

NOAA OAR Special Report

PMEL Tsunami Forecast Series: Vol. NNNN
**Development of a Tsunami Forecast Model for Point
Reyes, California**

Michael C. Spillane ^{1,2}

¹Joint Institute for the Study of the Atmosphere and Ocean (JISAO),
University of Washington, Seattle, WA

²NOAA/Pacific Marine Environmental Laboratory (PMEL), Seattle, WA

June 2011

DRAFT

NOTICE from NOAA

Mention of a commercial company or product does not constitute an endorsement by NOAA/OAR. Use of information from this publication concerning proprietary products or the tests of such products for publicity or advertising purposes is not authorized. Any opinions, findings, and conclusions or recommendations expressed in this material are those of the authors and do not necessarily reflect the views of the National Oceanic and Atmospheric Administration.

Contribution No. XXXX from NOAA/Pacific Marine Environmental Laboratory

Also available from the National Technical Information Service (NTIS)
(<http://www.ntis.gov>)

DRAFT

Contents

List of Figures

List of Tables

Foreword

Abstract

1.0 Background and Objectives

- 1.1 The Setting
- 1.2 Natural Hazards
- 1.3 Tsunami Warning and Risk Assessment

2.0 Forecast Methodology

- 2.1 The Tsunami Model
- 2.2 The SIFT Forecast System

3.0 Model Development

- 3.1 Digital Elevation Models
- 3.2 Tides and Sea Level Variation
- 3.3 The CFL Condition and other considerations for grid design
- 3.4 Specifics of the model grids
- 3.5 Model Run Input and Output Files

4.0 Results and Discussion

- 4.1 The “Null” Tests
- 4.2 The Extreme Case Tests
- 4.3 Model Validation: The Honshu-2011 Tsunami
- 4.4 Model Validation with other Standard Historical Events
- 4.5 Further Historical Simulations
- 4.6 The Mendocino Earthquake of April 25, 1992
- 4.7 Simulation of the remaining Synthetic Mega-events

5.0 Conclusions

6.0 Acknowledgements

7.0 References

FIGURES

Appendix A

- A1. Reference Model Input (*.in) File for Point Reyes, CA
- A2. Forecast Model Input (*.in) File for Point Reyes, CA

Appendix B Propagation Database: Pacific Ocean Unit Sources

Appendix C Synthetic Testing Report

DRAFT

List of Figures

- Figure 1.** The Point Reyes area of west and south Marin County, CA.
- Figure 2.** Extract from the oblique 3-D view of the San Francisco DEM provided by NGDC. The focus is Point Reyes; areas of potential inundation identified by CalEMA are highlighted in red.
- Figure 3.** View of the Point Reyes headland and Drake's Bay in its lee.
- Figure 4.** Distribution of the historical tsunami sources employed for the development of the Point Reyes forecast model. Those highlighted in red are more extensively investigated using the reference model.
- Figure 5.** A sample time interval from the Point Reyes tsunami-capable tide gage, unrelated to tsunami activity. The evolving surface wave spectrum is shown in the lower panel.
- Figure 6.** The setting of Point Reyes and its nested FM grids. The C-grids of other west coast forecast models are marked, as are various sites with data available for this study. The closest unit sources of the propagation database lie north of Cape Mendocino, and the epicenter of the most recent Cascadia thrust event is marked.
- Figure 7.** Nested grid representation for the Reference Model (RM).
- Figure 8.** Nested grid representation for the Forecast Model (FM).
- Figure 9.** Comparison of the RM and FM time series at the reference point for three "Null" sources in the Western Pacific. The lowest panel illustrates the appearance of model instability before the RM C-grid bathymetry was finalized.
- Figure 10.** Locations of synthetic tsunami scenarios employed in model development.
- Figure 11.** Comparison of Reference (RM) and Forecast (FM) model results for the ACSZ 56-65 synthetic mega-event, representing the Cascadia Subduction Zone. **a)** Maximum amplitude from the RM (upper panel), the FM (lower panel), time series at the Point Reyes tide gage (upper panel inset: black for RM, red for FM). The lagged correlation at the TG (lower inset) shows that there is only a few minutes difference in the model arrival times. **b)** Comparison of maximum speed from the Reference Model (upper panel) and Forecast Model (lower panel). Inset panels compare the time series of the velocity components at the TG. **c)** Comparison of the amplitude and vector current fields at the time indicated by the green line in the upper inset panel. **d)** As for c) but at a later time in the model runs.
- Figure 12.** As in Figure 11, but for the KISZ 01-10 scenario representing Kamchatka.
- Figure 13.** As in Figure 11, but for the NTSZ 30-39 scenario representing Samoa.
- Figure 14.** As in Figure 11, but for a synthetic moderate event at NTSZ B36 near Samoa.
- Figure 15.** Observed time series from DART and MARS bottom pressure sensors during the Honshu-2011 event, compared with the model representation based on the propagation database (see Table 1). Model time series in the right hand panel have been lagged, and a common scale factor of 1.2 applied.
- Figure 16.** Comparison with RM and FM-predicted time series at selected locations where tide gage data are available: a) Point Reyes, Arena Cove, and San Francisco, b) Bolinas (6-minute data), Alameda, and Richmond.

- Figure 17.** Intercomparison of RM and FM predictions for the Honshu-2011 event. a) maximum amplitude and zero-lag correlation in the style of Figure 11, b) maximum speed distribution, c), d) and e) contrast snapshots of amplitude and velocity at discrete times, marked in the upper panel inset. RM and FM C-grid results are in the upper and lower panels; the RM fields are truncated to the FM domain.
- Figure 18.** Inundation forecast for the Honshu-2011 event in the RM C-grid, compared with the CalEMA inundation line. The inset in the upper right shows tide gage data from Point Reyes. Actual tides were well below MHW so the inundation forecast was overly conservative.
- Figure 19.** Reference and Forecast Model comparison for the Chile-2010 event: a) maximum amplitude and correlation, in the style of Figure 11, b) maximum speed distribution, c) snapshot of amplitude and current at the indicated time.
- Figure 20.** Model and observed time series comparison for the Chile-2010 event.
- Figure 21.** RM and FM comparison, as in Figure 19 but for the Samoa-2009 event.
- Figure 22.** Model and observed time series comparison for the Samoa-2009 event.
- Figure 23.** RM and FM comparison, as in Figure 19 but for the Kuril-2006 event.
- Figure 24.** Model and observed time series comparison for the Kuril-2006 event.
- Figure 25.** RM and FM comparison, as in Figure 19 but for the Alaska-1964 event.
- Figure 26.** Model and observed time series comparison for the Alaska-1964 event.
- Figure 27.** RM and FM comparison, as in Figure 19 but for the Unimak-1946 event.
- Figure 28.** Model and observed time series comparison for the Unimak-1946 event.
- Figure 29.** The Sanriku event of June 15, 1896.
- Figure 30.** The Kamchatka event of November 4, 1952.
- Figure 31.** The Chile event of May 22, 1960.
- Figure 32.** The Andeanof event of June 10, 1996.
- Figure 33.** The Peru event of June 23, 2001.
- Figure 34.** The Hokkaido event of September 25, 2003.
- Figure 35.** The Rat Island event of November 17, 2003.
- Figure 36.** The Tonga event of May 3, 2006.
- Figure 37.** The normal thrust event off the Kuril Islands on January 13, 2007.
- Figure 38.** The Solomon event of April 1, 2007.
- Figure 39.** The Peru event of August 15, 2007.
- Figure 40.** The Chile event of November 14, 2007.
- Figure 41.** The Cape Mendocino event of April 25, 1992. The upper panels show the frequency of non-thrust events in the vicinity, with only two having a focal mechanism characteristic of subduction. Lower panel: comparison of model with observation at Arena Cove and Point Reyes.
- Figure 42.** Predicted maximum sea level (from the FM) at the Point Reyes tide gage that might result were “mega-events” to occur at various locations around the Pacific Basin.
- Figure 43.** Chart of the area inundated by one or more of the mega-tsunami scenarios modeled with the FM. Shown in blue is the CalEMA inundation line, which is based on a similar ensemble of scenarios.

List of Tables

- Table 1a.** Source characterization for historical tsunami events employed in Point Reyes model testing. Those in bold text were used in RM/FM inter-comparison. Sources identified as “ad hoc” may not be identically defined in other Forecast Model reports.
- Table 1b.** Supplementary historical tsunami events employed for Point Reyes, CA forecast model testing. Those identified as “ad hoc” and may not be identically implemented in other Forecast Model reports.
- Table 2.** The main features of the San Francisco Digital Elevation Model (DEM), which includes Point Reyes, California.
- Table 3.** Tidal characteristics of the Point Reyes, CA Tide Gage (9415020).
- Table 4.** Specifics of the Reference (RM) and Forecast model (RM) grids employed for Point Reyes, CA. For the paired values in the resolution and grid points columns, the zonal (East to West) value is listed first, followed by meridional (North to South).
- Table 5.** Grid file names and grid-related parameters. The time steps for the A and B-grids must be integer multiples of the basic time step chosen for the C-grid.
- Table 6.** Synthetic tsunami events employed in Point Reyes, CA model testing. The RM and FM solutions of those shown in bold text were inter-compared extensively.
- Table 7.** Mega-tsunami scenario impacts, represented by flooding (km² in the sub-region 123.1:122.5W, 37.8:38.1N) and maximum amplitude (cm) at several sites within the model domain (identified in the footnote). The maxima are highlighted and ranked.

This page is intentionally blank.

DRAFT

PMEL Tsunami Forecast Series: Vol. NNNN
**Development of a Tsunami Forecast Model for Point
Reyes, California**
Michael C. Spillane ^{1,2}

Foreword

Tsunamis have been recognized as a potential hazard to United States coastal communities since the mid-twentieth century, when multiple destructive tsunamis caused damage to the states of Hawaii, Alaska, California, Oregon, and Washington. In response to these events, the United States, under the auspices of the National Oceanic and Atmospheric Administration (NOAA), established the Pacific and Alaska Tsunami Warning Centers, dedicated to protecting United States interests from the threat posed by tsunamis. NOAA also created a tsunami research program at the Pacific Marine Environmental Laboratory (PMEL) to develop improved warning products.

The scale of destruction and unprecedented loss of life following the December 2004 Sumatra tsunami served as the catalyst to refocus efforts in the United States on reducing tsunami vulnerability of coastal communities, and on 20 December 2006, the United States Congress passed the “Tsunami Warning and Education Act” under which education and warning activities were thereafter specified and mandated. A “tsunami forecasting capability based on models and measurements, including tsunami inundation models and maps.” is a central component for the protection of United States coastlines from the threat posed by tsunamis. The forecasting capability for each community described in the PMEL Tsunami Forecast Series is the result of collaboration between the National Oceanic and Atmospheric Administration office of Oceanic and Atmospheric Research, National Weather Service, National Ocean Service, National Environmental Satellite Data and Information Service, the University of Washington’s Joint Institute for the Study of the Atmosphere and Ocean, National Science Foundation, and United States Geological Survey.

Abstract. Operational tsunami forecasting by NOAA’s Tsunami Warning Centers relies on the detection of tsunami wave trains in the open ocean, inversion of these data (telemetered via satellite) to quantify their source characteristics, and real-time modeling of the impact on threatened coastal communities. The latter phase of the process involves, for each such community, a pre-tested Forecast Model capable of predicting the impact, in terms of inundation and dangerous inshore currents, with sufficient resolution and within the time constraints appropriate to an emergency response.

In order to achieve this goal, considerable advance effort is required to tune each forecast model to the specific bathymetry and topography, both natural and manmade, of the impact area, and to validate its performance with a broad set of tsunami sources. Where possible the validation runs should replicate observed responses to historical events, but the sparse instrumental record of these rare but occasionally devastating occurrences dictates that comprehensive testing should include a suite of scenarios that represent potential future events.

During the forecast model design phase, and in research mode outside the pressures of an emergency situation, more detailed and slower-running models can be investigated. Such a model, referred to as a Reference Model, represents the most credible numerical representation of tsunami response for the study region, using the most detailed bathymetry available and without the run-time constraint of operational use. Once a reference model has been developed, the process of forecast model design is to determine where efficiencies can be gained, through reducing the grid resolution and increasing the model time step, while still adequately representing the salient features of the full solution.

This report documents the reference and forecast model development for Point Reyes and vicinity, comprising much of western Marin County, CA. The Point Reyes headland juts out into the Pacific and its lighthouse is a prominent navigation landmark northwest of the entrance to San Francisco Bay. A tide gage within Drake's Bay, in the lee of the headland, provides observations for model validation. While much of the study region lies within a National Seashore area, limiting the population and waterfront infrastructure, there are a number of nearby communities exposed to tsunami impact. Beaches and other natural amenities and the mild climate foster extensive recreational use, and there is a clear need for emergency preparedness. This report addresses the tsunami aspects of the natural hazard spectrum.

¹ Joint Institute for the Study of the Atmosphere and Ocean (JISAO), University of Washington, Seattle, WA

²NOAA/Pacific Marine Environmental Laboratory (PMEL), Seattle, WA

1.0 Background and Objectives

1.1. The Setting

Point Reyes, lying to the northwest of the entrance to San Francisco Bay is a prominent navigational landmark. As illustrated in Figure 1 (composed of orthographic images from “MarinMaps” (mmgis.marinmap.org/OrthoGrid/viewer.htm), the headland is the site of a lighthouse and, in Drake’s Bay in its lee adjacent to the historic Point Reyes Lifeboat station, is the tide gage bearing the same name. All lie within the Point Reyes National Seashore (PRNS), comprising most of west Marin County, which is essentially unpopulated and in a natural state, with the exception of some agricultural activity that was allowed to continue when the PRNS was established in 1962. As seen in the inset to Figure 1, the San Andreas Fault strongly delineates the eastern boundary of the region though it is submerged in Tomales Bay, in the north, and Bolinas Lagoon in the south. In the neck of land between them are the communities of Olema and Point Reyes Station, which are close to the epicenter of the 1906 San Francisco Earthquake. Several small communities lie on the shores of Tomales Bay (20.4km in length but with a mean depth of only 3.1m, Nieme and Hall, 1996). The connection to Bodega Bay is shallow and constricted. At the southern end, Bolinas (2010 Pop. 1,620) and Stinson Beach (2010 Pop. 632) have greater exposure to damage from tsunami or winter storm waves. Between Stinson Beach and Point Bonita, the southernmost point of Marin County, is Muir Beach, a community of about 310. It is notable, from the tsunami perspective, in that it reported major run-ups during the Unimak-1946 and Alaska-1964 events.

North of Tomales Bay is Bodega Bay whose shores lie both in Marin and Sonoma counties. Apart from the shallow Bodega Harbor, and the communities of Bodega Bay (2010 Pop. 1,077) and Doran Beach extending onto the spit at its mouth, this area too is sparsely populated. The natural beauty of the region, with its mild climate and proximity to the San Francisco area and other urban centers, provides outstanding recreational opportunities, resulting in large numbers of visitors throughout the year. Normally, in selecting the domain of a tsunami forecast model, the location of a tide gage provides the focus but, in this case, a somewhat larger region is included to provide forecast capability to population centers and primary recreational assets. Initially it was hoped that a forecast model could cover the entire region from Bodega Bay to Muir Beach. This proved to be impossible, given the time constraints on model run time imposed by emergency usage, without an unacceptable reduction in spatial resolution. While the C-grid of the Reference Model (RM) does include Tomales Bay and a portion of Bodega Bay, these are excluded from the Forecast Model (FM), which focuses on the south and southwest of Marin County.

The University of Southern California Tsunami Research Center conducted a comprehensive study of potential tsunami inundation, for the entire California coastline. Funded through the California Emergency Management Agency (CalEMA), by the National Tsunami Hazard Program, the study (Barberopoulou et al, 2011) has produced a set of inundation maps for emergency planning purposes accessible online in various forms, including MyHazard (myhazards.calema.ca.gov) which enables users to acquire information specific to their site of interest. The CalEMA inundation results are available in GIS form and those specific to the Point Reyes area are used throughout this report. In

addition to underpinning the modeling effort, the digital elevation model (DEM) for the San Francisco region, provided by the National Geophysical Data Center (NGDC), includes a 3-D oblique view that assists greatly in visualizing the study area. In Figure 2, the CalEMA inundation information is overlaid, together with descriptive labels on an extract from the NGDC image. The full 3-D image is available in the San Francisco DEM Report (Carnigan et al., 2010).

A striking series of aerial photographs (www.californiacoastline.org) show that the study region contains both high cliffs (also seen in Figure 3) that limit potential impact by tsunamis and broad beaches and shallow coastal inlets that are more exposed. Queries to the CalEMA “MyHazards” site for Bolinas and Stinson Beach show flooding and earthquake as other hazards to which they are prone, in addition to tsunami. Available online is a video “Marin Tsunami” (Loeffler and Gesell, 2010), produced for the USGS in cooperation with the Marin County Sheriff – Office of Emergency Services. In addition to providing an overview of the comprehensive level of preparedness for tsunami impact on the communities of Bolinas, Stinson Beach, Dillon Beach/Lawson’s Landing, and the popular Limantour Beach within the National Parks area of responsibility, this excellent resource for residents and visitors alike gives insight into the character of the area.

1.2. Natural Hazards

Instances of mild tsunami signals are evident in the tide gage records for Point Reyes (established in 1975), and Marin County sites appears several times in the records compiled by Lander and Lockridge (1989) and its regularly updated online equivalent: NGDC Tsunami Hazard Database (Dunbar, 2007; see www.ngdc.noaa.gov/hazard/). The historical record first mentions Marin County with a wave observed at Sausalito, on the north shore of the Golden Gate, from a Chilean event in 1877. The first time series currently available for analysis is a digitized marigram from Sausalito, recorded during the Sanriku event of 1896 and available in the Alaska/West Coast Tsunami Warning Center (WCATWC) archives. O’Brien (1946) described a 2.6 meter wave (above MLLW) in Drake’s Bay during the 1946 Unimak tsunami, with a boat washed onto the highway. While Marin County sites are not explicitly mentioned in connection with the Kamchatka-1952 or Andreanof-1957 events, waves were observed at Bodega and within San Francisco Bay. During the 1960 Chile event, a 1.5 meter run-up was reported at Stinson Beach, and during the 1964 Alaska tsunami waves were observed at several sites within Marin County including Drake’s Beach. Time series from several tsunamis are available from the Point Reyes tide gage in recent years, culminating in the major event east of Honshu on March 11, 2011 (also referred to as the Tohoku earthquake.) The latter will be discussed extensively in this report.

Combining events impacting northern California with those that have occurred since the Point Reyes tide gage was upgraded to 1-minute sampling, a total of 27 historical events are available for study. Nineteen of these, listed in Table 1a, are the standards for forecast

Table 1a. Source characterization for historical tsunami events employed in Point Reyes model testing. Those in bold text were used in RM/FM inter-comparison. Sources identified as “ad hoc” may not be identically defined in other Forecast Model reports.

Event	Earthquake / Seismic				Model			
	USGS		CMT		Tsunami Magnitude	Subduction Zone	Tsunami Source (Reference/Derivation)	
	Date Time (UTC) Epicenter	Date Time (UTC) Centroid	Magnitude M_w					
1946 Unimak	01 Apr 12:28:56 52.75°N 163.50°W		8.5		8.5	ACSZ	7.5×B23 + 19.7×B24 + 3.7×B25 (López & Okal, 2006)	
1952 Kamchatka	04 Nov 16:58:26.0 52.76°N 160.06°E		9.0		9.0	KISZ	19.71 × (A4 + Y4 + Z4 + A5 + Y5 + Z5 + A6 + Y6 + Z6) (ad hoc)	
1957 Andreanof	09 Mar 14:22:31 51.56°N 175.39°W		8.6		8.7	ACSZ	31.4×A15 + 10.6×A16 + 12.2×A17 (Preliminary)	
1960 Chile	22 May 19:11:14 38.29°S 73.05°W		9.5		9.5	CSSZ	125×(A93 + B93 + Z93 + A94 + B94 + Z94 + A95 + B95) Kanamori & Cipar (1974)	
1964 Alaska	28 Mar 03:36:00 61.02°N 147.65°W		9.2		8.9	ACSZ	15.4×A34 + 18.3×B34 + 48.3×Z34 + 19.4×A35 + 15.1×B35 (Tang et al., 2006, 2009)	
1994 East Kuril	04 Oct 13:22:58 43.73°N 147.32°E	04 Oct 13:23:28.5 43.60°N 147.63°E	8.3		8.1	KISZ	9.0×A20 (ad hoc)	
1996 Andreanof	10 Jun 04:03:35 51.56°N 175.39°W	10 Jun 04:04:03.4 51.10°N 177.410°W	7.9		7.8	ACSZ	2.40×A15 + 0.80×B16 (Preliminary)	
2001 Peru	23 Jun 20:33:14 16.26°S 73.64°W	23 Jun 20:34:23.3 17.28°S 72.71°W	8.4		8.2	CSSZ	5.7×A15 + 2.9×B16 + 1.98×A16 (Preliminary)	
2003 Hokkaido	25 Sep 19:50:06 41.77°N 143.904°E	25 Sep 19:50:38.2 42.21°N 143.84°E	8.3		8.3	KISZ	3.95 × (A22 + B22 + A23 + B23) (ad hoc)	
2003 Rat Island	17 Nov 06:43:07 51.13°N 178.74°E	17 Nov 06:43:31.0 51.14°N 177.86°E	7.7		7.8	ACSZ	2.81×B11 (Real-time)	
2006 Tonga	03 May 15:26:39 20.13°S 174.16°W	03 May 15:27:03.7 20.39°S 173.47°W	8.0		8.0	NTSZ	6.6×B29 (ad hoc)	
2006 Kuril	15 Nov 11:14:16 46.607°N 153.230°E	15 Nov 11:15:08 46.71°N 154.33°E	8.3		8.1	KISZ	4.0×A12 + 0.5×B12 + 2.0×A13 + 1.5×B13 (Real-time)	
2007 Kuril	13 Jan 04:23:20 46.272°N 154.455°E	13 Jan 04:23:48.1 46.17°N 154.80°E	8.1		7.9	KISZ	-3.64 × B13 (Real-time)	
2007 Solomon	01 Apr 20:39:56 8.481°S 156.978°E	01 Apr 20:40:38.9 7.76°S 156.34°E	8.1		8.2	NVSZ	12.0×B10 (Preliminary)	
2007 Peru	15 Aug 23:40:57 13.354°S 76.509°W	15 Aug 23:41:57.9 13.73°S 77.04°W	8.0		8.1	CSSZ	0.9×A61 + 1.25×B61 + 5.6×A62 + 6.97×B62 + 3.5×Z62 (Preliminary)	
2007 Chile	14 Nov 15:40:50 22.204°S 69.869°W	14 Nov 15:41:11.2 22.64°S 70.62°W	7.7		7.6	CSSZ	1.65×Z73 (Real-time)	
2009 Samoa	29 Sep 17:48:10 15.509°S 172.034°W	29 Sep 17:48:26.8 15.13°S 171.97°W	8.1		8.1	NTSZ	3.96×A34 + 3.96×B34 (Real-time)	
2010 Chile	27 Feb 06:34:14 35.909°S 72.733°W	27 Feb 06:35:15.4 35.95°S 73.15°W	8.8		8.8	CSSZ	17.24×A88 + 8.82×A90 + 11.84×B88 + 18.39×B89 + 16.75×B90 + 20.78×Z88 + 7.06×Z90 (Real-time)	
2011 Honshu	11 Mar 05:47:24 38.297°N 142.372°E	11 Mar 05:47:47.2 38.486°N 142.597°E	9.0		9.0	KISZ	4.66 × B24 + 12.23×B25 + 26.31×A26 + 21.27×B26 + 22.75×A27 + 4.98×B27 (Real-time; Tang et al., 2012)	

Table 1b. Supplementary historical tsunami events employed for Point Reyes, CA forecast model testing. Those identified as “ad hoc” and may not be identically implemented in other Forecast Model reports.

Event	Earthquake / Seismic			Tsunami Source (Reference/Derivation)		
	USGS Date Time (UTC) Epicenter	GMT Date Time (UTC) Centroid	Magnitude M_w	Tsunami Magnitude	Subduction Zone	Tsunami Source
1896 Samriku	15 Jun 10:33:00 39.5°N 144.0°E		7.6	7.6	KISZ	b25 x 1.413 (ad hoc)
1992 Mendoza	25 Apr 18:06:04 40.368°N 124.316°W	25 Apr 18:06:11.8 38.56°N 123.31°W	7.2	7.2	ACSZ	a65 x 0.355 or b65 x 0.355 (ad hoc)
1995 Chile	30 Jul 05:11:24 23.340°S 70.294°W	30 Jul 05:11:56.9 24.17°S 70.74°W	8.0	8.0	CSSZ	2.812 x (a75 + b75) (ad hoc)
1995 Kuril	03 Dec 18:01:09 44.663°N 149.300°E	03 Dec 18:01:36.1 44.82°N 150.17°E	7.9	7.9	KISZ	1.991 x (a17 + z17) (ad hoc)
1996 Irian Jaya	17 Feb 05:59:31 0.891°S 136.952°E	17 Feb 06:00:02.8 0.67°S 136.62°E	8.2	8.2	NGSZ	2.7984 x (a9 + b9 + a10 + b10) (ad hoc)
2009 PapuaNG	03 Jan 19:43:51 0.414°S 132.885°E	03 Jan 19:44:09.0 0.38°S 132.83°E	7.6	7.6	NGSZ	0.7046 x (b13 + b14) (ad hoc)
2009 Kuril	15 Jan 17:49:39 46.857°N 155.154°E	15 Jan 17:49:48.3 46.97°N 155.39°E	7.4	7.4	KISZ	b12 x 0.7063 (ad hoc)
2009 Vanuatu / Santa Cruz	07 Oct 22:03:15 13.032°S 166.187°E	07 Oct 22:03:28.9 12.59°S 166.27°E	7.6	7.6	NVSZ	1.2xB24 + 0.26xA23 followed after 15minutes by 2.6xB23 + 0.9xA23
	07 Oct 22:18:26 12.554°S 166.320°E	07 Oct 22:19:15.3 11.86°S 166.01°E	7.8	7.9	NVSZ	(Preliminary Wei 2009, Personal Communication)

model testing in the Pacific because their sea floor deformation is reasonably well known, either from the literature or, more recently, derived from direct observation of the wave trains they generated. The remaining eight, listed in Table 1b, have source characteristics that are less well known; they are included to expand the geographical coverage or because of their special relevance to the West Coast. The M_w 7.2 earthquake north of Cape Mendocino on April 25, 1992 was a very mild foretaste of a Cascadia Subduction Zone (CSZ) event but was registered in marigrams at Arena Cove and Point Reyes. Others, due to significant noise in the tide gage, do not produce a clear signal but shed light on Point Reyes as a reference point for coastal impacts. Figure 4 illustrates the distribution of the 27 historical sources. Those highlighted in red were employed for intercomparison of the reference and forecast versions of the model.

Direct seismic impact is another natural hazard to which Point Reyes area is exposed. Its proximity to the rupture zone of the SAF in the San Francisco earthquake of 1906 resulted in significant damage to the town and the destruction of the lighthouse. While the SAF enters the ocean at Bolinas, its strike-slip nature reduces the likelihood of severe tsunami wave generation should ruptures occur in the immediate vicinity. Submarine landslides or collapse of sections of sea cliff are however a potential local source for tsunami damage. Landslides triggered by seismic events caused significant loss of life during the 1929 Newfoundland event and accentuated the 1996 New Guinea tsunami. Landslide-generated tsunami waves are not currently included in the SIFT forecast methodology, nor are those generated meteorologically. However, to the extent that the waves they produce are detected by the DART array, some warning of their presence may be available.

Another local hazard that has been a frequent cause of damage in the Bolinas-Stinson Beach area has been ocean wave action. Originating locally, or as swell from distant storms, such waves in the winters of 1977-78 and 1982-83 caused the loss of several beachfront homes. Another impact of ocean waves, of relevance to tsunami detection and modeling, is in the noise they produce in the tide gage records. Although the Point Reyes tide gage is in the lee of the headland, excessive wave action and resonance can mask weak tsunami signals.

1.3. Tsunami Warning and Risk Assessment

The forecast model development, described here, will permit Point Reyes, CA, to be incorporated into the tsunami forecasting system SIFT, developed at NCTR (NOAA Center for Tsunami Research) and now in operational use at the U.S. Tsunami Warning Centers (TWC's). The system has had considerable success is accurately forecasting the impact of both moderate and severe tsunami events in recent years and in the following section the methodology that permits such forecasts is discussed as prelude to a description of development of the forecast model for Point Reyes. With the model in hand, validated with historical events and with its stability verified by extensive testing against extreme scenarios, real-time forecasts will be available to inform local emergency response. Additionally, the synthetic scenarios investigated during model development, and reported here, provide an initial tsunami risk assessment as described in the Results and Discussion section.

2.0 Forecast Methodology

2.1 The Tsunami Model

In operational use, a tsunami forecast model is used to extend a pre-computed deep-water solution into the shallows, and onshore as inundation if appropriate. The model consists of a set of three nested grids, of increasingly fine resolution that, in a real-time application of the MOST model (Method of Splitting Tsunami: Titov and Synolakis, 1998; Titov and González, 1997), permits forecasts at spatial scales (as little a few tens of meters) relevant to local emergency management. The validity of the MOST model applied in this manner, and the operational effectiveness of the forecast system built around it, has been demonstrated during unplanned tests triggered by several mild to moderate tsunami events in the years since the 2004 Indian Ocean disaster (Wei et al., 2008). Successful hindcasting of observed historic events, even mild ones, during forecast model development lends credence to the ability to accurately forecasting the impact of future events. Such validation of tsunami modeling procedures is documented in other volumes of the series of which this report is but one. Before proceeding to a description of the forecast model development for Point Reyes, it is useful to describe the steps in the overall forecast process.

2.2 The SIFT Forecast System

Operational tsunami forecasts are generated at Tsunami Warning Centers, staffed 24/7 in Alaska and Hawaii, using the SIFT (Short-term Inundation Forecasting for Tsunamis) tool, developed at NCTR. The semi-automated process facilitates the steps by which TWC operators assimilate data from an appropriate subset of the DART® tsunami sensors, “invert” the data to determine the linear combination of pre-computed propagation solutions that best match the observations, then initiate a set of forecast model runs if coastal communities are threatened or, if warranted, cancel the warning.

Steps in the process are as follows:

- When a submarine earthquake occurs the global network of seismometers registers it. Based on the epicenter, the unit sources in the Propagation Database (Gica et al., 2008) that are most likely to be involved in the event, and the DART® array elements (Spillane et al., 2008) best placed to detect the waves passage are identified. TWC watch-standers can trigger DART®s into rapid sampling mode in the event that this did not occur automatically in response to the seismic signal.
- There is now an unavoidable delay while the tsunami waves are in transit to the DART®s; at least a quarter of a cycle of the first wave in the train must be sampled before moving to the “inversion” step.
- When sufficient data have accumulated, at one or more DART®s, the observed time series are compared with the model series from the candidate unit sources. Since the latter are pre-computed (using the MOST code), and the dynamics of tsunami waves in deep water is linear, a least squares approach taking very little time can identify the unit sources, (and the appropriate scale factors for each,) that

best fit the observations. The “inversion” methodology is described by Percival et. al., (2009).

- Drawing again on the Propagation Database, the scale factors are applied to produce a composite basin-wide solution with which to identify the coastal regions most threatened by the radiating waves.
- It is at this point that one or more forecast models are run. The composite propagation solution is employed as the boundary condition to the outermost (A-grid) domain of a nested set of three real-time MOST models that telescope with increasingly fine scale to the community of concern. A-grid results provide boundary conditions to the B-grid, which in turn forces the innermost C-grid. Non-linear processes including inundation are modeled so that, relying on the validation procedures during model development, credible forecasts of the current event are available.
- Each forecast model provides quantitative and graphic forecast products with which to inform the emergency response, or to serve as the basis for canceling or reducing the warnings. Unless the tsunami source is local, the forecast is generally available before the waves arrive but, even when lead-time cannot be provided, the several hour duration of a significant event (in which the first wave may not be the most damaging) give added value to the multi-hour forecasts provided.

Because multiple communities may be potentially at risk, it may be necessary to run simultaneously, or in a prioritized manner, multiple forecast models. Each must be optimized to run efficiently in as little time as possible; the current standard is that an operational forecast model should be capable of simulating 4 hours of real time within about 10 minutes of CPU time on a fast workstation computer.

3.0 Model Development

3.1 Digital Elevation Models

Water depth determines local tsunami wave speed and sub-aerial topography determines the extent to which tsunami waves inundate the land. Thus a prerequisite for credible tsunami modeling is the availability of accurate gridded bathymetric and topographic datasets, termed DEM's (Digital Elevation Models.) Given their expertise in this area, and the number of coastal communities needing tsunami forecast capability, NCTR relies heavily on the National Geophysical Data Center (NGDC) to provide the DEM's needed. In the case of Point Reyes, a sub-region of the San Francisco DEM is employed. The DEM, a composite of multiple data sources merged and converted to a common datum of Mean High Water (MHW), was produced and documented by Carignan et al. (2010). The use of MHW as the "zero level" for forecast results is standard. The MOST model does not include tidal fluctuations and, since a tsunami may arrive at any stage of the tide, it is best to employ a "worst-case" approach by assuming high tide when forecasting inundation. For some Forecast Models grounding of vessels and the strong and the rapidly varying currents often associated with even mild tsunamis are of concern. For Point Reyes, lacking a marina and shoreline infrastructure, low water impacts are less important.

The Point Reyes sub-region of the San Francisco DEM was illustrated in Figure 2; its salient features listed in Table 2 are reproduced from DEM documentation (Carnigan et al., 2010). The NGDC report thoroughly describes the data sources and methods employed in constructing the DEM. With one-third arc second (~10m) resolution, the DEM provides the basis for the B and C-grids for both reference and forecast model usage. NCTR maintains an atlas of lower resolution gridded bathymetries, which can be used for the A-grids, as described later. All of the DEMs employed were verified for consistency with charts, satellite imagery, and other datasets during the course of MOST grid development.

Table 2. The main features of the San Francisco Digital Elevation Model (DEM), which includes Point Reyes, California.

Grid Area	San Francisco, California
Coverage Area	123.30° to 121.85° W; 37.32° to 38.48° N
Coordinate System	Geographic decimal degrees
Horizontal Datum	World Geodetic System 1984 (WGS84)
Vertical Datum	Mean High Water (MHW)
Vertical Units	Meters
Cell Size	1/3 arc-second
Grid Format	ESRI Arc ASCII grid
Version Employed	Update of February 24, 2011

The bathymetry and topography used in the development of this forecast model was based on the digital elevation model provided by the National Geophysical Data Center and the author considers it to be a good representation of the local topography/bathymetry. As new digital elevation models become available, forecast models will be updated and report updates will be posted at http://nctr.pmel.noaa.gov/forecast_reports/.

3.2 Tides and Sea Level Variation

The history of tidal observation at Point Reyes dates back only to 1975. The tide station (9415020) is located near the end of the pier projecting into Drake's Bay just west of the historic Lifeboat station. The pilings raise the deck well above sea level and do not impede water movement. The instrumentation was upgraded in 2006 to include a tsunami-capable gage sampling at 1-minute intervals (and, on demand at 15-second intervals); some earlier data was sampled at 6-minute intervals and several historical events are only available as marigrams on microfiche. An ongoing project at NGDC will digitize the more critical images in this archive; a few are available in digitized form in the WCATWC archives.

Station characteristics for 9415020 are provided in Table 3, based on the wealth of online tidal information available at NOAA's CO-OPS (Center for Operational Oceanographic Products and Services) website (tidesandcurrents.noaa.gov). Note the sizeable diurnal range of about 1.7 meters and that, while the long-term rate of change in sea level is low (compared to more seismically active areas), there is substantial seasonal, interannual and short-term variability.

Table 3. Tidal characteristics of the Point Reyes, CA Tide Gage (9415020).

Point Reyes, CA		Station#9415020		37°59.7'N, 122°58.6'W	
Tidal Datum and Range Values (Epoch 1983-2001)					
MHHW (Mean Higher High)	2.964m	Great Diurnal Range 1.758m	Mean Range 1.193m		
MHW (Mean High Water)	2.760m				
MSL (Mean Sea Level)	2.152m				
MLW (Mean Low Water)	1.567m				
MLLW (Mean Lower Low)	1.206m				
Sea Level Trends and Cycles					
Long Term SL Trend	Increasing 2.10±1.52mm/year				
Seasonal Cycle Range	Minimum -89mm(April); Maximum 59mm(September)				
Interannual Variation (from 1980)	Minimum -20mm(1989); Maximum +21mm(1998)				
Extremes to date (June 2011)					
Maximum	3.810m on 06 Feb, 1998				
Minimum	0.387 on 19 Jan, 1988				

A sample section of the tide gage record, extracted from the CO-OPS website for the period following the Honshu-2011 is included in Figure 18 from Section 4.3. In a several hour section of one-minute data, the signature of an arriving tsunami is generally a burst of higher frequency energy with a sudden onset. However, during the winter months in particular, similar bursts unrelated to tsunami activity are quite common. In January 2011 for example several occurred, one of which is illustrated in Figure 5. The tidal signal has been removed with a Butterworth band-pass filter with cutoff periods at 5 and 120 minutes. This filter will be used through the report is preprocessing tide gage records for comparison with model prediction. The lower panel of Figure 5 is the spectral wave

energy at hourly intervals from NDBC buoy 46026, 18nm west of San Francisco. There is a clear correlation between enhanced swell at this site and the detided residuals in Drake's Bay suggesting that surface waves can excite a coastal response. The amplitude of this noise for the example shown is perhaps 10-20cm and would likely obscure a mild tsunami signature were one to arrive during such an episode. Deviations (or residuals) from the astronomically predicted tide can be several centimeters and the variability strong. In particular the highest water level reported for the Point Reyes gage is 1.05m above MHW (Feb 6, 1998) so the use of MHW as the zero level of modeled sea level may underestimate the truly worse case. While the simultaneous arrival of the crest of a large tsunami at high tide during a storm surge has low probability, a feature of the simulated events reported below is that sustained oscillations at a resonant period may extend the duration of the threat. This effect is notorious at Crescent City, CA which is frequently the most heavily impacted U.S. west coast location for remote events.

3.3 The CFL Condition and other considerations for grid design

Water depth dependent wave speed, in conjunction with the spacing of the spatial grid representation, place an upper limit on the time step permissible for stable numerical solutions employing an explicit scheme. This is the CFL limit (Courant-Friedrichs-Levy), which requires careful consideration when the grids employed for a reference or forecast model are being designed. Finer-scale spatial grids, or greater water depths, require shorter time steps thereby increasing the amount of computation required to simulate a specific real time interval.

Another feature of the application of gridded numerical solutions to the tsunami wave problem is the shortening that the wave train encounters in moving from deep water onto the shelf. In deep water a grid spacing of 4 arc-seconds (of latitude and longitude, corresponding to ~7km) is normally used to represent propagating wave trains whose wavelength is typically of the order of a few hundred kilometers. The stored results of such propagation model runs are typically decimated by a factor of 4, resulting in a database of ~30km spacing (and 1 minute temporal sampling) with which to generate the boundary conditions for the outermost of the nested grids in a model solution. The extraction of the boundary conditions (of wave height and the two horizontal velocity components) is achieved by linear interpolation in space and time. To provide realistic interpolated values the stored fields for these variables must be smoothly varying, and have adequate sampling in space and time to resolve their structure. This necessitates the placement of the offshore boundary of the forecast model domain well offshore. The presence of the Mendocino Escarpment is another incentive to do so, in order that its role in topographic steering of trans-Pacific wave trains is adequately represented.

3.4 Specifics of the model grids

After several rounds of experimentation, the extents and resolutions of the nested grids were chosen, and are illustrated in Figures 7 and 8; details are provided in Tables 4 and 5. The Reference Model (RM) grid extents were set early in the process when the hope was to provide forecast results from Bodega Bay to Muir Beach, but have further value in ensuring adequate representation of waves entering the domain from remote sources. The RM grids are displayed in Figure 7; in the A- and B-grid panels, rectangles show the

nested grid domain within. In the case of the RM grid-C panel, the reduced extent of the equivalent FM grid is indicated. Figure 8 depicts the nested grids of the Forecast Model. The main focus of the FM, and this report, is on the southwestern and southern portion of Marin County. Some mention of the northern portion will be made as appropriate but, with the exception of some results that can be derived from the A-grid, comprehensive forecasts for Bodega Bay will require a dedicated model.

Table 4. Specifics of the Reference (RM) and Forecast model (RM) grids employed for Point Reyes, CA. For the paired values in the resolution and grid points columns, the zonal (East to West) value is listed first, followed by meridional (North to South).

Point Reyes, CA Reference Model (RM)						
Grid	Zonal Extent		Meridional Extent		Resolution	Grid Points
A	128.000°W	121.500°W	36.000°N	42.500°N	30"x30"	781 x 781
B	123.300°W	122.100°W	37.475°N	38.475°N	4"x3"	1081 x 1201
C	123.150°W	122.533°W	37.825°N	38.350°N	$\frac{4}{3}$ "x1"	1666 x 1891

Point Reyes, CA Forecast Model (FM)						
Grid	Zonal Extent		Meridional Extent		Resolution	Grid Points
A	125.000°W	122.000°W	37.00°N	39.00°N	60"x60"	181 x 121
B	123.300°W	122.100°W	37.550°N	38.475°N	18" x 15"	241 x 233
C	123.130°W	122.533°W	37.825°N	38.100°N	4" x 3"	538 x 331

Table 5. Grid file names and grid-related parameters. The time steps for the A and B-grids must be integer multiples of the basic time step chosen for the C-grid.

Grid	Filename	Maximum Depth (m)	Minimum CFL (s)	Model Time Step (s)	Water Cells
A	PtReyesCA_RM_A	5002	3.350	1.2 (2x)	436,723
	PtReyesCA_FM_A	4379	7.137	6.0 (3x)	15,977
B	PtReyesCA_RM_B	2166	0.637	0.6 (1x)	664,682
	PtReyesCA_FM_B	2114	3.062	2.0 (1x)	26,598
C	PtReyesCA_RM_C	98.6	0.995	0.6	1,411,698
	PtReyesCA_FM_C	94.7	3.045	2.0	103,086

Both C-grids lie entirely within the NGDC-provided DEM; A and B-grids incorporate bathymetry and topography from other DEM datasets available at NCTR. Some smoothing and editing were necessary to eliminate erroneous points or grid features that tend to cause model instability. For example, "point" islands where an isolated grid cell stands above water are eliminated, as are narrow channels or inlets one grid unit wide; these tend to resonate in the numerical solution. Large depth changes between adjacent grid cells can also cause numerical problems; customized tools (such as "bathcorr") are available to correct many of these grid defects. An additional constraint on the bathymetry is the SSL (Elena Tolikova, personal communication), which identifies excessive depth changes in the discrete representation.,

Details of the model grids are provided in Tables 4 and 5. The latter lists the maximum depth, the CFL time step requirement that must not be exceeded, and the actual time steps chosen for the reference and forecast model runs. Since in the current version of MOST, employed by SIFT, the numerical solutions in the three grids proceed simultaneously, there is a requirement that the A and B-grid time steps be integer multiples of the (innermost) C-grid time step in addition to satisfying the appropriate CFL requirement. For both reference and forecast models the CFL requirement of the C-grid was the most stringent. The values chosen are shown in the final column of Table 4 and are such that an integer multiple of each time step (15x for the forecast model; 50x for the reference) is identically 30 seconds, the chosen output time interval for both models. When run on an Intel® Xeon® E5670 2.93GHz processor the forecast model produces four hours of simulation in 9.78 minutes, within the desired 10-minute value for this metric.

3.5 Model Run Input and Output Files

In addition to providing the bathymetry file names and the appropriate time step and A, B grid multiples as provided in the tables above, the designer must provide a number of additional parameters in an input file. These include the Manning Friction Coefficient, a depth threshold to determine when a grid point becomes inundated, and the threshold amplitude at the A-grid boundary that will start the model. An upper limit is specified in order to terminate the run if the wave amplitude grows beyond reasonable expectation. Standard values are used: 0.0009 for the friction coefficient and 0.1m for the inundation threshold. The latter causes the inundation calculation to be avoided for insignificant water encroachments that are probably below the uncertainty in the topographic data. Inundation can, optionally, be ignored in the A and B-grids, as is the norm in the (non-nested) MOST model runs that generate the propagation database. When A and/or B-grid inundation is excluded, water depths less than a specified “minimum offshore depth” are treated as land; in effect a “wall” is placed at the corresponding isobath. When invoked, a value of 5m is applied as the threshold, though A and B inundation is normally permitted as a way to gain some knowledge of tsunami impact beyond the scope of the C-grid domain. Other parameter settings allow decimation of the output in space and/or time. As noted earlier, 30-second output has been the target and output at every spatial node is preferred. These choices avoid aliasing in the output fields that may be suggestive of instability (particularly in graphical output), when none in fact exists.

Finally the input file (supplied in Appendix A) provides options that control the output produced. Output of the three variables: wave amplitude, and the zonal (positive to the east) and meridional (positive to the north) velocity components can be written (in netCDF format) for any combination of the A, B, and C-grids. These files can be very large! A separate file, referred to as a “SIFT” file, contains the time series of wave amplitude at each time step at discrete cells of a selected grid. Normally the time series at a “reference” or “warning point”, typically the location of a tide gage is selected to permit validation in the case of future or historical events. Also output in the SIFT file is the distribution of the overall minimum and maximum wave amplitude and speed in each grid. By contrast with the complete space-time results of a run, the SIFT file (also netCDF) is very compact and, if more than a single grid point is specified, a broader view of the response is provided.

By default two additional output files are generated: a listing file, which summarizes run specifications, progress, and performance in terms of run time. Also included in this file is information to determine the reason, should a run not start or terminate early. Finally a “restart” file is produced so that a run can be resumed, beginning at the time it ended, either normally or by operator intervention.

The input files described above are specific to the model itself. For an actual run, the program must be pointed toward the files that contain the boundary conditions of wave amplitude (HA), and velocity components (UA, VA), to be imposed at the A-grid boundary. Time varying conditions are generally extracted as a subset of a basin-wide propagation solution (either a single unit source or several, individually scaled and linearly combined) that mimic a particular event. These boundary-forcing files typically consist of 24 hours of values (beginning at the time of the earthquake), sampled at 1-minute intervals and available on a 16 arc-minute grid. Occasionally, for more remote seismic sources (or when delayed arrival of secondary waves due to reflections are a concern, as has been seen at Hawaii,) the time span of the propagation run available for forcing is extended beyond one day.

DRAFT

4.0 Results and Discussion

Before proceeding to an extensive suite of model runs, that explore the threat to Marin County from various source regions, the stability of the model is tested in both low and extreme amplitude situations. The former we refer to as “null source” testing: where the boundary forcing is at such a low level (but not precisely zero of course) that the response is expected to be negligible. These tests can be highly valuable in revealing localized instabilities that may result from undesirable features in the discretized bathymetric representation. Inlets or channels that are only one grid cell wide may “ring” or resonate in a non-physical way in the numerical solution. An instability may not grow large enough to cause the model to fail but, in a run with typical tsunami amplitudes, may be masked by actual wave variability.

Forcing by extreme events should also be tested. In addition to the need to test model stability under such circumstances, there is a parameter in the input file that truncates the run if a prescribed threshold is exceeded. For operational use, the threshold must be set high enough so that an extreme event run is not unnecessarily terminated. Both tests should be done for test sources whose waves enter the model domain from different directions since, although stable for one set of incoming waves, an instability may be encountered for another. The “null” and “extreme” case testing of the forecast and reference models is reported in the following subsections. Further evidence of stability is provided by the extensive set of scenarios, aimed at exploring the dependence of impact to source location, described later in the report, and in independent testing by other members of the NCTR team before the model is released for operational use.

4.1 The “Null” Tests

Three null test cases (see Table 6) were run representing sources in the western Aleutians, the Philippines, and south of Japan. Based on sources from the propagation database (Gica et al., 2008), their amplitudes were scaled down by a factor of 10,000 so as to mimic an $M_w=4.8333$ / Slip 0.0001m source rather than the $M_w=7.5$ / Slip 1m standard. A number of grid cells in the B and C grids emerged as potential sources of instability. These were generally minor indentations of the coastline, barely resolved by the grids, or narrow channels. The region contains several inlets (called Esteros) extending far inland that, at a practical level of spatial resolution, proved difficult to accommodate. Among these are the upper reaches of the multiple arms of Drake’s Estero and, feeding into Bodega Bay, Estero Americano and Estero de San Antonio. A limited number of grid cells in the outermost (A) grid required correction. Generally these were associated with non-physical features in the topographic database, such as where a track of ship-based soundings were improperly merged with other data sources. After an iterative process of grid correction and retesting using these “null” sources, both of the reference (RM) and forecast model (FM) grids were deemed satisfactory and the testing of realistic events can begin. Figure 9 illustrates a step in the process where a deficiency in the RM grid generated a mild instability (in the EPSZ B19 micro-tsunami scenario – see Table 6) causing the RM time series at the reference point, initially in close agreement with the FM, to develop unrealistic, high frequency oscillations. Though still

Table 6. Synthetic tsunami events employed in Point Reyes, CA model testing. The RM and FM solutions of those shown in bold text were inter-compared extensively.

Scenario Name	Source Zone	Tsunami Source	α [m]
Mega-tsunami Scenario			
KISZ 1-10	Kamchatka-Yap-Mariana-Izu-Bonin	A1-A10, B1-B10	25
KISZ 22-31	Kamchatka-Yap-Mariana-Izu-Bonin	A22-A31, B22-B31	25
KISZ 32-41	Kamchatka-Yap-Mariana-Izu-Bonin	A32-A41, B32-B41	25
KISZ 56-65	Kamchatka-Yap-Mariana-Izu-Bonin	A56-A65, B56-B65	25
ACSZ 6-15	Aleutian-Alaska-Cascadia	A6-A15, B6-B15	25
ACSZ 16-25	Aleutian-Alaska-Cascadia	A16-A25, B16-B25	25
ACSZ 22-31	Aleutian-Alaska-Cascadia	A22-A31, B22-B31	25
ACSZ 50-59	Aleutian-Alaska-Cascadia	A50-A59, B50-B59	25
ACSZ 56-65	Aleutian-Alaska-Cascadia	A56-A65, B56-B65	25
CSSZ 1-10	Central and South America	A1-A10, B1-B10	25
CSSZ 37-46	Central and South America	A37-A46, B37-B46	25
CSSZ 89-98	Central and South America	A89-B98, B89-B98	25
CSSZ 102-111	Central and South America	A102-A111, B102-B111	25
NTSZ 30-39	New Zealand-Kermadec-Tonga	A30-A39, B30-B39	25
NVSZ 28-37	New Britain-Solomons-Vanuatu	A28-A37, B28-B37	25
MOSZ 1-10	ManusOCB	A1-A10, B1-B10	25
NGSZ 3-12	North New Guinea	A3-A12, B3-B12	25
EPSZ 6-15	East Philippines	A6-A15, B6-B15	25
RNSZ 12-21	Ryukus-Kyushu-Nankai	A12-A21, B12-B21	25
Mw 7.5 Scenario			
NTSZ B36	New Zealand-Kermadec-Tonga	B36	1
Micro-tsunami Scenario			
EPSZ B19	East Philippines	B19	0.01
RNSZ B14	Ryukus-Kyushu-Nankai	B14	0.01
ACSZ B6	Aleutian-Alaska-Cascadia	B6	0.01

generally tracking the FM result, and not growing without bound, the feature could behave erratically in simulating real events. Modification of the RM bathymetry eliminated the problem, as seen in the lower panel, and “null” tests involving other sources (RNSZ B14 and ACSZ B6) did not reveal other issues.

4.2 The Extreme Case Tests

The record of tsunami impact on the northern California coast discussed later reveals that sources around the entire periphery of the Pacific can be felt. Indeed the catastrophic Indian Ocean tsunami of 2004 was detectable at Point Reyes as it was throughout the global ocean. A broad suite of 19 extreme events (so-called mega-tsunamis) whose locations are standard for testing of Pacific basin forecast models, are described in Table 6. Their locations are shown in Figure 10. To simulate each mega-tsunami source, ten A-B pairs of unit sources are used, with an evenly distributed slip of 25m. As described by Gica et al. (2008), each unit source represents a 100x50km area of the fault surface with the long axis parallel to the plate boundary. The B-row is shallowest, sloping from a nominal depth of 5km (unless a depth estimate has been provided by the USGS based on the earthquake catalogs), row-A is deeper, followed by rows Z, Y, X, ... where appropriate. Thus, the extreme case sources represent 1,000 km long ruptures with a width of 100km; the corresponding magnitude is $M_w=9.3$.

Discussion of the entire set in greater detail is provided later in the report, once the validity of the Forecast Model has been established. Here we focus on a subset of three synthetic cases, highlighted in Figure 10 and Table 6, to contrast the Forecast Model (FM) with the more highly resolved Reference Model (RM). In Figures 11-13 the RM results (from the subregion spanned by the FM) are shown in the upper panel. The corresponding FM results in the lower panel employ the same scale. Insets are used to show the time series (black for RM, red for FM) of H, U, and V at the reference point (the Point Reyes tide gage). The lagged correlation of H at the reference point is drawn in the lower inset and illustrates that there is generally only a few minutes lag between the time series with the RM lagging FM. This behavior is repeated in other scenarios illustrated later in the report. It is a general feature of MOST and is due to the tendency of more finely resolved features in the bathymetry slowing the progress of long waves and is discussed further in the context of model validation using observations.

The agreement between the RM and FM results for the three mega-events is good, both for the maximum amplitude and speed distributions, the reference point time series, and the discrete “snapshots” of the amplitude and vector velocity fields. The earliest waves show the best agreement; later in the solution the RM and FM results begin to diverge as multiple reflections with the coastline occur. A qualitative difference between the solutions is often seen along the straight coastline north of Point Reyes Light (see Figures 1 and 2). The straight shoreline, bounded by rocky headlands at the south and north, supports edge waves that appear most noticeably in the RM results almost as a standing wave pattern, but generally do not propagate around the headland and into Drake’s Bay.

It is noticeable that, in all three of the cases shown, the RM tends to oscillate longer and have somewhat larger amplitude than does the FM though the two solutions are in close

agreement for the first few tsunami waves. This is likely a physical reality: the more highly resolved bathymetry and coastline of the RM providing greater scope for non-linear features or reflected waves to develop as, for example, near the rocky headland west of Bodega Bay. This observation suggests a caveat to operational use of the FM: while accurate portrayal of the early history of an event is to be expected, the duration of the event and the amplitude of later waves may be under-estimated. Tide gage data will be needed to verify this conjecture, which is pursued later in the report.

The snapshot comparisons in the lower panels of Figures 11-12 are quite reasonable, illustrating that the solutions match not just at the reference point. It is worth noting too that, although the ACSZ 56-65 mega-event represents a massive Cascadia tsunami, the scale of the impact to the Point Reyes area (~ 3m) is not substantially greater than from trans-Pacific locations (KISZ 01-10 off Kamchatka and NTSZ 30-39 near Samoa.) The Crescent City response to the same synthetic Cascadia mega-event exceeds 10m (Arcas and Uslu, 2010). It would appear that the energy propagated along shore to the south, perhaps due to sheltering by Cape Mendocino, is reduced and that perhaps the greatest impact to Marin County may be associated with source regions elsewhere in the Pacific basin.

In Figure 13 the comparison time was intentionally chosen later in the event as a counterexample. While the reference point amplitudes and nearby fields the FM and RM may be in reasonable agreement, the broader wave patterns may have substantial phase differences. The comparisons in these lower panels is restricted to the portion of C-grid area common to both models, There is a suggestion that the near shore velocity fields at the north and south FM boundaries differ somewhat from the RM for which these are internal points.

Before proceeding to validate the model with historical events, one other synthetic event is usual in the testing protocol: a mild source of magnitude 7.5 at a remote location. A single unit source near Samoa (NTSZ-B36) is employed and its representation by the RM and FM are compared in Figure 14. Such an event results in a response of about 4cm in Point Reyes sea level and again there is excellent agreement between both model representations in the earlier portion of the event.

The results presented above, for a variety of synthetic events, suggest that the RM and FM versions of the model are in good agreement. The match is particularly good in the early stages of a wave train; later, as reflections and other interactions with the coastline occur, the solutions may diverge. The next task is to ascertain whether the models reflect observations from actual tsunami events. Given the manner in which the MOST model is forced, at its boundary (with wave amplitudes and currents not available in real observations), it is not possible to validate the model independently. Rather, as described earlier in Section 2.2, the validation will rely on the results of an external model, based perhaps on DART observations or on a description of the tsunami source in the literature. As a result, the success of the model in replicating observations within its domain is in part dependent on the adequacy of the forcing employed to represent the actual external wave field. For historical events preceding the DART array, the unit source representations are based on seismic observations or coastal tide gage data. Past experience suggests that, in the far field at least, the propagation solution is not overly

sensitive to variation in the unit source weights. Nonetheless, imperfections in forecast model predictions of coastal observations will not necessarily indicate a defect in the model itself. Neither are the tide-gage observations, available for comparison with model prediction, perfect. They may include noise from wind wave activity, possibly amplified by harbor resonances.

4.3 Model Validation : The Honshu-2011 Tsunami

In addition to its disastrous impact on the coast of Japan, the Honshu tsunami of March 11, 2011 radiated waves throughout the Pacific Basin. Those arriving at nearby DART's were of unprecedented amplitude and their signal/noise ratios facilitated accurate and early source characterization. Further afield, the waves were detectable at all operational DART's in the basin and, while major damage was mainly confined to Japan, significant signals were obtained at multiple coastal tide gages. Prior to this event, the Kuril-2006 tsunami event was the best available for model validation. For the U.S. West Coast at least, that role has now been taken by Honshu-2011. The adequacy of the composite propagation solution can be assessed by comparison with the BPR signals from the West Coast DART's. An additional BPR record is available for this purpose: the MARS cabled observatory in Monterey Canyon has, since July 2010, had a pair of bottom pressure sensors at a depth of about 870 meters. One is a standard BPR, reporting at the standard DART 15-second recording interval. The other is an experimental sensor – the “Nano” (Paros et al., 2011) sampling at 40Hz with enhanced sensitivity. For this report we employ only data from the standard BPR.

The locations of the West Coast BPR's, reporting during Honshu-2011, are shown in Figure 15. To the left of the locator chart, the actual and propagation model results interpolated to the BPR locations are compared. There is clearly a strong agreement but, even for the earliest waves, there are two points of difference. Firstly the model “waves” arrive about 8 minutes early, a difference that is small compared to the several hours of transit time. Early arrival by the model is typical and is associated with the limited resolution of the basin-wide bathymetry. Finer-scale features in the actual bathymetry slow down the real wave trains. The other feature of the model vs. observation comparison is that the model underestimates the observed signal by about 20% at all locations. In the right-hand panel, the lagged and scaled-up versions of the model time series are seen to be in excellent agreement with observation. Since these results are likely the best obtainable with the current state of the DART array and inversion methodology, less than perfect agreement between forecast model and observations is not necessarily indicative of a major defect in the FM itself.

With that caveat, we proceed with the model validation. The prime location for this purpose is the Point Reyes tide gage itself. However within the forecast system, predictions from elsewhere in the model domain are employed to enhance the “coastal forecast”. In its basic form, the “coastal forecast”, at selected locations around the basin, is generated by extrapolating offshore values from the propagation solution to the coast using Green's Law. Based on simple assumptions this law indicates that the waves should grow in inverse proportion to the one-fourth power of the depth ratio. The assumption is crude at best and it makes sense that, when a forecast model has been run, the predictions within its domain are likely to be superior to the Green's Law equivalent. For the Point

Reyes model, tide gage observations are available at several points within the domain and, in the case of Honshu-2011 all of these had detectable signals. The auxiliary sites are Bolinas, lying within the C-grid but within the lagoon and with only 6-minute sampling; San Francisco, Alameda, and Richmond within San Francisco Bay and the model B-grid and with 1-minute sampling; Arena Cove, near the northern bound of the FM A-grid and also with 1-minute sampling. The results of the comparison may be seen in Figure 16a,b where the RM (black) and FM (red) versions of the model response are compared to the observations (drawn in green.) The model curves have been lagged to facilitate the comparison but the amplitudes have not been altered. For the first six hours of the event, the agreement is quite gratifying, particularly at Point Reyes itself and at San Francisco. For Arena Cove the agreement is limited more to the early waves; perhaps as a result of resonance associated with Cove geometry, the observed response grows and shifts to a higher frequency than appears in the model signals. The RM solution is a better match in amplitude to the observations from Arena Cove than is the FM whose representation of the geometry is quite coarse.

For Alameda and Richmond, progressing deeper into San Francisco Bay, the match between the models themselves and with the observations, is degraded compared with the better agreement near the entrance. Nonetheless the agreement is quite good and shows promise for an improved “coastal forecast” usage of FM results. Least satisfying, but understandable, is the comparison at Bolinas. The tide gage there lies within the mouth of the lagoon and an adequate representation of the narrow entrance channel is difficult, particularly in the FM. As is common with narrow-mouthed entrances to enclosed regions, there is a tendency for the model to retain water within and clearly (the red curve) the lagoon increasingly does not empty during the “ebb” phase of the tsunami wave train. The RM solution, perhaps as a result of excessive modifications of inaccurate representation of entrance geometry in the DEM, seems to resonate far more than the observational record. It is possible however that, with its 6-minute sampling and placement, the Bolinas tide gage is not well suited to tsunami detection. On a positive note, the timing and amplitude are not grossly dissimilar to the data. The purpose of the FM is more to predict the impact on the seaward side of the Stinson Beach spit and, based on the success at San Francisco, forecasts outside constricted regions of the model domain are likely to be quite useful for warning purposes.

We now step back in order to verify the agreement between the RM and FM solutions throughout the common portion of the C-grid domain. In Figure 17, as was done for the purely synthetic scenarios, the solutions are compared based on their maximum amplitude and speed fields, and the time series and lagged correlation at the Point Reyes tide gage site. The distribution patterns of the maximum fields are comparable and, based on the Point Reyes time series sample, it is not unexpected that the RM should be the greater with the mismatch coming perhaps for the later waves. A point wise (zero lag) correlation distribution (not shown), between RM and FM throughout the FM C-grid domain, indicates that the over 60% of the variance is explained except in constricted areas. The lagged correlation inset confirms a phase difference of only a few minutes between the RM and FM time series at the tide gage. As a further means of comparing the RM and FM solutions, snapshots of the amplitude and velocity fields are also provided in Figure 17. For both the RM (upper panel) and FM (lower panel) a common scale is used. The agreement is particularly close when the comparison time (indicated by

the green line) is close to the first peak's arrival at the tide gage. Two later sample times are shown in Figures 17d,e illustrating that phase differences can increase.

The analysis of the Honshu-2011 in the Point Reyes model is concluded with an examination of the pattern of inundation in Figure 18. For this purpose the full RM C-grid domain is drawn. The model suggests that, had the waves arrived at or above mean high water (MHW), both the Limantour Spit and much of Stinson Beach and the low-lying parts of Bolinas may have been inundated. In fact, as illustrated in the inset based on the observed water level at the Point Reyes tide gage, the waves barely attained MHW. Though the reporting of the impact on the U.S. may have been somewhat muted, given the gravity of the imagery from Japan, it appears that on the U.S. West Coast the main evidence of the tsunami was in excessive currents, notably at Santa Cruz and Crescent City. As designed, with model sea level set at MHW, the forecast erred on the side of conservatism. In the northern portion of the RM domain (excluded in the FM C-grid) the greatest response was predicted with inundation of the Doran Beach spit and the Dillon Beach/Lawson's Landing area at the north and south ends of Bodega Bay. Although in reality no actual inundation occurred due to the state of the tide, a video clips posted online document strong currents beneath the Lawson's Landing pier, and oscillations of 2-3 feet with 20-minute periodicity are reported for Dillon Beach. Examination of the model time series, both RM and FM, from Bodega Bay (not shown) indicate that the northern and southern portions were rising and falling together, so the large amplitudes responsible for the inundation pattern were not associated with the excitation of an alongshore standing wave mode. Also shown in Figure 18 is the CalEMA Inundation Line, based on an ensemble of synthetic mega events scenarios. The MHW-based model prediction does impact, albeit at a lesser level, the regions the CalEMA study identifies as vulnerable.

4.4 Model Validation with other Standard Historical Events

We now proceed to examine how well the RM and FM solutions compare with observation for several other historical cases highlighted in Table 1 and Figure 6. The RM and FM time series are inter-compared at Point Reyes tide gage, Arena Cove, and San Francisco and validated where possible with observation, and the same representations of maximum amplitude, point wise correlation, and snapshots of the RM and FM fields are drawn.

The results, displayed and described below, represent other DART-detected and well-documented recent events: Chile-2010, Samoa-2009, and Kuril-2006, the latter being the first substantial event for which direct observation of the tsunami wave train was available from multiple deep-water DART sites. These events occurred subsequent to the installation the tide gage at Point Reyes. Two pre-DART cases are examined in this section: Alaska-1964 and Unimak-1946 whose large amplitudes caused severe damage to Hawaii and provided the impetus for the establishment of the TWC's. Source characterization for these events is based on the literature, with the source mechanism estimated from the seismic record.

For Chile-2010 the direct comparison of RM and FM is shown in Figure 19 with satisfactory results both in terms of RM-FM intercomparison and agreement with the

observed time series at three locations displayed in Figure 20. The amplitude series match well throughout the six-hour period shown and there is strong point wise correlation throughout the common domain. Comparisons of observations with predictions based on the dedicated forecast models are to be found in the FM reports for Arena Cove (Spillane, 2010) and San Francisco (Uslu et al., 2010) and in post-event reports online at the NCTR website. Excellent agreement is seen for Point Reyes and San Francisco, though the leading wave at Point Reyes is over-estimated and the timing of some later features at San Francisco is less than perfect. The observational record at Arena Cove is noisier, though the amplitude of the first wave is captured well by both models.

For Samoa-2009, the equivalent set of results is shown in Figures 21 and 22. Despite the considerably more complex structure of the maximum amplitude field, the FM pattern is in good agreement with that from the RM and the time series for the first few hours agree well. Later the FM solution appears to decay faster than the RM. Considering the Point Reyes observations in Figure 22, the RM is in better agreement with the amplitude of later waves. At San Francisco the situation is less clear with the RM perhaps overestimating the observed response, while at Arena Cove neither model (as extracted from the A-grid) reproduces the severe ringing evident in the observations.

Figures 23 and 24 represent the Kuril-2006 event. Agreement between the models is strong both for the early and later portions of the record shown. However, in comparisons with observation, the models underestimate later features in the San Francisco observations and, at Arena Cove, the FM response decays far too rapidly. At both locations outside the C-grid, the predicted maxima are less than 50% of what was observed. To summarize these three events, with weaker impacts than Honshu-2011, the accuracy of a revised “coastal forecast” based on the A- and B-grids may be reduced. It remains to be demonstrated whether they are significantly better than those based on Green’s Law.

The Unimak-1946 and Alaska-1964 events were widely felt along the U.S. west coast, though the greatest impact was to the Hawaiian Islands. Reported run-ups associated with Unimak-1946 were 240cm at Arena Cove, 130cm at Bolinas and 256cm at Muir Beach; run-up at San Francisco and Alameda were 26 and 20cm respectively. During the Alaska-1964 event a run-up of 240cm was reported for Drake’s Bay (Point Reyes) with 274cm at Muir Beach and 113cm at San Francisco. Arena Cove and Bodega experienced run-up of 183 and 76cm. were 2.40 and 1.83 meters respectively. The model representations of these major pre-DART events are illustrated in Figures 25-28. In 1946 only the tide gage record for San Francisco is available but shows good agreement with the model-based values. The model time series for Arena Cove are in good agreement but substantially underestimate the reported run-up there, as do the maximum FM amplitudes of 58cm near Bolinas and 96cm at Muir Beach. For the Alaska-1964 event too, only the San Francisco tide gage record is readily available, showing good agreement between model and data. At Point Reyes the model intercomparison is good but while the FM and RM representations of the leading wave match closely, the FM decays more rapidly for later waves. Maximum amplitudes from the sites of reported run-up are 217cm at Drake’s Beach, 173cm at Muir Beach and 116cm at San Francisco. These and the values of 140cm at Arena Cove and 129cm near Bodega are far better with observation than was the case for the Unimak event. Other measures of the intercomparison between FM and

RM: the maximum amplitude and correlation, and the amplitude and velocity fields at a selected comparison time, are good for both events.

4.5 Further Historical Simulations

The above analysis has documented good agreement between the forecast model and the slower running reference version. This permits us to simulate the balance of the historical cases in Table 1, where impacts to the study area have been reported (and the remaining mega-tsunami scenarios) with the forecast model alone. These runs are intended to further validate the stability of the FM but also provide some information on the exposure of the region to tsunamis generated at various points on the periphery of the Pacific.

The quality of the historical events highlighted above is likely to be the result of good characterizations of the source, based on DART observations in the case of recent tsunamis or extensive post-event analysis in the case of the historical examples. In the absence of direct and timely observations, the successes of the forecast models are likely to be much reduced. An extreme case in point is the Sanriku-1896 event, a so-called “tsunami-earthquake” (Dudley and Lee, 1998), causing devastating losses in Japan despite its modest magnitude and scant warning in the form of ground motion. A digitized marigram from Sausalito (across the Golden Gate from San Francisco) is available from the WCATWC archives and is drawn in the lower panel of Figure 29. While the timing is reasonably represented, the amplitude considerably underestimates the reported run-up of 10cm at Sausalito and 20cm at San Francisco. Reports are not available from nearby locations outside the bay, the closest being 150cm at Santa Cruz.

For the Andreanof-1957 event reported run-up of 29cm at Bodega, 26cm at San Francisco and 18cm at Alameda are in reasonable agreement with the model results (35cm, 46cm, and 23cm respectively). No observed time series is available for comparison for this event, nor for East Kuril-1994. For the later only a 4cm run-up, reported at Alameda is available for validation; the maximum model amplitude for Alameda at 2.5cm is in good agreement. For the remaining events in Table 1, Part A time series are available for more thorough validation and are displayed in Figures 30-NN without extensive comment; run-up values where available are added as annotations to the graphics.

Kamchatka-1952 with M_w 8.6 is available as a marigram from San Francisco (Figure 30.) It's amplitude there is well represented by the model, suggesting that a run-up of three meters or more may have occurred at Point Reyes and elsewhere in Marin County. For the Chile-1960 M_w 9.5 event, whose San Francisco marigram was also obtained from the WCATWC archive, the character of the observed response is quite different from the model representation. As seen in Figure 31, the model exceeds the observed amplitude response by a factor of 2-3, and lacks the higher frequency components evident in the observations some hours into the event. The model wave arrived about 20 minutes early. At Alameda, also within San Francisco Bay, the maximum amplitude of the model, at 68cm, is about twice the reported run-up of 31cm. At Stinson Beach the model exaggeration is less severe: 217cm compared to the observed 152cm, but is again large (68cm compared to the observed 25cm) near Bodega.

Figure 32 presents the validation results for the Andeanof-1996 event. At Point Reyes the agreement is quite good and at Alameda the weak model waves seem to capture some of the features of the observed series. At Arena Cove however the signal is far too weak to be visible against the high noise background. For the Peru-2001 (Figure 33) and Hokkaido-2003 (Figure 34) events the validation is quite satisfactory, but for the winter Rat Island-2003 event, as seen in Figure 35, there is considerable noise at the validation sites, limiting the visibility of signals as weak as the model predicts. This event is however notable in that, aided by direct observations of BPR, from pre-cursors to the DART array, useful forecasts were provided to inform the Hawaii emergency response. The Tonga-2006 event proved useful for validation of the Point Reyes model, with a strong response, shown in Figure 36, that agrees well with the observations.

The year 2007 brought several events with which to validate the model, beginning with the normal thrust seaward of the Kuril Trench on January 2007. As seen in Figure 37, the model correctly captured the leading trough and amplitude seen at Point Reyes and San Francisco, though at Arena Cove the background noise limits the usefulness of the observations. The Solomon-2007 event (Figure 38) is reasonably satisfactory, though the signal in both the model and the observations is weak. In August an event off Peru (Figure 39) appears to match well the observations at Point Reyes but, at Arena Cove and San Francisco, while the model seems to capture the amplitude and timing of the early waves, the later portion of the event is less satisfactory. The final event to be treated, from the standard suite of Table 1, Part A is the weak winter Chile-2007 event. Not surprisingly, since the forecast amplitudes are very small off California, there is not a lot to be learned from this event displayed in Figure 40.

Several additional events, listed in Table 1, Part B are available for analysis. Of these, the Sanriku-1894 event has been presented earlier, and the Cape Mendocino tsunami of 1992 as the sole, albeit weak, representative of a Cascadia event is described later in the next Section. The remainder, generally weak in terms of their impact and most occurring in winter where the noise background limits the S/N ratio, are not reported other than to state that all ran without difficulty or evidence of instability.

To summarize the analysis of historical events, given above and in subsection 4.6, it would appear that the Arena Cove FM is capable of producing accurate forecasts for this open coast site on the U.S. west coast. Though the actual waves may be difficult to observe accurately at the tide gage during winter storms, the objective of producing credible forecasts of sizeable tsunami impacts appears to have been met.

4.6 The Mendocino Earthquake of April 25, 1992

Of special interest to northern California is the Mendocino earthquake of April 25, 1992. This has the distinction of being the most recent substantial thrust event on the Cascadia subduction zone. While strike-slip events are commonplace offshore in this region, as shown in the upper right panel of Figure 41, it is thrust faults that have the potential to generate significant vertical displacements of the sea floor that cause large tsunamis. The epicenter of the 1992 event was on land to the southeast of the plate triple-junction off Cape Mendocino. Uplift of the order of a meter of a 25km stretch of the nearshore, between Cape Mendocino and Punta Gorda to the south was evident in a die-off of

intertidal organisms, reported by Carver et al., (1994). Presumably extending offshore too, this deformation is not well represented well by either of the southernmost unit sources (ACSZ-A/B65) now available in the propagation database (see Figure 6 where the epicenter is marked by the seismic “beach ball”). A custom source, available from NCTR but not part of the propagation database, is used to model the event for comparison with two digitized marigrams, plotted in the lower panels of Figure 41. These were obtained from the WCATWC archives. The model performs reasonably in representing the leading wave, though the model series had to be delayed by 30 minutes to achieve alignment. This time offset, greater both in actual time units and as a percentage of travel time, than those typically necessary to adjust trans-basin predictions, may be the result of the coarse representation of the near shore bathymetry. Another possible explanation is that this event, described by González et al. (1995), may have generated a train of coastal-trapped edge waves. Traveling slower than normal tsunami waves taking a deep-water route, the edge waves may have resulted in a delayed arrival and an extended duration for the event. This possibility, and the suggestion that the ACSZ source line ought to be extended at least one unit further south, make this an event worth further study. The reference and forecast models for Point Reyes, and others existing or planned for the west coast (Point Reyes, Eureka, Crescent City, etc.), have a major role in ongoing risk assessment studies for Cascadia.

4.7 Simulation of the remaining Synthetic Mega-events

We conclude this section with a summary of other model runs that were made in order to verify its stability, but which provide useful information on the exposure of Point Reyes to potentially hazardous future events within the Pacific. As noted earlier, the sparse instrumental record of actual events needs to be augmented with credible scenarios to permit risk assessment. While not pretending to be a full-blown risk assessment for the Point Reyes and southwest Marin County area, the full set of mega-tsunamis modeled during stability testing can provide some early estimates.

Results for the set of 19 mega-tsunamis, based on the FM are presented in Figure 42. Each source is a composite of 10 unit sources from the A and B rows with an evenly distributed slip representing an M_w 9.3 event. A color-coded square, drawn at the geometric center of each synthetic source, is used to represent the impact at Point Reyes resulting from that source. The measure of impact employed in Figure 42 is the maximum amplitude of the predicted time series at the reference point. There is not any simple relationship apparent between source orientation, location, or great circle distance to Point Reyes; focusing associated with seafloor features can more than compensate for the decay associated with geometric spreading. It is notable that the greatest impact at Point Reyes comes from trans-basin sources, rather than from those representing Cascadia. The latter apparently beam most of their energy directly onshore or offshore into the open ocean; arrows normal to the plate boundary are used in Figure 42 as an approximate indicator of main beam direction.

Further results from the suite of mega-event scenarios are presented in Table 7. Seven sites within the C and B-grids of the FM are represented; the first being Point Reyes tide gage that was illustrated graphically in Figure 42. Limatour Beach is a well-visited recreational site within the PRNS; Stinson Beach, adjacent to Bolinas, and Muir Beach

Table 7. Mega-tsunami scenario impacts, represented by flooding (km² in the sub-region 123.1:122.5W, 37.8:38.1N) and maximum amplitude (cm) at several sites within the model domain (identified in the footnote). The maxima are highlighted and ranked.

Scenario (km)	Flooding		Impact Sites							Amp. Rank
	Area		PTR ¹	LIM ²	STN ³	MUR ⁴	DOR ⁵	LAW ⁶	SFO ⁷	
AC 56-65 (688)	5.18	7	159	152	160	182	201	224	115	13
AC 50-59 (1278)	4.72	11	202	106	217	373	194	193	203	4
CS 1-10 (2994)	1.18	18	99	69	64	72	48	52	37	18
AC 22-31 (3277)	6.34	4	239	221	288	227	251	333	150	6
AC 16-25 (3731)	4.97	8	266	121	234	275	162	194	102	8
AC 6-15 (4731)	2.55	17	134	87	117	136	118	120	81	17
KI 1-10 (5856)	4.93	10	354	152	184	245	144	189	90	6
CS 37-46 (6070)	0	19	42	36	38	35	37	38	25	19
KI 22-31 (7724)	4.24	12	251	129	170	231	212	182	74	11
NT 30-39 (8054)	7.00	2	402	226	263	277	239	309	127	3
KI 32-41 (8368)	6.39	3	318	169	288	502	361	440	159	2
RN 12-21 (8808)	3.27	15	209	84	115	162	110	121	57	14
KI 56-65 (9429)	3.94	13	166	96	145	233	171	204	87	12
NV 28-37 (9553)	4.96	9	258	131	149	149	173	202	88	10
MO 1-10 (9943)	7.71	1	460	295	324	513	240	277	200	1
CS89-98 (10063)	3.48	14	140	134	102	78	102	136	43	16
NG 3-12 (10801)	3.15	16	162	107	143	145	133	131	104	15
EP 6-15 (10932)	6.31	5	246	160	264	296	211	235	137	7
CS102-11(11010)	3.27	6	265	132	156	193	157	172	77	9
	Overall Max		402	295	324	513	361	440	203	

C-Grid: 1-Point ReyesTG, 2-Limantour Beach, 3-Stinson Beach, 4-Muir Beach,
B-Grid: 5-Doran Spit, 6-Lawson's Landing, 7-San Francisco TG.

are coastal communities between Point Reyes and the southern limit of the FM C-grid at Point Bonita. Doran Beach and Lawson's Landing represent communities within Bodega Bay, which is only represented in the FM B-grid. San Francisco, also in the B-grid, is included owing to the wealth of tsunami records available there. While Point Reyes has the most instances (10) of having the greatest amplitude among the selected sites, for the mega-events treated here, Muir Beach with 7 and the two overall greatest impacts, is clearly threatened; these results are consonant with the large run-up reported at Muir Beach in the historical record. Lawson's Landing too, with the remaining two cases (one representing the southern end of Cascadia, the other the mid-Aleutians, is clearly at risk and given the inundation that might have resulted had the Honshu-2011 waves arrived under adverse tidal condition (Figure 18) and statements by emergency responders in the "Marin Tsunami" video, Bodega Bay warrants a dedicated forecast model, though lacking an instrumented reference point. Given the linear geometry and orientation of Bodega and Tomales Bays Version 4 of MOST, which is not limited to north-south and east-west grid lines, should be well suited.

Finally the set of 19 mega-tsunami scenarios evaluated here is an approximate match to the set employed in the CalEMA study that established an inundation line for California. In Figure 43, an ensemble of the inundation predictions by the Point Reyes FM is compared with the CalEMA result. The FM C-grid cells inundated by one or more of the meta-tsunami scenarios are colored red; the CalEMA inundation line is drawn in blue. (The flooded area, in square kilometers, associated with each scenario is included in Table 7.) As underlying topography Figure 43 uses the RM grid to better indicate coastal indentations. The FM provides a reasonable match in most of the threatened areas, particularly the Limantour Spit and Beach areas and Stinson Beach. In some areas, such as Muir Beach, the reduced resolution of the FM limits the penetration of flooding there. No attempt has been made to adequately represent Tomales Bay in the Forecast Model. Its shallowness and the constrictions at its mouth cannot be adequately represented at the spatial resolution necessitated by the run-time constraints for emergency usage.

5.0 Conclusions

To conclude, good agreement between observations and model predictions for a subset of historical events, including the recent Honshu-2011 tsunami, has been established and the stability of the model for numerous synthetic events has been demonstrated. In particular the reliability of the forecast model, designed to run rapidly in a real time emergency conditions, has been proven by the favorable comparison with reference model predictions, particularly during the early hours of an event. The model will be included in the SIFT system employed operationally at the Tsunami Warning Centers, and will permit the Point Reyes beaches and the communities of Bolinas, Stinson Beach, and Muir Beach to be added to the coastal communities for which forecast capability is available. Additionally it will provide a tool of use in risk assessment studies.

In addition to the scenarios run by the author, and reported here, further tests have been made by other members of the group at NCTR, and will continue to be made by staff at the Warning Centers and others, perhaps in training situations. Among the many related tools developed at NCTR is ComMIT (Community Model Interface for Tsunami, nctr.pmel.noaa.gov/ComMIT/), which provides a highly intuitive graphical environment in which to exercise and explore forecast models for any combination of propagation database unit sources. Were any of these avenues to reveal a problem with the model, its origin (most likely in some quirk of the bathymetric files) would be located and corrected then the revised version re-installed for operational use. The development of the forecast system will be a dynamic process, with new models added (and old ones revisited) from the current list of U.S interests and globally. In the coming years it is expected that further capabilities (for example landslides) will be added as algorithms and methodologies mature.

6. Acknowledgments

Many members of the NCTR GROUP provided valuable assistance in the production of this report. In particular Diego Arcas edited the first draft for content and style. CalEMA and other California entities distribute GIS online dataset used in the graphics. The modeling could not proceed without the detailed DEM produced at NGDC by the painstaking combination of numerous bathymetric and topographic surveys. Digitized marigrams for a number of historic events were acquired from the WCATWC archives. This publication is [partially] funded by the Joint Institute for the Study of the Atmosphere and Ocean (JISAO) under NOAA Cooperative Agreements NA17RJ1232 and NA10OAR4320148, Contribution No. XXXX. It is PMEL Contribution No. NNNN

7. References

- Arcas, D. and B. Uslu (2009): PMEL Tsunami Forecast Series: Vol. 2. A Tsunami Forecast Model for Crescent City, California
- Barberopoulou, A., J. C. Borrero, B. Uslu, M. R. Legg and C. E. Synolakis (2011): A Second Generation of Tsunami Inundation Maps for the State of California. *Pure and Appl. Geophys.* DOI: 10.1007/s00024-011-0293-3
- Carignan, K.S., L.A. Taylor, B.W. Eakins, R.J. Caldwell, D.Z. Friday, P.R. Grothe and E. Lim (2010): Digital Elevation Models of Central California and San Francisco Bay: Procedures, Data Sources and Analysis. www.ngdc.noaa.gov/dem/report/download/1220
- Carver, G.A., A.S. Jayko, D.W. Valentine and W.H. Li (1994): Coastal uplift associated with the 1992 Cape Mendocino earthquake, northern California. *Geology* 22(3), 195-198.
- Dudley, W.C. and Min Lee (1998): Tsunami! University of Hawai'i Press, 362pp.
- Dunbar, P. (2007): Increasing public awareness of natural hazards via the Internet. *Nat. Hazards* 42(3) 529-536, DOI: 10.1007/s11069-006-9072-3
- Gica, E., M. Spillane, V.V. Titov, C.D. Chamberlin, and J.C. Newman (2008): Development of the forecast propagation database for NOAA's Short-term Inundation Forecast for Tsunamis (SIFT). NOAA Tech. Memo. OAR PMEL-139, NTIS: PB2008-109391, 89 pp.
- González, F.I., K. Satake, E.F. Boss and H.O. Mofjeld (1995): Edge wave and non-trapped modes of the 25 April 1992 Cape Mendocino tsunami. *Pure and Appl. Geophys.* 144, 409-426, DOI: 10.1007/BF00874375
- Kanamori, H. and J.J. Ciper (1974): Focal process of the great Chilean earthquake, May 22, 1960. *Phys Earth Planet. In.*, 9, 128-136.
- Lander, J.F., and P.A. Lockridge (1989): United States Tsunamis, 1690 to 1988, Publ. 41-2. National Geophysical Data Center, Boulder, CO, 265 pp.
- Loeffler, Kurt, and Gesell, Justine, editors/cinematographers, 2010, Marin Tsunami: U.S. Geological Survey General Information Product 95 (video).
URL: pubs.usgs.gov/gip/95/index.html
- López, A.M., and E.A. Okal (2006): A seismological reassessment of the source of the 1946 Aleutian "tsunami" earthquake. *Geophys. J. Int.*, 165(3), 835-849, doi: 10.1111/j.1365-246x.2006.02899.x.
- Niemi, T.M. and N.T. Hall (1996): Historical Changes in the Tidal Marsh of Tomales

Bay and Olema Creek, Marin County, California. *J. Coastal Res.*, 12(1): 90-102.

- O'Brien, M.P. (1946): Preliminary Report on Seismic Sea Waves from Aleutian Earthquake of April 1, 1946, *Tech. Rep. HE 116207*, Wave Project, Fluid Mechanics Lab., U. Cal. (Berkeley).
- Paros, J., E. Bernard, J. Delaney, C. Meinig, M. Spillane, P. Migliacio, L. Tang, W. Chadwick, T. Schaad, and S. Stalin (2011): Breakthrough underwater technology holds promise for improved local tsunami warnings. Oceans '11 Paper
- Percival, D.B., D. Arcas, D.W. Denbo, M.C. Eble, E. Gica, H.O. Mofjeld, M.C. Spillane, L. Tang, and V.V. Titov (2009): Extracting tsunami source parameters via inversion of DART® buoy data. NOAA Tech. Memo. OAR PMEL-144, 22 pp.
- Spillane, M.C., E. Gica, V.V. Titov, and H.O. Mofjeld (2008): Tsunameter network design for the U.S. DART® arrays in the Pacific and Atlantic Oceans. NOAA Tech. Memo. OAR PMEL-143, 165 pp.
- Spillane, M.C. (2011): Development of a Tsunami Forecast Model for Arena Cove, California. NOAA OAR Special Report, PMEL Tsunami Forecast Series: Vol. , pp.
- Tang, L., C. Chamberlin, E. Tolkova, M. Spillane, V.V. Titov, E.N. Bernard, and H.O. Mofjeld (2006): Assessment of potential tsunami impact for Pearl Harbor, Hawaii. NOAA Tech. Memo. OAR PMEL-131, NTIS: PB2007-100617, 36 pp.
- Tang, L., V.V. Titov, and C.D. Chamberlin (2009): Development, testing, and applications of site-specific tsunami inundation models for real-time forecasting. *J. Geophys. Res.*, 114, C12025, doi: 10.1029/2009JC005476.
- Titov, V., and F.I. González (1997): Implementation and testing of the Method of Splitting Tsunami (MOST) model. NOAA Tech. Memo. ERL PMEL-112, NTIS: PB98-122773, NOAA/Pacific Marine Environmental Laboratory, Seattle, WA, 11 pp.
- Titov, V.V., and C.E. Synolakis (1998): Numerical modeling of tidal wave run-up. *J. Waterw. Port Coast. Ocean Eng.*, 124(4), 157–171.
- Titov, V.V., F.I. González, E.N. Bernard, M.C. Eblé, H.O. Mofjeld, J.C. Newman, and A.J. Venturato (2005): Real-time tsunami forecasting: Challenges and solutions. *Nat. Hazards*, 35(1), Special Issue, U.S. National Tsunami Hazard Mitigation Program, 41–58.
- Uslu, B., D. Arcas, V.V. Titov, and A.J. Venturato (2010): A Tsunami Forecast Model for San Francisco, California. NOAA OAR Special Report, PMEL Tsunami Forecast Series: Vol. 3, 88 pp.
- Wei, Y., E. Bernard, L. Tang, R. Weiss, V. Titov, C. Moore, M. Spillane, M. Hopkins,

and U. Kânođlu (2008): Real-time experimental forecast of the Peruvian tsunami of August 2007 for U.S. coastlines. *Geophys. Res. Lett.*, 35, L04609, doi: 10.1029/2007GL032250.

DRAFT

FIGURES

DRAFT



Figure 1. The Point Reyes area of west and south Marin County, CA.

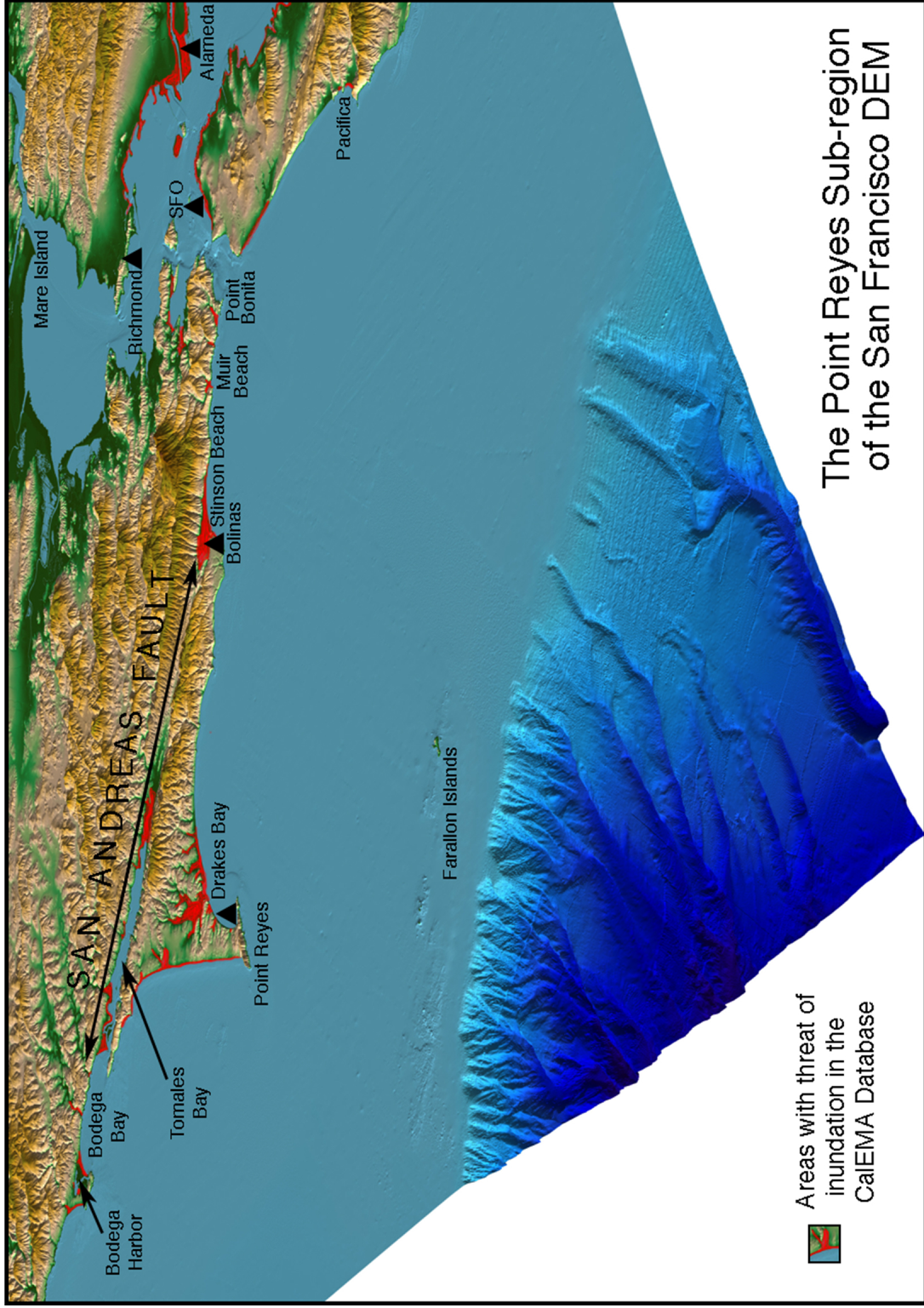


Figure 2. Extract from the oblique 3-D view of the San Francisco DEM provided by NGDC. The focus is Point Reyes; areas of potential inundation identified by CalEMA are highlighted in red.



Figure 3. View of the Point Reyes headland and Drake's Bay in its lee.

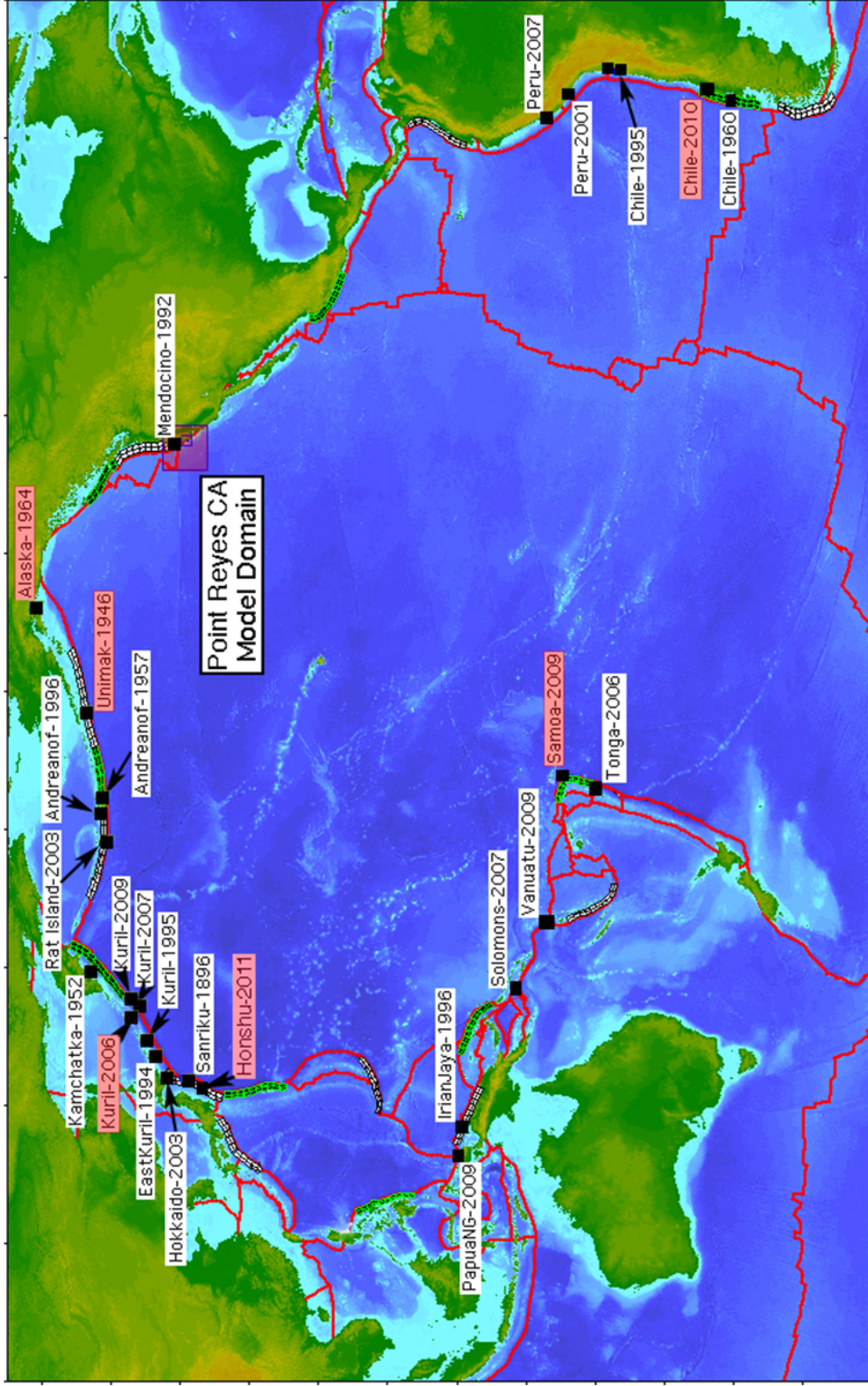


Figure 4. Distribution of the historical tsunami sources employed for the development of the Point Reyes forecast model. Those highlighted in red are more extensively investigated using the reference model.

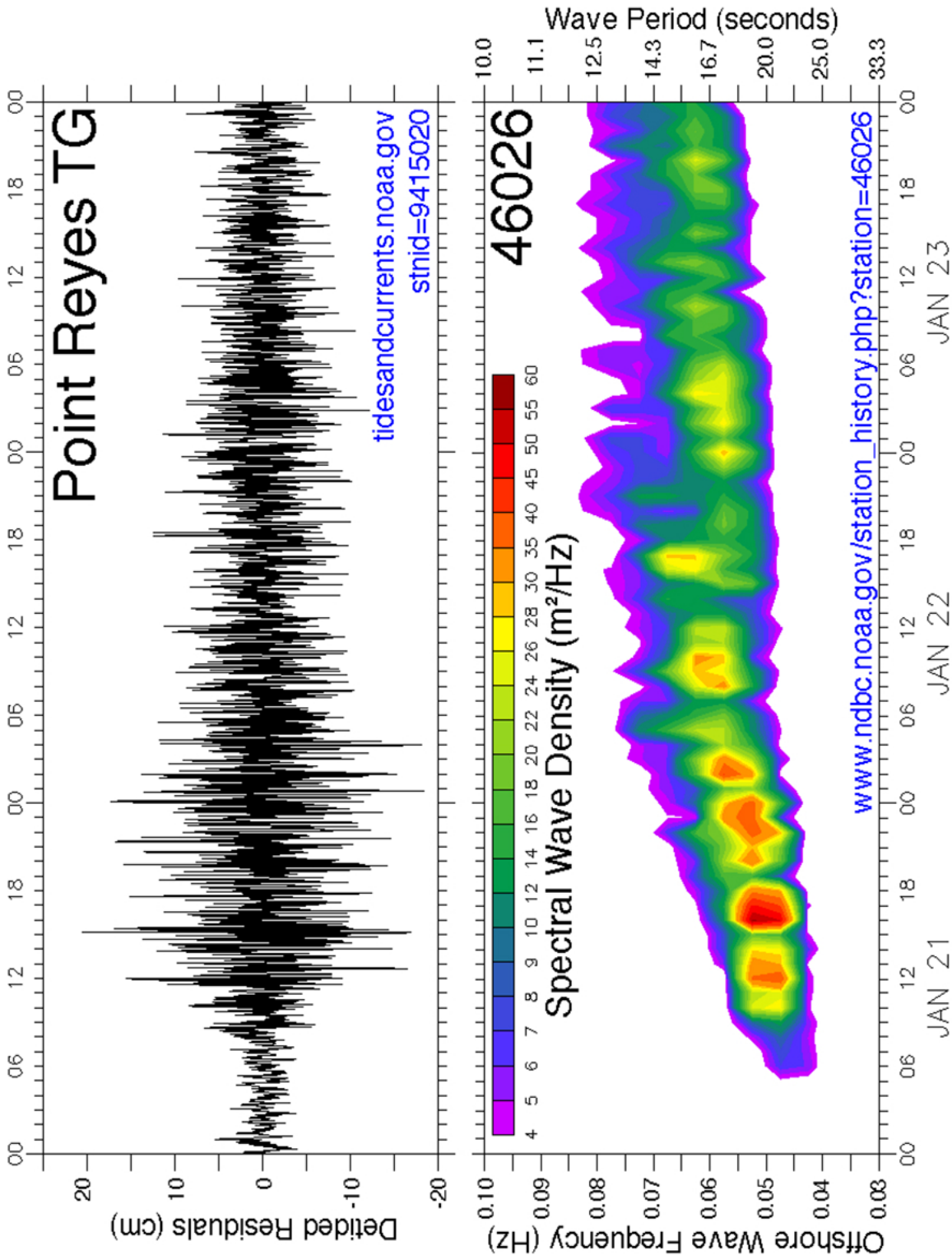


Figure 5. A sample time interval from the Point Reyes tsunami-capable tide gage, unrelated to tsunami activity. The evolving surface wave spectrum is shown in the lower panel.

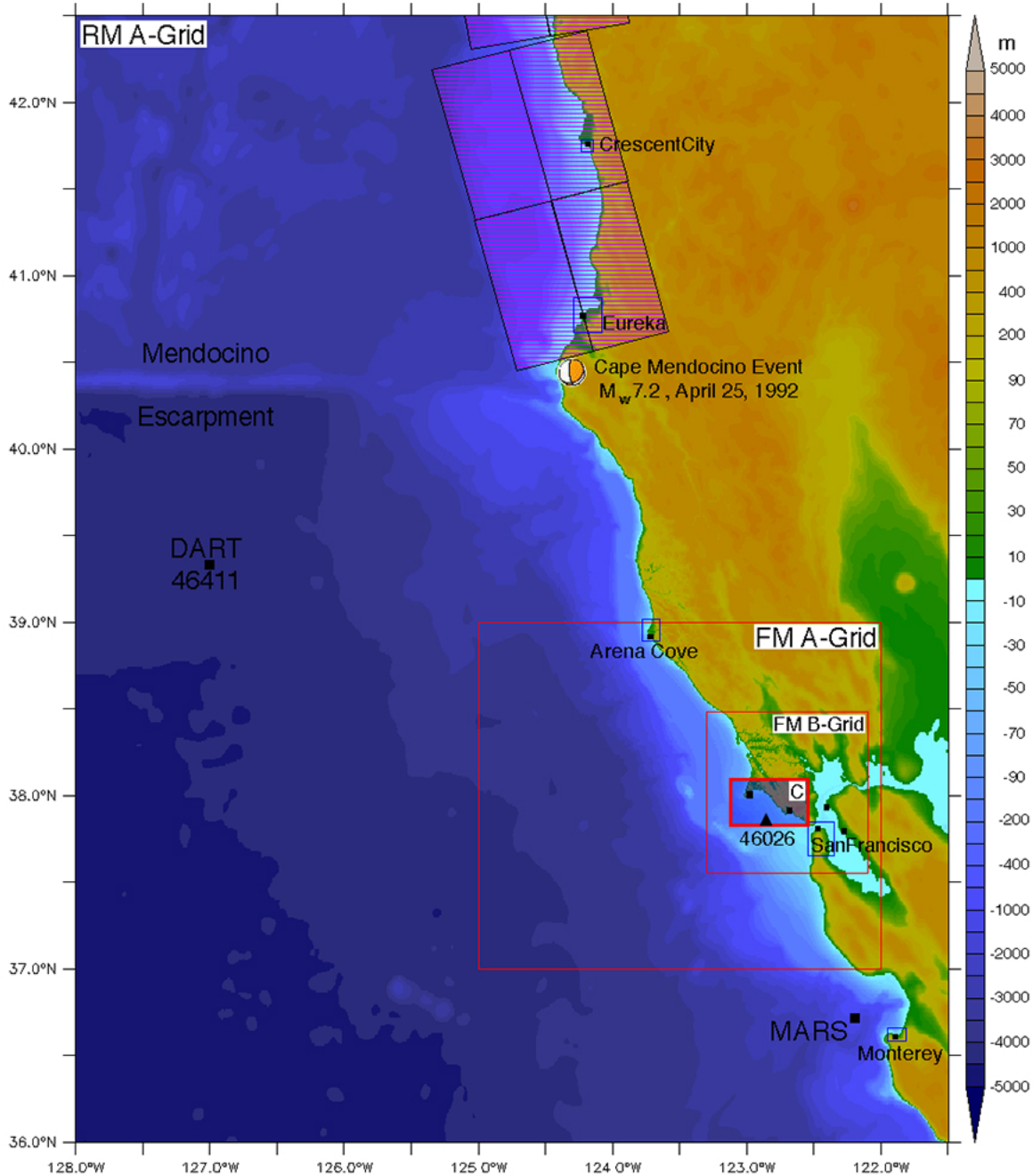


Figure 6. The setting of Point Reyes and its nested FM grids. The C-grids of other west coast forecast models are marked, as are various sites with data available for this study. The closest unit sources of the propagation database lie north of Cape Mendocino, and the epicenter of the most recent Cascadia thrust event is marked.

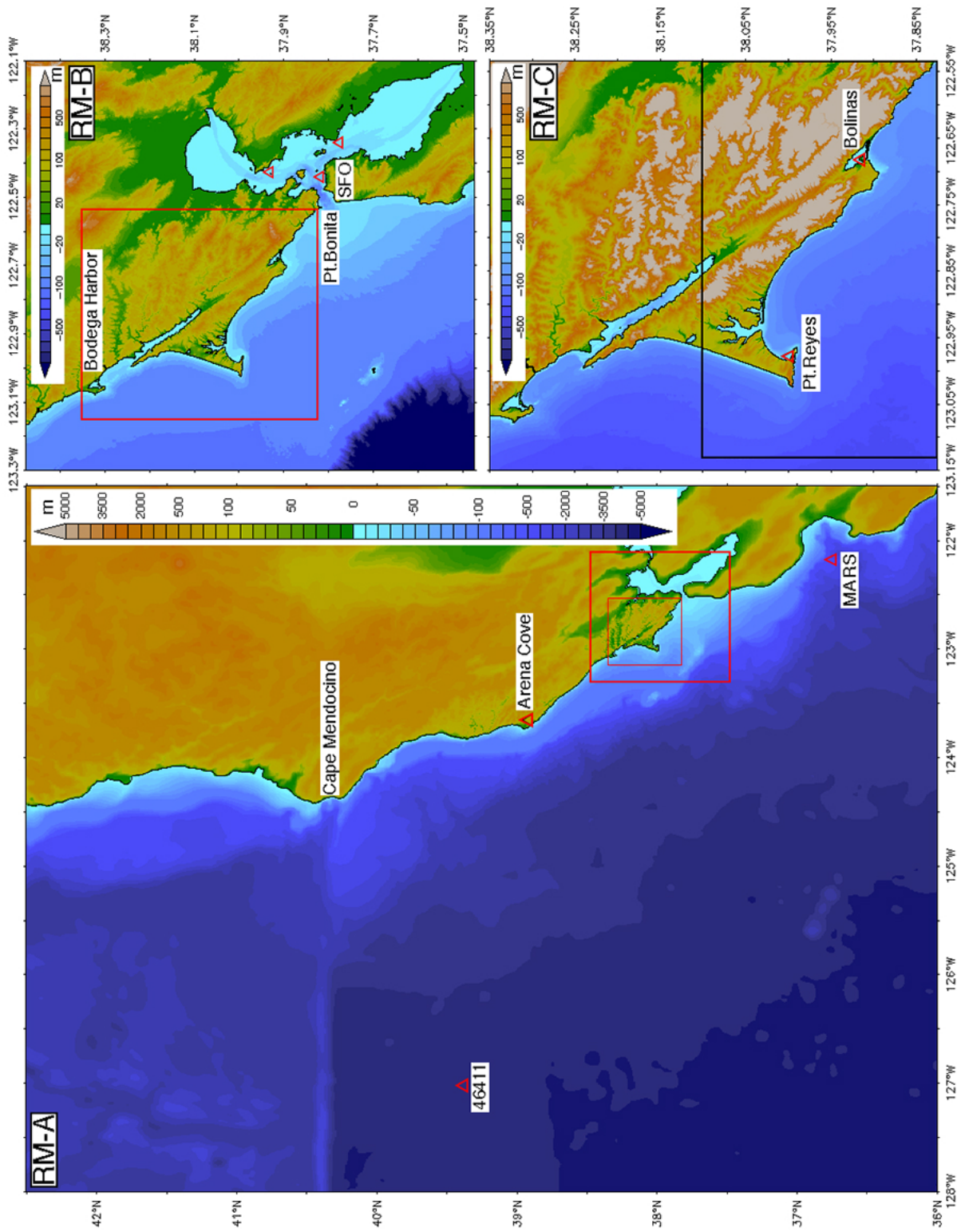


Figure 7. Nested grid representation for the Reference Model (RM).

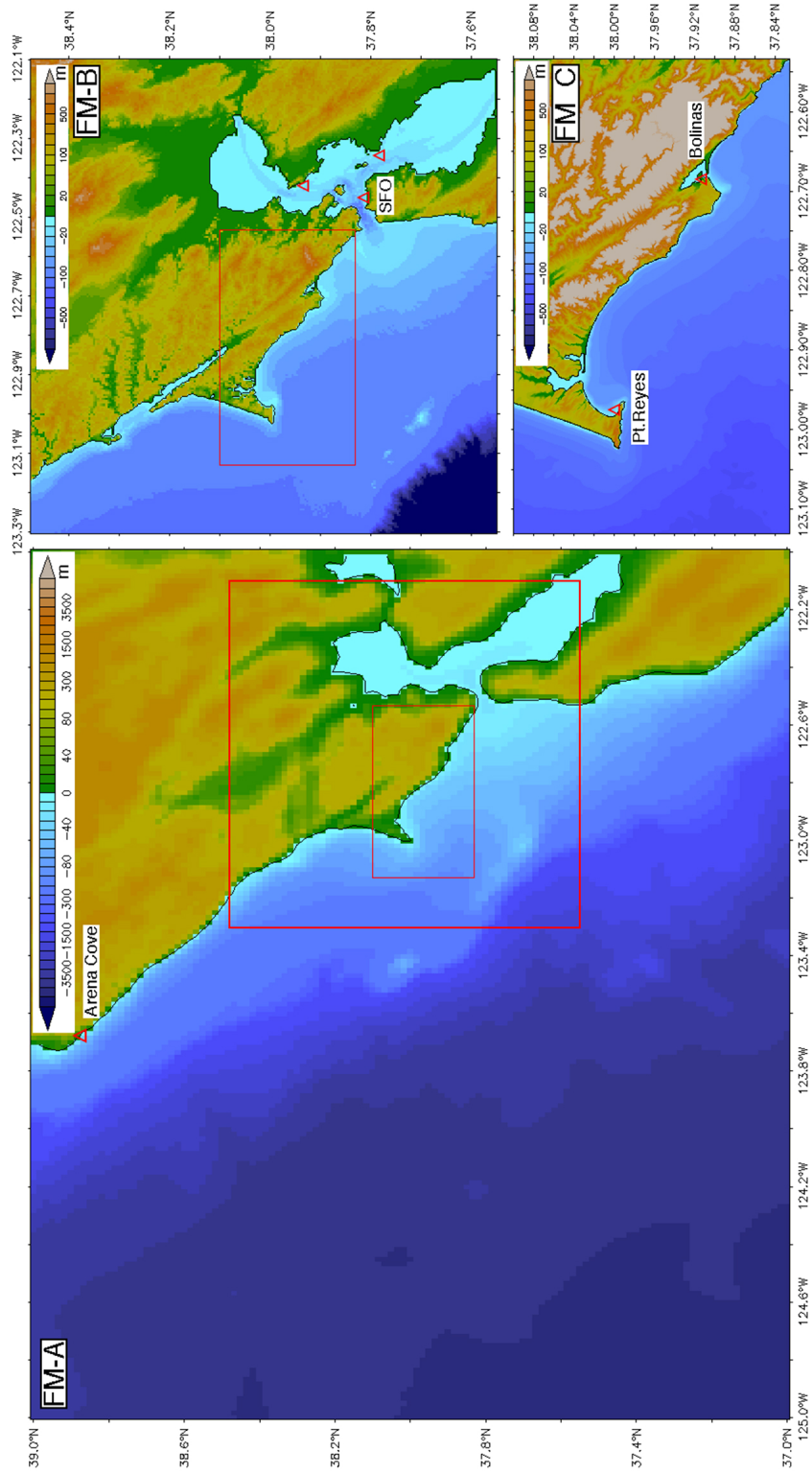


Figure 8. Nested grid representation for the Forecast Model (FM).

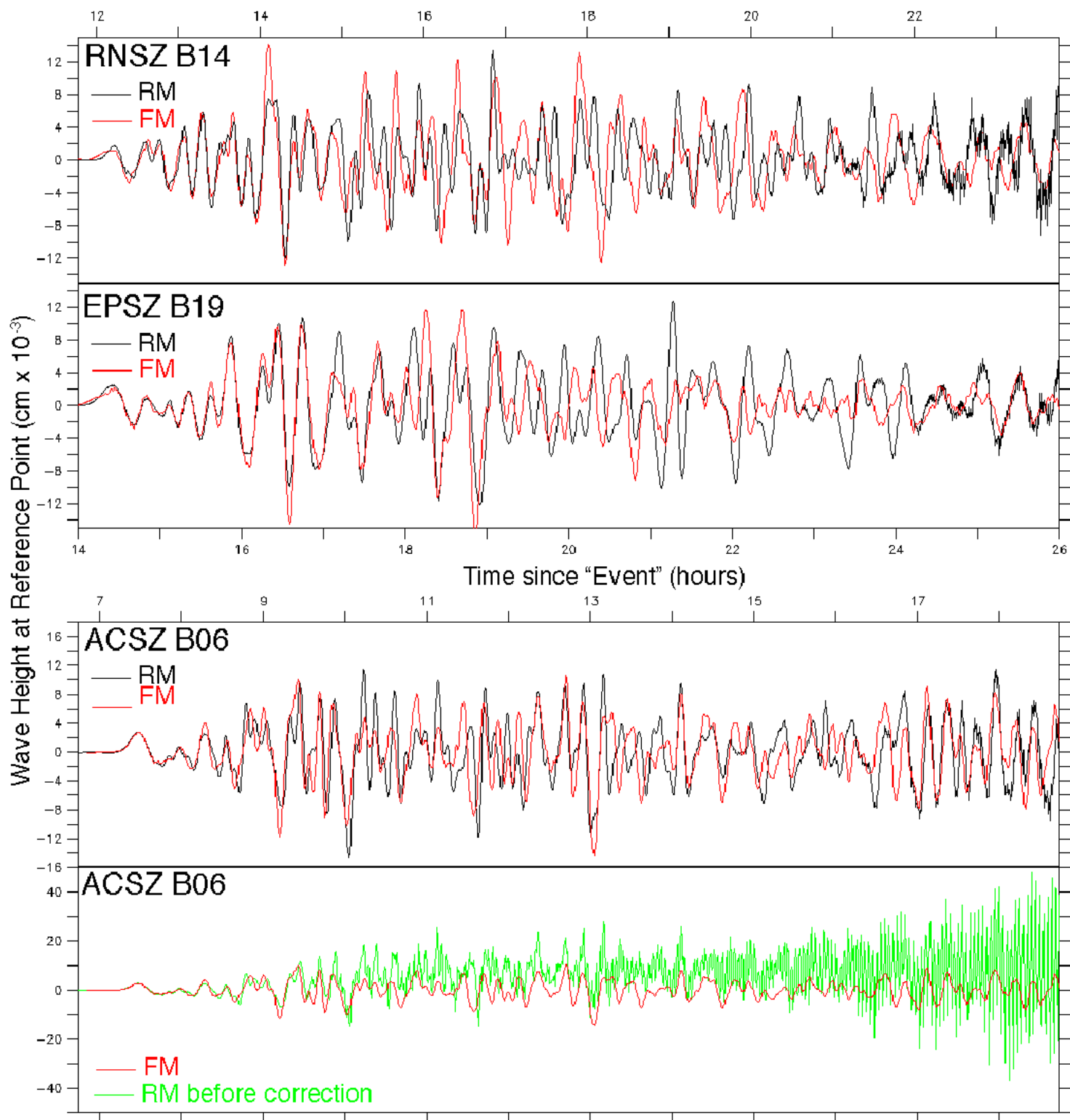


Figure 9. Comparison of the RM and FM time series at the reference point for three "Null" sources in the Western Pacific. The lowest panel illustrates the appearance of model instability before the RM C-grid bathymetry was finalized.

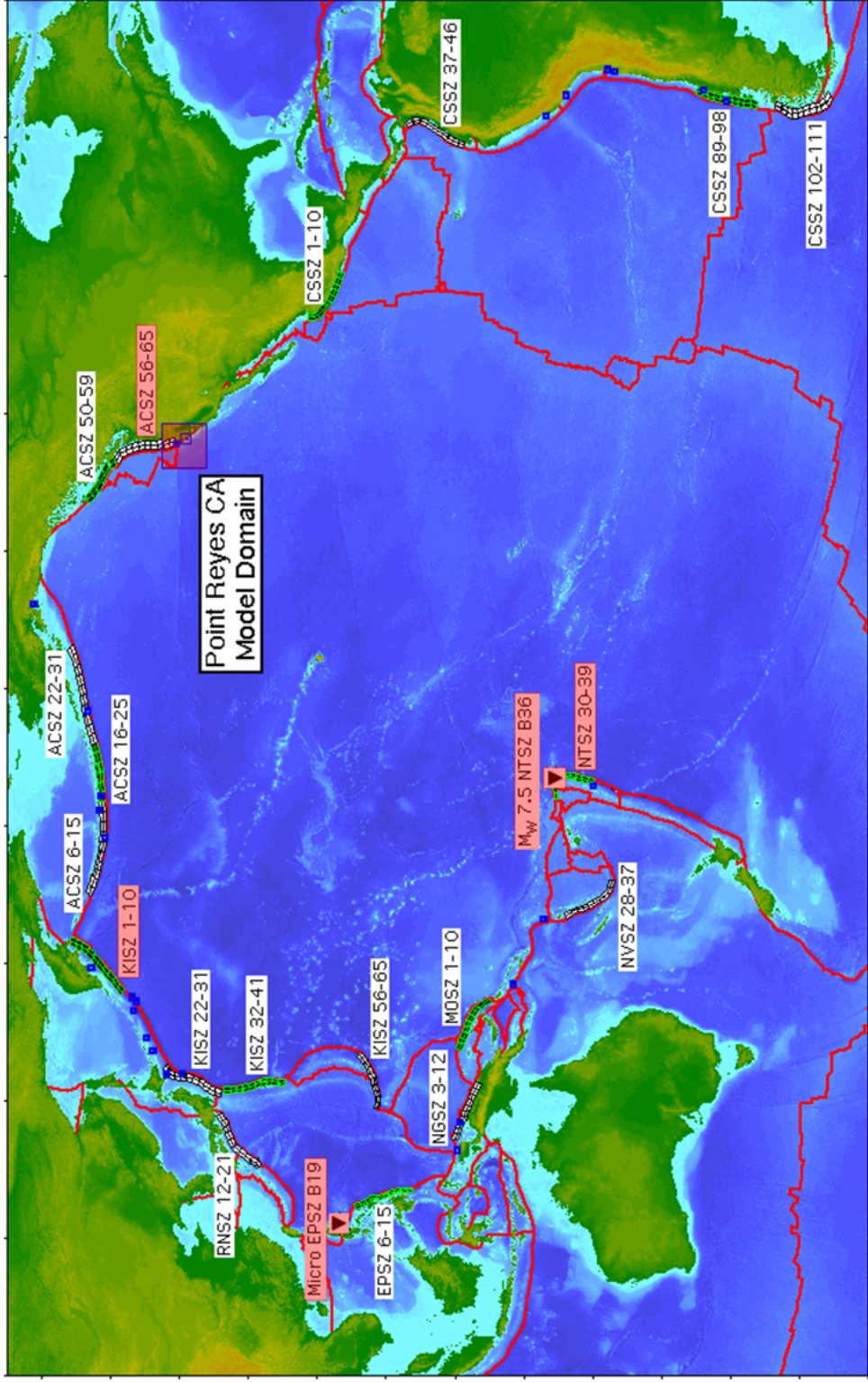


Figure 10. Locations of synthetic tsunami scenarios employed in model development.

ACSZ 56-65

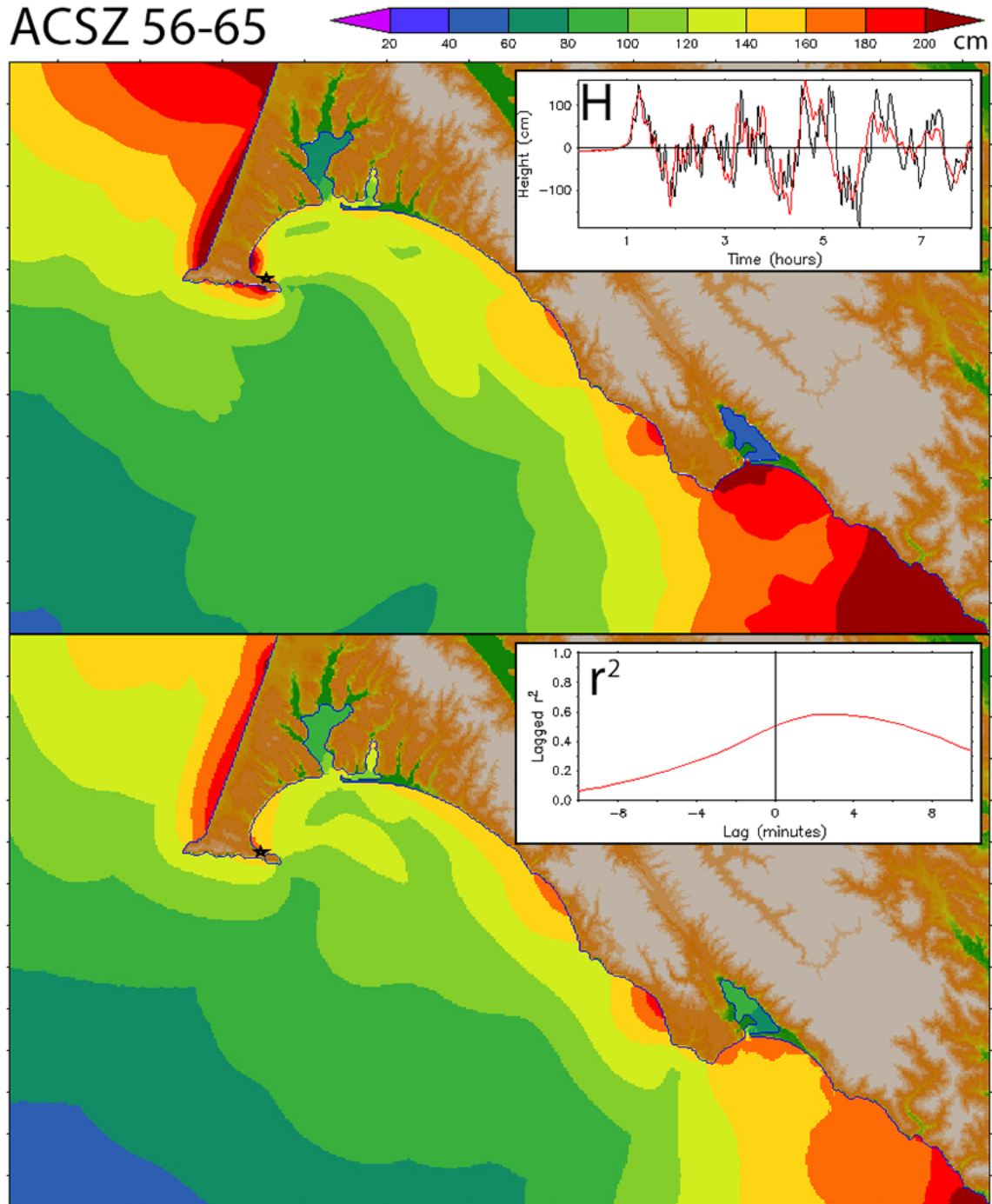


Figure 11. Comparison of Reference (RM) and Forecast (FM) model results for the ACSZ 56-65 synthetic mega-event, representing the Cascadia Subduction Zone. a) Maximum amplitude from the RM (upper panel), the FM (lower panel), time series at the Point Reyes tide gage (upper panel inset: black for RM, red for FM). The lagged correlation at the TG (lower inset) shows that there is only a few minutes difference in the model arrival times.

ACSZ 56-65

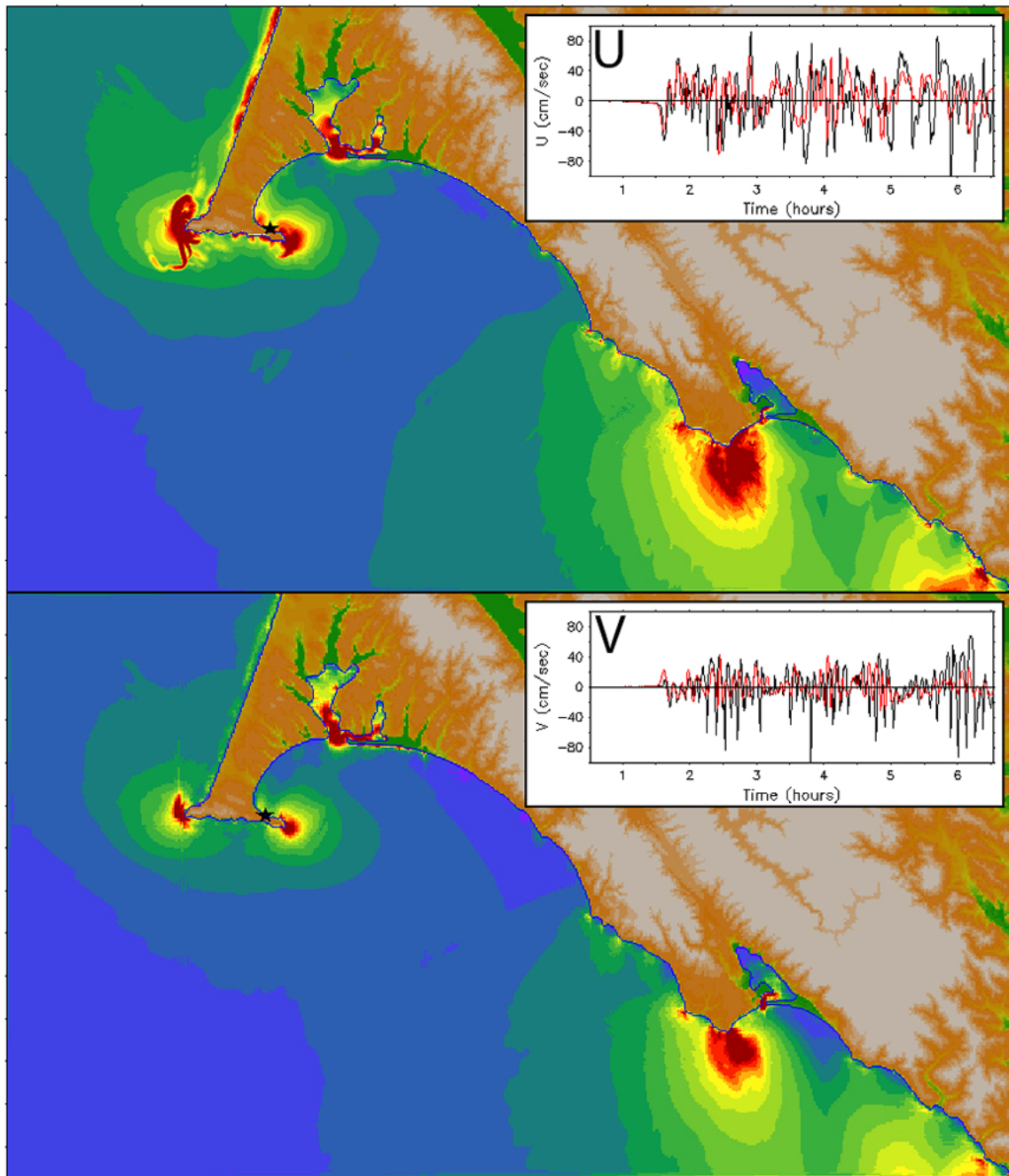


Figure 11 continued. . b) Comparison of maximum speed from the Reference Model (upper panel) and Forecast Model (lower panel). Inset panels compare the time series of the velocity components at the TG.

ACSZ 56-65

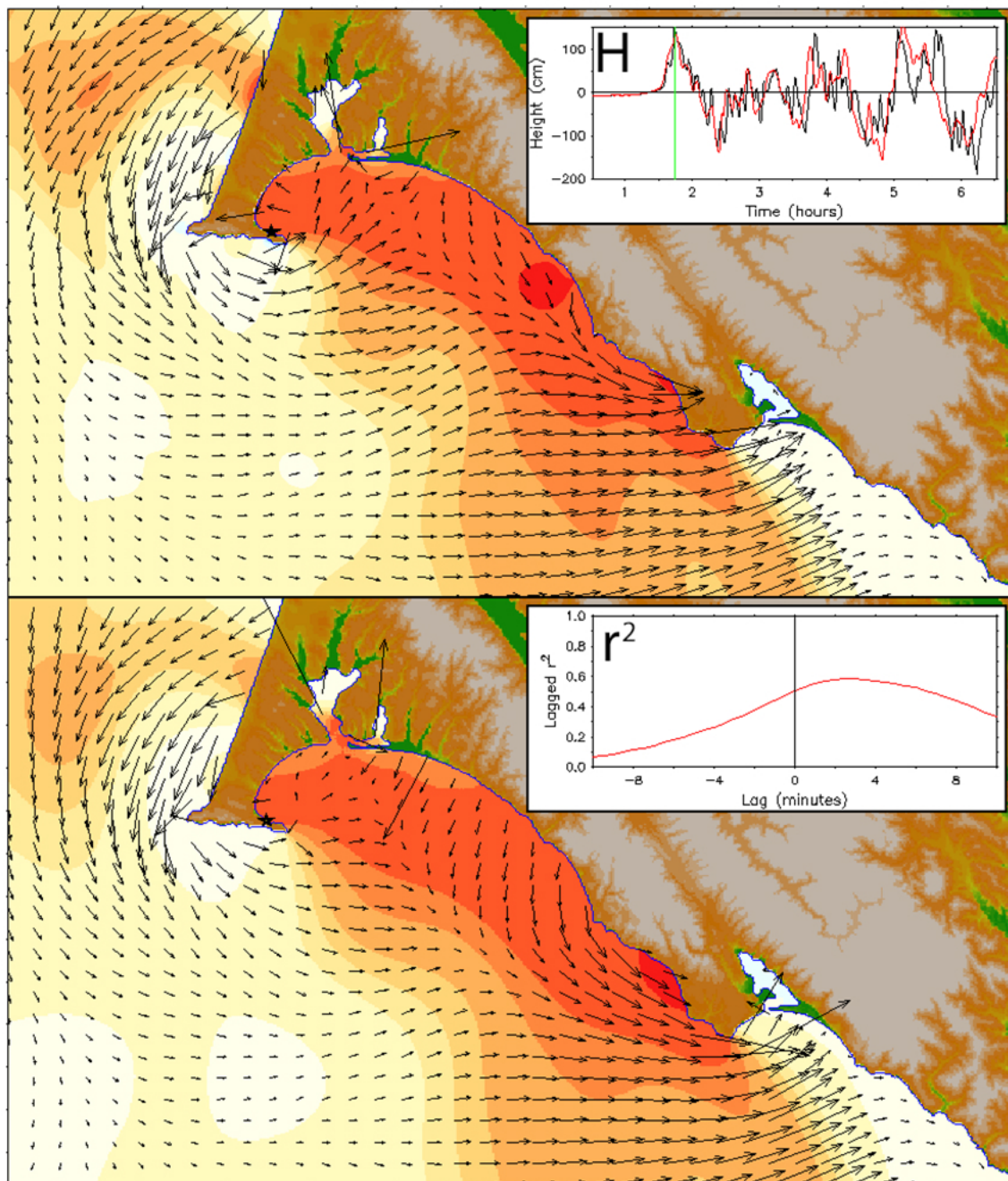
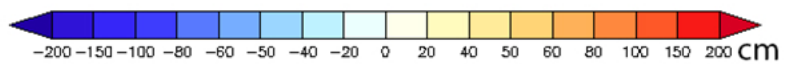


Figure 11 continued. c) Comparison of the amplitude and vector current fields at the time indicated by the green line in the upper inset panel.

ACSZ 56-65

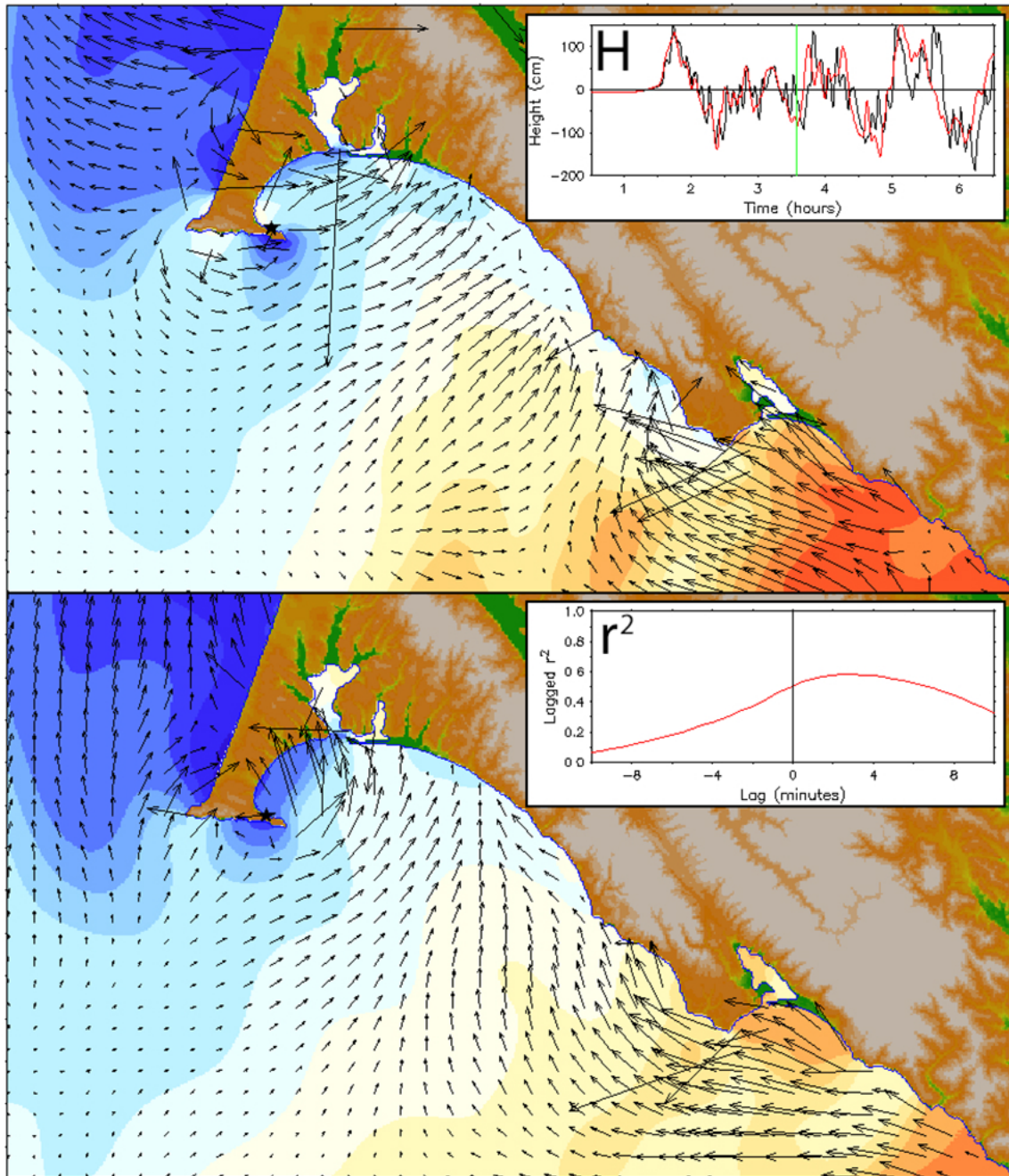
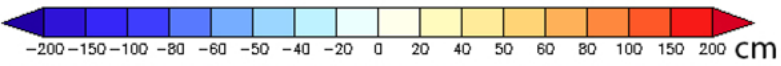


Figure 11 continued. d) As for c) but at a later time in the model runs.

KISZ 01-10

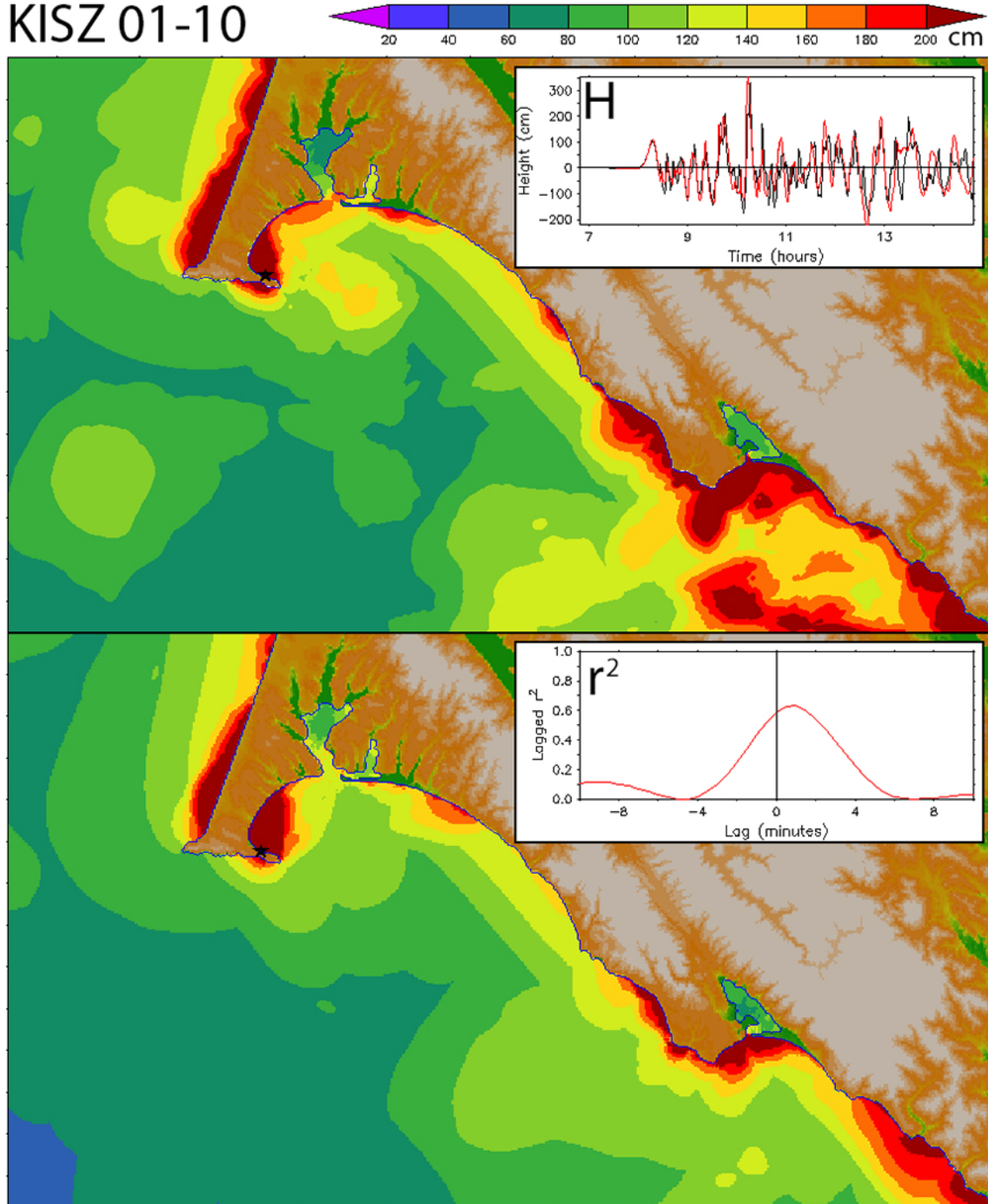


Figure 12. As in Figure 11, but for the KISZ 01-10 scenario representing Kamchatka.
a) Maximum amplitude for RM (upper panel) and FM (lower panel).

KISZ 01-10

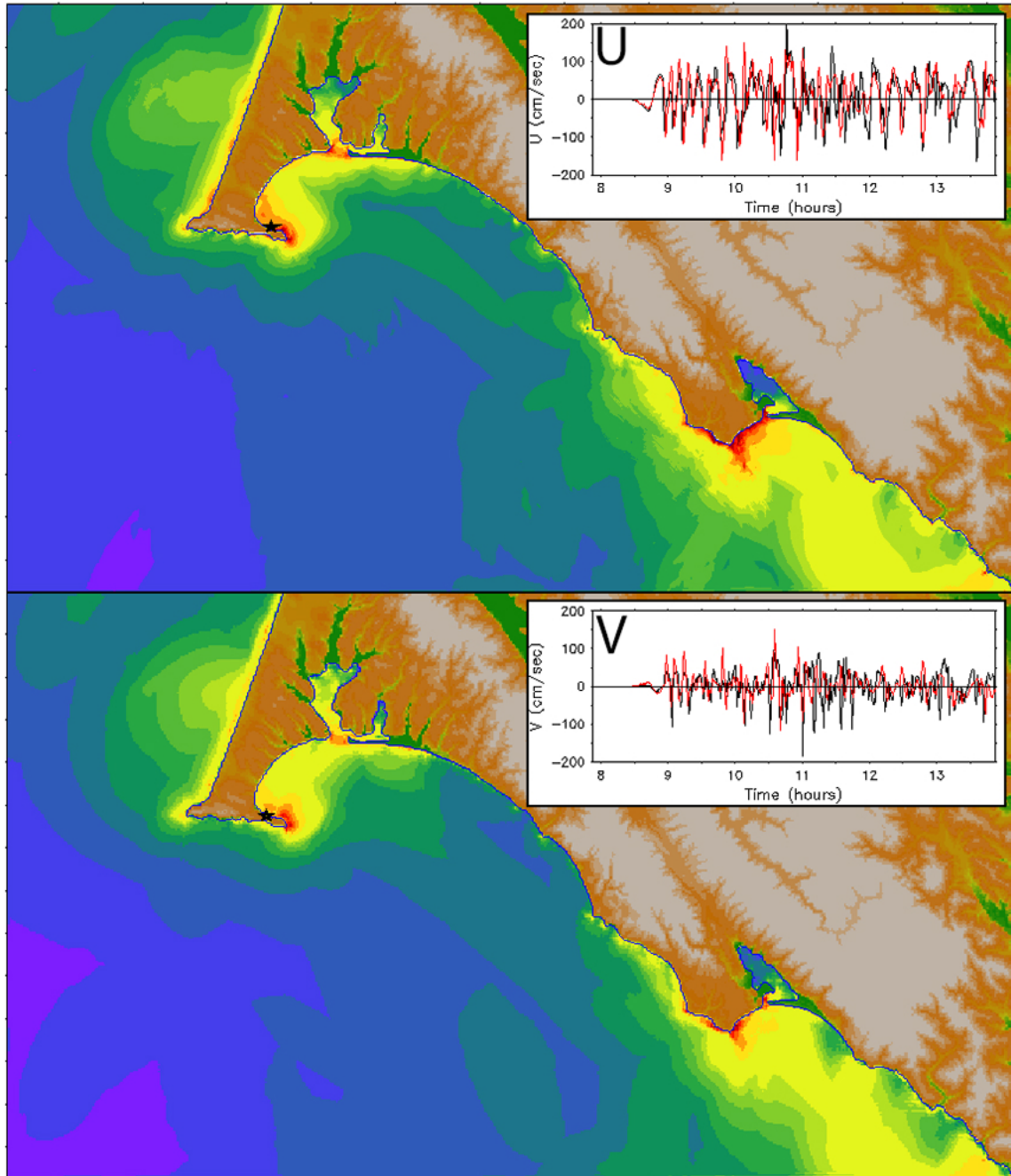


Figure 12 continued. As in Figure 11b, but for the KISZ 01-10 scenario representing Kamchatka.

KISZ 01-10

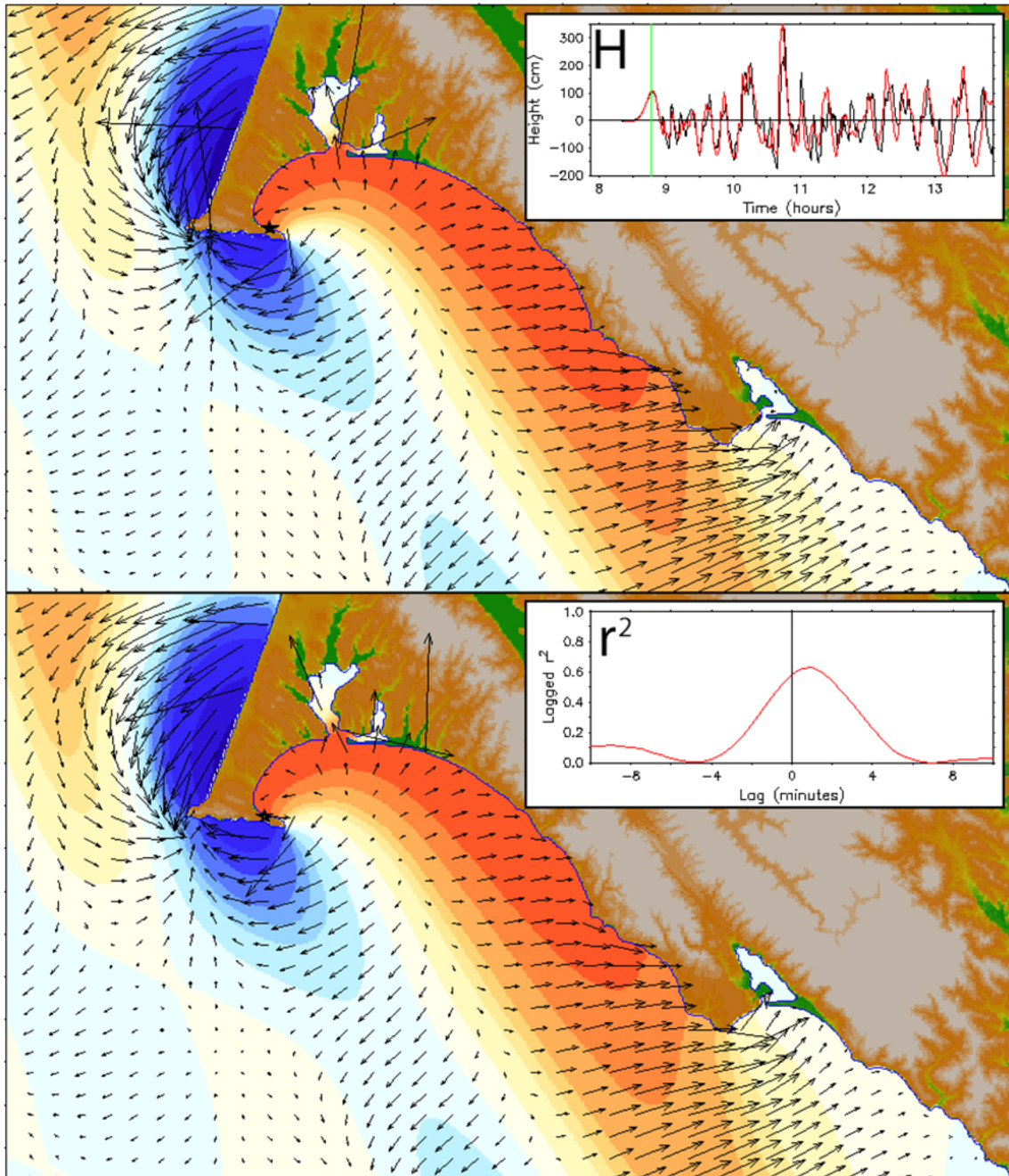
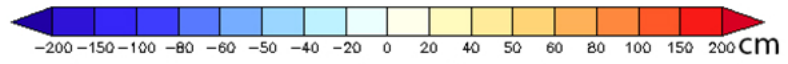


Figure 12 continued. As in Figure 11c, but for the KISZ 01-10 scenario representing Kamchatka.

KISZ 01-10

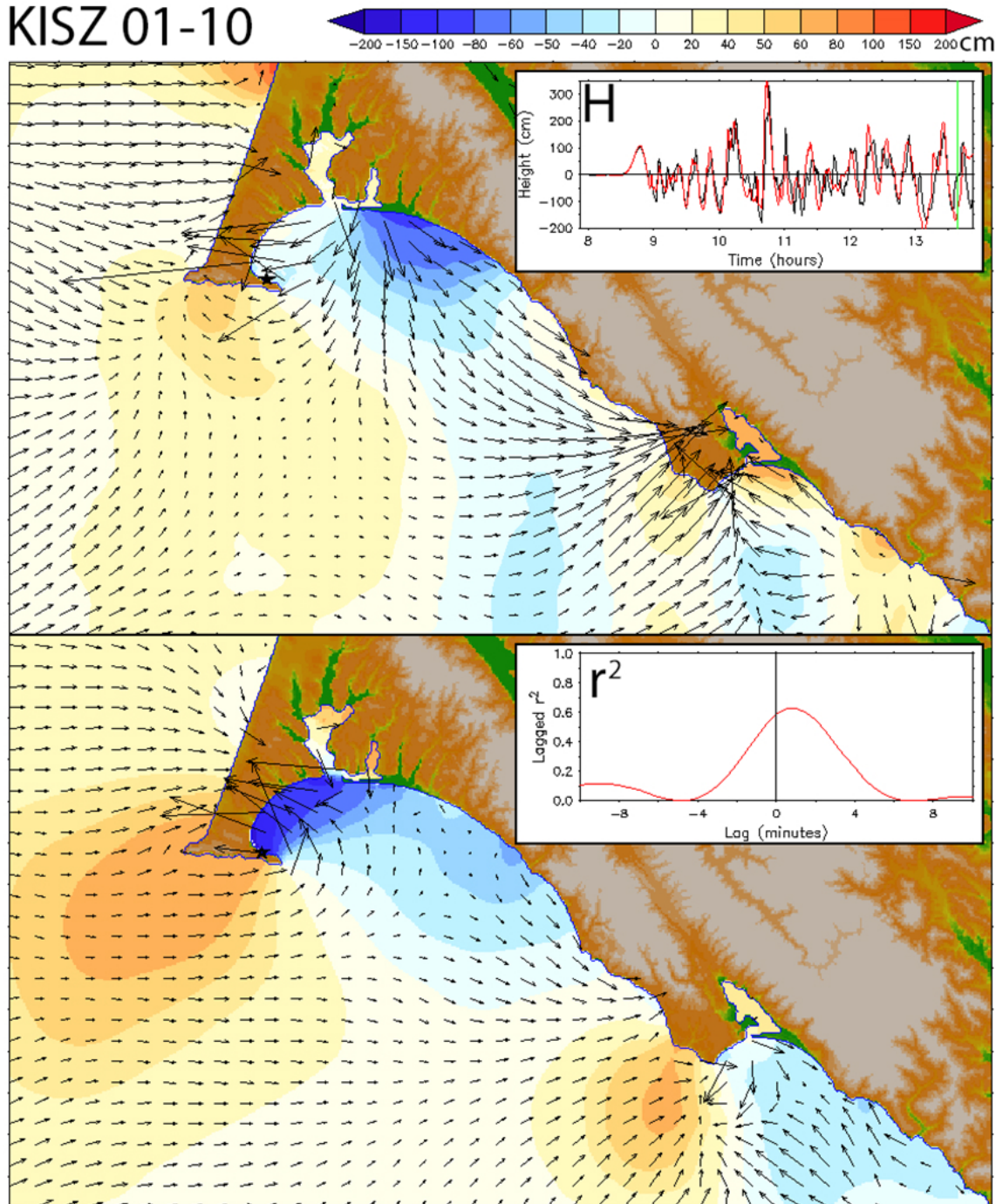


Figure 12d. As in Figure 11d, but for the KISZ 01-10 scenario representing Kamchatka.

NTSZ 30-39

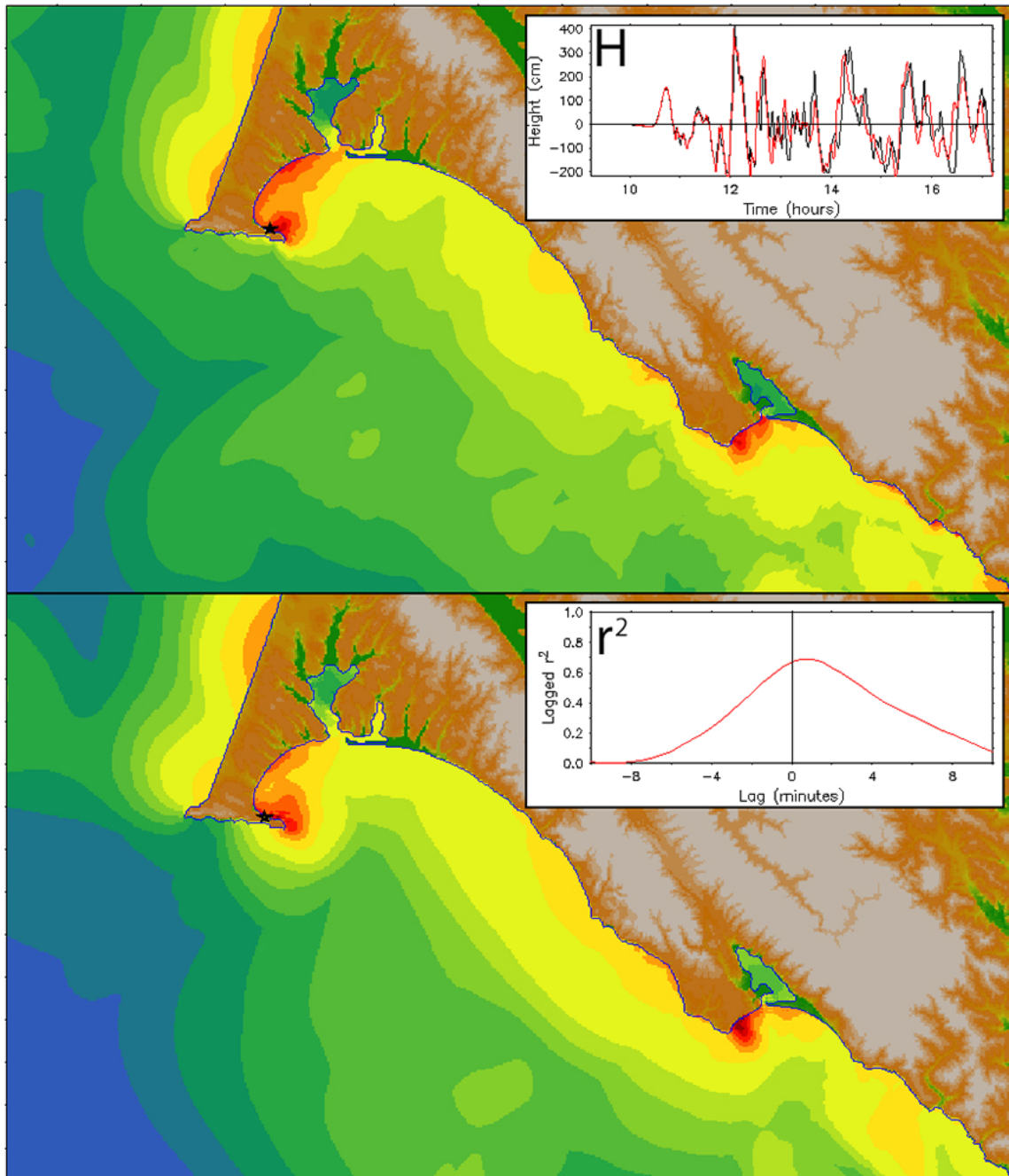
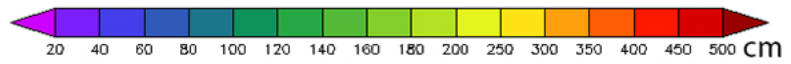


Figure 13. As in Figure 11, but for the NTSZ 30-39 scenario representing Samoa.
a) Maximum amplitude for RM (upper panel) and FM (lower panel).

NTSZ 30-39

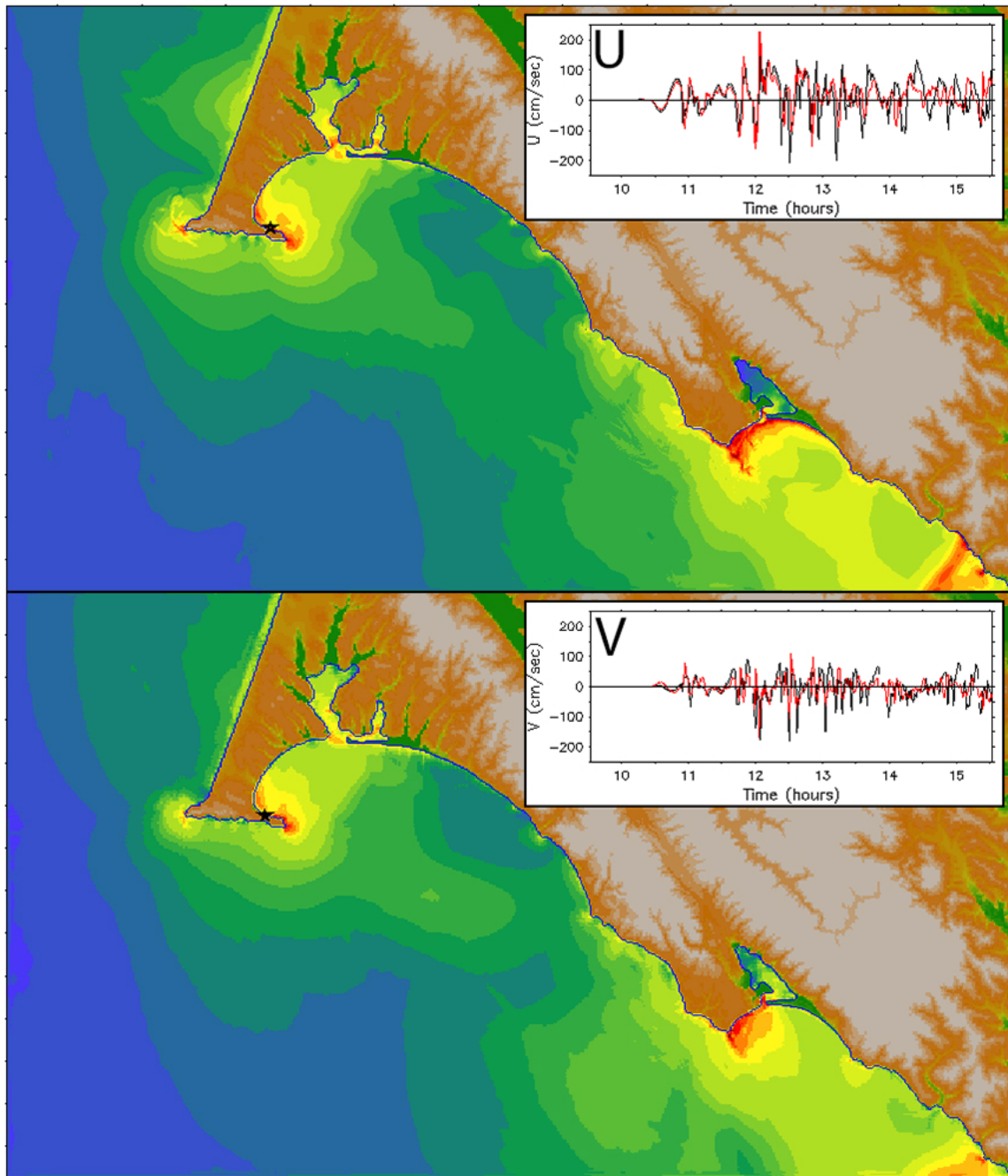


Figure 13 continued. As in Figure 11b, but for the NTSZ 30-39 scenario representing Samoa.

NTSZ 30-39

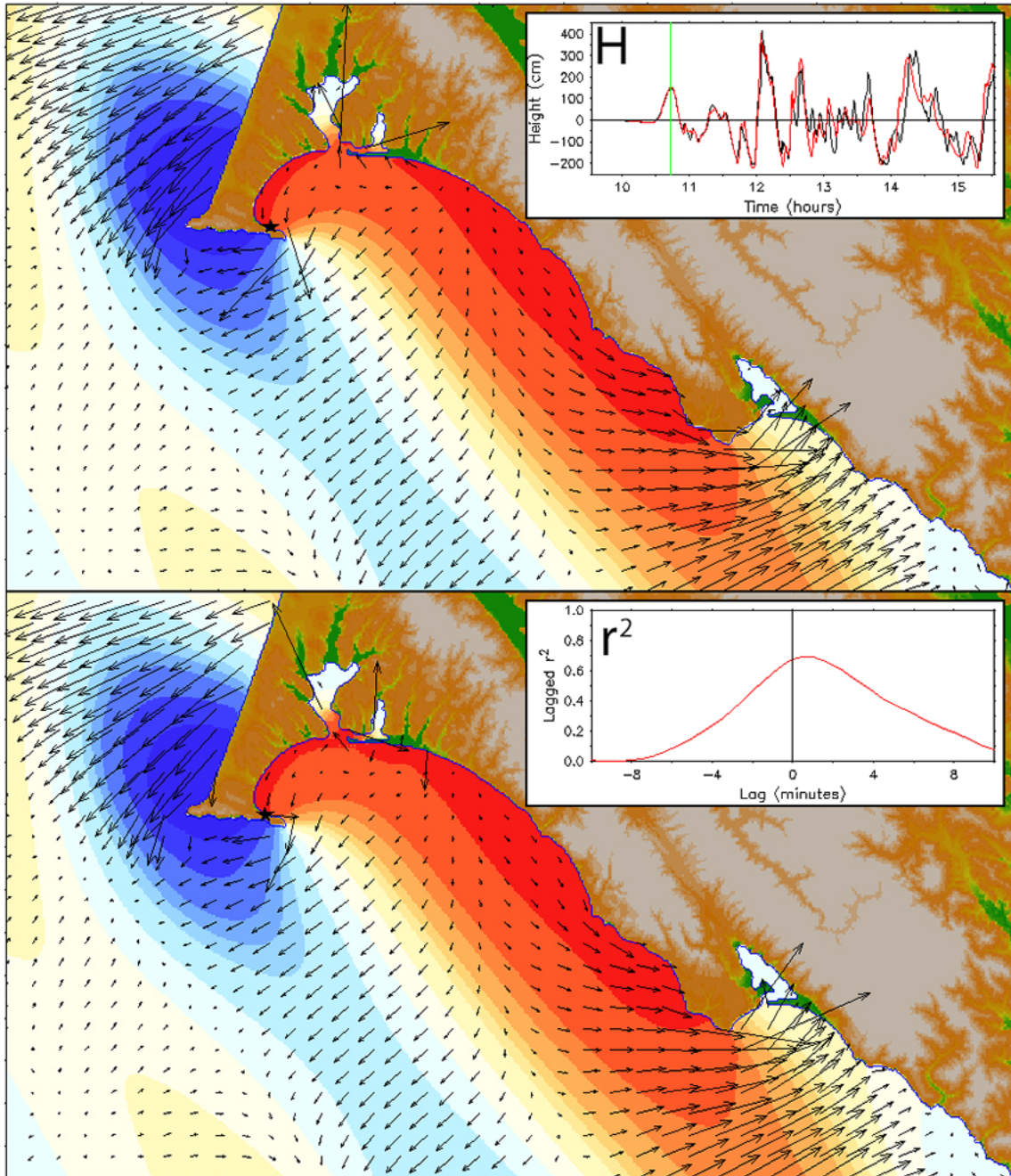
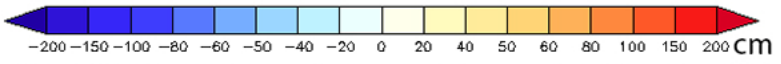


Figure 13c. As in Figure 11c, but for the NTSZ 30-39 scenario representing Samoa.

NTSZ 30-39

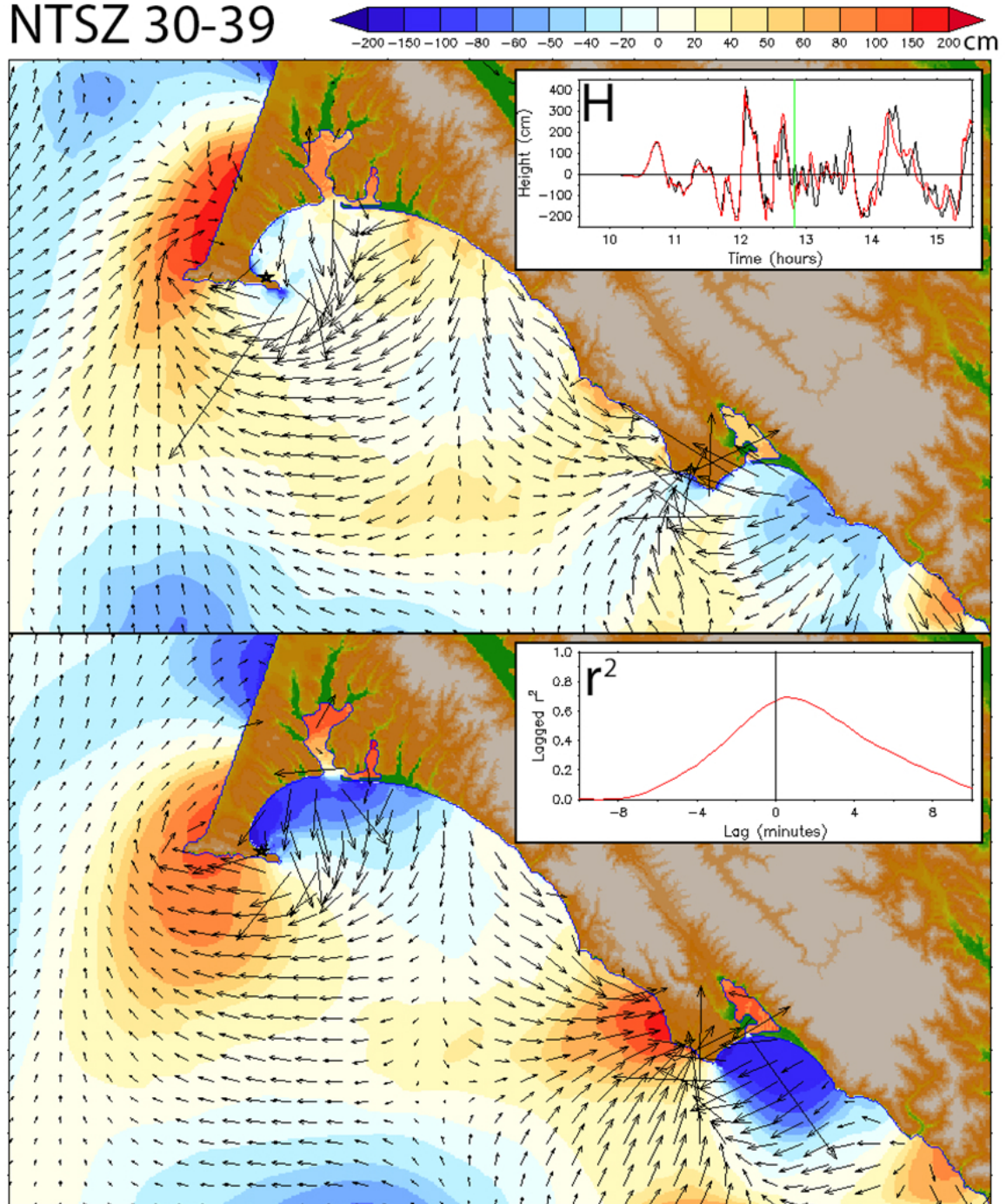


Figure 13d. As in Figure 11d, but for the NTSZ 30-39 scenario representing Samoa.

NTSZ B36

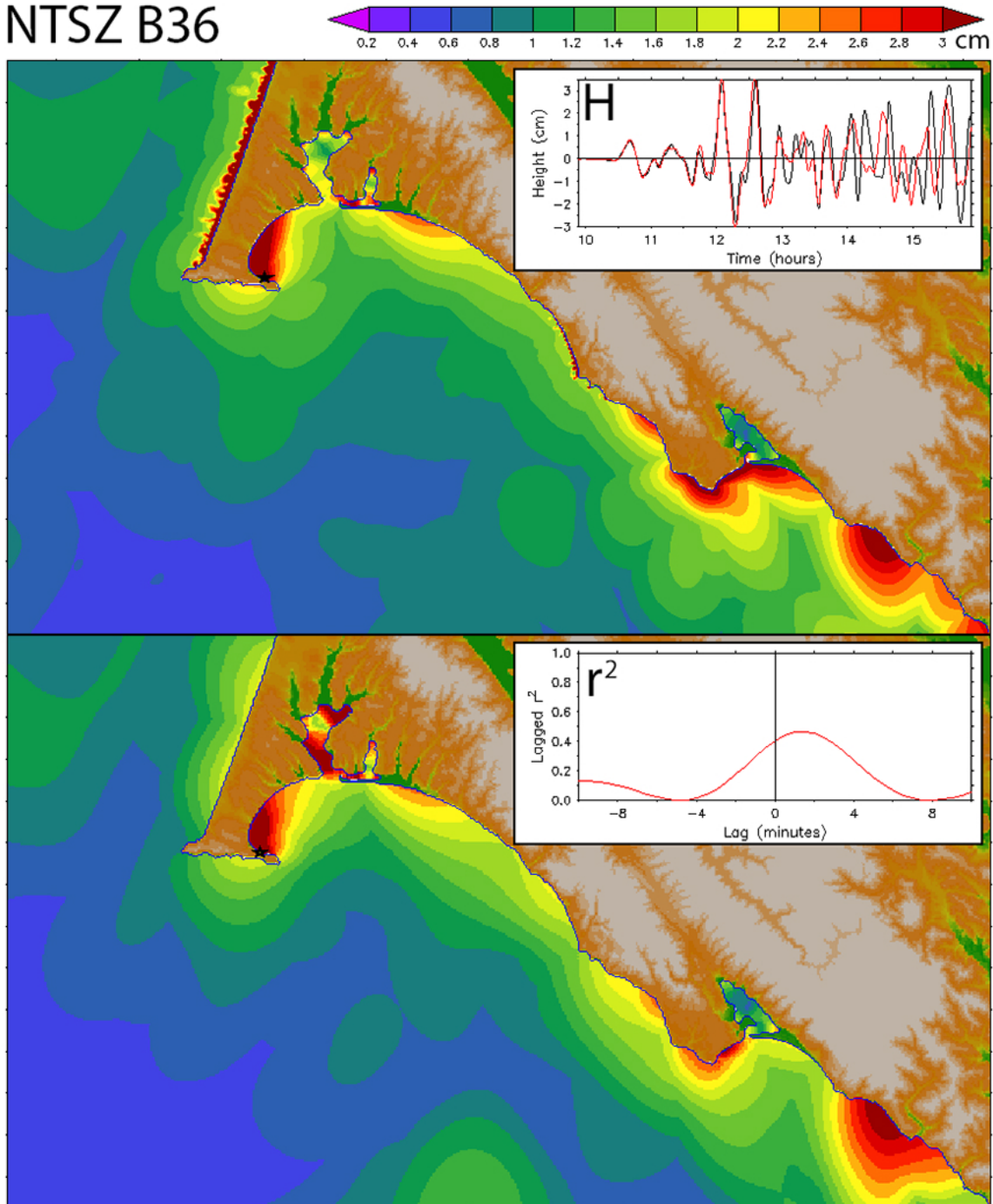


Figure 14. As in Figure 11, but for a synthetic moderate event at NTSZ B36 near Samoa.
a) Maximum amplitude for RM (upper panel) and FM (lower panel).

NTSZ B36

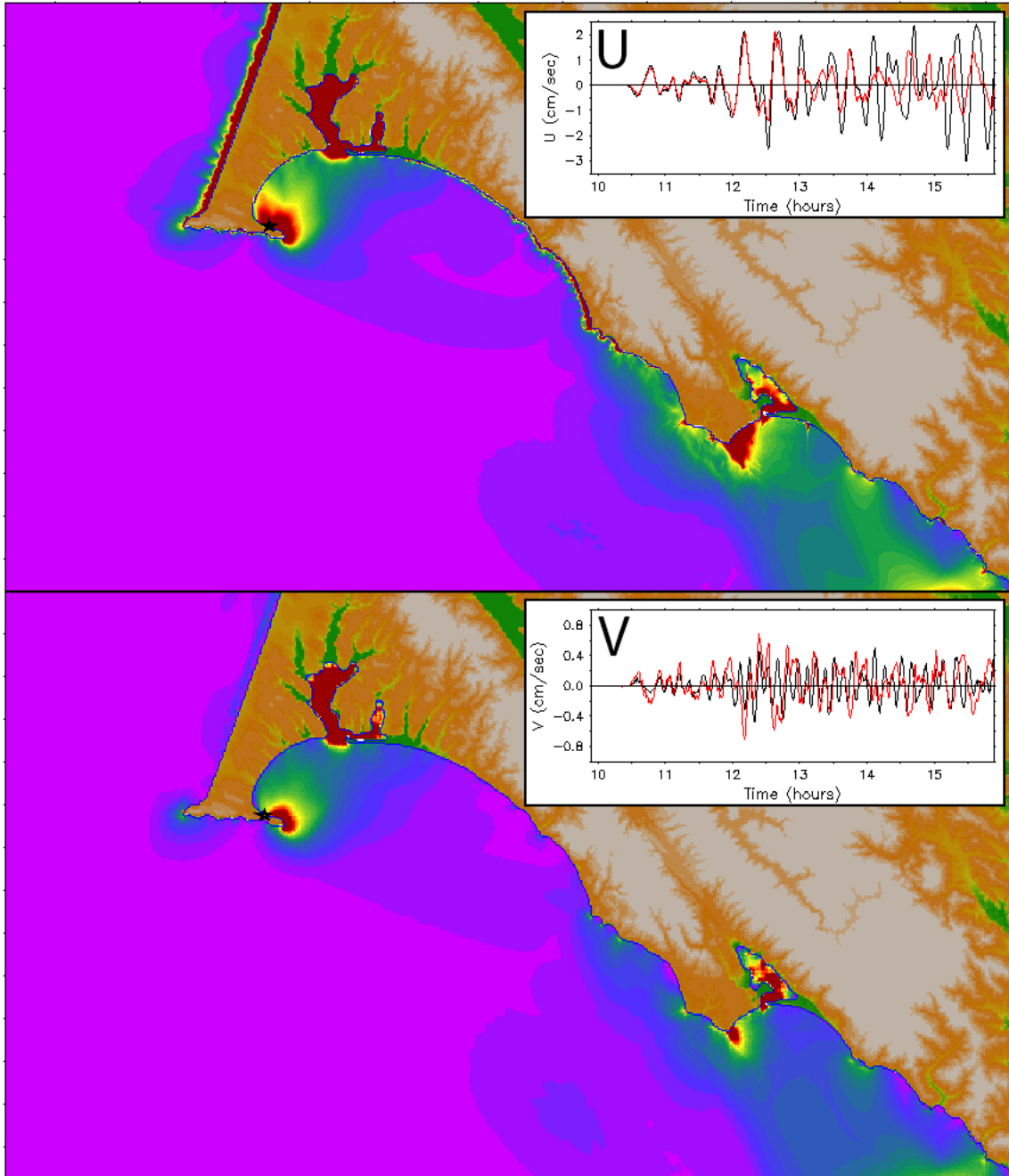


Figure 14b. As in Figure 11b, but for a synthetic moderate event at NTSZ B36 near Samoa.

NTSZ B36

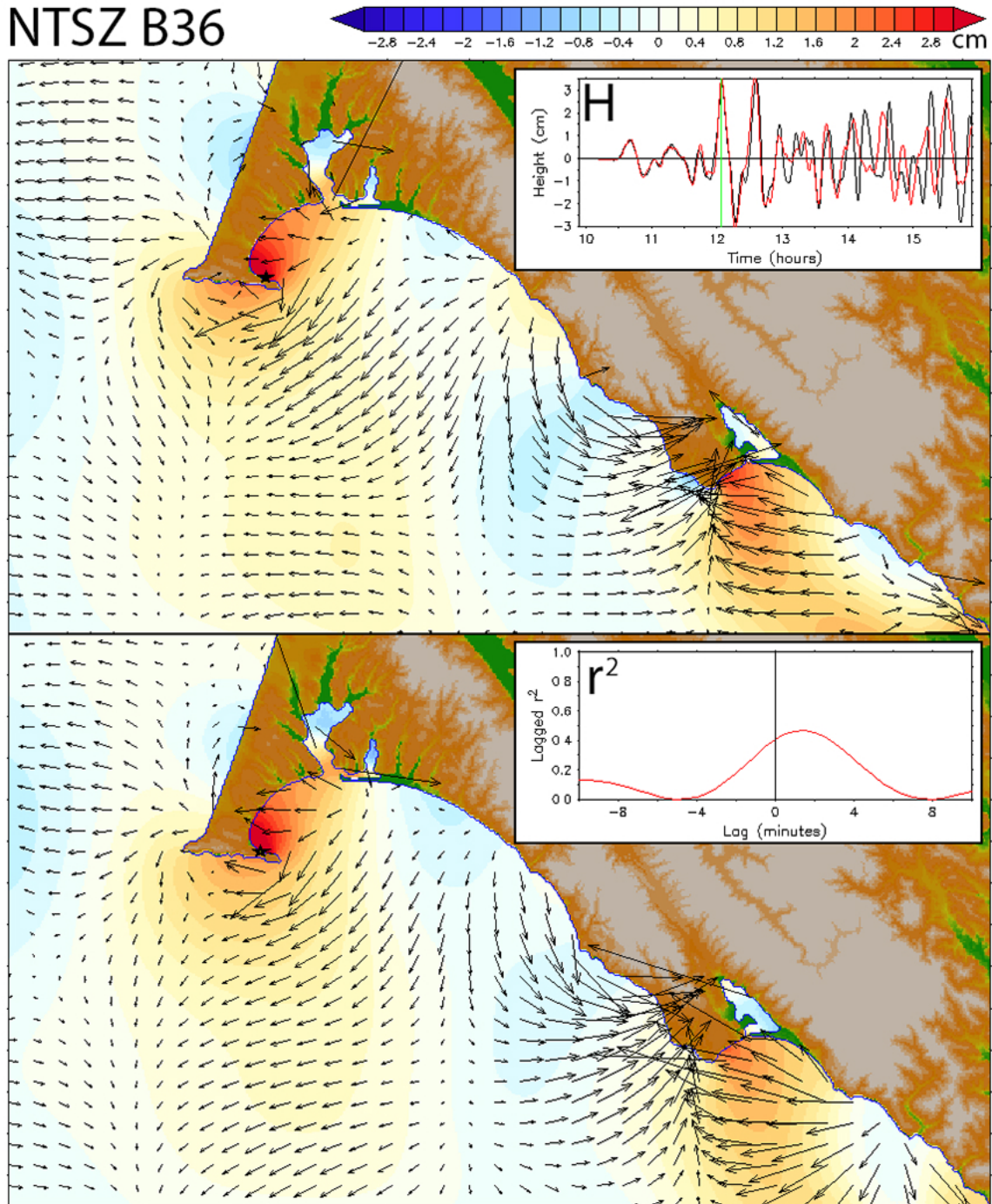


Figure 14c. As in Figure 11c, but for a synthetic moderate event at NTSZ B36 near Samoa.

NTSZ B36

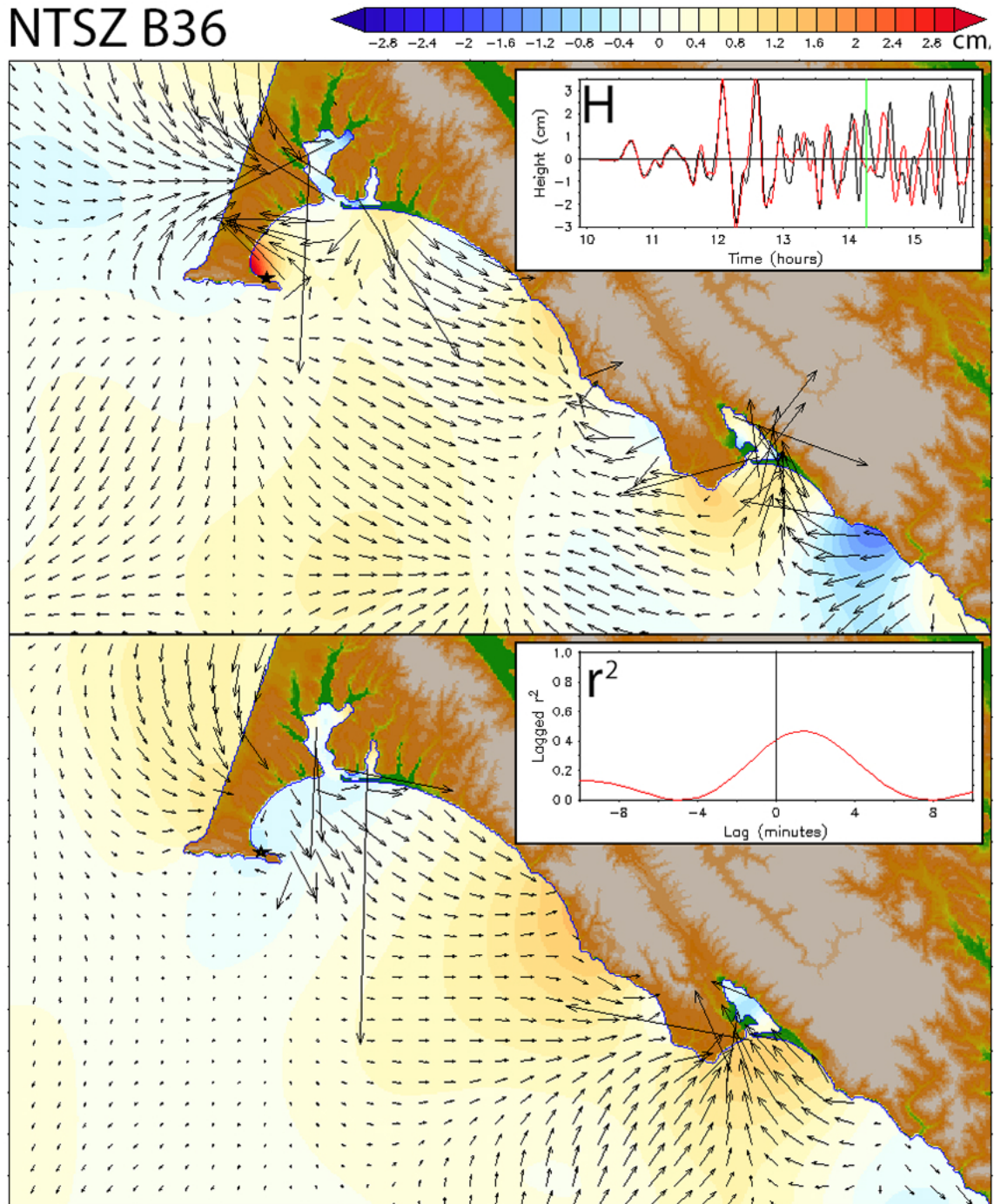


Figure 14d. As in Figure 11d, but for a synthetic moderate event at NTSZ B36 near Samoa.

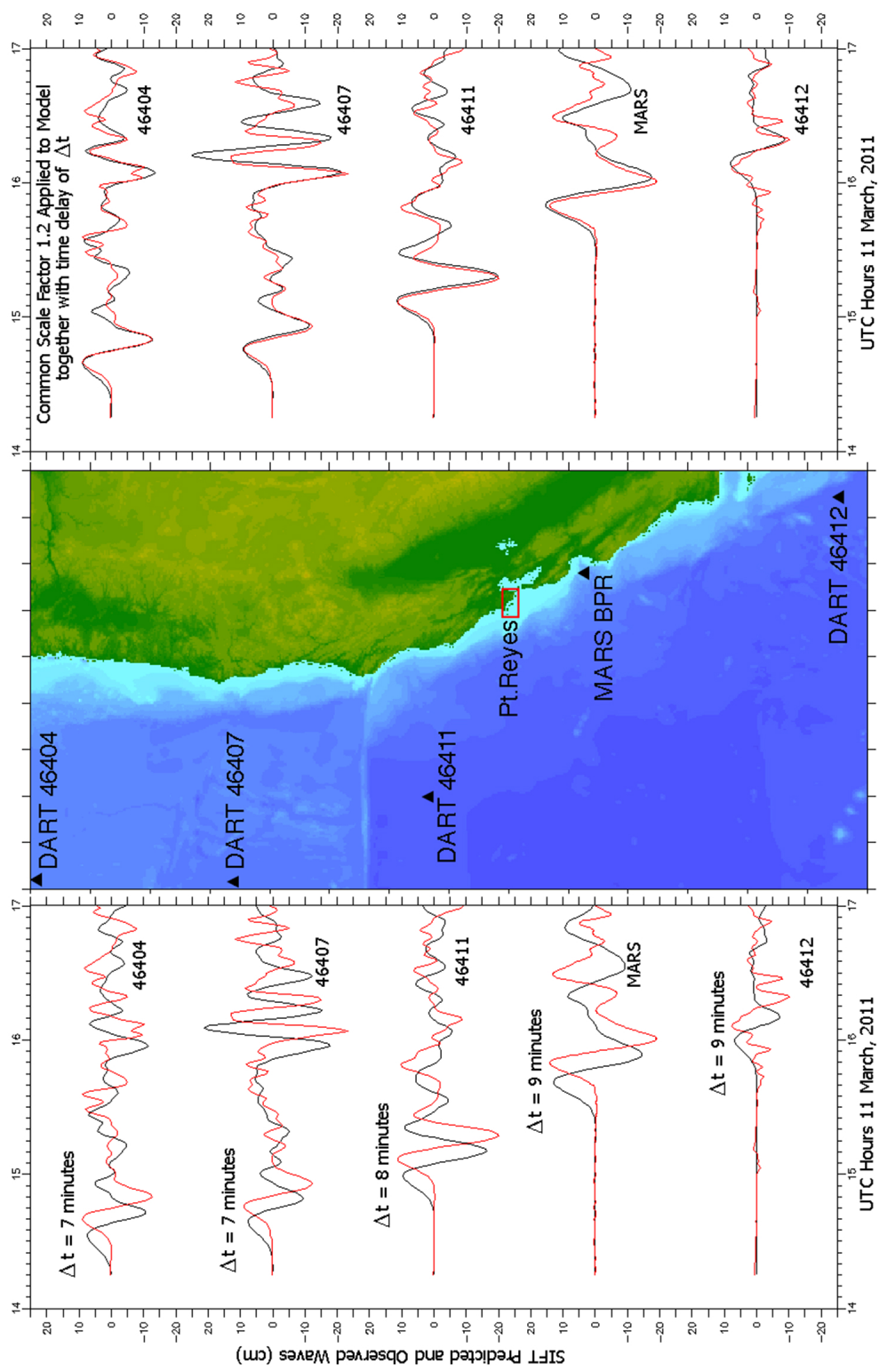


Figure 15. Observed time series from DART and MARS bottom pressure sensors during the Honshu-2011 event, compared with the model representation based on the propagation database (see Table 1). Model time series in the right hand panel have been lagged, and a common scale factor of 1.2 applied.

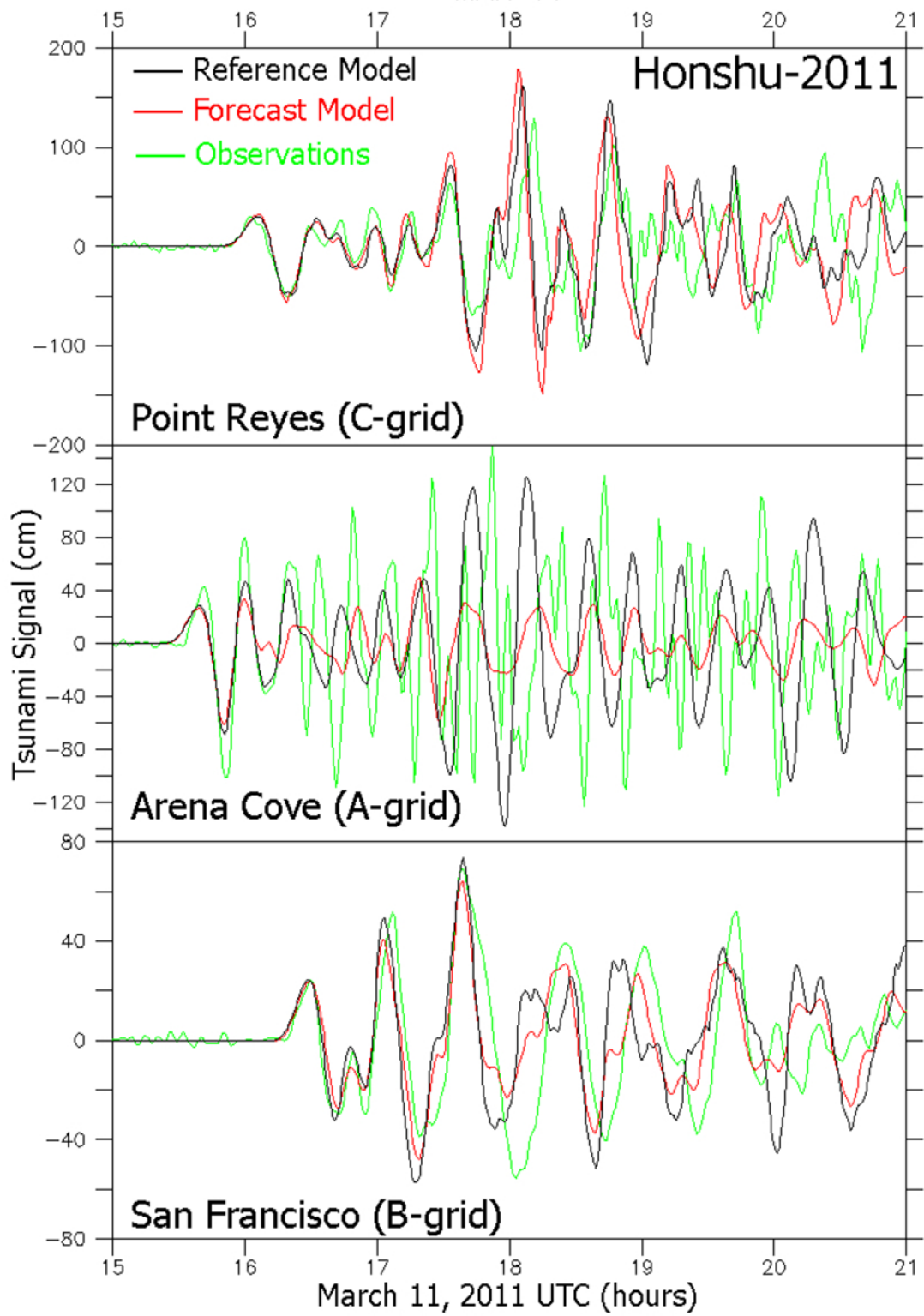


Figure 16. Comparison with RM and FM-predicted time series at selected locations where tide gage data are available: a) Point Reyes, Arena Cove, and San Francisco.

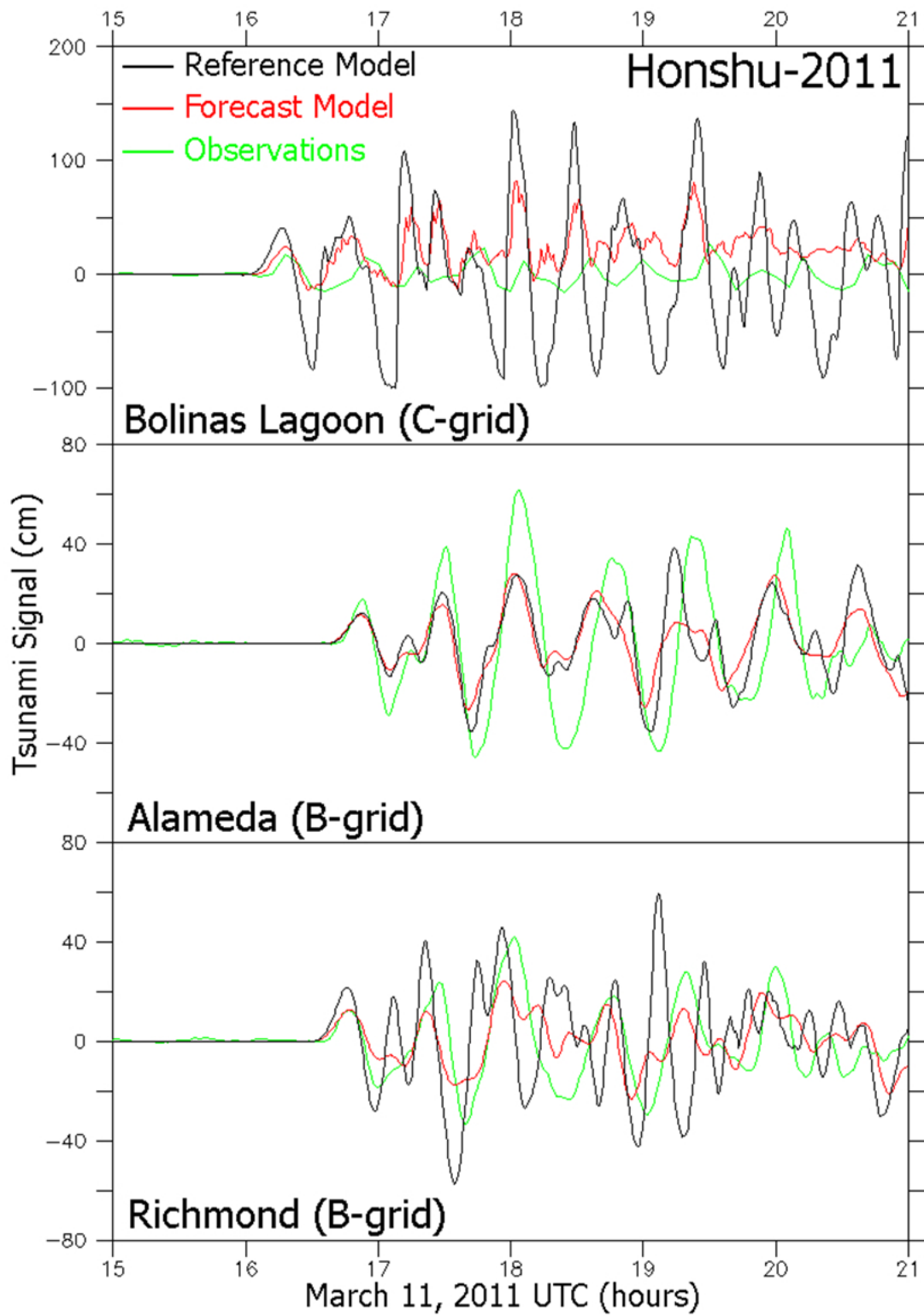


Figure 16 continued. b) Bolinas (6-minute data), Alameda, and Richmond.

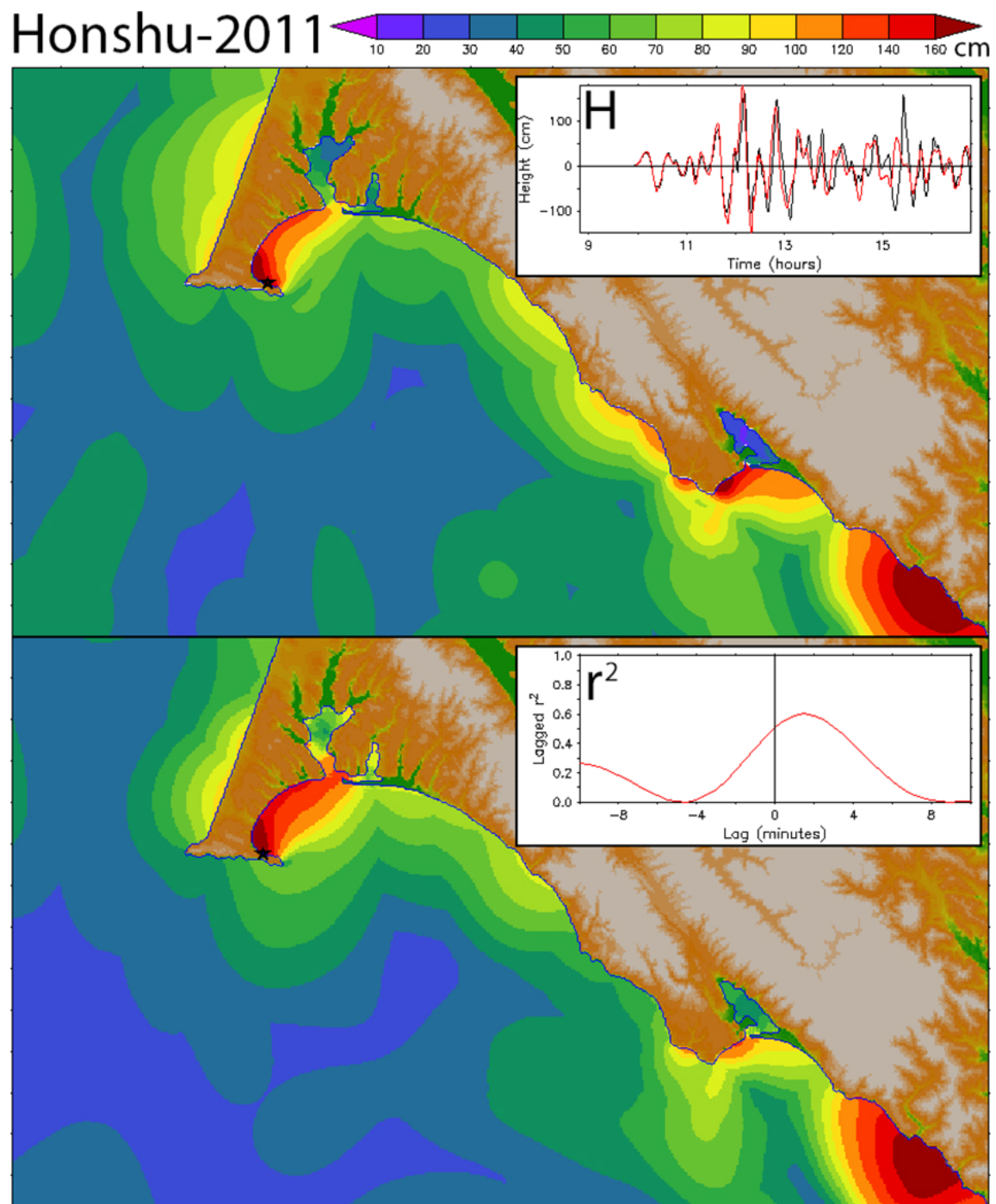


Figure 17. Intercomparison of RM and FM predictions for the Honshu-2011 event.
a) Maximum amplitude for the RM (upper panel) and FM (lower panel).

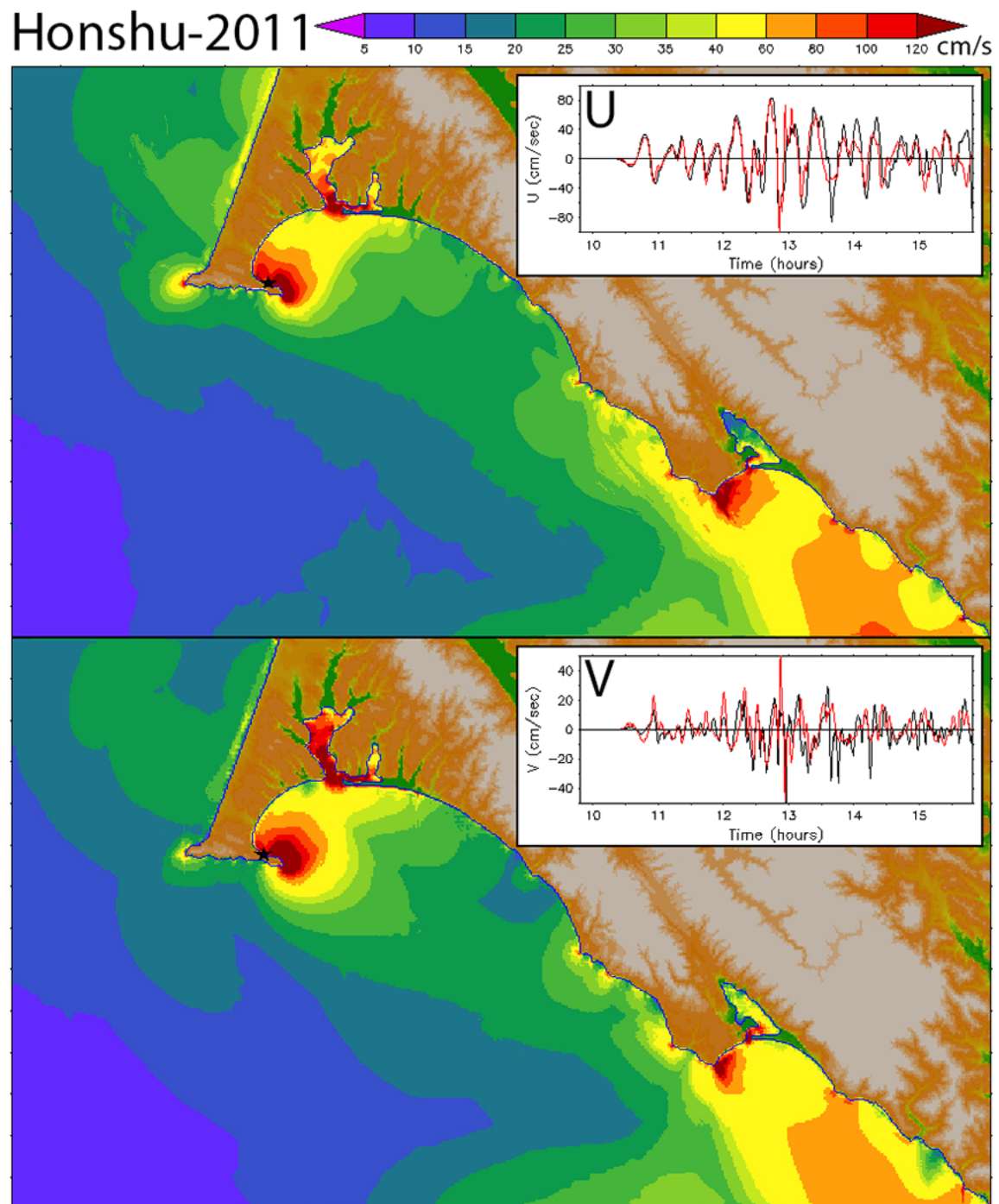


Figure 17 continued. Intercomparison of RM and FM predictions for the Honshu-2011 event.
b) Maximum speed distribution in the style of Figure 11 b.

Honshu-2011

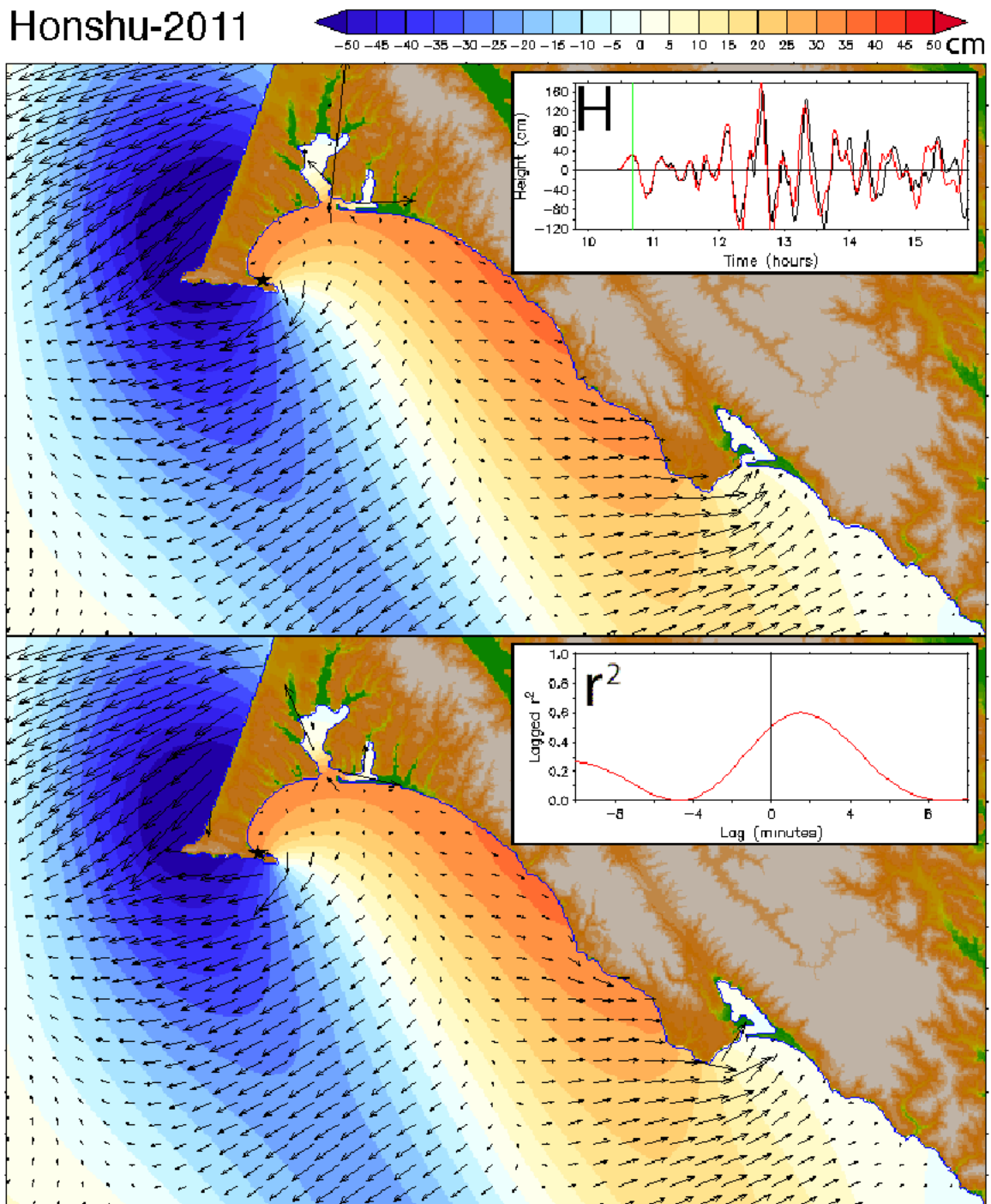


Figure 17 continued. Intercomparison of RM and FM predictions for the Honshu-2011 event. c) snapshot of amplitude and velocity at the discrete time, marked in the upper panel inset. RM and FM C-grid results are in the upper and lower panels.

Honshu-2011

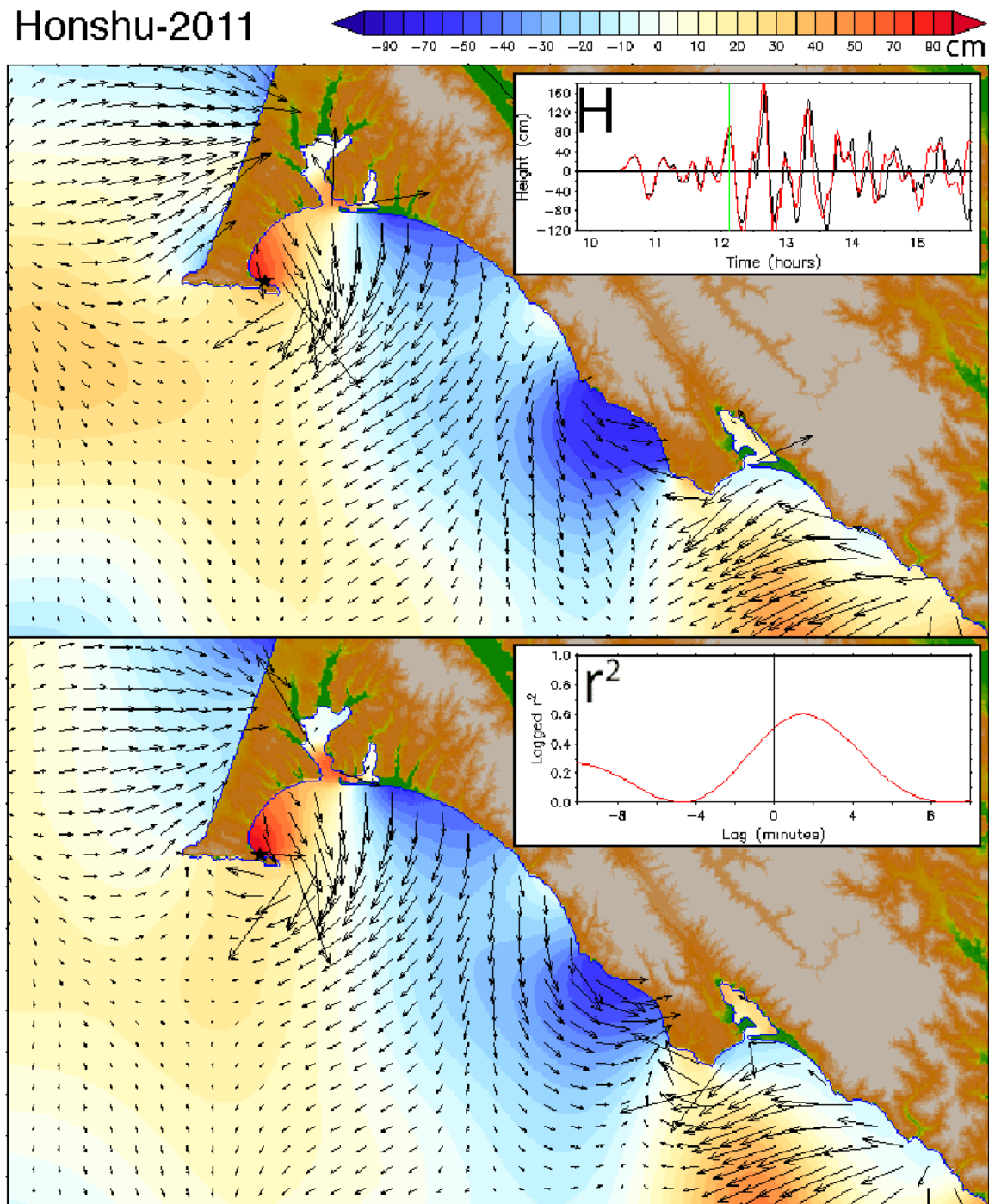


Figure 17 continued. Intercomparison of RM and FM predictions for the Honshu-2011 event. d) as in Figure 17c but at the later time indicated in the upper panel inset.

Honshu-2011

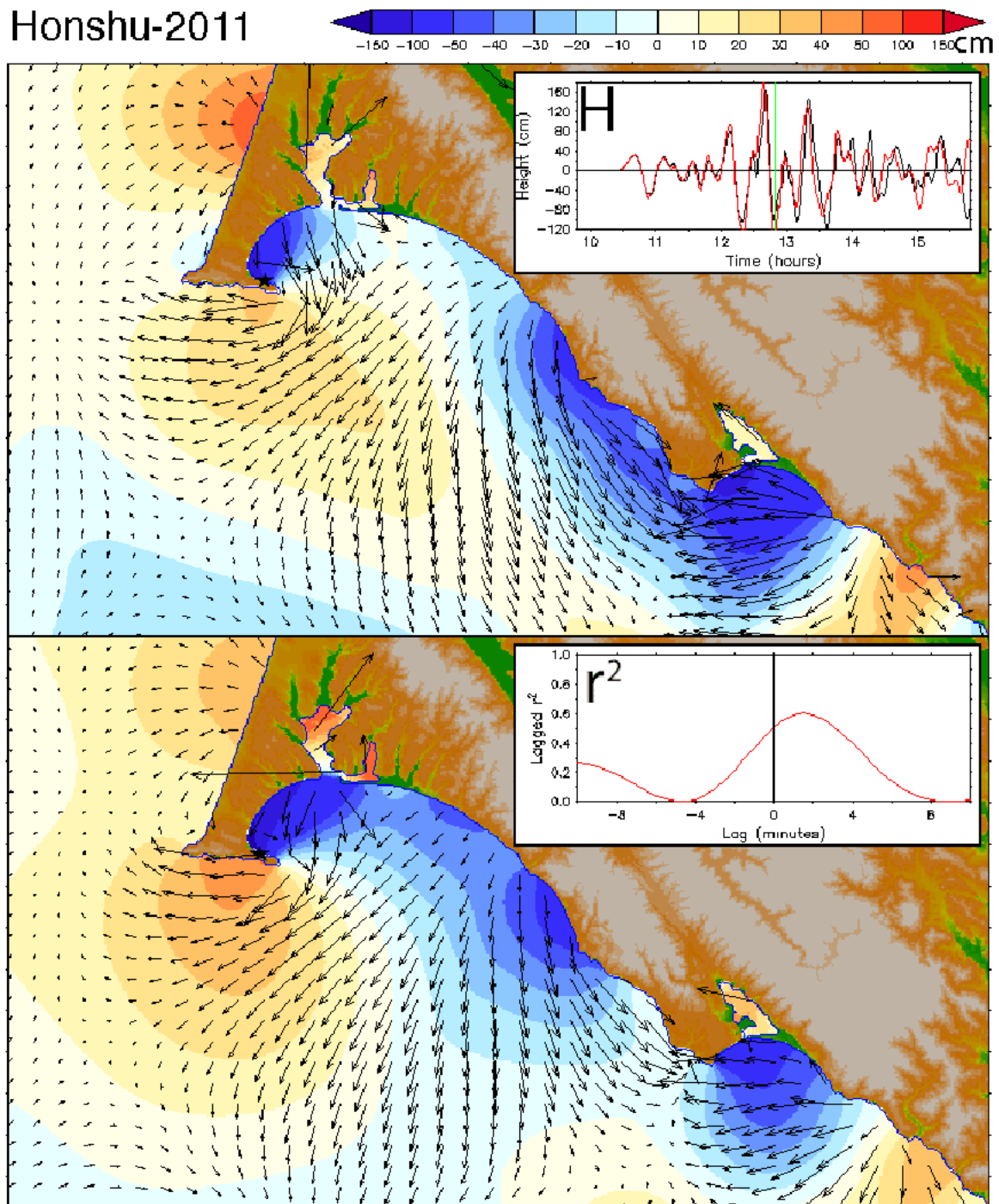


Figure 17 continued. Intercomparison of RM and FM predictions for the Honshu-2011 event. e) as in Figure 17c but at the later time indicated in the upper inset panel.

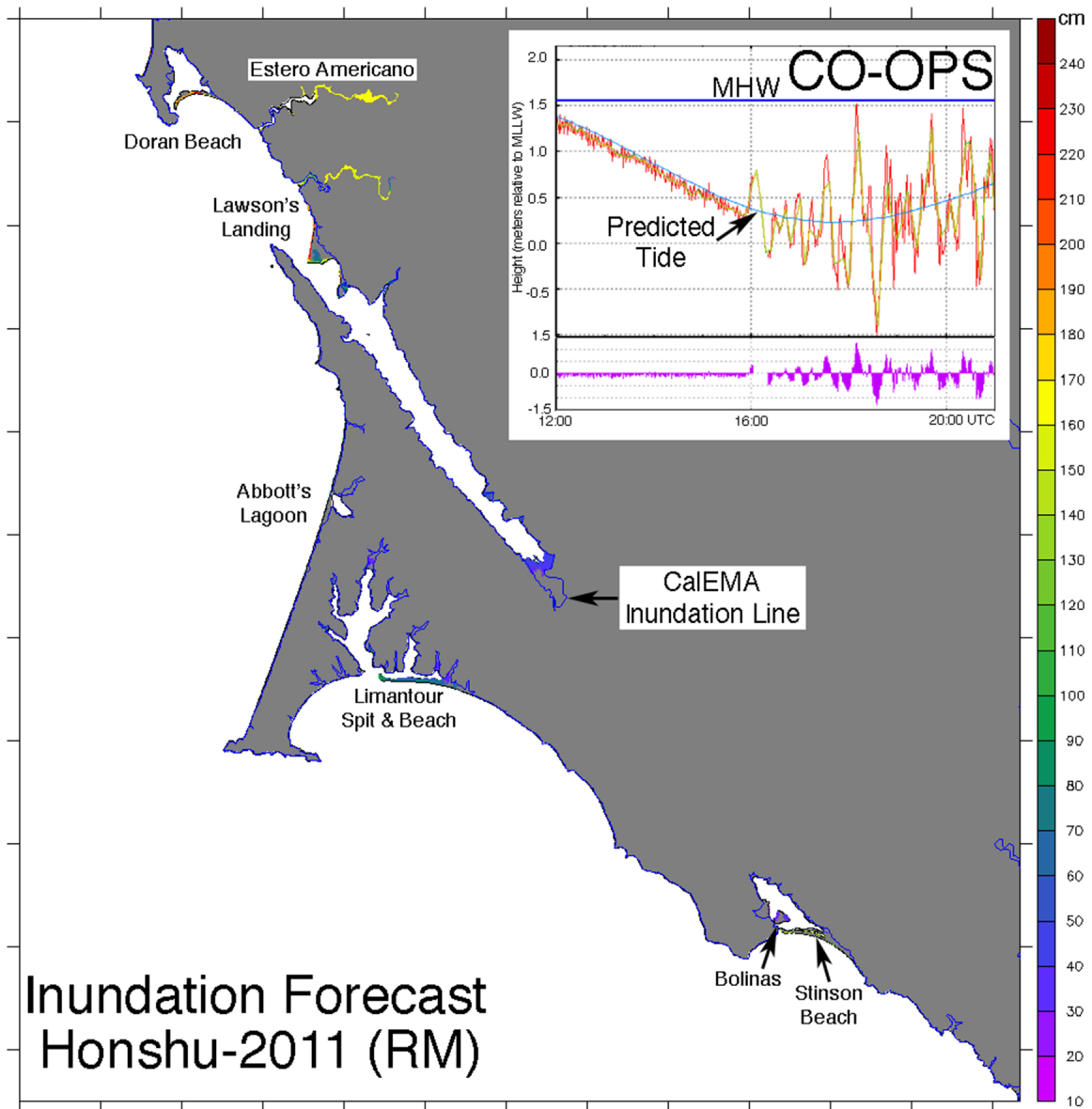


Figure 18. Inundation forecast for the Honshu-2011 event in the RM C-grid, compared with the CalEMA inundation line. The inset in the upper right shows tide gage data from Point Reyes. Actual tides were well below MHW so the inundation forecast was overly conservative.

Chile-2010

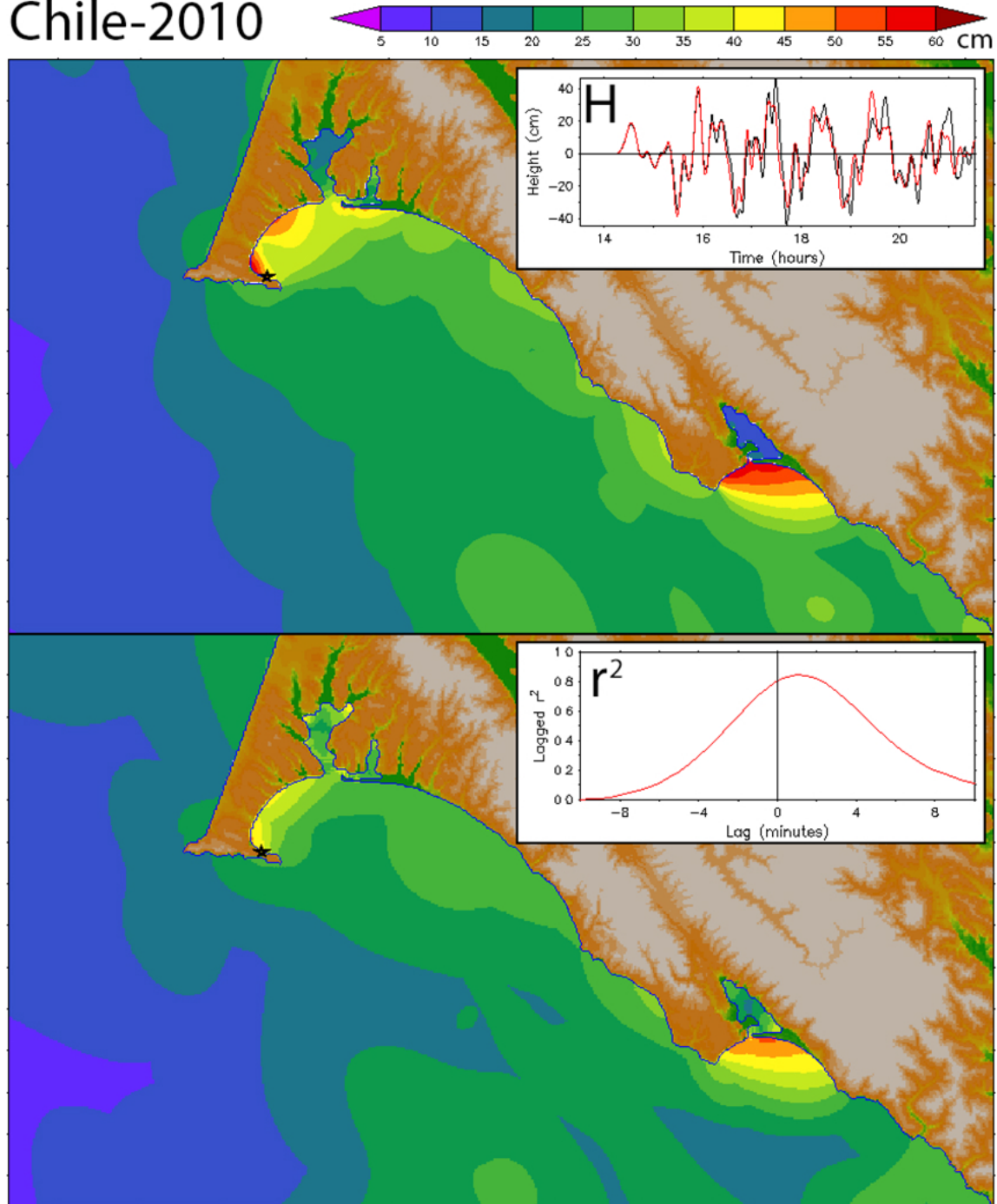
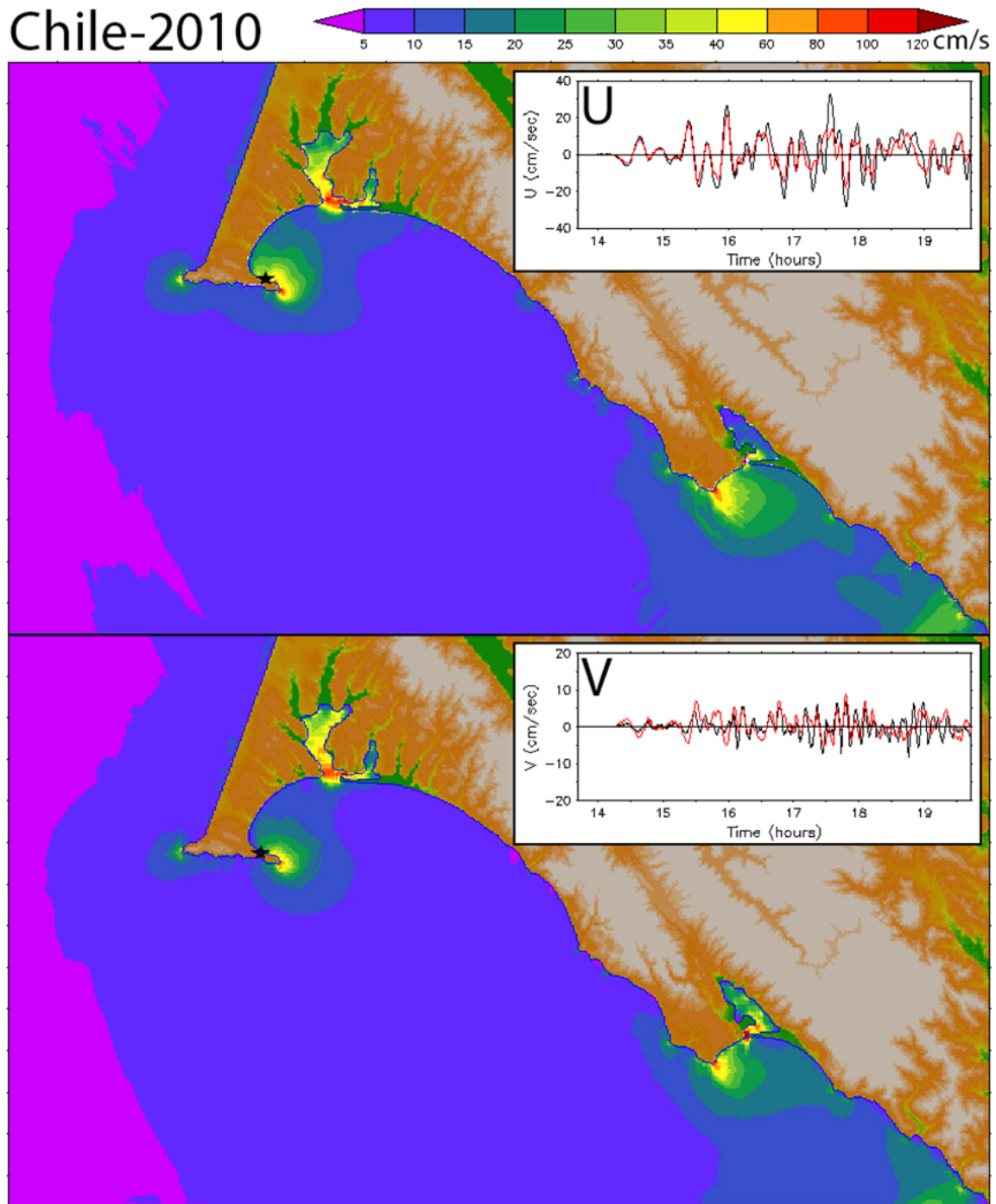


Figure 19. Reference and Forecast Model comparison for the Chile-2010 event.
a) Maximum amplitude for the RM (upper panel) and FM (lower panel).

Chile-2010



Chile-2010

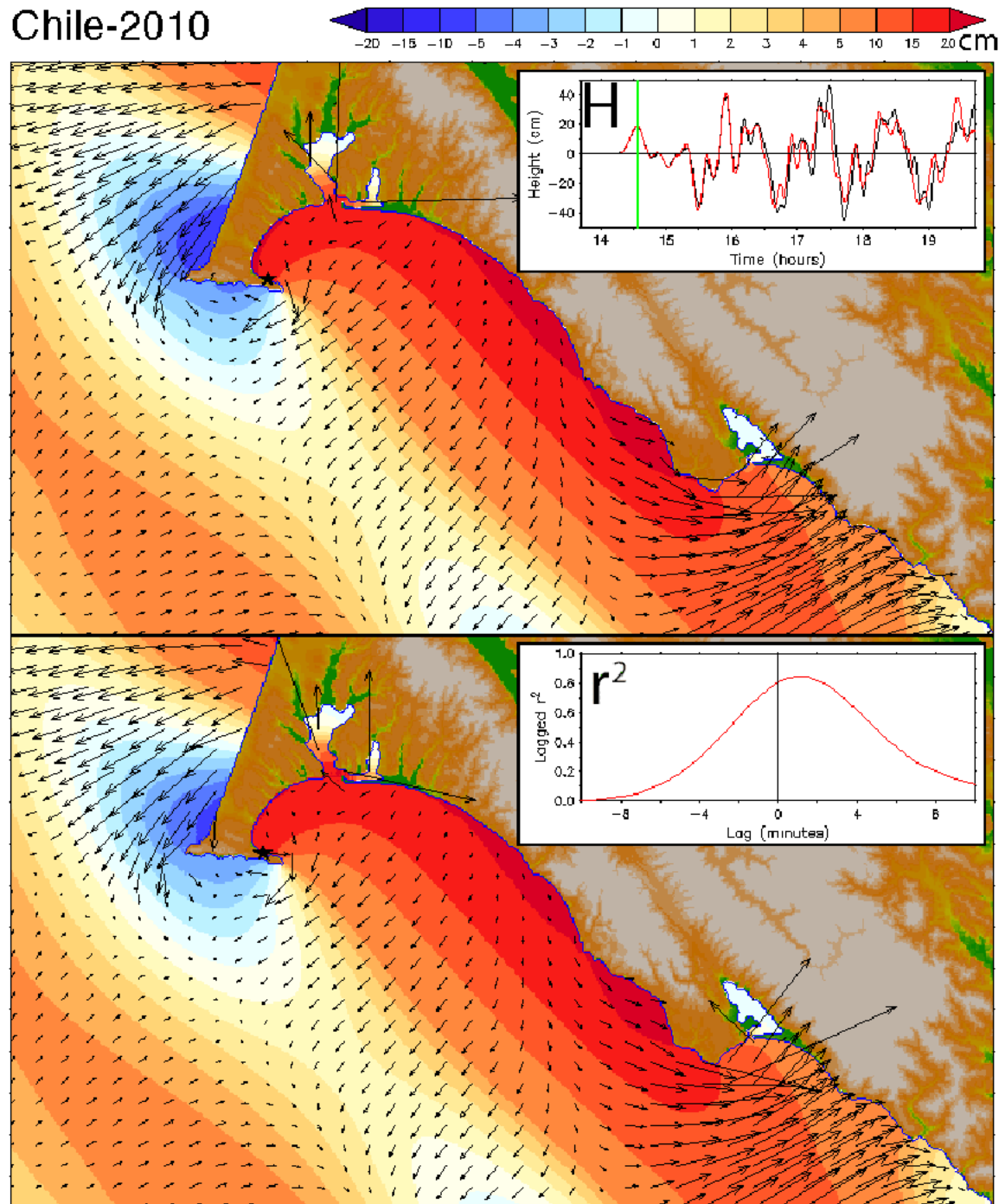


Figure 19 continued. Reference and Forecast Model comparison for the Chile-2010 event.
c) snapshot of amplitude and current at the indicated time.

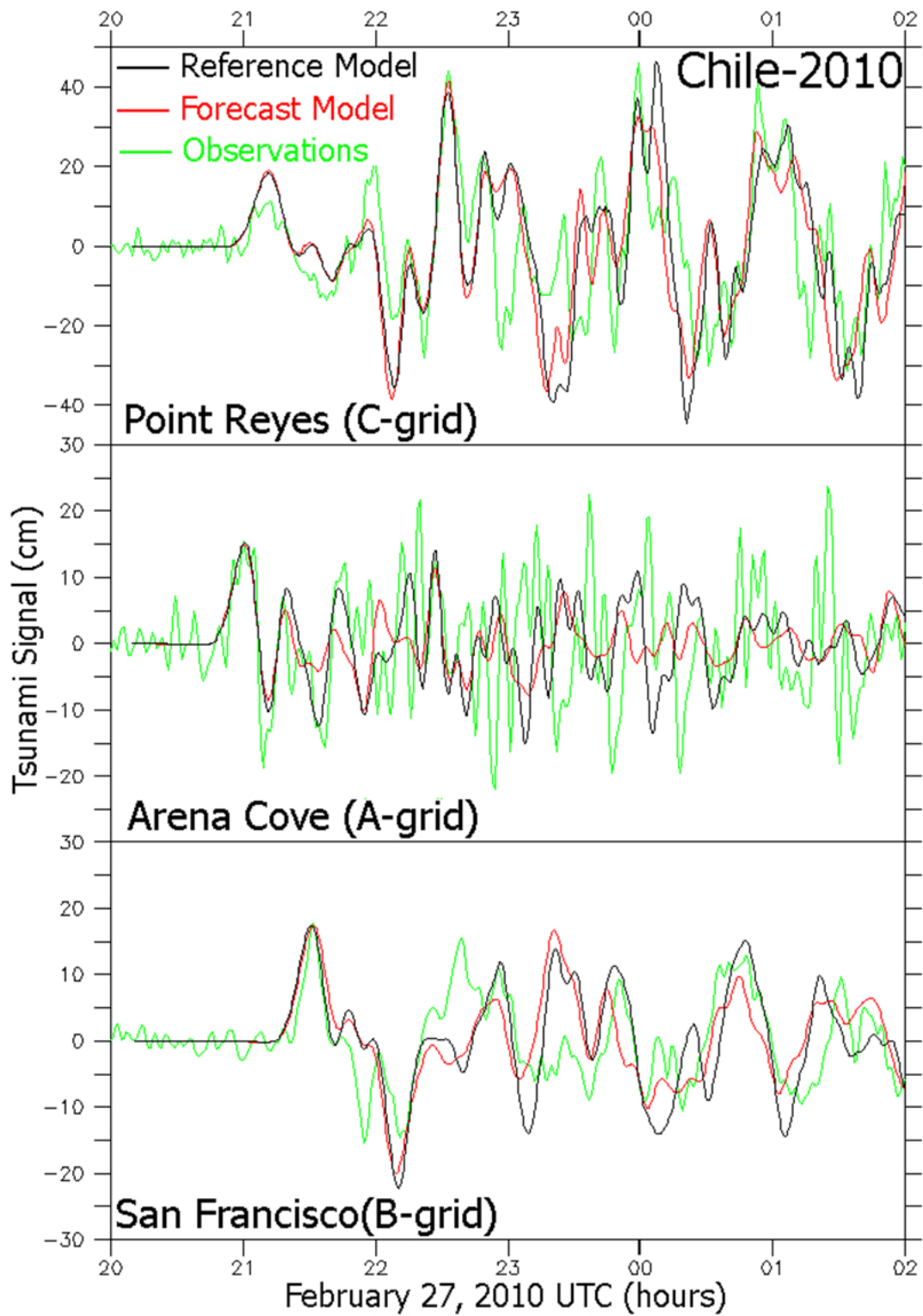


Figure 20. Model and observed time series comparison for the Chile-2010 event.

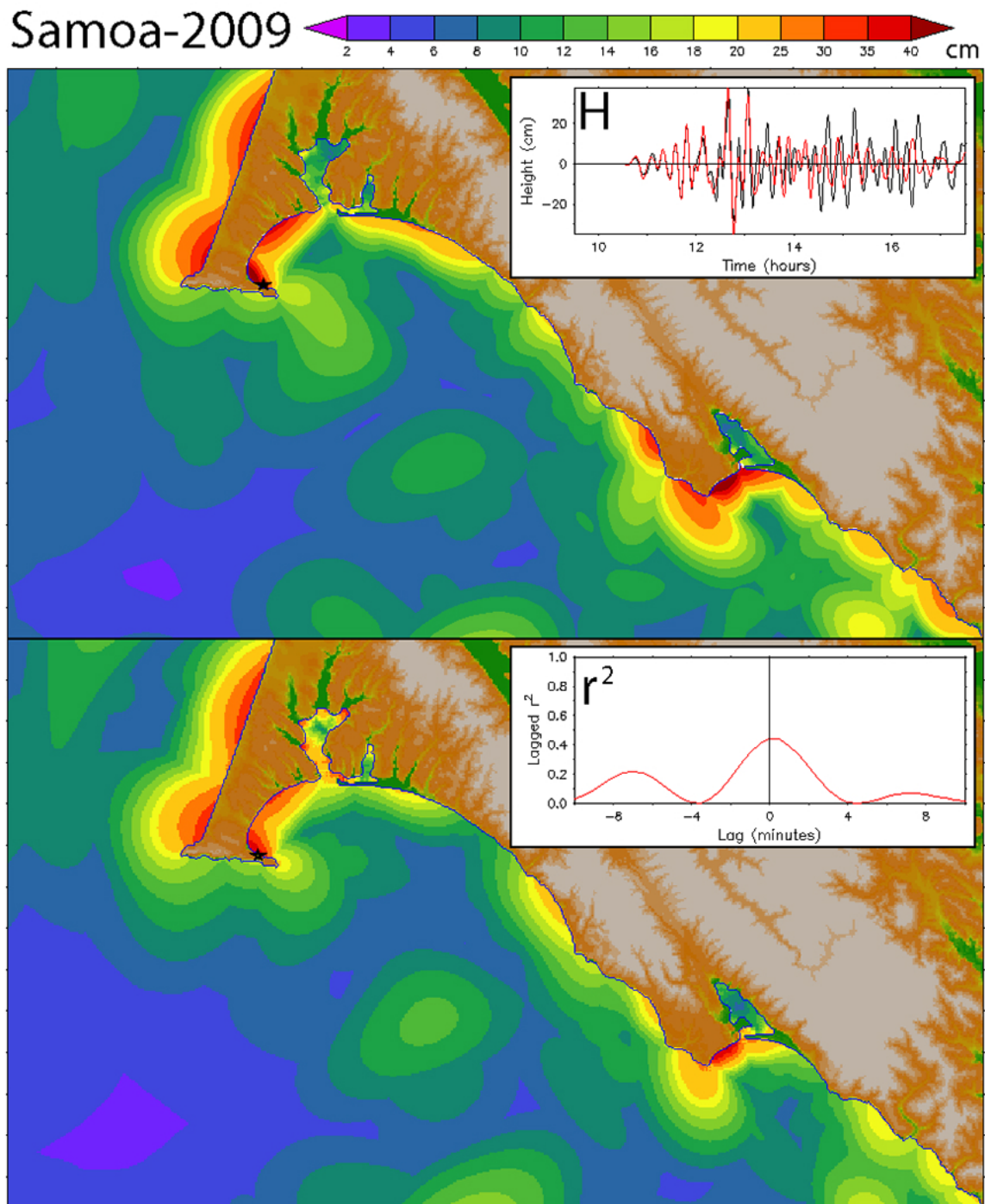


Figure 21. RM and FM comparison, as in Figure 19 but for the Samoa-2009 event.
 a) Maximum amplitude for the RM (upper panel) and FM (lower panel).

Samoa-2009

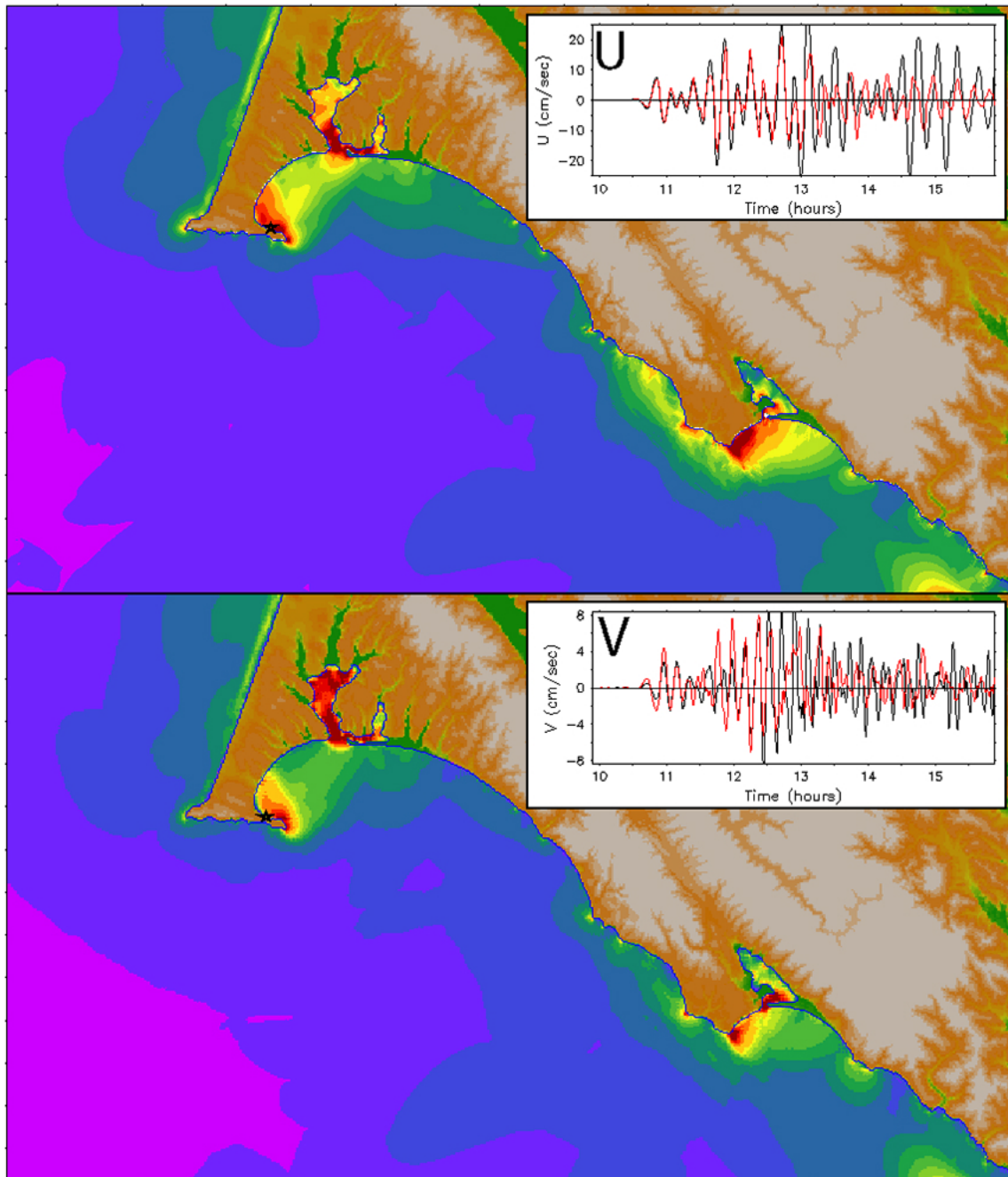


Figure 21 continued. RM and FM comparison, as in Figure 19 but for the Samoa-2009 event.
b) Maximum speed for the RM (upper panel) and FM (lower panel).

Samoa-2009

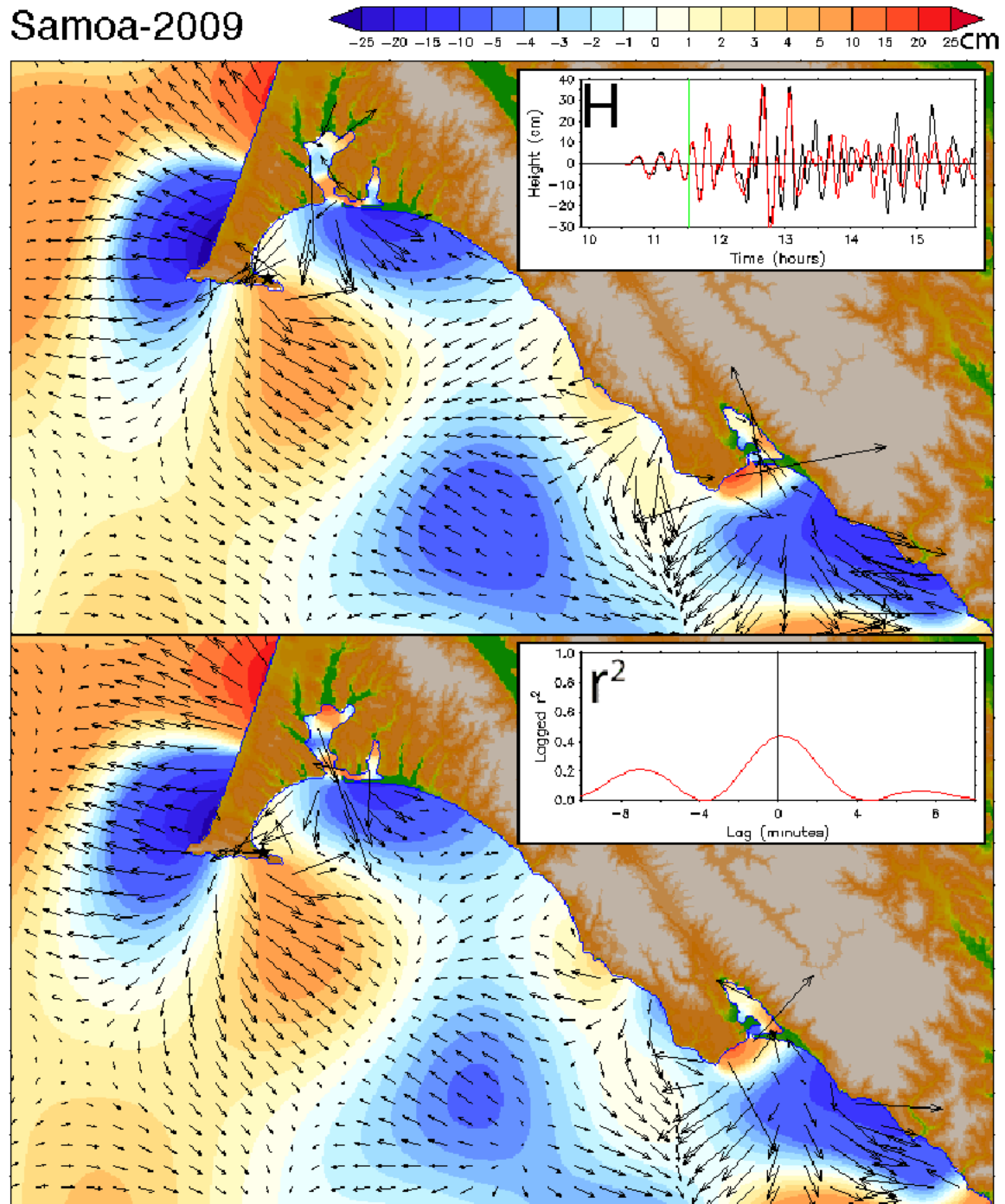


Figure 21 continued. RM and FM comparison, as in Figure 19 but for the Samoa-2009 event.
c) snapshot of amplitude and current at the indicated time.

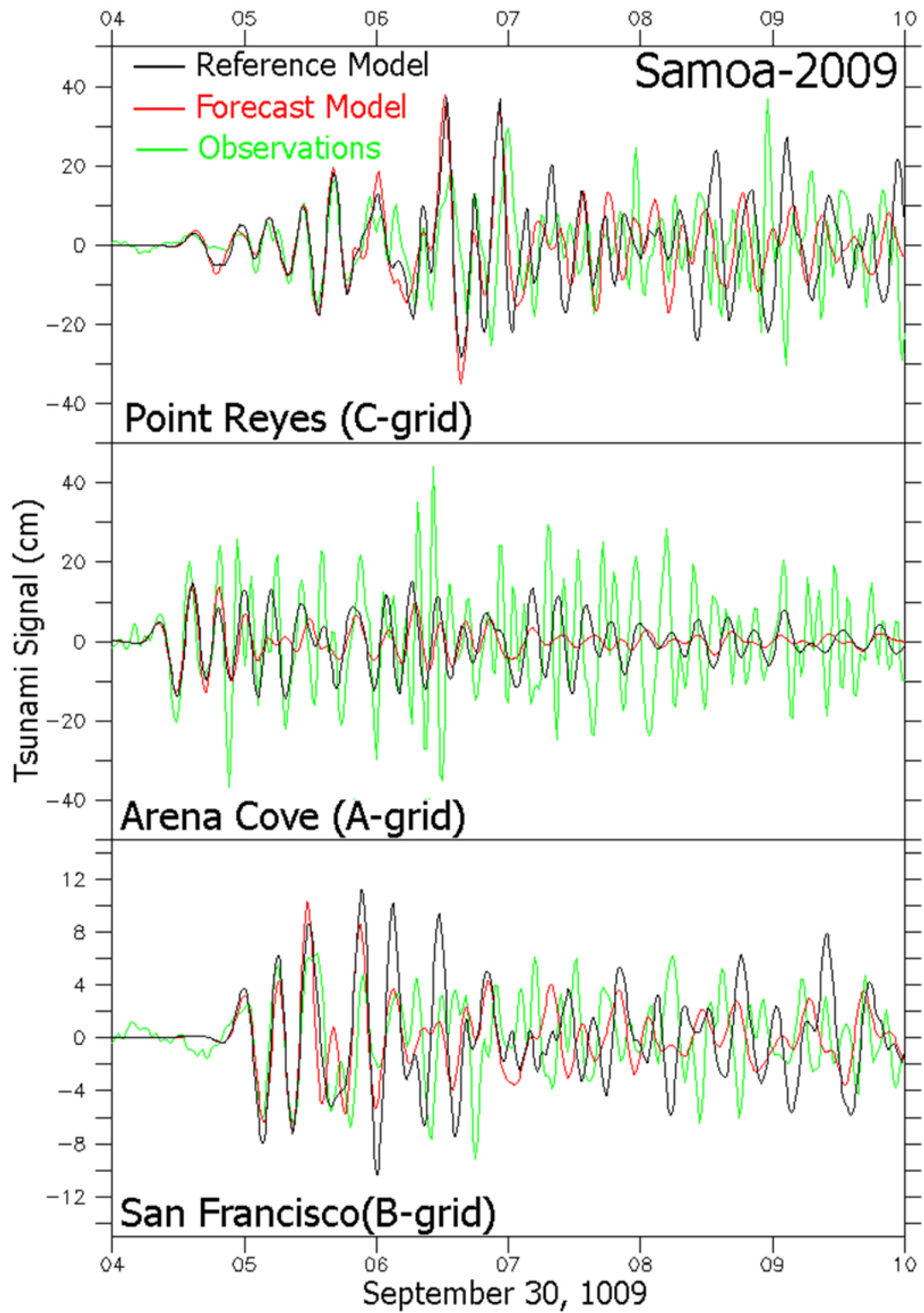


Figure 22. Model and observed time series comparison for the Samoa-2009 event.

Kuril-2006

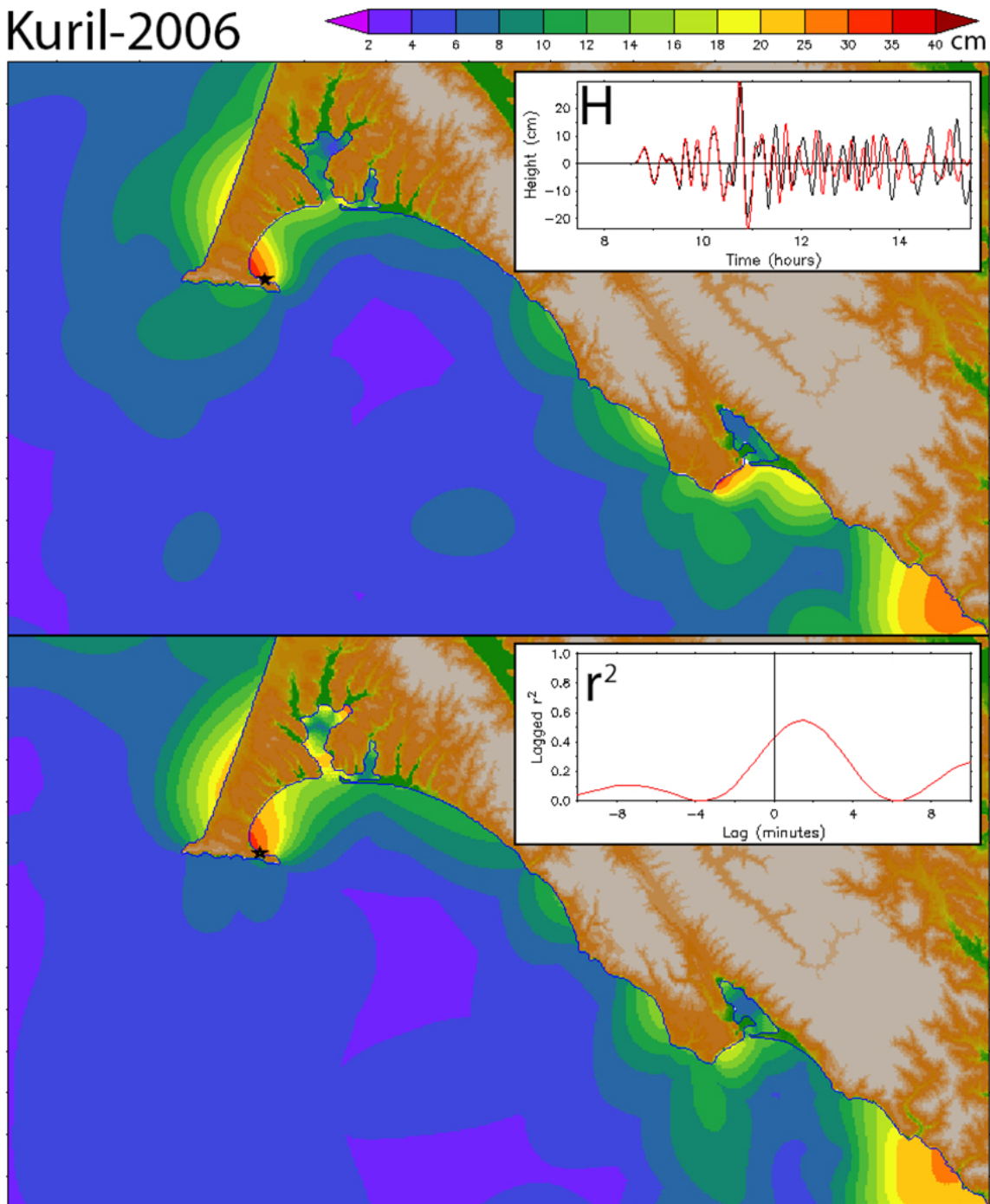


Figure 23. RM and FM comparison, as in Figure 19 but for the Kuril-2006 event.
a) Maximum amplitude for the RM (upper panel) and FM (lower panel).

Kuril-2006

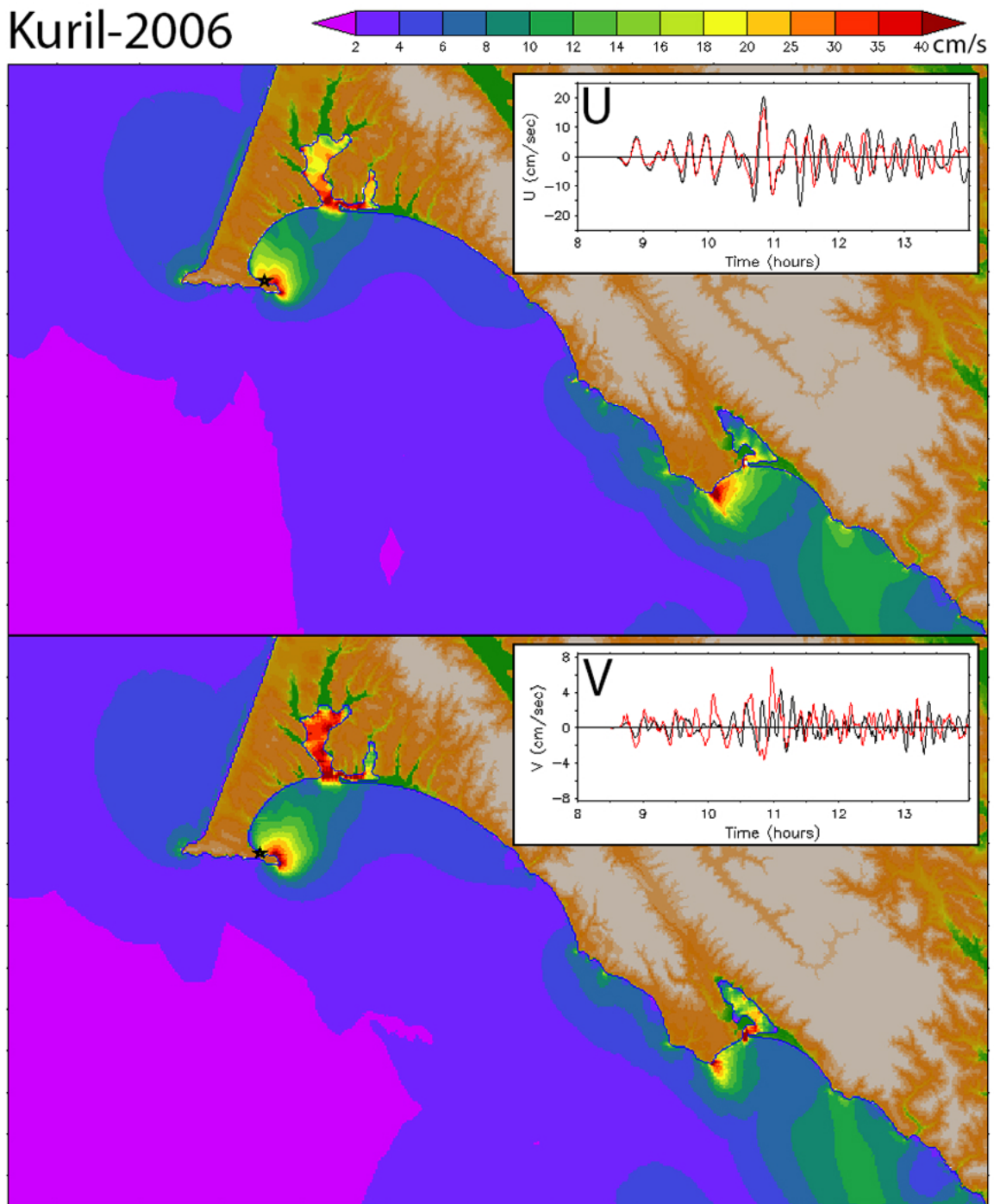


Figure 23 continued. RM and FM comparison, as in Figure 19 but for the Kuril-2006 event.
b) Maximum speed for the RM (upper panel) and FM (lower panel).

Kuril-2006

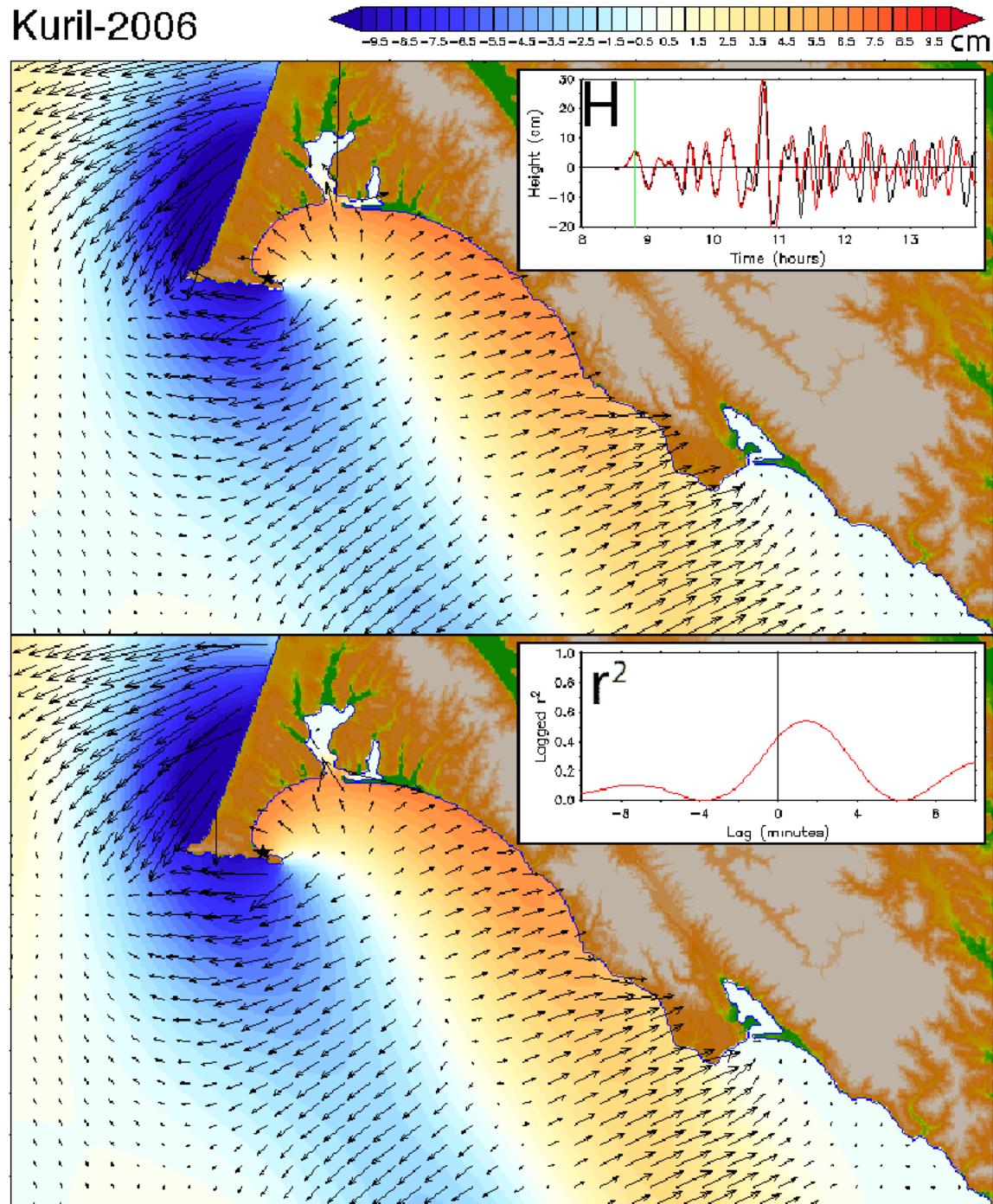


Figure 23 continued. RM and FM comparison, as in Figure 19 but for the Kuril-2006 event.
c) snapshot of amplitude and current at the indicated time.

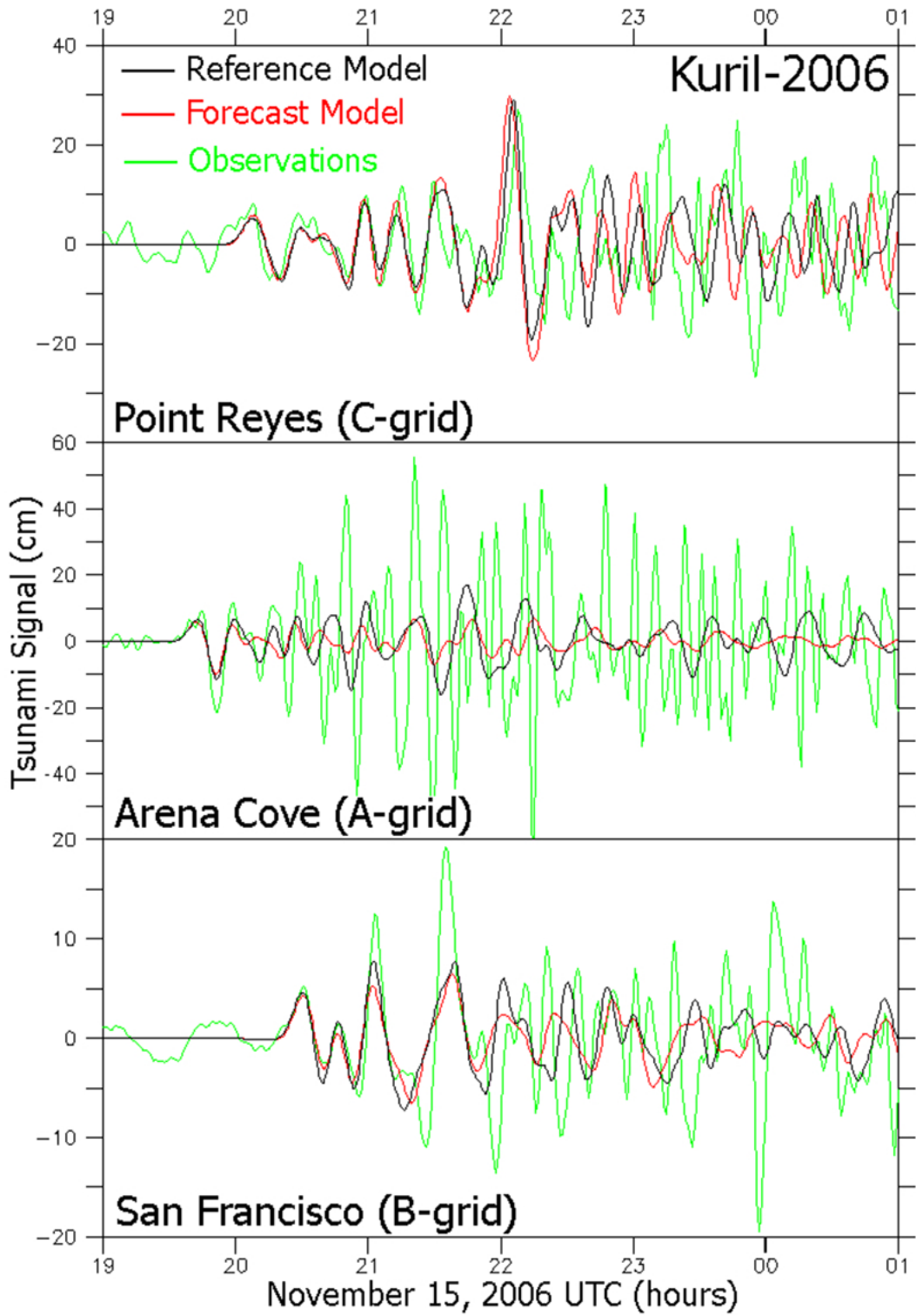


Figure 24. Model and observed time series comparison for the Kuril-2006 event.

Alaska-1964

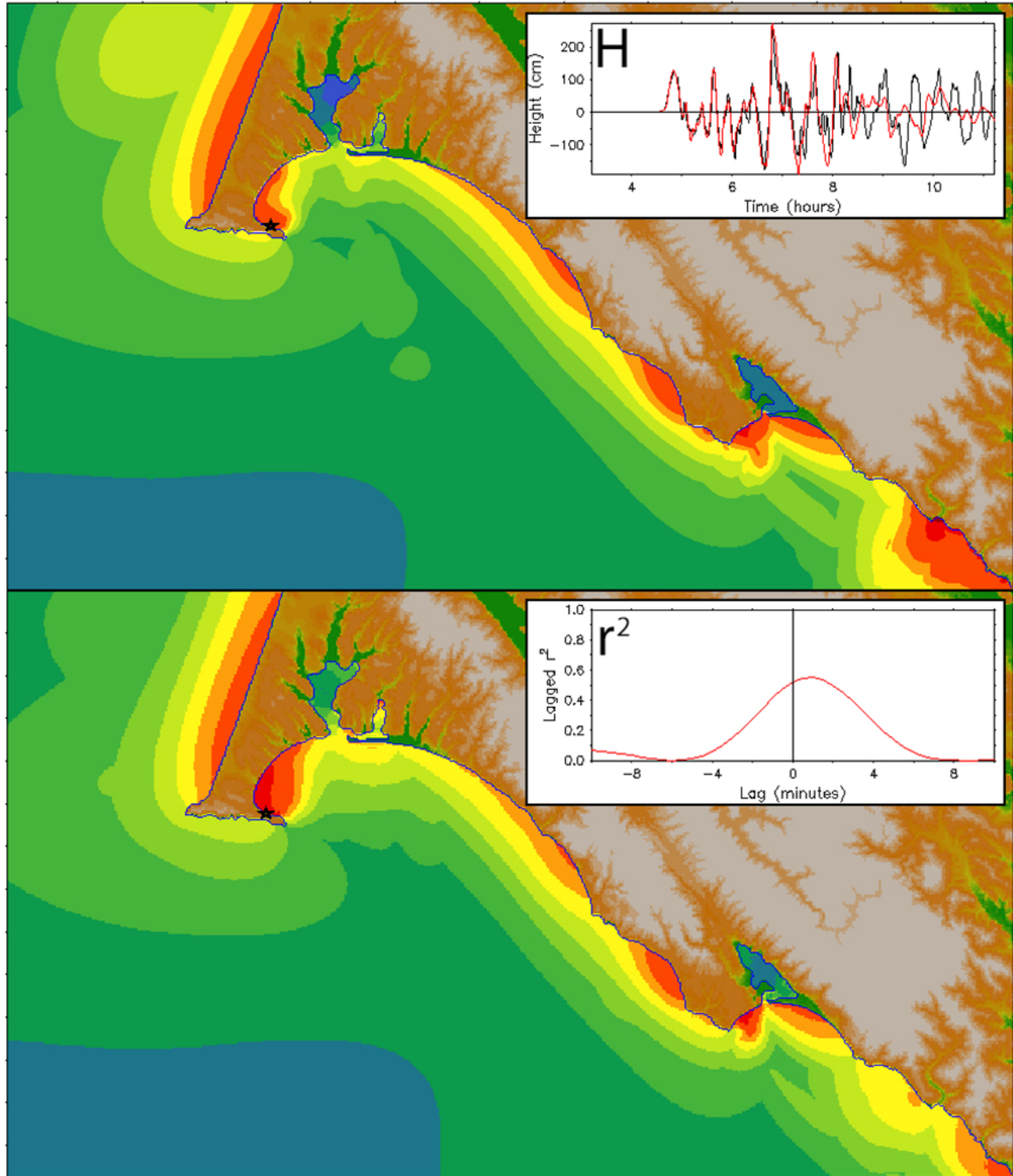
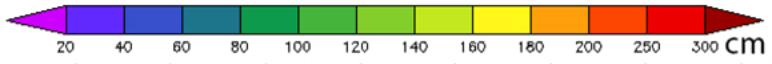


Figure 25. RM and FM comparison, as in Figure 19 but for the Alaska-1964 event.
a) Maximum amplitude for the RM (upper panel) and FM (lower panel).

Alaska-1964

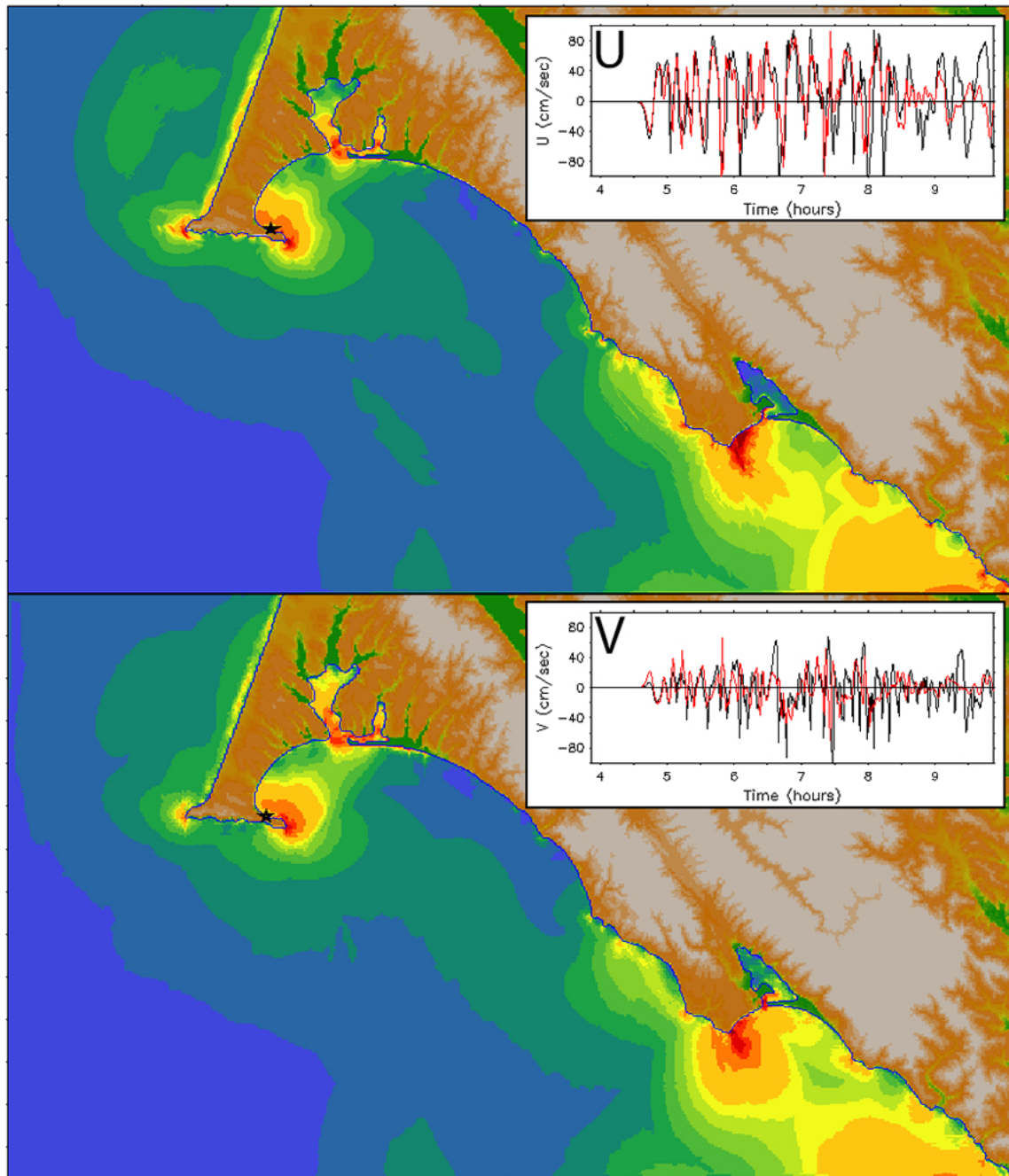


Figure 25 continued. RM and FM comparison, as in Figure 19 but for the Alaska-1964 event.
b) Maximum speed for the RM (upper panel) and FM (lower panel).

Alaska-1964

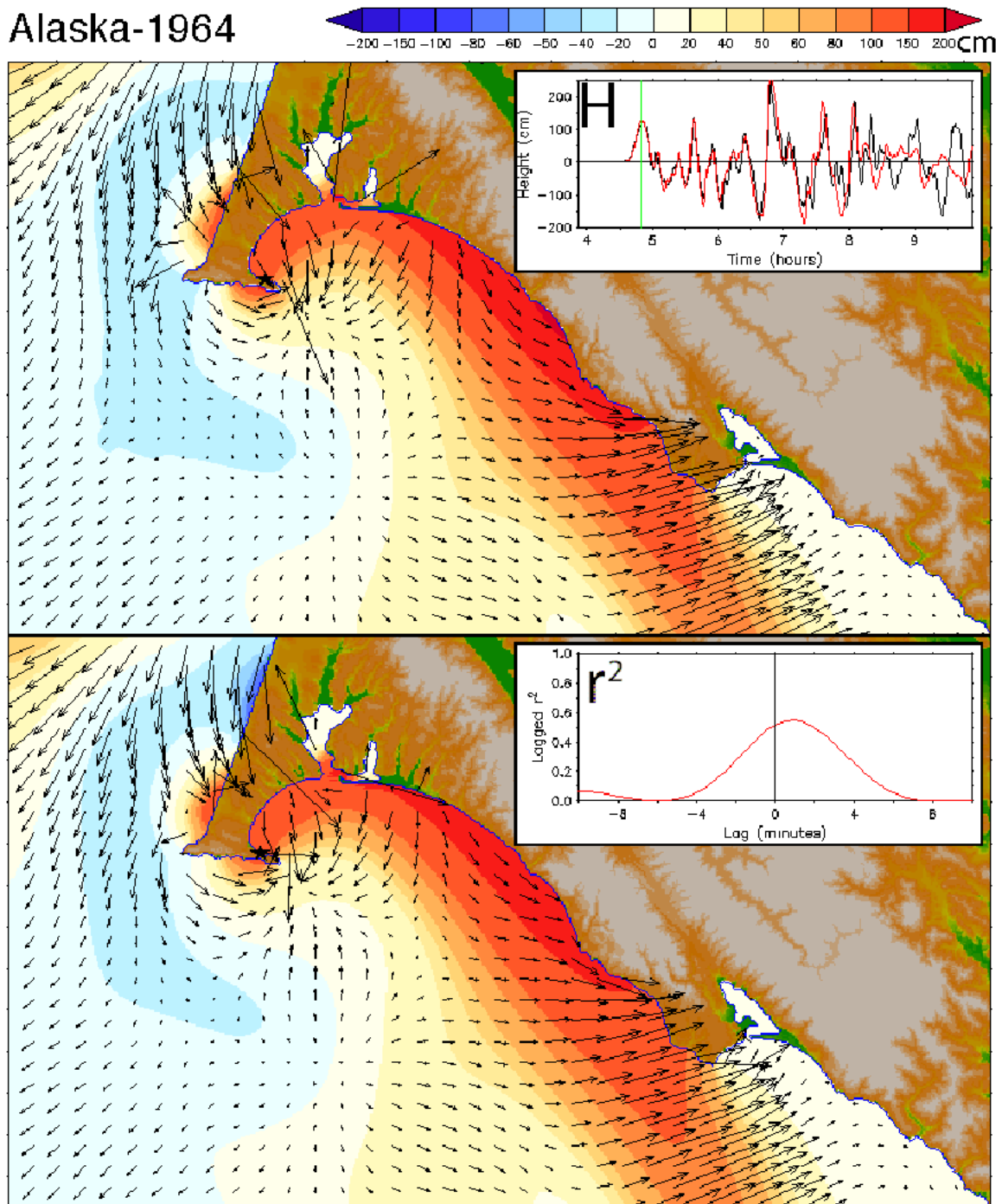


Figure 25 continued. RM and FM comparison, as in Figure 19 but for the Alaska-1964 event.
c) snapshot of amplitude and current at the indicated time.

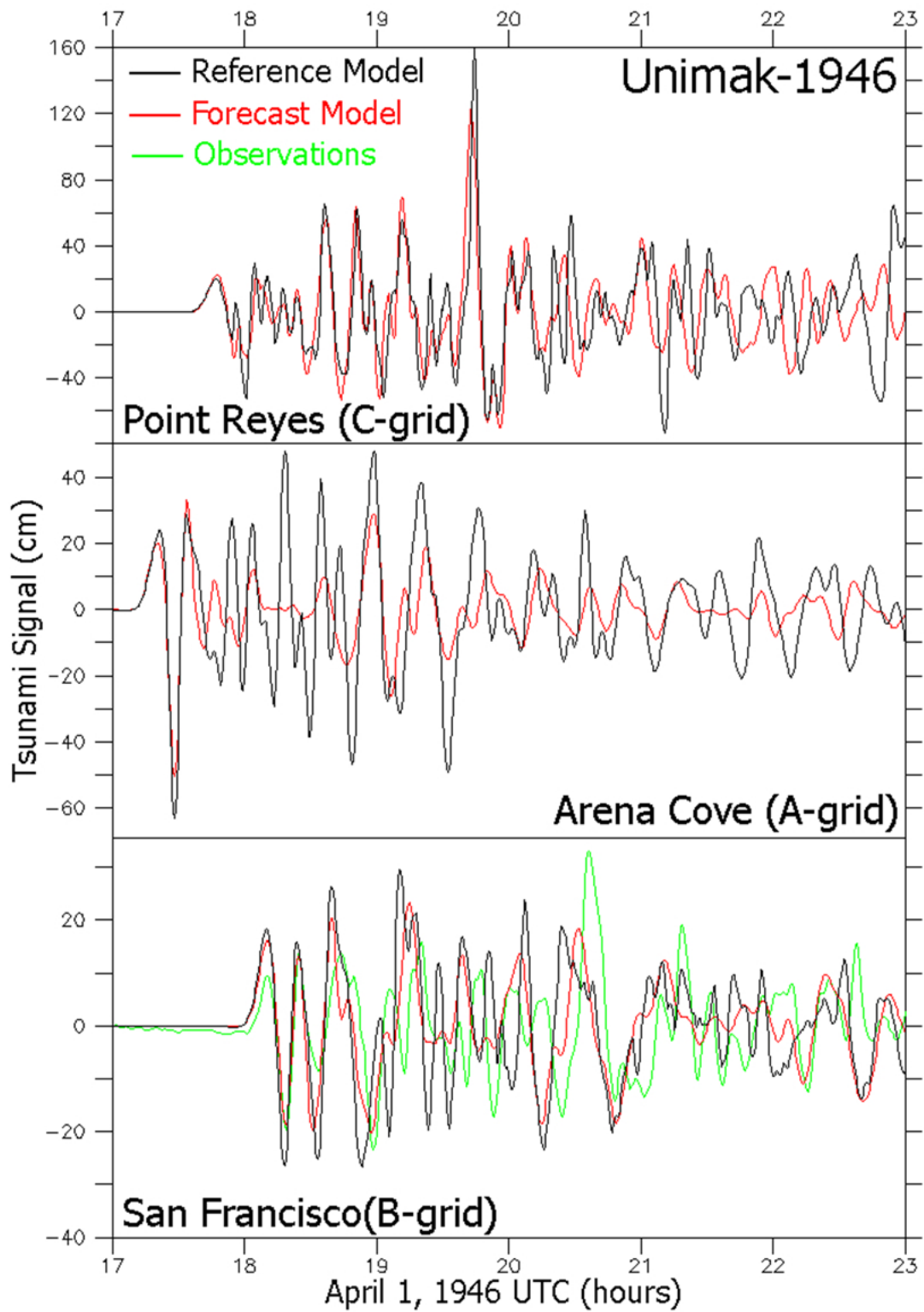


Figure 26. Model and observed time series comparison for the Alaska-1964 event.

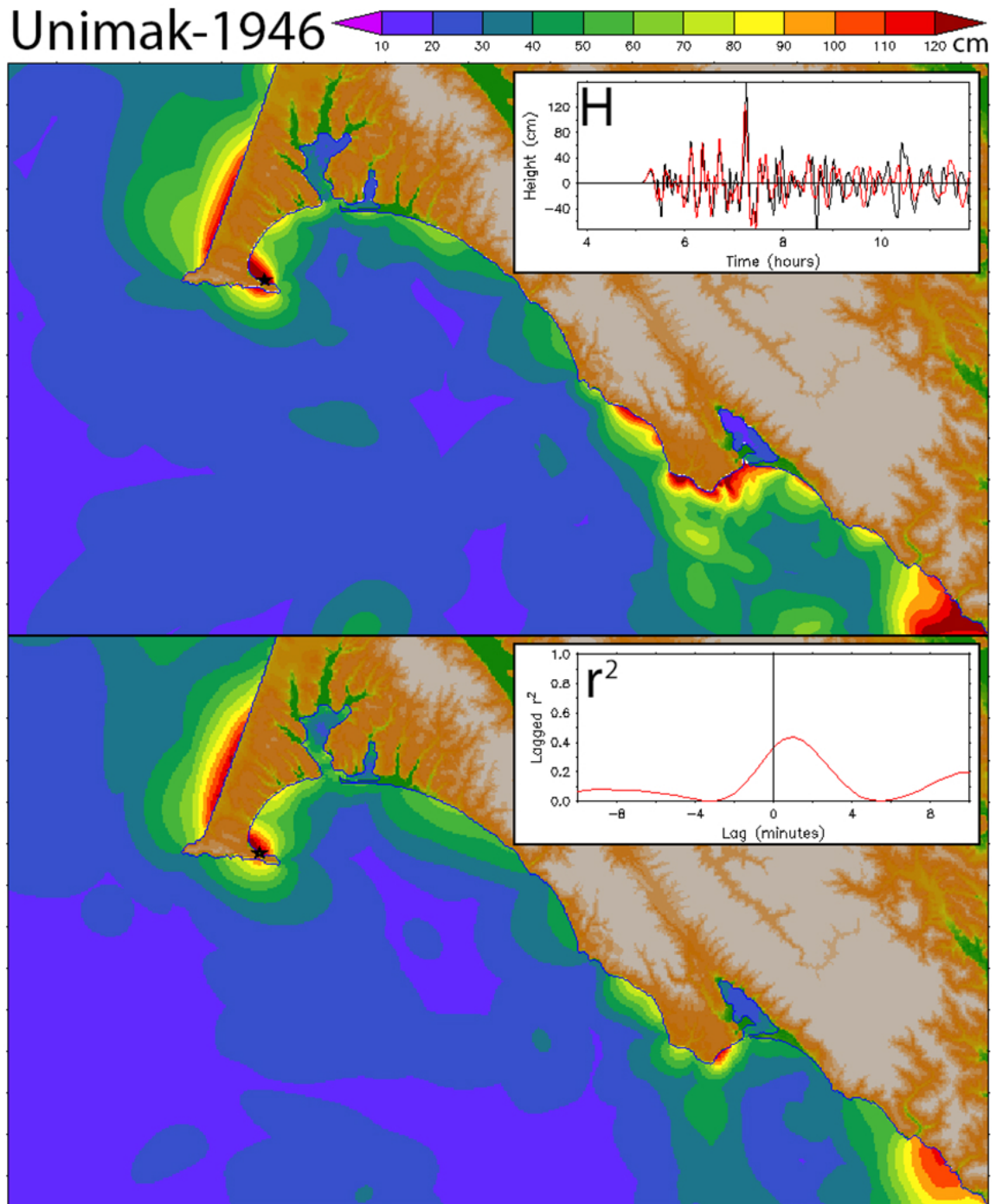


Figure 27. RM and FM comparison, as in Figure 19 but for the Unimak-1946 event.
 a) Maximum amplitude for the RM (upper panel) and FM (lower panel).

Unimak-1946

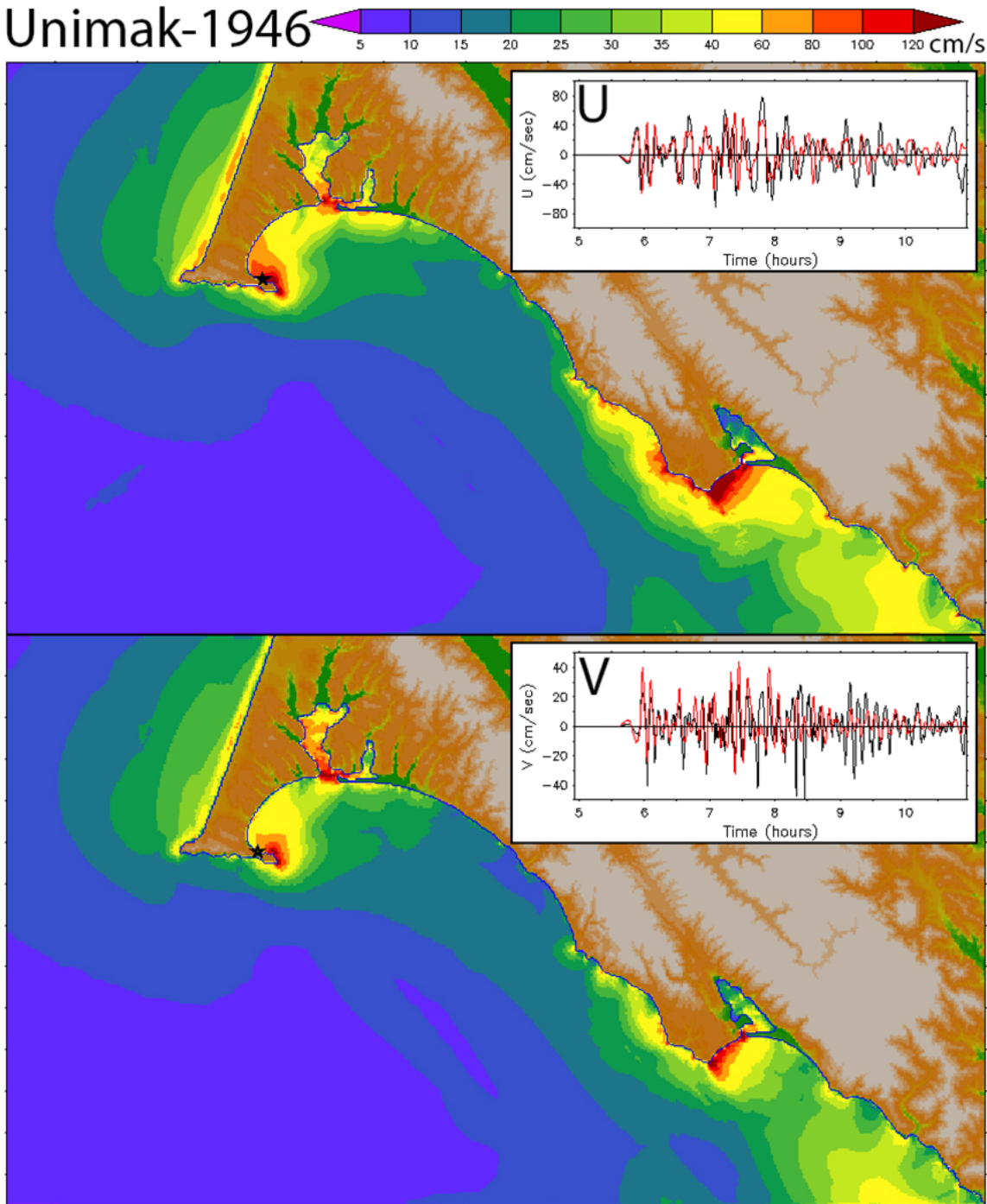


Figure 27continued. RM and FM comparison, as in Figure 19 but for the Unimak-1946 event.
b) Maximum speed for the RM (upper panel) and FM (lower panel).

Unimak-1946

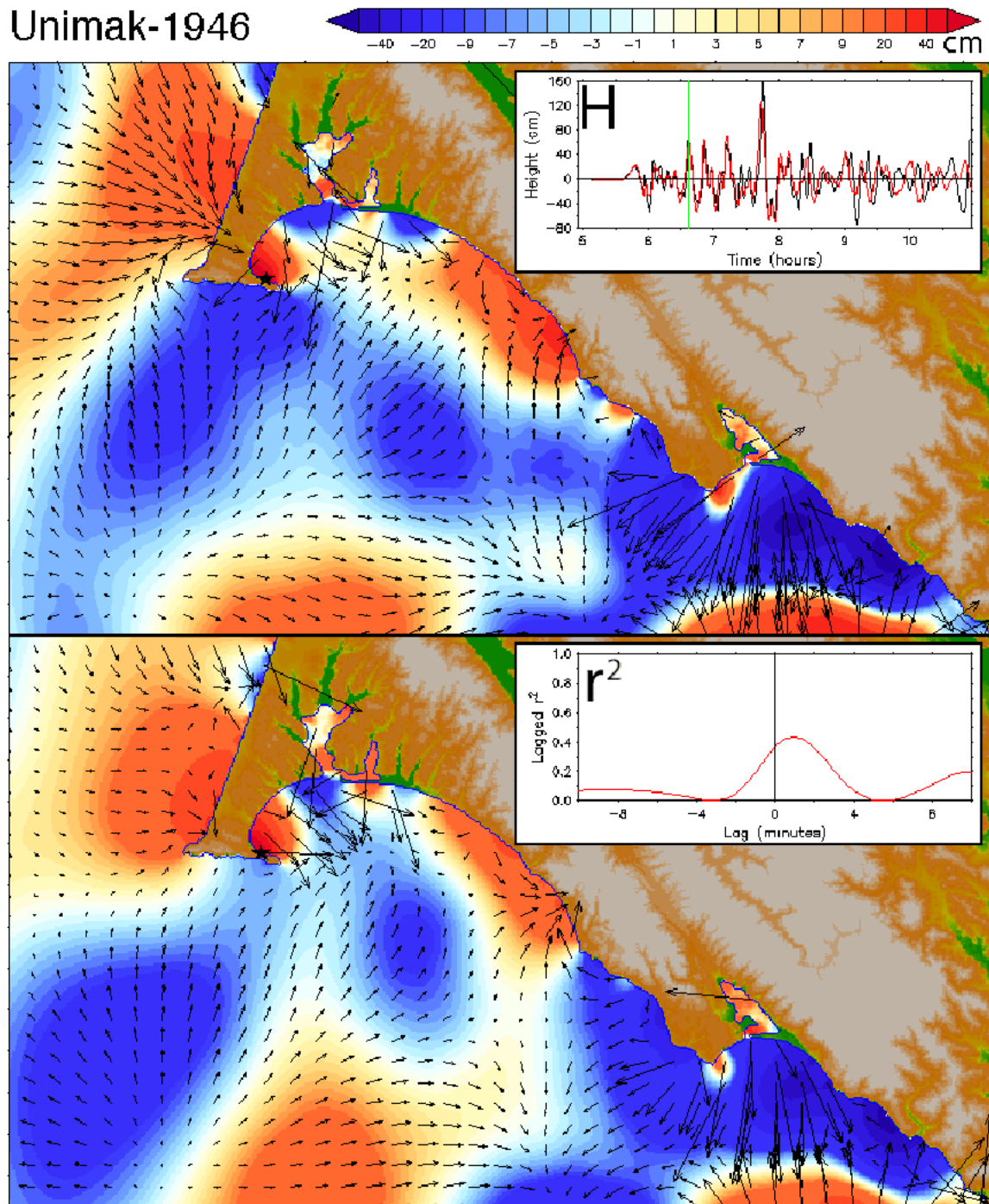


Figure 27 continued. RM and FM comparison, as in Figure 19 but for the Unimak-1946 event.
c) snapshot of amplitude and current at the indicated time.

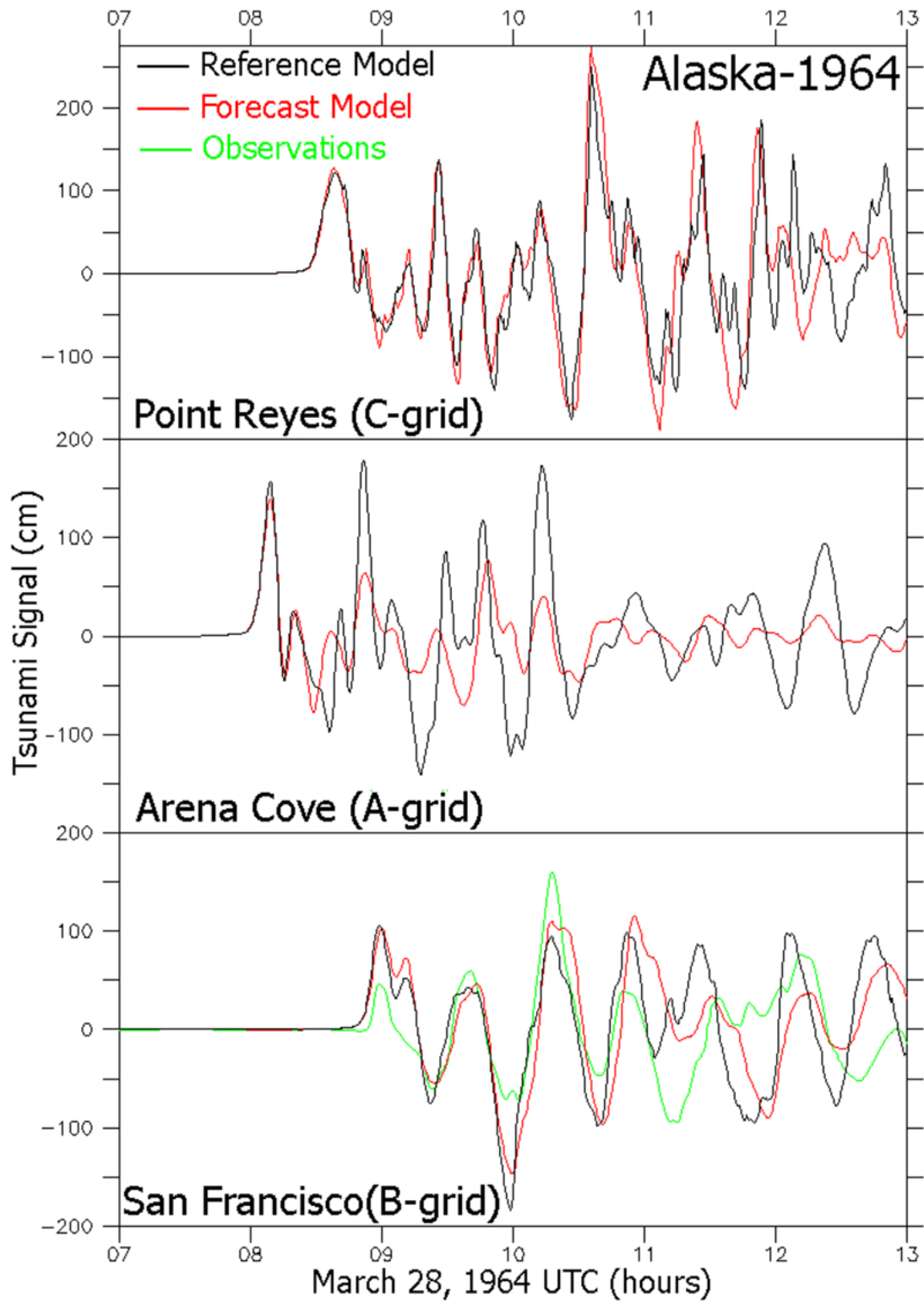


Figure 28. Model and observed time series comparison for the Unimak-1946 event.

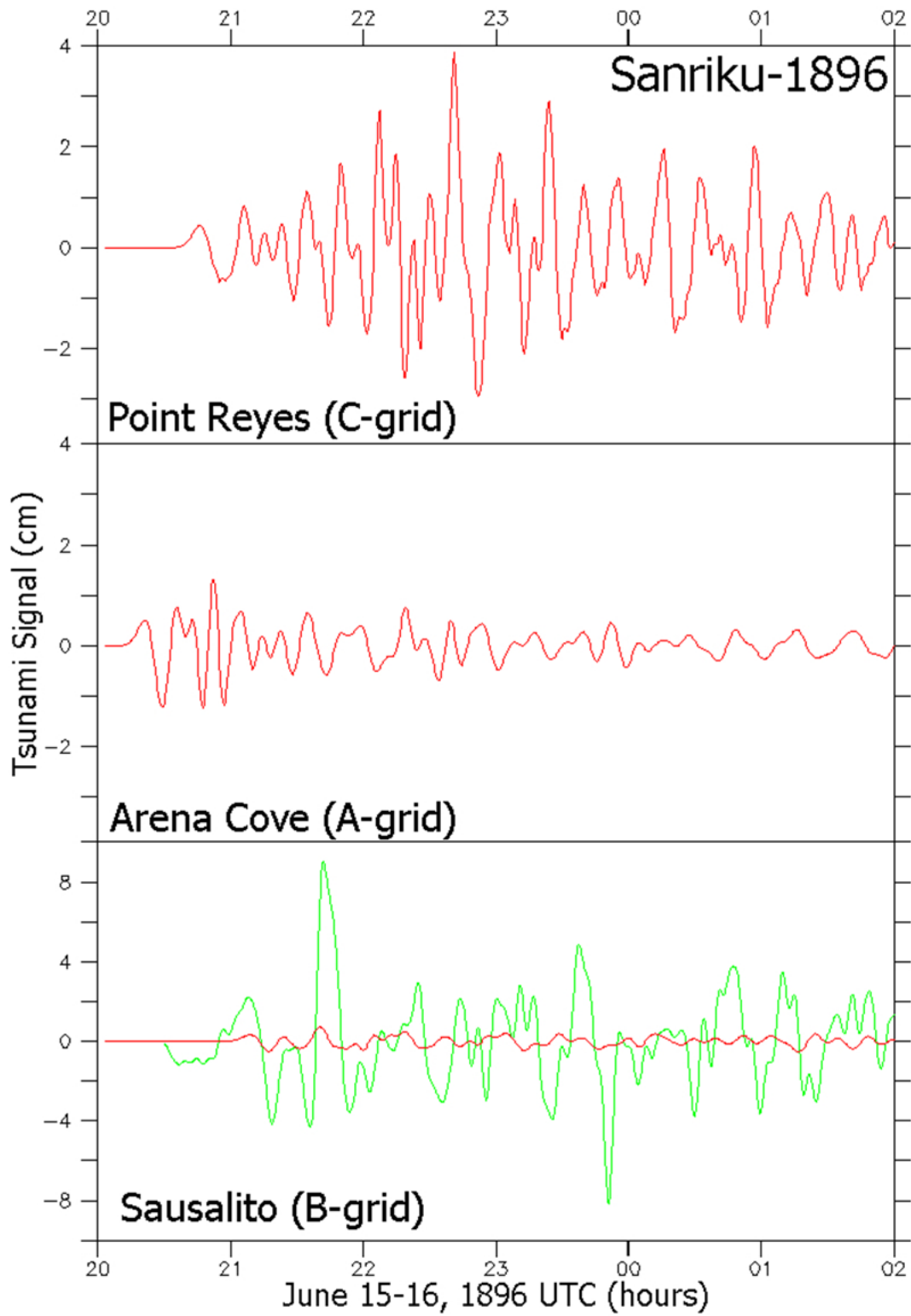


Figure 29. The Sanriku event of June 15, 1896.

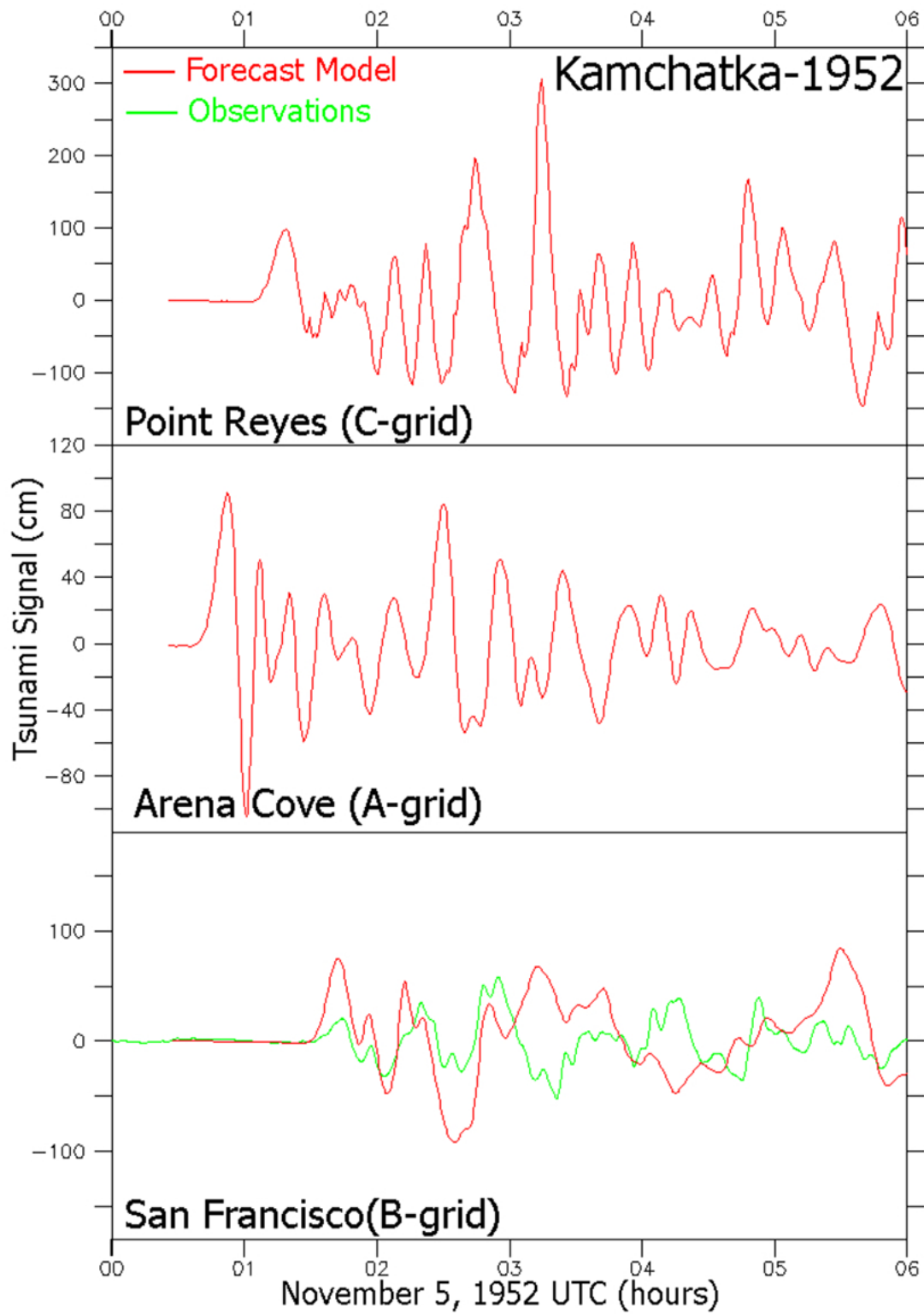


Figure 30. The Kamchatka event of November 4, 1952.

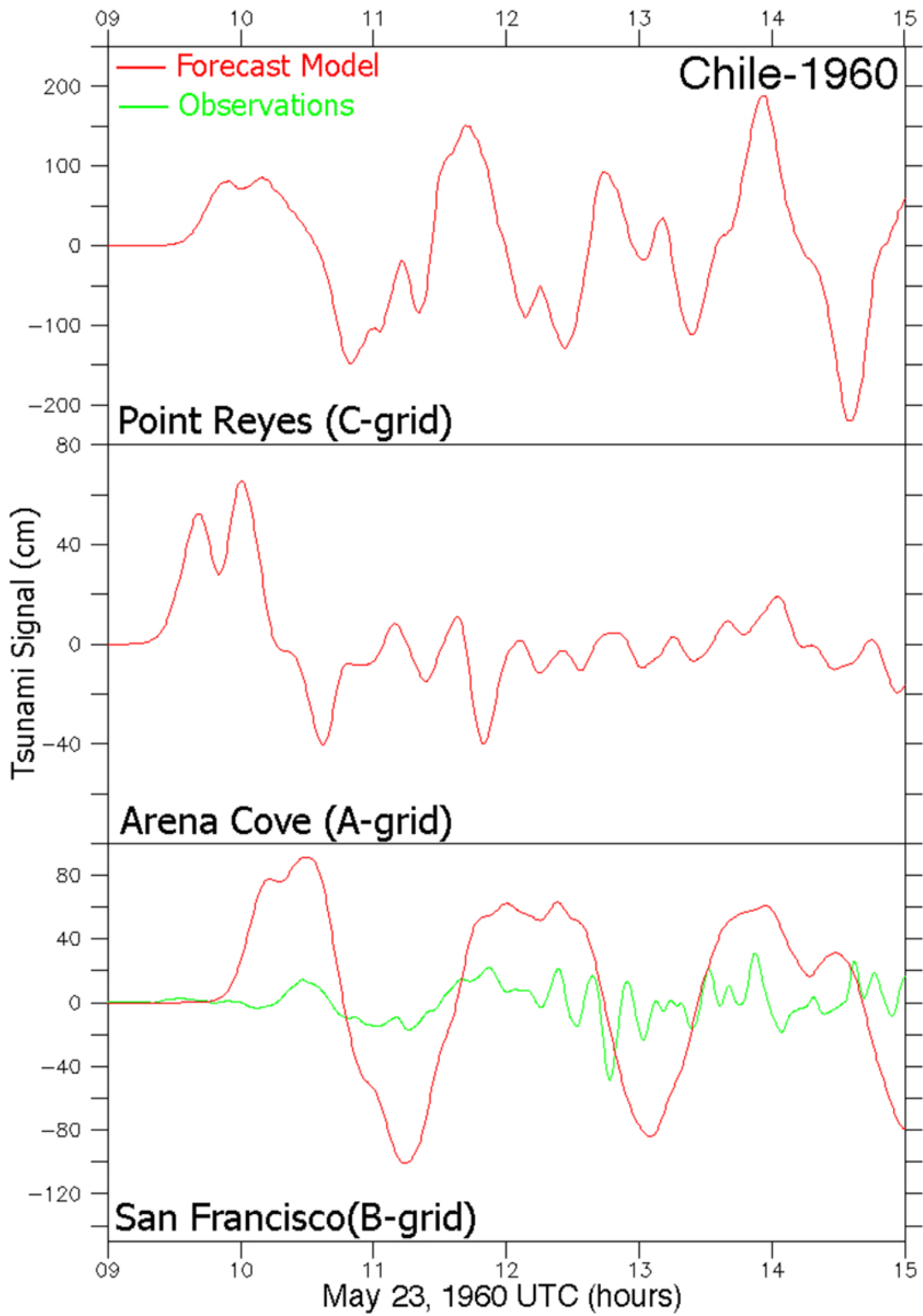


Figure 31. The Chile event of May 22, 1960.

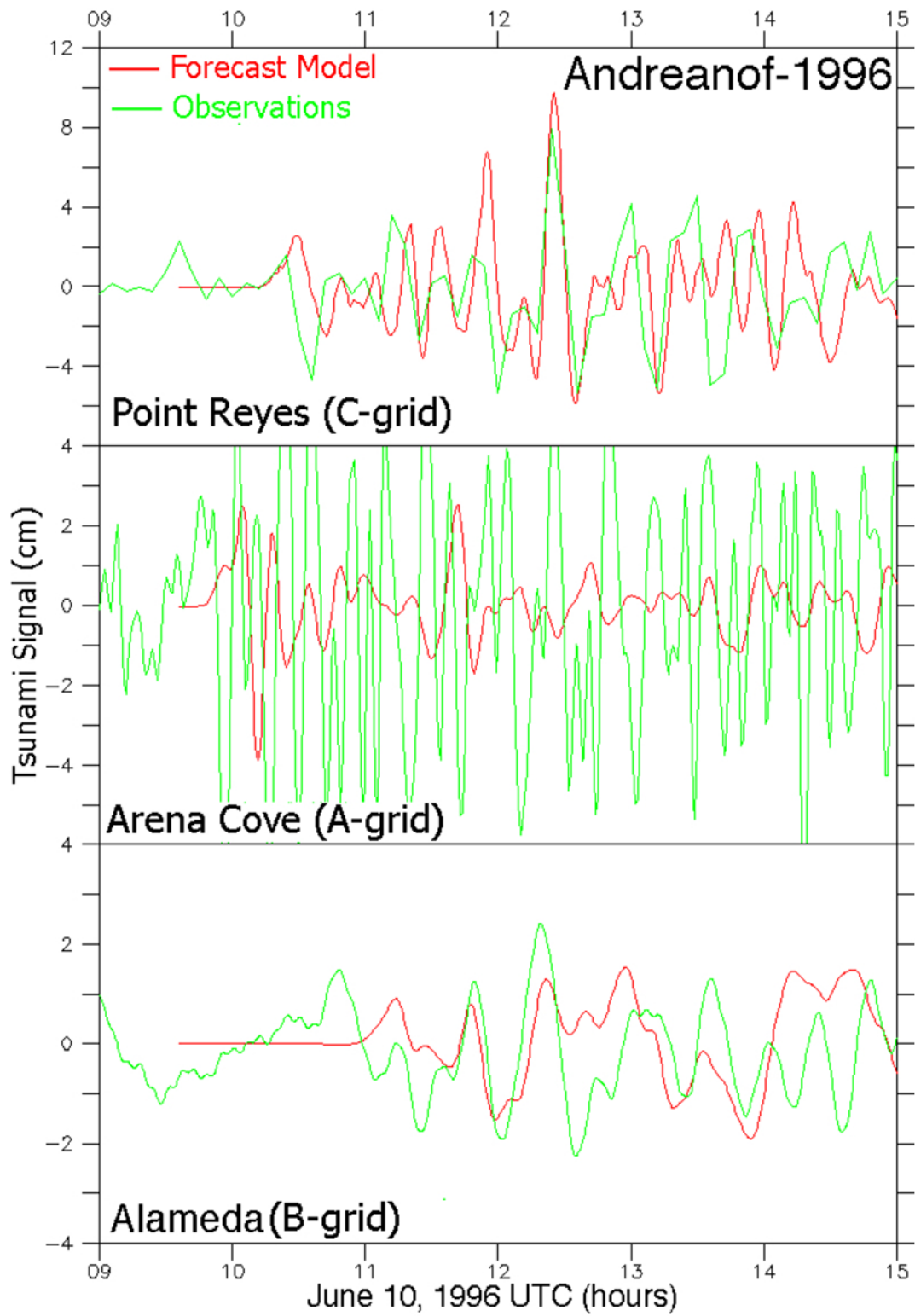


Figure 32. The Andreanof event of June 10, 1996.

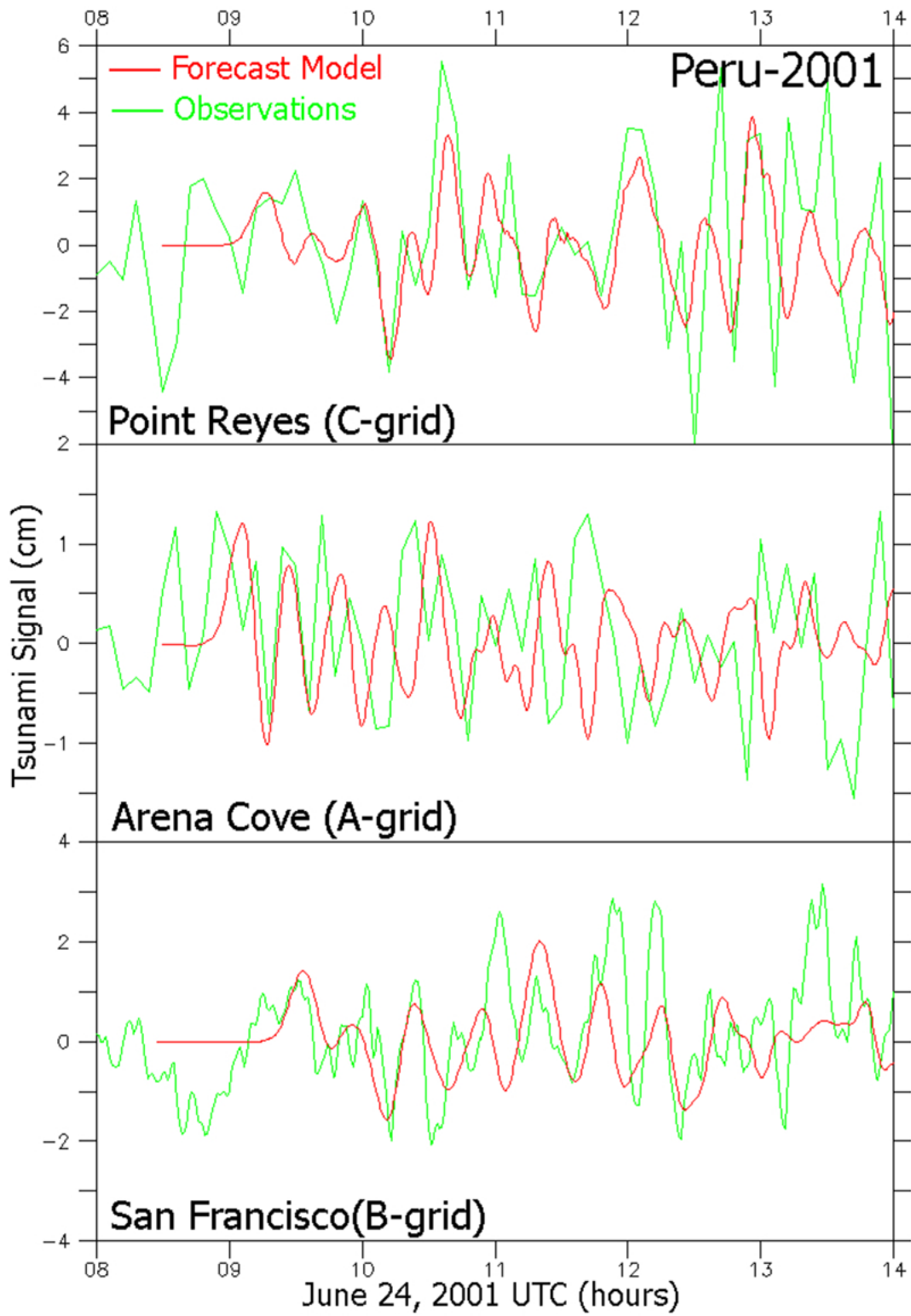


Figure 33. The Peru event of June 23, 2001.

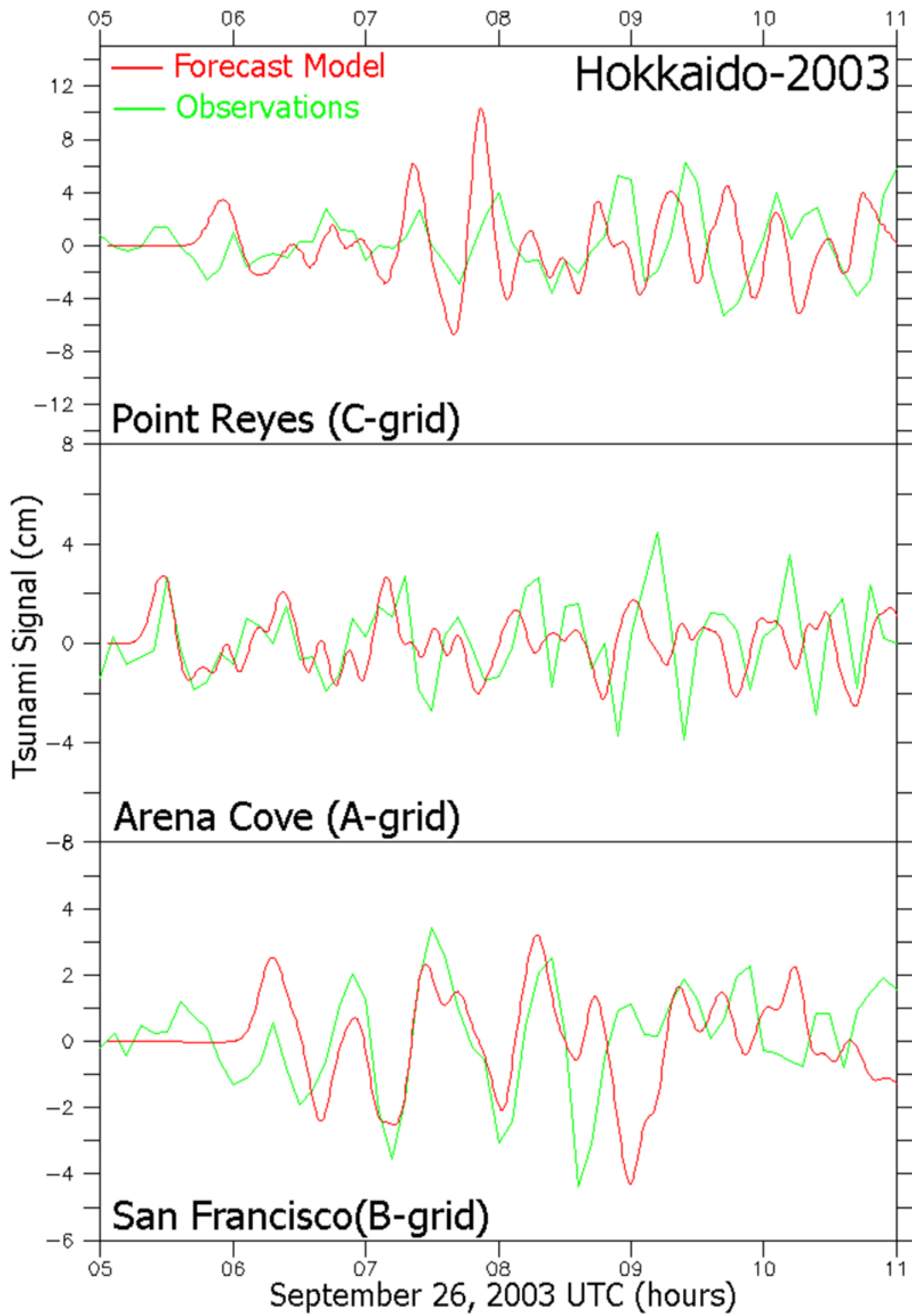


Figure 34. The Hokkaido event of September 25, 2003.

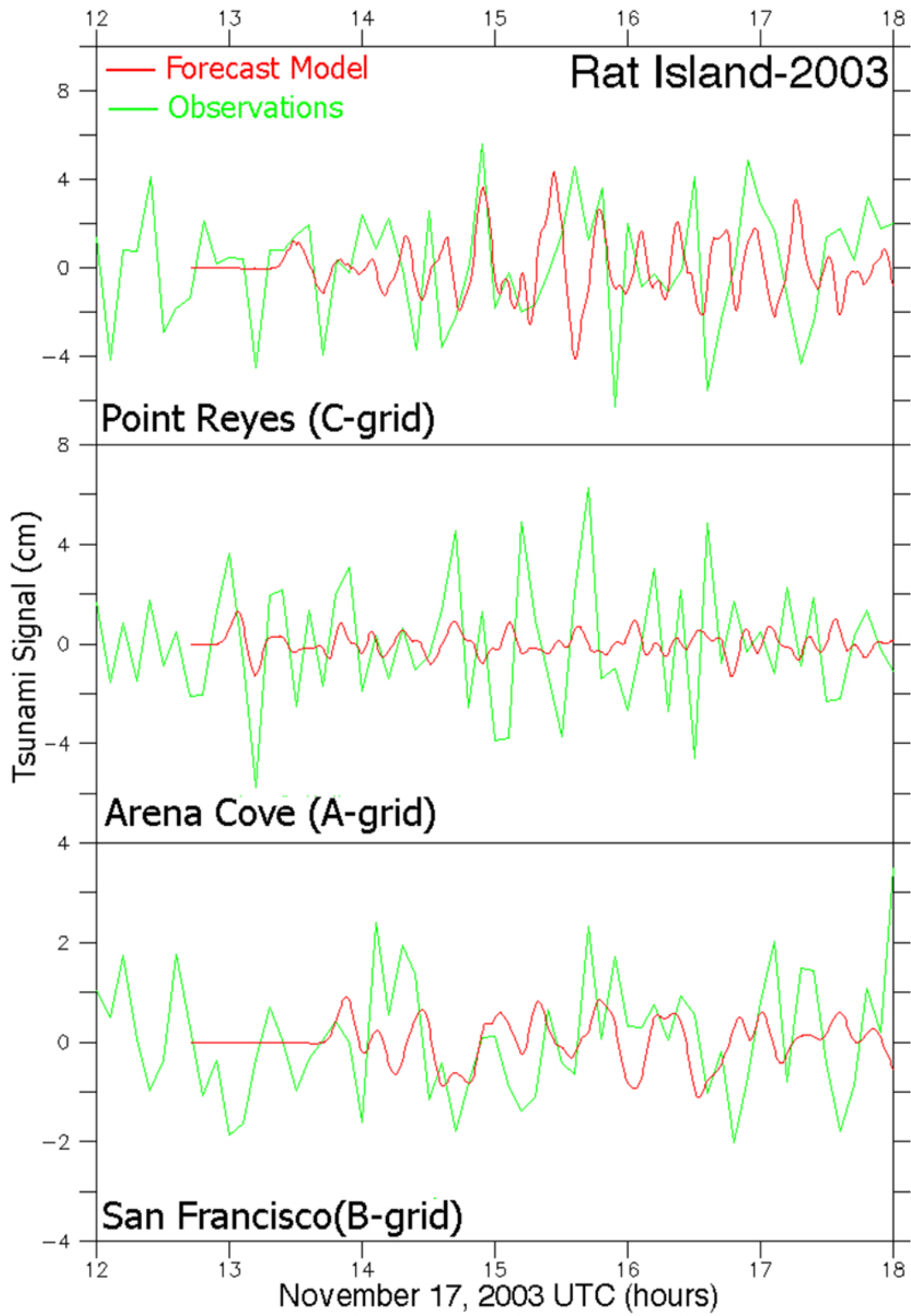


Figure 35. The Rat Island event of November 17, 2003.

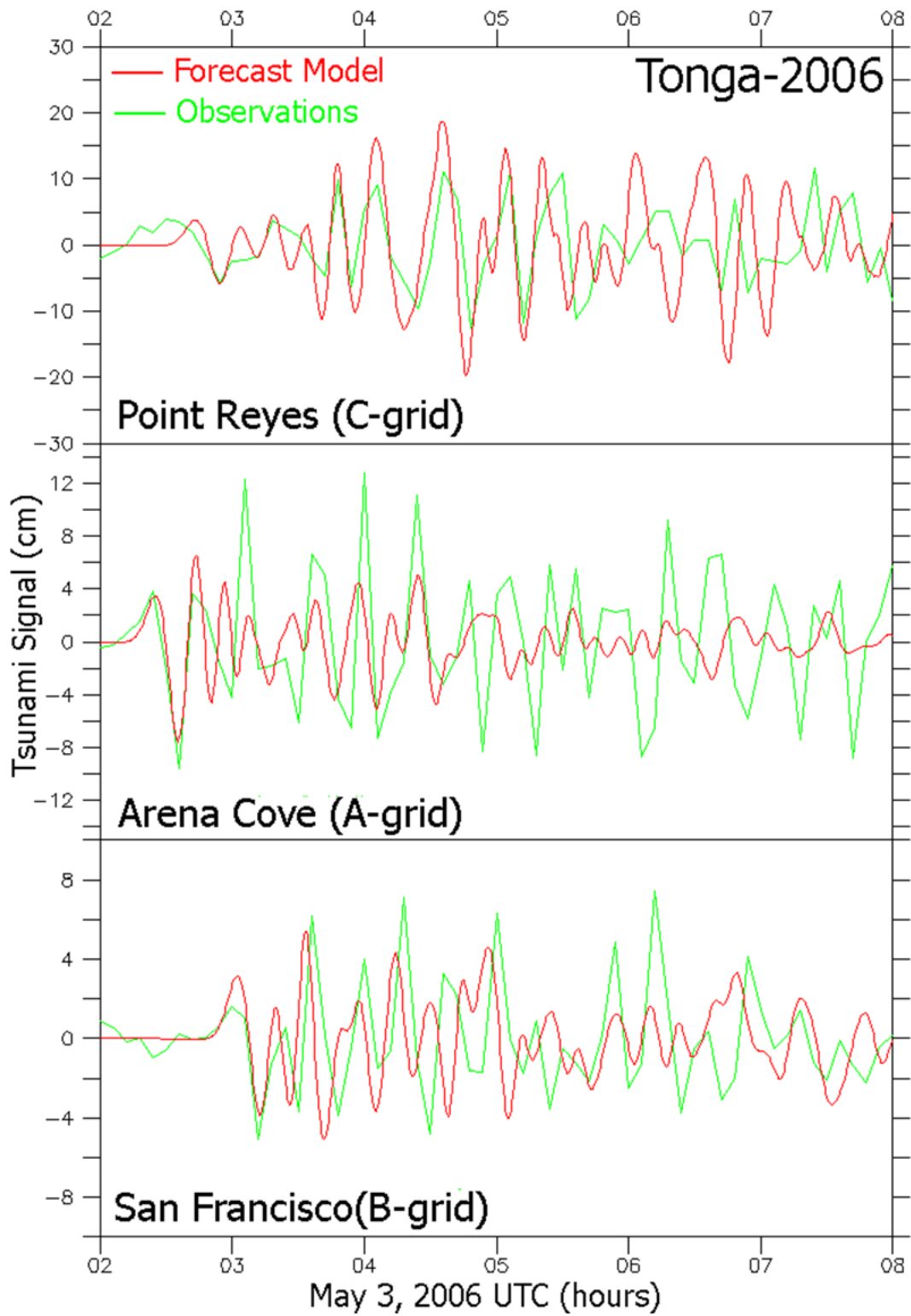


Figure 36. The Tonga event of May 3, 2006.

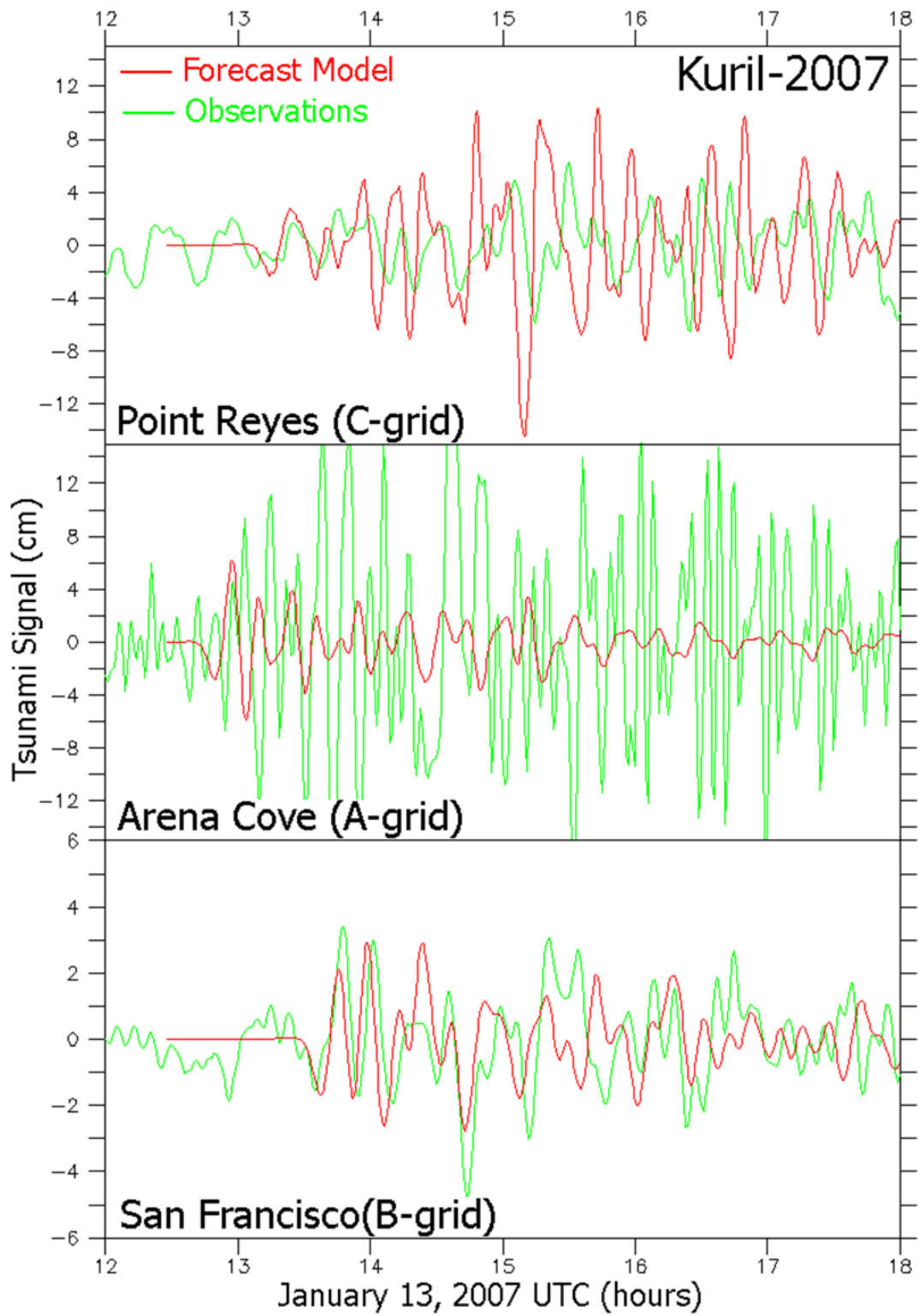


Figure 37. The normal thrust event off the Kuril Islands on January 13, 2007.

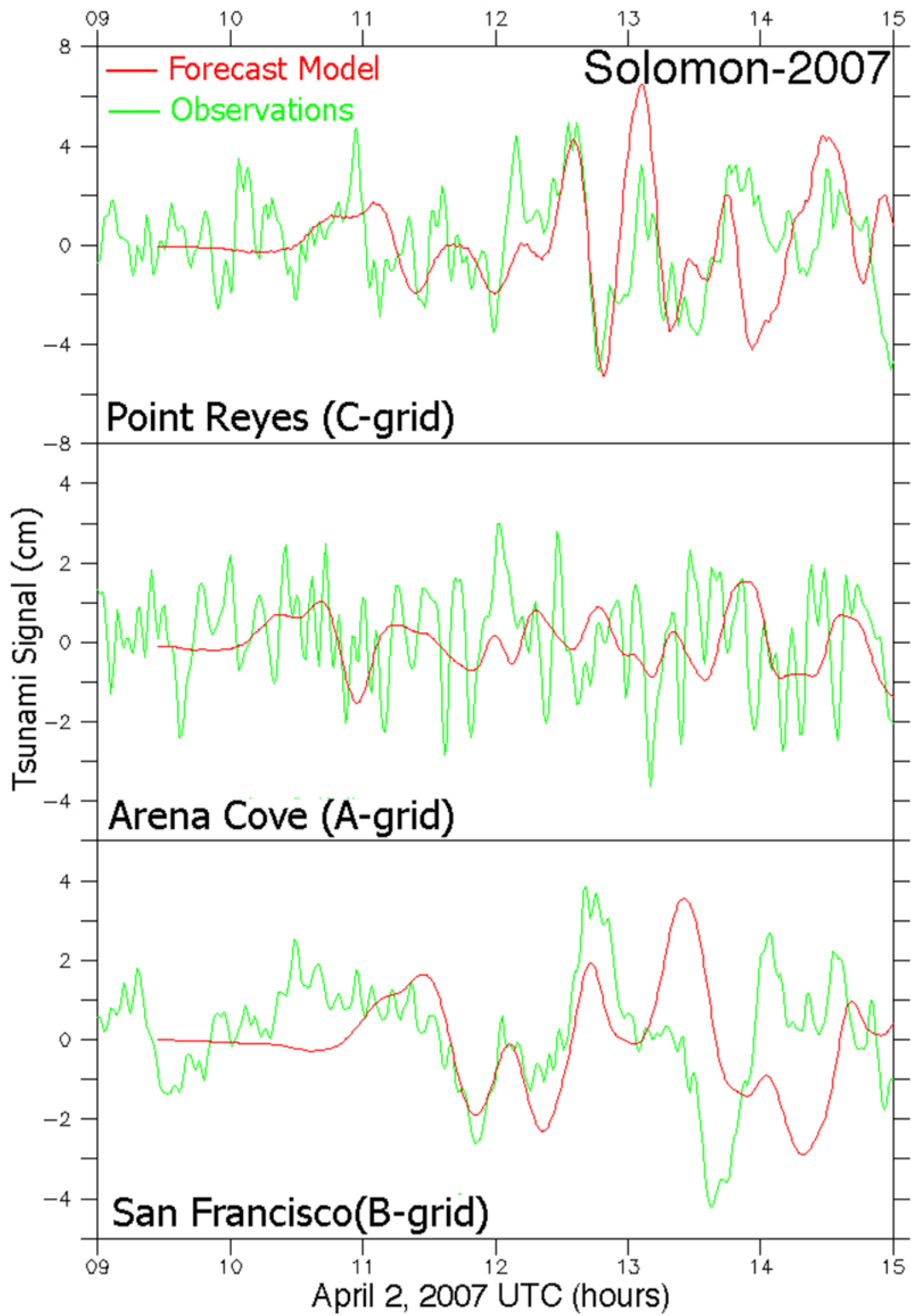


Figure 38. The Solomon event of April 1, 2007.

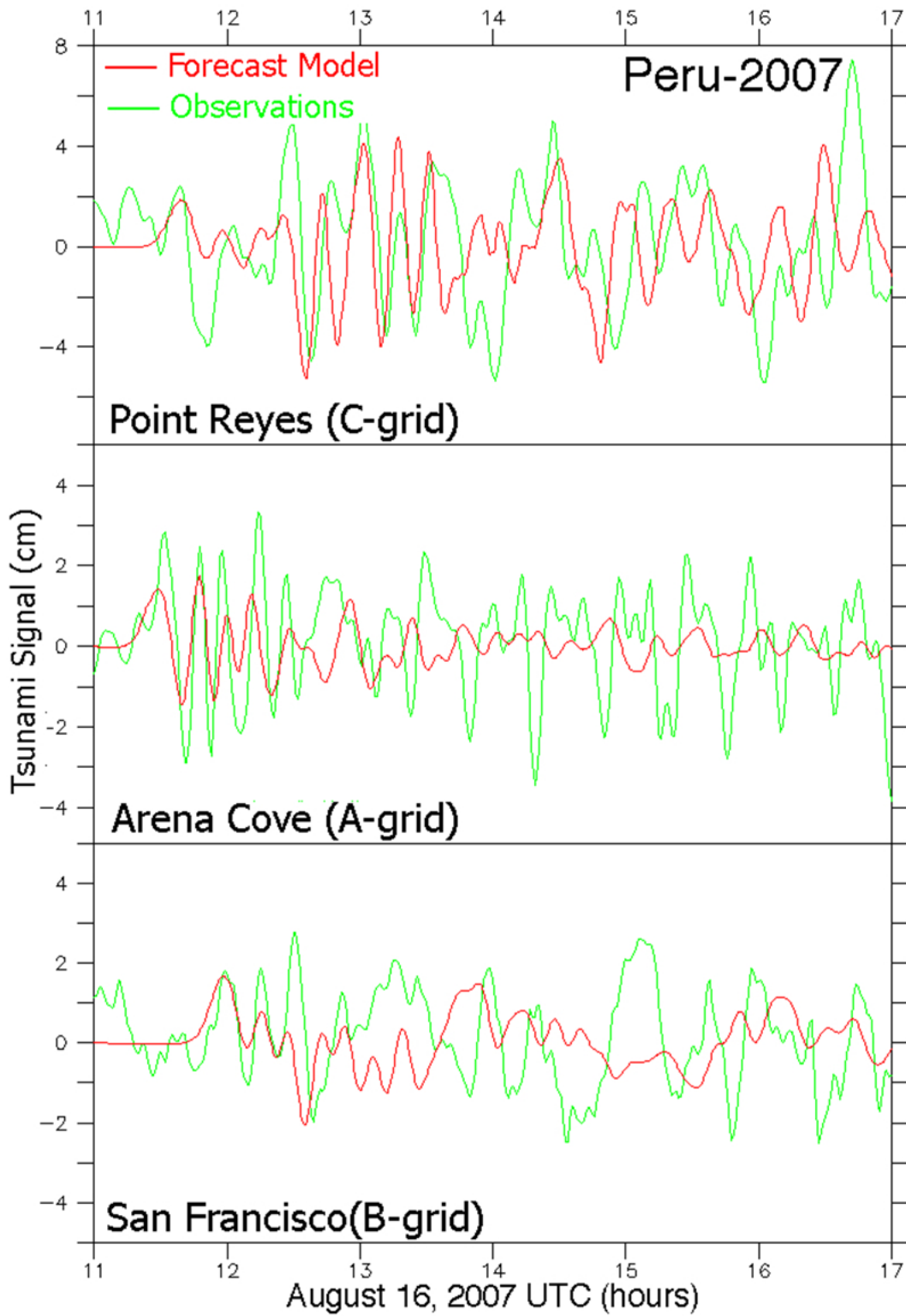


Figure 39. The Peru event of August 15, 2007.

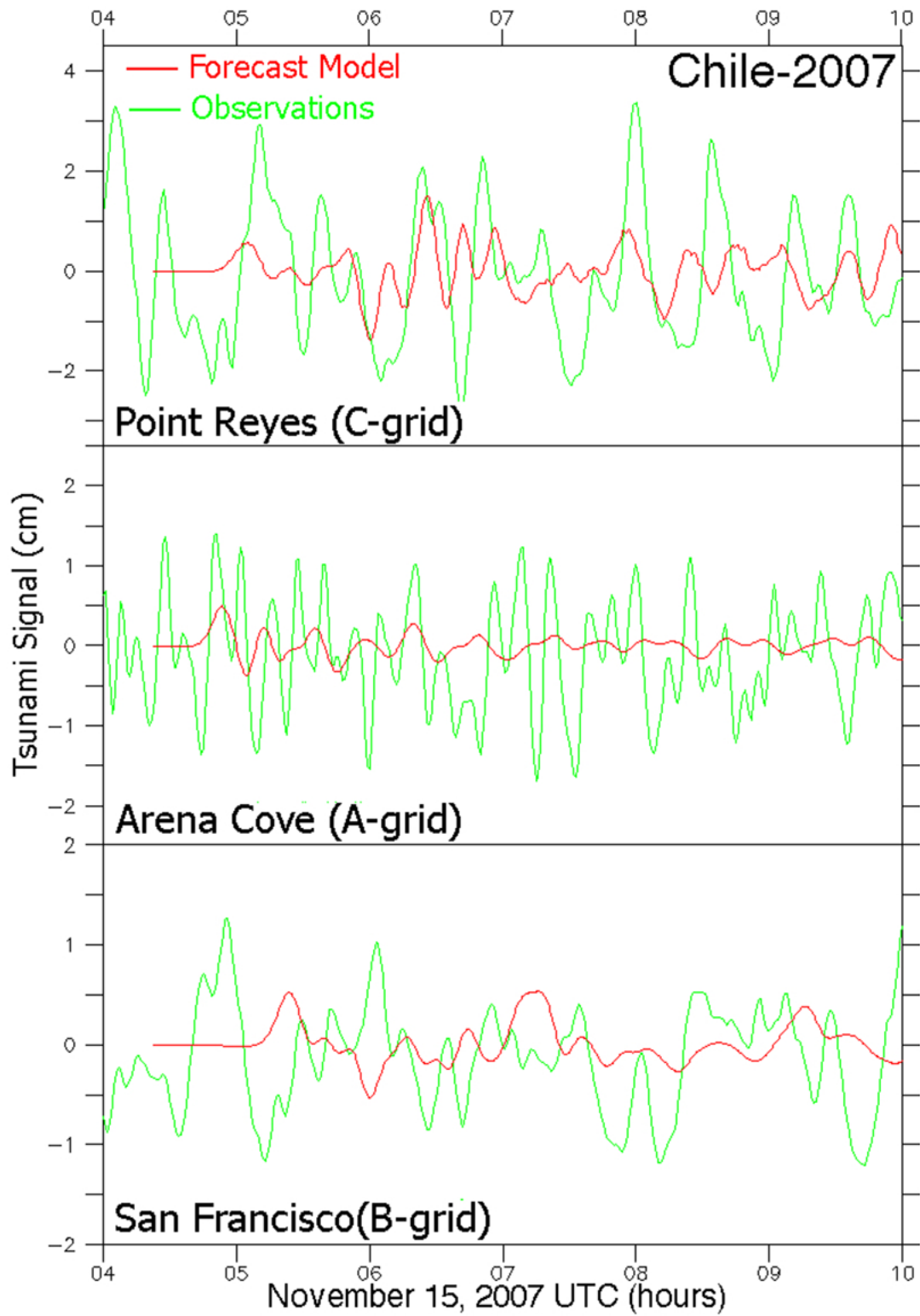


Figure 40. The Chile event of November 14, 2007.

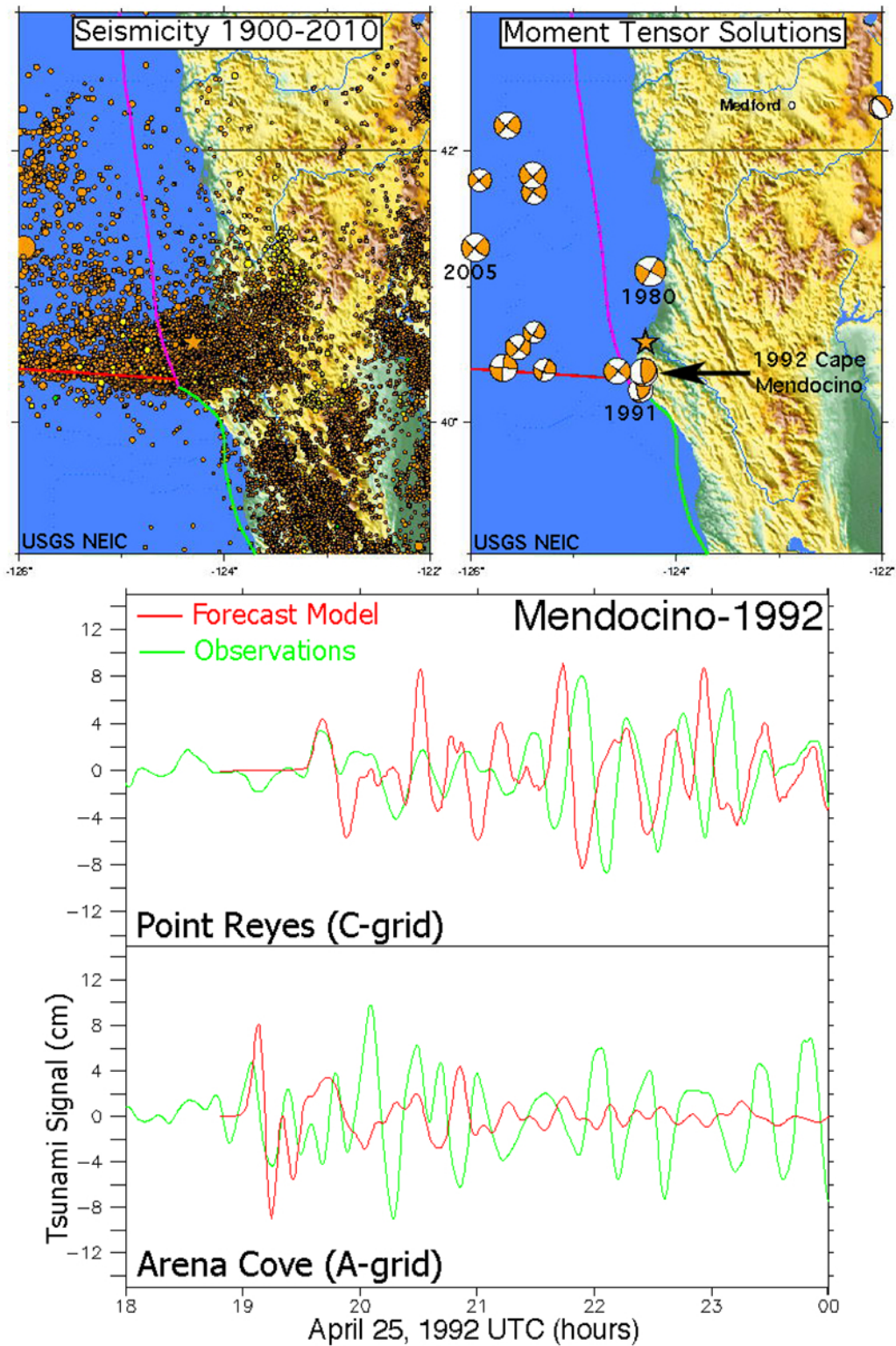


Figure 41. The Cape Mendocino event of April 25, 1992. The upper panels show the frequency of non-thrust events in the vicinity, with only two having a focal mechanism characteristic of subduction. Lower panel: comparison of model with observation at Arena Cove and Point Reyes.

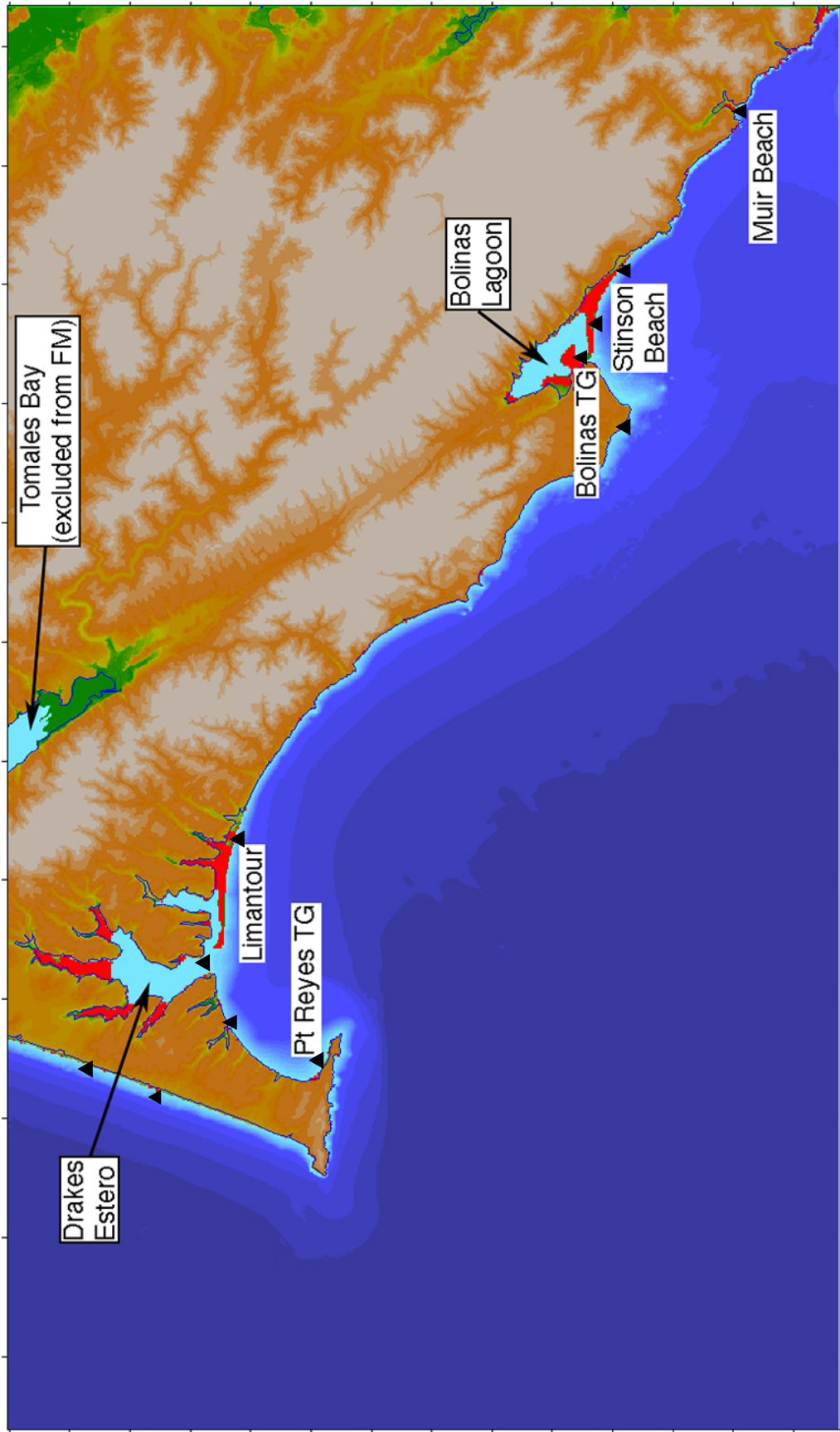


Figure 43. Chart of the area inundated by one or more of the mega-tsunami scenarios modeled with the FM. Shown in blue is the CalEMA inundation line, which is based on a similar ensemble of scenarios.

Appendix A

A1. Reference Model Input (*.in) File for Point Reyes, CA

The following table contains the parameter and file choices used in the input file for the SIFT implementation (most3_facts_nc.in) of the reference model (RM) for Point Reyes, CA.

Parameter/File*	Purpose
0.0010	Minimum amp. of input offshore wave (m)
1.5	Minimum depth of offshore (m)
0.1	Dry land depth of inundation (m)
0.0009	Friction coefficient (n^{*2})
1	Let A-Grid and B-Grid run up
900.0	Max eta before blow-up (m)
0.6	Time step (sec)
48000	Total number of time steps in run
2	Time steps between A-Grid computations
1	Time steps between B-Grid computations
50	Time steps between output steps
0	Time steps before saving first output step
1	Save output every n-th grid point
PtReyesCA_RM_A.most	A-grid bathymetry file
PtReyesCA_RM_B.most	B-grid bathymetry file
PtReyesCA_RM_C.most	C-grid bathymetry file
./	Directory of source files
./	Directory for output files

* The column headings are not part of most3_facts_nc.in

A2. Forecast Model Input (*.in) File for Point Reyes, CA

The following table contains the parameter and file choices used in the input file for the SIFT implementation (most3_facts_nc.in) of the optimized forecast model (FM) for Point Reyes, CA. When run on an Intel® Xeon® E5670 2.93GHz processor the forecast model produces four hours of simulation in 9.78 minutes, within the desired 10-minute value for this metric.

Parameter/File*	Purpose
0.0010	Minimum amp. of input offshore wave (m)
2.5	Minimum depth of offshore (m)
0.1	Dry land depth of inundation (m)
0.0009	Friction coefficient (n^{*2})
1	Let A-Grid and B-Grid run up
900.0	Max eta before blow-up (m)
2.0	Time step (sec)
14400	Total number of time steps in run
3	Time steps between A-Grid computations
1	Time steps between B-Grid computations
15	Time steps between output steps
0	Time steps before saving first output step
1	Save output every n-th grid point
PtReyesCA_FM_A.most	A-grid bathymetry file
PtReyesCA_FM_B.most	B-grid bathymetry file
PtReyesCA_FM_C.most	C-grid bathymetry file
./	Directory of source files
./	Directory for output files

* The column headings are not part of most3_facts_nc.in

Appendix B Propagation Database: Pacific Ocean Unit Sources

Appendix C Synthetic Testing Report

DRAFT

Appendix B

Propagation Database: Pacific Ocean Unit Sources

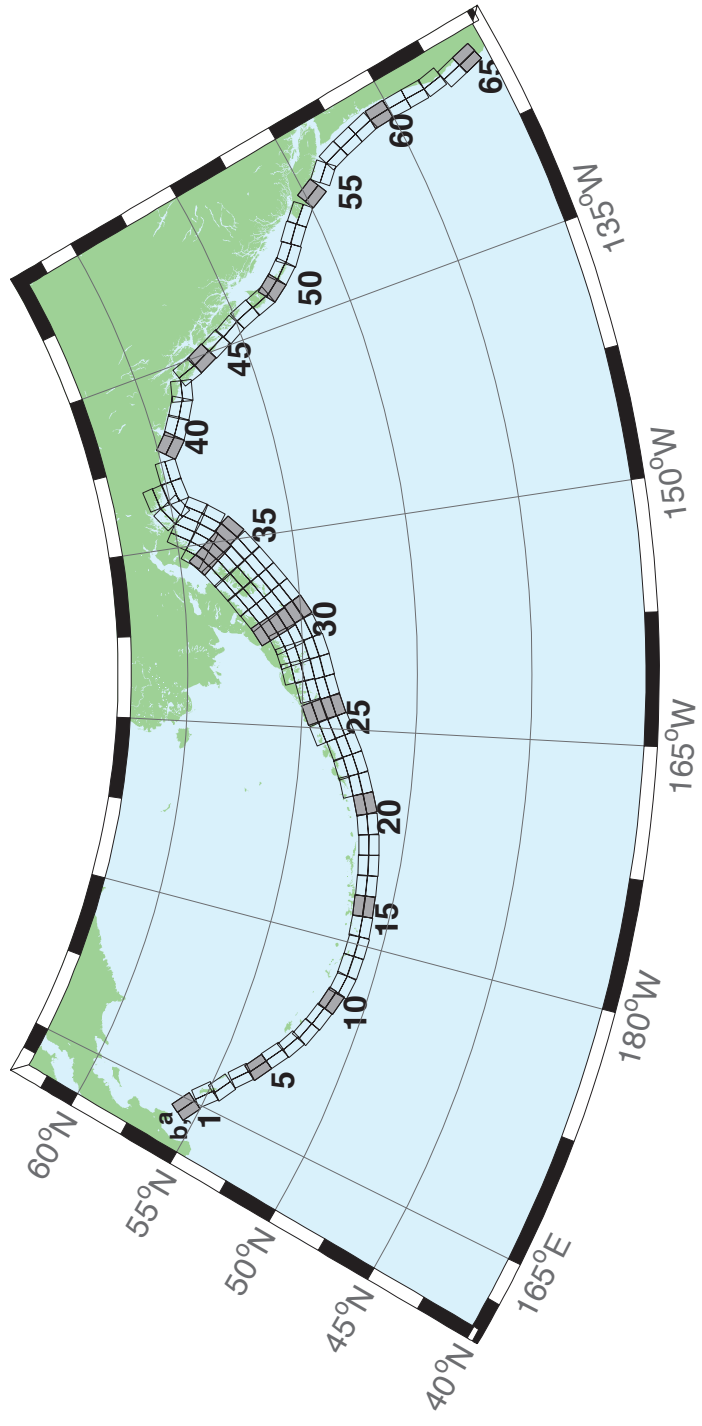


Figure B.1: Aleutian–Alaska–Cascadia Subduction Zone unit sources.

Table B.1: Earthquake parameters for Aleutian–Alaska–Cascadia Subduction Zone unit sources.

Segment	Description	Longitude(°E)	Latitude(°N)	Strike(°)	Dip(°)	Depth (km)
acsz-1a	Aleutian–Alaska–Cascadia	164.7994	55.9606	299	17	19.61
acsz-1b	Aleutian–Alaska–Cascadia	164.4310	55.5849	299	17	5
acsz-2a	Aleutian–Alaska–Cascadia	166.3418	55.4016	310.2	17	19.61
acsz-2b	Aleutian–Alaska–Cascadia	165.8578	55.0734	310.2	17	5
acsz-3a	Aleutian–Alaska–Cascadia	167.2939	54.8919	300.2	23.36	24.82
acsz-3b	Aleutian–Alaska–Cascadia	166.9362	54.5356	300.2	23.36	5
acsz-4a	Aleutian–Alaska–Cascadia	168.7131	54.2852	310.2	38.51	25.33
acsz-4b	Aleutian–Alaska–Cascadia	168.3269	54.0168	310.2	24	5
acsz-5a	Aleutian–Alaska–Cascadia	169.7447	53.7808	302.8	37.02	23.54
acsz-5b	Aleutian–Alaska–Cascadia	169.4185	53.4793	302.8	21.77	5
acsz-6a	Aleutian–Alaska–Cascadia	171.0144	53.3054	303.2	35.31	22.92
acsz-6b	Aleutian–Alaska–Cascadia	170.6813	52.9986	303.2	21	5
acsz-7a	Aleutian–Alaska–Cascadia	172.1500	52.8528	298.2	35.56	20.16
acsz-7b	Aleutian–Alaska–Cascadia	171.8665	52.5307	298.2	17.65	5
acsz-8a	Aleutian–Alaska–Cascadia	173.2726	52.4579	290.8	37.92	20.35
acsz-8b	Aleutian–Alaska–Cascadia	173.0681	52.1266	290.8	17.88	5
acsz-9a	Aleutian–Alaska–Cascadia	174.5866	52.1434	289	39.09	21.05
acsz-9b	Aleutian–Alaska–Cascadia	174.4027	51.8138	289	18.73	5
acsz-10a	Aleutian–Alaska–Cascadia	175.8784	51.8526	286.1	40.51	20.87
acsz-10b	Aleutian–Alaska–Cascadia	175.7265	51.5245	286.1	18.51	5
acsz-11a	Aleutian–Alaska–Cascadia	177.1140	51.6488	280	15	17.94
acsz-11b	Aleutian–Alaska–Cascadia	176.9937	51.2215	280	15	5
acsz-12a	Aleutian–Alaska–Cascadia	178.4500	51.5690	273	15	17.94
acsz-12b	Aleutian–Alaska–Cascadia	178.4130	51.1200	273	15	5
acsz-13a	Aleutian–Alaska–Cascadia	179.8550	51.5340	271	15	17.94
acsz-13b	Aleutian–Alaska–Cascadia	179.8420	51.0850	271	15	5
acsz-14a	Aleutian–Alaska–Cascadia	181.2340	51.5780	267	15	17.94
acsz-14b	Aleutian–Alaska–Cascadia	181.2720	51.1290	267	15	5
acsz-15a	Aleutian–Alaska–Cascadia	182.6380	51.6470	265	15	17.94
acsz-15b	Aleutian–Alaska–Cascadia	182.7000	51.2000	265	15	5
acsz-16a	Aleutian–Alaska–Cascadia	184.0550	51.7250	264	15	17.94
acsz-16b	Aleutian–Alaska–Cascadia	184.1280	51.2780	264	15	5
acsz-17a	Aleutian–Alaska–Cascadia	185.4560	51.8170	262	15	17.94
acsz-17b	Aleutian–Alaska–Cascadia	185.5560	51.3720	262	15	5
acsz-18a	Aleutian–Alaska–Cascadia	186.8680	51.9410	261	15	17.94
acsz-18b	Aleutian–Alaska–Cascadia	186.9810	51.4970	261	15	5
acsz-19a	Aleutian–Alaska–Cascadia	188.2430	52.1280	257	15	17.94
acsz-19b	Aleutian–Alaska–Cascadia	188.4060	51.6900	257	15	5
acsz-20a	Aleutian–Alaska–Cascadia	189.5810	52.3550	251	15	17.94
acsz-20b	Aleutian–Alaska–Cascadia	189.8180	51.9300	251	15	5
acsz-21a	Aleutian–Alaska–Cascadia	190.9570	52.6470	251	15	17.94
acsz-21b	Aleutian–Alaska–Cascadia	191.1960	52.2220	251	15	5
acsz-21z	Aleutian–Alaska–Cascadia	190.7399	53.0443	250.8	15	30.88
acsz-22a	Aleutian–Alaska–Cascadia	192.2940	52.9430	247	15	17.94
acsz-22b	Aleutian–Alaska–Cascadia	192.5820	52.5300	247	15	5
acsz-22z	Aleutian–Alaska–Cascadia	192.0074	53.3347	247.8	15	30.88
acsz-23a	Aleutian–Alaska–Cascadia	193.6270	53.3070	245	15	17.94
acsz-23b	Aleutian–Alaska–Cascadia	193.9410	52.9000	245	15	5
acsz-23z	Aleutian–Alaska–Cascadia	193.2991	53.6768	244.6	15	30.88
acsz-24a	Aleutian–Alaska–Cascadia	194.9740	53.6870	245	15	17.94
acsz-24b	Aleutian–Alaska–Cascadia	195.2910	53.2800	245	15	5
acsz-24y	Aleutian–Alaska–Cascadia	194.3645	54.4604	244.4	15	43.82
acsz-24z	Aleutian–Alaska–Cascadia	194.6793	54.0674	244.6	15	30.88

Continued on next page

Table B.1 – continued

Segment	Description	Longitude(°E)	Latitude(°N)	Strike(°)	Dip(°)	Depth (km)
acsz-25a	Aleutian-Alaska-Cascadia	196.4340	54.0760	250	15	17.94
acsz-25b	Aleutian-Alaska-Cascadia	196.6930	53.6543	250	15	5
acsz-25y	Aleutian-Alaska-Cascadia	195.9009	54.8572	247.9	15	43.82
acsz-25z	Aleutian-Alaska-Cascadia	196.1761	54.4536	248.1	15	30.88
acsz-26a	Aleutian-Alaska-Cascadia	197.8970	54.3600	253	15	17.94
acsz-26b	Aleutian-Alaska-Cascadia	198.1200	53.9300	253	15	5
acsz-26y	Aleutian-Alaska-Cascadia	197.5498	55.1934	253.1	15	43.82
acsz-26z	Aleutian-Alaska-Cascadia	197.7620	54.7770	253.3	15	30.88
acsz-27a	Aleutian-Alaska-Cascadia	199.4340	54.5960	256	15	17.94
acsz-27b	Aleutian-Alaska-Cascadia	199.6200	54.1600	256	15	5
acsz-27x	Aleutian-Alaska-Cascadia	198.9736	55.8631	256.5	15	56.24
acsz-27y	Aleutian-Alaska-Cascadia	199.1454	55.4401	256.6	15	43.82
acsz-27z	Aleutian-Alaska-Cascadia	199.3135	55.0170	256.8	15	30.88
acsz-28a	Aleutian-Alaska-Cascadia	200.8820	54.8300	253	15	17.94
acsz-28b	Aleutian-Alaska-Cascadia	201.1080	54.4000	253	15	5
acsz-28x	Aleutian-Alaska-Cascadia	200.1929	56.0559	252.5	15	56.24
acsz-28y	Aleutian-Alaska-Cascadia	200.4167	55.6406	252.7	15	43.82
acsz-28z	Aleutian-Alaska-Cascadia	200.6360	55.2249	252.9	15	30.88
acsz-29a	Aleutian-Alaska-Cascadia	202.2610	55.1330	247	15	17.94
acsz-29b	Aleutian-Alaska-Cascadia	202.5650	54.7200	247	15	5
acsz-29x	Aleutian-Alaska-Cascadia	201.2606	56.2861	245.7	15	56.24
acsz-29y	Aleutian-Alaska-Cascadia	201.5733	55.8888	246	15	43.82
acsz-29z	Aleutian-Alaska-Cascadia	201.8797	55.4908	246.2	15	30.88
acsz-30a	Aleutian-Alaska-Cascadia	203.6040	55.5090	240	15	17.94
acsz-30b	Aleutian-Alaska-Cascadia	203.9970	55.1200	240	15	5
acsz-30w	Aleutian-Alaska-Cascadia	201.9901	56.9855	239.5	15	69.12
acsz-30x	Aleutian-Alaska-Cascadia	202.3851	56.6094	239.8	15	56.24
acsz-30y	Aleutian-Alaska-Cascadia	202.7724	56.2320	240.2	15	43.82
acsz-30z	Aleutian-Alaska-Cascadia	203.1521	55.8534	240.5	15	30.88
acsz-31a	Aleutian-Alaska-Cascadia	204.8950	55.9700	236	15	17.94
acsz-31b	Aleutian-Alaska-Cascadia	205.3400	55.5980	236	15	5
acsz-31w	Aleutian-Alaska-Cascadia	203.0825	57.3740	234.5	15	69.12
acsz-31x	Aleutian-Alaska-Cascadia	203.5408	57.0182	234.9	15	56.24
acsz-31y	Aleutian-Alaska-Cascadia	203.9904	56.6607	235.3	15	43.82
acsz-31z	Aleutian-Alaska-Cascadia	204.4315	56.3016	235.7	15	30.88
acsz-32a	Aleutian-Alaska-Cascadia	206.2080	56.4730	236	15	17.94
acsz-32b	Aleutian-Alaska-Cascadia	206.6580	56.1000	236	15	5
acsz-32w	Aleutian-Alaska-Cascadia	204.4129	57.8908	234.3	15	69.12
acsz-32x	Aleutian-Alaska-Cascadia	204.8802	57.5358	234.7	15	56.24
acsz-32y	Aleutian-Alaska-Cascadia	205.3385	57.1792	235.1	15	43.82
acsz-32z	Aleutian-Alaska-Cascadia	205.7880	56.8210	235.5	15	30.88
acsz-33a	Aleutian-Alaska-Cascadia	207.5370	56.9750	236	15	17.94
acsz-33b	Aleutian-Alaska-Cascadia	207.9930	56.6030	236	15	5
acsz-33w	Aleutian-Alaska-Cascadia	205.7126	58.3917	234.2	15	69.12
acsz-33x	Aleutian-Alaska-Cascadia	206.1873	58.0371	234.6	15	56.24
acsz-33y	Aleutian-Alaska-Cascadia	206.6527	57.6808	235	15	43.82
acsz-33z	Aleutian-Alaska-Cascadia	207.1091	57.3227	235.4	15	30.88
acsz-34a	Aleutian-Alaska-Cascadia	208.9371	57.5124	236	15	17.94
acsz-34b	Aleutian-Alaska-Cascadia	209.4000	57.1400	236	15	5
acsz-34w	Aleutian-Alaska-Cascadia	206.9772	58.8804	233.5	15	69.12
acsz-34x	Aleutian-Alaska-Cascadia	207.4677	58.5291	233.9	15	56.24
acsz-34y	Aleutian-Alaska-Cascadia	207.9485	58.1760	234.3	15	43.82
acsz-34z	Aleutian-Alaska-Cascadia	208.4198	57.8213	234.7	15	30.88
acsz-35a	Aleutian-Alaska-Cascadia	210.2597	58.0441	230	15	17.94
acsz-35b	Aleutian-Alaska-Cascadia	210.8000	57.7000	230	15	5

Continued on next page

Table B.1 – continued

Segment	Description	Longitude(°E)	Latitude(°N)	Strike(°)	Dip(°)	Depth (km)
acsz-35w	Aleutian-Alaska-Cascadia	208.0204	59.3199	228.8	15	69.12
acsz-35x	Aleutian-Alaska-Cascadia	208.5715	58.9906	229.3	15	56.24
acsz-35y	Aleutian-Alaska-Cascadia	209.1122	58.6590	229.7	15	43.82
acsz-35z	Aleutian-Alaska-Cascadia	209.6425	58.3252	230.2	15	30.88
acsz-36a	Aleutian-Alaska-Cascadia	211.3249	58.6565	218	15	17.94
acsz-36b	Aleutian-Alaska-Cascadia	212.0000	58.3800	218	15	5
acsz-36w	Aleutian-Alaska-Cascadia	208.5003	59.5894	215.6	15	69.12
acsz-36x	Aleutian-Alaska-Cascadia	209.1909	59.3342	216.2	15	56.24
acsz-36y	Aleutian-Alaska-Cascadia	209.8711	59.0753	216.8	15	43.82
acsz-36z	Aleutian-Alaska-Cascadia	210.5412	58.8129	217.3	15	30.88
acsz-37a	Aleutian-Alaska-Cascadia	212.2505	59.2720	213.7	15	17.94
acsz-37b	Aleutian-Alaska-Cascadia	212.9519	59.0312	213.7	15	5
acsz-37x	Aleutian-Alaska-Cascadia	210.1726	60.0644	213	15	56.24
acsz-37y	Aleutian-Alaska-Cascadia	210.8955	59.8251	213.7	15	43.82
acsz-37z	Aleutian-Alaska-Cascadia	211.6079	59.5820	214.3	15	30.88
acsz-38a	Aleutian-Alaska-Cascadia	214.6555	60.1351	260.1	0	15
acsz-38b	Aleutian-Alaska-Cascadia	214.8088	59.6927	260.1	0	15
acsz-38y	Aleutian-Alaska-Cascadia	214.3737	60.9838	259	0	15
acsz-38z	Aleutian-Alaska-Cascadia	214.5362	60.5429	259	0	15
acsz-39a	Aleutian-Alaska-Cascadia	216.5607	60.2480	267	0	15
acsz-39b	Aleutian-Alaska-Cascadia	216.6068	59.7994	267	0	15
acsz-40a	Aleutian-Alaska-Cascadia	219.3069	59.7574	310.9	0	15
acsz-40b	Aleutian-Alaska-Cascadia	218.7288	59.4180	310.9	0	15
acsz-41a	Aleutian-Alaska-Cascadia	220.4832	59.3390	300.7	0	15
acsz-41b	Aleutian-Alaska-Cascadia	220.0382	58.9529	300.7	0	15
acsz-42a	Aleutian-Alaska-Cascadia	221.8835	58.9310	298.9	0	15
acsz-42b	Aleutian-Alaska-Cascadia	221.4671	58.5379	298.9	0	15
acsz-43a	Aleutian-Alaska-Cascadia	222.9711	58.6934	282.3	0	15
acsz-43b	Aleutian-Alaska-Cascadia	222.7887	58.2546	282.3	0	15
acsz-44a	Aleutian-Alaska-Cascadia	224.9379	57.9054	340.9	12	11.09
acsz-44b	Aleutian-Alaska-Cascadia	224.1596	57.7617	340.9	7	5
acsz-45a	Aleutian-Alaska-Cascadia	225.4994	57.1634	334.1	12	11.09
acsz-45b	Aleutian-Alaska-Cascadia	224.7740	56.9718	334.1	7	5
acsz-46a	Aleutian-Alaska-Cascadia	226.1459	56.3552	334.1	12	11.09
acsz-46b	Aleutian-Alaska-Cascadia	225.4358	56.1636	334.1	7	5
acsz-47a	Aleutian-Alaska-Cascadia	226.7731	55.5830	332.3	12	11.09
acsz-47b	Aleutian-Alaska-Cascadia	226.0887	55.3785	332.3	7	5
acsz-48a	Aleutian-Alaska-Cascadia	227.4799	54.6763	339.4	12	11.09
acsz-48b	Aleutian-Alaska-Cascadia	226.7713	54.5217	339.4	7	5
acsz-49a	Aleutian-Alaska-Cascadia	227.9482	53.8155	341.2	12	11.09
acsz-49b	Aleutian-Alaska-Cascadia	227.2462	53.6737	341.2	7	5
acsz-50a	Aleutian-Alaska-Cascadia	228.3970	53.2509	324.5	12	11.09
acsz-50b	Aleutian-Alaska-Cascadia	227.8027	52.9958	324.5	7	5
acsz-51a	Aleutian-Alaska-Cascadia	229.1844	52.6297	318.4	12	11.09
acsz-51b	Aleutian-Alaska-Cascadia	228.6470	52.3378	318.4	7	5
acsz-52a	Aleutian-Alaska-Cascadia	230.0306	52.0768	310.9	12	11.09
acsz-52b	Aleutian-Alaska-Cascadia	229.5665	51.7445	310.9	7	5
acsz-53a	Aleutian-Alaska-Cascadia	231.1735	51.5258	310.9	12	11.09
acsz-53b	Aleutian-Alaska-Cascadia	230.7150	51.1935	310.9	7	5
acsz-54a	Aleutian-Alaska-Cascadia	232.2453	50.8809	314.1	12	11.09
acsz-54b	Aleutian-Alaska-Cascadia	231.7639	50.5655	314.1	7	5
acsz-55a	Aleutian-Alaska-Cascadia	233.3066	49.9032	333.7	12	11.09
acsz-55b	Aleutian-Alaska-Cascadia	232.6975	49.7086	333.7	7	5
acsz-56a	Aleutian-Alaska-Cascadia	234.0588	49.1702	315	11	12.82
acsz-56b	Aleutian-Alaska-Cascadia	233.5849	48.8584	315	9	5

Continued on next page

Table B.1 – continued

Segment	Description	Longitude(°E)	Latitude(°N)	Strike(°)	Dip(°)	Depth (km)
acsz-57a	Aleutian-Alaska-Cascadia	234.9041	48.2596	341	11	12.82
acsz-57b	Aleutian-Alaska-Cascadia	234.2797	48.1161	341	9	5
acsz-58a	Aleutian-Alaska-Cascadia	235.3021	47.3812	344	11	12.82
acsz-58b	Aleutian-Alaska-Cascadia	234.6776	47.2597	344	9	5
acsz-59a	Aleutian-Alaska-Cascadia	235.6432	46.5082	345	11	12.82
acsz-59b	Aleutian-Alaska-Cascadia	235.0257	46.3941	345	9	5
acsz-60a	Aleutian-Alaska-Cascadia	235.8640	45.5429	356	11	12.82
acsz-60b	Aleutian-Alaska-Cascadia	235.2363	45.5121	356	9	5
acsz-61a	Aleutian-Alaska-Cascadia	235.9106	44.6227	359	11	12.82
acsz-61b	Aleutian-Alaska-Cascadia	235.2913	44.6150	359	9	5
acsz-62a	Aleutian-Alaska-Cascadia	235.9229	43.7245	359	11	12.82
acsz-62b	Aleutian-Alaska-Cascadia	235.3130	43.7168	359	9	5
acsz-63a	Aleutian-Alaska-Cascadia	236.0220	42.9020	350	11	12.82
acsz-63b	Aleutian-Alaska-Cascadia	235.4300	42.8254	350	9	5
acsz-64a	Aleutian-Alaska-Cascadia	235.9638	41.9818	345	11	12.82
acsz-64b	Aleutian-Alaska-Cascadia	235.3919	41.8677	345	9	5
acsz-65a	Aleutian-Alaska-Cascadia	236.2643	41.1141	345	11	12.82
acsz-65b	Aleutian-Alaska-Cascadia	235.7000	41.0000	345	9	5
acsz-238a	Aleutian-Alaska-Cascadia	213.2878	59.8406	236.8	15	17.94
acsz-238y	Aleutian-Alaska-Cascadia	212.3424	60.5664	236.8	15	43.82
acsz-238z	Aleutian-Alaska-Cascadia	212.8119	60.2035	236.8	15	30.88

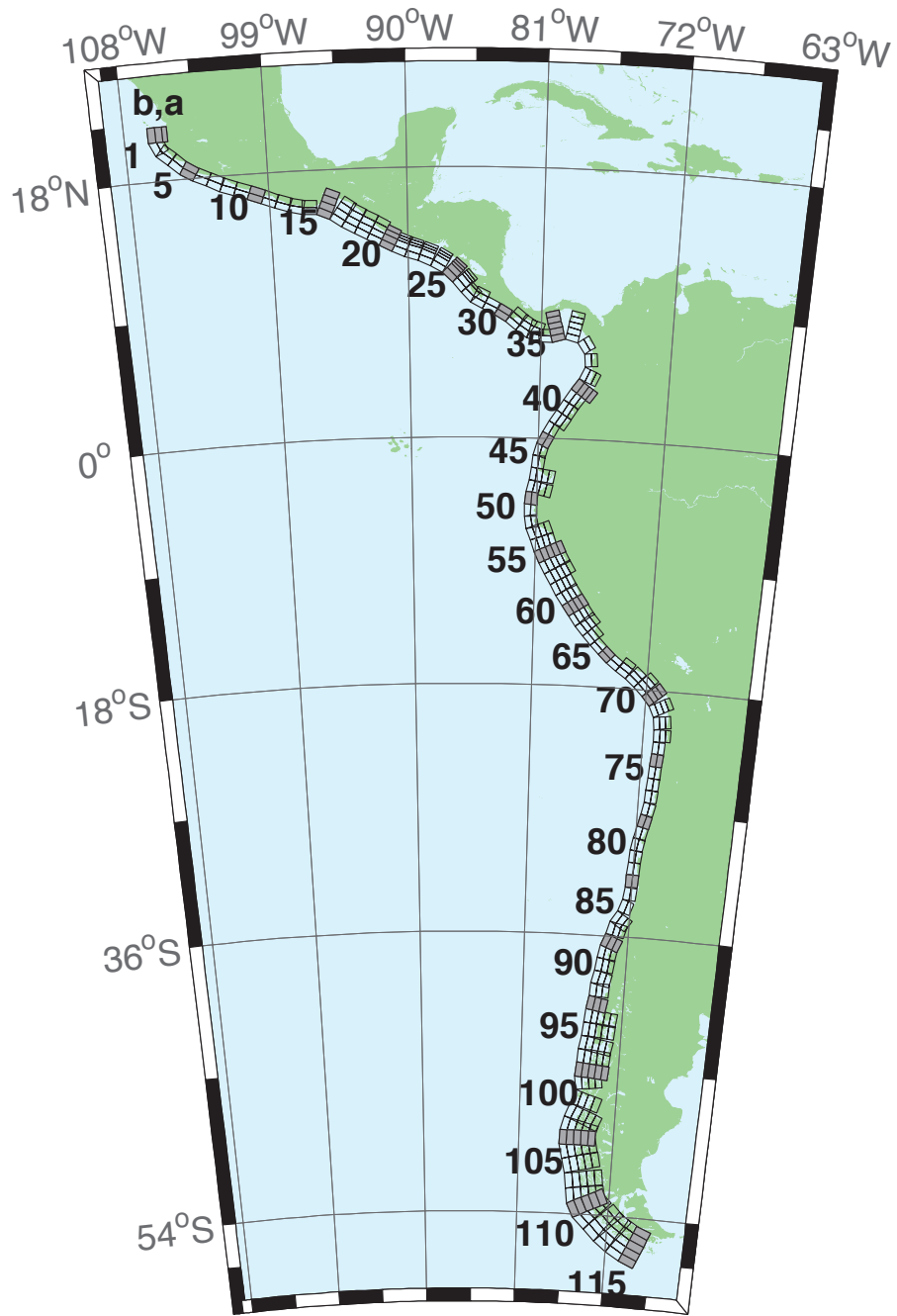


Figure B.2: Central and South America Subduction Zone unit sources.

Table B.2: Earthquake parameters for Central and South America Subduction
Zone unit sources.

Segment	Description	Longitude(°E)	Latitude(°N)	Strike(°)	Dip(°)	Depth (km)
cssz-1a	Central and South America	254.4573	20.8170	359	19	15.4
cssz-1b	Central and South America	254.0035	20.8094	359	12	5
cssz-1z	Central and South America	254.7664	20.8222	359	50	31.67
cssz-2a	Central and South America	254.5765	20.2806	336.8	19	15.4
cssz-2b	Central and South America	254.1607	20.1130	336.8	12	5
cssz-3a	Central and South America	254.8789	19.8923	310.6	18.31	15.27
cssz-3b	Central and South America	254.5841	19.5685	310.6	11.85	5
cssz-4a	Central and South America	255.6167	19.2649	313.4	17.62	15.12
cssz-4b	Central and South America	255.3056	18.9537	313.4	11.68	5
cssz-5a	Central and South America	256.2240	18.8148	302.7	16.92	15
cssz-5b	Central and South America	255.9790	18.4532	302.7	11.54	5
cssz-6a	Central and South America	256.9425	18.4383	295.1	16.23	14.87
cssz-6b	Central and South America	256.7495	18.0479	295.1	11.38	5
cssz-7a	Central and South America	257.8137	18.0339	296.9	15.54	14.74
cssz-7b	Central and South America	257.6079	17.6480	296.9	11.23	5
cssz-8a	Central and South America	258.5779	17.7151	290.4	14.85	14.61
cssz-8b	Central and South America	258.4191	17.3082	290.4	11.08	5
cssz-9a	Central and South America	259.4578	17.4024	290.5	14.15	14.47
cssz-9b	Central and South America	259.2983	16.9944	290.5	10.92	5
cssz-10a	Central and South America	260.3385	17.0861	290.8	13.46	14.34
cssz-10b	Central and South America	260.1768	16.6776	290.8	10.77	5
cssz-11a	Central and South America	261.2255	16.7554	291.8	12.77	14.21
cssz-11b	Central and South America	261.0556	16.3487	291.8	10.62	5
cssz-12a	Central and South America	262.0561	16.4603	288.9	12.08	14.08
cssz-12b	Central and South America	261.9082	16.0447	288.9	10.46	5
cssz-13a	Central and South America	262.8638	16.2381	283.2	11.38	13.95
cssz-13b	Central and South America	262.7593	15.8094	283.2	10.31	5
cssz-14a	Central and South America	263.6066	16.1435	272.1	10.69	13.81
cssz-14b	Central and South America	263.5901	15.7024	272.1	10.15	5
cssz-15a	Central and South America	264.8259	15.8829	293	10	13.68
cssz-15b	Central and South America	264.6462	15.4758	293	10	5
cssz-15y	Central and South America	265.1865	16.6971	293	10	31.05
cssz-15z	Central and South America	265.0060	16.2900	293	10	22.36
cssz-16a	Central and South America	265.7928	15.3507	304.9	15	15.82
cssz-16b	Central and South America	265.5353	14.9951	304.9	12.5	5
cssz-16y	Central and South America	266.3092	16.0619	304.9	15	41.7
cssz-16z	Central and South America	266.0508	15.7063	304.9	15	28.76
cssz-17a	Central and South America	266.4947	14.9019	299.5	20	17.94
cssz-17b	Central and South America	266.2797	14.5346	299.5	15	5
cssz-17y	Central and South America	266.9259	15.6365	299.5	20	52.14
cssz-17z	Central and South America	266.7101	15.2692	299.5	20	35.04
cssz-18a	Central and South America	267.2827	14.4768	298	21.5	17.94
cssz-18b	Central and South America	267.0802	14.1078	298	15	5
cssz-18y	Central and South America	267.6888	15.2148	298	21.5	54.59
cssz-18z	Central and South America	267.4856	14.8458	298	21.5	36.27
cssz-19a	Central and South America	268.0919	14.0560	297.6	23	17.94
cssz-19b	Central and South America	267.8943	13.6897	297.6	15	5
cssz-19y	Central and South America	268.4880	14.7886	297.6	23	57.01
cssz-19z	Central and South America	268.2898	14.4223	297.6	23	37.48
cssz-20a	Central and South America	268.8929	13.6558	296.2	24	17.94
cssz-20b	Central and South America	268.7064	13.2877	296.2	15	5
cssz-20y	Central and South America	269.1796	14.2206	296.2	45.5	73.94
cssz-20z	Central and South America	269.0362	13.9382	296.2	45.5	38.28

Continued on next page

Table B.2 – continued

Segment	Description	Longitude(°E)	Latitude(°N)	Strike(°)	Dip(°)	Depth (km)
cssz-21a	Central and South America	269.6797	13.3031	292.6	25	17.94
cssz-21b	Central and South America	269.5187	12.9274	292.6	15	5
cssz-21x	Central and South America	269.8797	13.7690	292.6	68	131.8
cssz-21y	Central and South America	269.8130	13.6137	292.6	68	85.43
cssz-21z	Central and South America	269.7463	13.4584	292.6	68	39.07
cssz-22a	Central and South America	270.4823	13.0079	288.6	25	17.94
cssz-22b	Central and South America	270.3492	12.6221	288.6	15	5
cssz-22x	Central and South America	270.6476	13.4864	288.6	68	131.8
cssz-22y	Central and South America	270.5925	13.3269	288.6	68	85.43
cssz-22z	Central and South America	270.5374	13.1674	288.6	68	39.07
cssz-23a	Central and South America	271.3961	12.6734	292.4	25	17.94
cssz-23b	Central and South America	271.2369	12.2972	292.4	15	5
cssz-23x	Central and South America	271.5938	13.1399	292.4	68	131.8
cssz-23y	Central and South America	271.5279	12.9844	292.4	68	85.43
cssz-23z	Central and South America	271.4620	12.8289	292.4	68	39.07
cssz-24a	Central and South America	272.3203	12.2251	300.2	25	17.94
cssz-24b	Central and South America	272.1107	11.8734	300.2	15	5
cssz-24x	Central and South America	272.5917	12.6799	300.2	67	131.1
cssz-24y	Central and South America	272.5012	12.5283	300.2	67	85.1
cssz-24z	Central and South America	272.4107	12.3767	300.2	67	39.07
cssz-25a	Central and South America	273.2075	11.5684	313.8	25	17.94
cssz-25b	Central and South America	272.9200	11.2746	313.8	15	5
cssz-25x	Central and South America	273.5950	11.9641	313.8	66	130.4
cssz-25y	Central and South America	273.4658	11.8322	313.8	66	84.75
cssz-25z	Central and South America	273.3366	11.7003	313.8	66	39.07
cssz-26a	Central and South America	273.8943	10.8402	320.4	25	17.94
cssz-26b	Central and South America	273.5750	10.5808	320.4	15	5
cssz-26x	Central and South America	274.3246	11.1894	320.4	66	130.4
cssz-26y	Central and South America	274.1811	11.0730	320.4	66	84.75
cssz-26z	Central and South America	274.0377	10.9566	320.4	66	39.07
cssz-27a	Central and South America	274.4569	10.2177	316.1	25	17.94
cssz-27b	Central and South America	274.1590	9.9354	316.1	15	5
cssz-27z	Central and South America	274.5907	10.3444	316.1	66	39.07
cssz-28a	Central and South America	274.9586	9.8695	297.1	22	14.54
cssz-28b	Central and South America	274.7661	9.4988	297.1	11	5
cssz-28z	Central and South America	275.1118	10.1643	297.1	42.5	33.27
cssz-29a	Central and South America	275.7686	9.4789	296.6	19	11.09
cssz-29b	Central and South America	275.5759	9.0992	296.6	7	5
cssz-30a	Central and South America	276.6346	8.9973	302.2	19	9.36
cssz-30b	Central and South America	276.4053	8.6381	302.2	5	5
cssz-31a	Central and South America	277.4554	8.4152	309.1	19	7.62
cssz-31b	Central and South America	277.1851	8.0854	309.1	3	5
cssz-31z	Central and South America	277.7260	8.7450	309.1	19	23.9
cssz-32a	Central and South America	278.1112	7.9425	303	18.67	8.49
cssz-32b	Central and South America	277.8775	7.5855	303	4	5
cssz-32z	Central and South America	278.3407	8.2927	303	21.67	24.49
cssz-33a	Central and South America	278.7082	7.6620	287.6	18.33	10.23
cssz-33b	Central and South America	278.5785	7.2555	287.6	6	5
cssz-33z	Central and South America	278.8328	8.0522	287.6	24.33	25.95
cssz-34a	Central and South America	279.3184	7.5592	269.5	18	17.94
cssz-34b	Central and South America	279.3223	7.1320	269.5	15	5
cssz-35a	Central and South America	280.0039	7.6543	255.9	17.67	14.54
cssz-35b	Central and South America	280.1090	7.2392	255.9	11	5
cssz-35x	Central and South America	279.7156	8.7898	255.9	29.67	79.22
cssz-35y	Central and South America	279.8118	8.4113	255.9	29.67	54.47

Continued on next page

Table B.2 – continued

Segment	Description	Longitude(°E)	Latitude(°N)	Strike(°)	Dip(°)	Depth (km)
cssz-35z	Central and South America	279.9079	8.0328	255.9	29.67	29.72
cssz-36a	Central and South America	281.2882	7.6778	282.5	17.33	11.09
cssz-36b	Central and South America	281.1948	7.2592	282.5	7	5
cssz-36x	Central and South America	281.5368	8.7896	282.5	32.33	79.47
cssz-36y	Central and South America	281.4539	8.4190	282.5	32.33	52.73
cssz-36z	Central and South America	281.3710	8.0484	282.5	32.33	25.99
cssz-37a	Central and South America	282.5252	6.8289	326.9	17	10.23
cssz-37b	Central and South America	282.1629	6.5944	326.9	6	5
cssz-38a	Central and South America	282.9469	5.5973	355.4	17	10.23
cssz-38b	Central and South America	282.5167	5.5626	355.4	6	5
cssz-39a	Central and South America	282.7236	4.3108	24.13	17	10.23
cssz-39b	Central and South America	282.3305	4.4864	24.13	6	5
cssz-39z	Central and South America	283.0603	4.1604	24.13	35	24.85
cssz-40a	Central and South America	282.1940	3.3863	35.28	17	10.23
cssz-40b	Central and South America	281.8427	3.6344	35.28	6	5
cssz-40y	Central and South America	282.7956	2.9613	35.28	35	53.52
cssz-40z	Central and South America	282.4948	3.1738	35.28	35	24.85
cssz-41a	Central and South America	281.6890	2.6611	34.27	17	10.23
cssz-41b	Central and South America	281.3336	2.9030	34.27	6	5
cssz-41z	Central and South America	281.9933	2.4539	34.27	35	24.85
cssz-42a	Central and South America	281.2266	1.9444	31.29	17	10.23
cssz-42b	Central and South America	280.8593	2.1675	31.29	6	5
cssz-42z	Central and South America	281.5411	1.7533	31.29	35	24.85
cssz-43a	Central and South America	280.7297	1.1593	33.3	17	10.23
cssz-43b	Central and South America	280.3706	1.3951	33.3	6	5
cssz-43z	Central and South America	281.0373	0.9573	33.3	35	24.85
cssz-44a	Central and South America	280.3018	0.4491	28.8	17	10.23
cssz-44b	Central and South America	279.9254	0.6560	28.8	6	5
cssz-45a	Central and South America	279.9083	-0.3259	26.91	10	8.49
cssz-45b	Central and South America	279.5139	-0.1257	26.91	4	5
cssz-46a	Central and South America	279.6461	-0.9975	15.76	10	8.49
cssz-46b	Central and South America	279.2203	-0.8774	15.76	4	5
cssz-47a	Central and South America	279.4972	-1.7407	6.9	10	8.49
cssz-47b	Central and South America	279.0579	-1.6876	6.9	4	5
cssz-48a	Central and South America	279.3695	-2.6622	8.96	10	8.49
cssz-48b	Central and South America	278.9321	-2.5933	8.96	4	5
cssz-48y	Central and South America	280.2444	-2.8000	8.96	10	25.85
cssz-48z	Central and South America	279.8070	-2.7311	8.96	10	17.17
cssz-49a	Central and South America	279.1852	-3.6070	13.15	10	8.49
cssz-49b	Central and South America	278.7536	-3.5064	13.15	4	5
cssz-49y	Central and South America	280.0486	-3.8082	13.15	10	25.85
cssz-49z	Central and South America	279.6169	-3.7076	13.15	10	17.17
cssz-50a	Central and South America	279.0652	-4.3635	4.78	10.33	9.64
cssz-50b	Central and South America	278.6235	-4.3267	4.78	5.33	5
cssz-51a	Central and South America	279.0349	-5.1773	359.4	10.67	10.81
cssz-51b	Central and South America	278.5915	-5.1817	359.4	6.67	5
cssz-52a	Central and South America	279.1047	-5.9196	349.8	11	11.96
cssz-52b	Central and South America	278.6685	-5.9981	349.8	8	5
cssz-53a	Central and South America	279.3044	-6.6242	339.2	10.25	11.74
cssz-53b	Central and South America	278.8884	-6.7811	339.2	7.75	5
cssz-53y	Central and South America	280.1024	-6.3232	339.2	19.25	37.12
cssz-53z	Central and South America	279.7035	-6.4737	339.2	19.25	20.64
cssz-54a	Central and South America	279.6256	-7.4907	340.8	9.5	11.53
cssz-54b	Central and South America	279.2036	-7.6365	340.8	7.5	5
cssz-54y	Central and South America	280.4267	-7.2137	340.8	20.5	37.29

Continued on next page

Table B.2 – continued

Segment	Description	Longitude(°E)	Latitude(°N)	Strike(°)	Dip(°)	Depth (km)
cssz-54z	Central and South America	280.0262	-7.3522	340.8	20.5	19.78
cssz-55a	Central and South America	279.9348	-8.2452	335.4	8.75	11.74
cssz-55b	Central and South America	279.5269	-8.4301	335.4	7.75	5
cssz-55x	Central and South America	281.0837	-7.7238	335.4	21.75	56.4
cssz-55y	Central and South America	280.7009	-7.8976	335.4	21.75	37.88
cssz-55z	Central and South America	280.3180	-8.0714	335.4	21.75	19.35
cssz-56a	Central and South America	280.3172	-8.9958	331.6	8	11.09
cssz-56b	Central and South America	279.9209	-9.2072	331.6	7	5
cssz-56x	Central and South America	281.4212	-8.4063	331.6	23	57.13
cssz-56y	Central and South America	281.0534	-8.6028	331.6	23	37.59
cssz-56z	Central and South America	280.6854	-8.7993	331.6	23	18.05
cssz-57a	Central and South America	280.7492	-9.7356	328.7	8.6	10.75
cssz-57b	Central and South America	280.3640	-9.9663	328.7	6.6	5
cssz-57x	Central and South America	281.8205	-9.0933	328.7	23.4	57.94
cssz-57y	Central and South America	281.4636	-9.3074	328.7	23.4	38.08
cssz-57z	Central and South America	281.1065	-9.5215	328.7	23.4	18.22
cssz-58a	Central and South America	281.2275	-10.5350	330.5	9.2	10.4
cssz-58b	Central and South America	280.8348	-10.7532	330.5	6.2	5
cssz-58y	Central and South America	281.9548	-10.1306	330.5	23.8	38.57
cssz-58z	Central and South America	281.5913	-10.3328	330.5	23.8	18.39
cssz-59a	Central and South America	281.6735	-11.2430	326.2	9.8	10.05
cssz-59b	Central and South America	281.2982	-11.4890	326.2	5.8	5
cssz-59y	Central and South America	282.3675	-10.7876	326.2	24.2	39.06
cssz-59z	Central and South America	282.0206	-11.0153	326.2	24.2	18.56
cssz-60a	Central and South America	282.1864	-11.9946	326.5	10.4	9.71
cssz-60b	Central and South America	281.8096	-12.2384	326.5	5.4	5
cssz-60y	Central and South America	282.8821	-11.5438	326.5	24.6	39.55
cssz-60z	Central and South America	282.5344	-11.7692	326.5	24.6	18.73
cssz-61a	Central and South America	282.6944	-12.7263	325.5	11	9.36
cssz-61b	Central and South America	282.3218	-12.9762	325.5	5	5
cssz-61y	Central and South America	283.3814	-12.2649	325.5	25	40.03
cssz-61z	Central and South America	283.0381	-12.4956	325.5	25	18.9
cssz-62a	Central and South America	283.1980	-13.3556	319	11	9.79
cssz-62b	Central and South America	282.8560	-13.6451	319	5.5	5
cssz-62y	Central and South America	283.8178	-12.8300	319	27	42.03
cssz-62z	Central and South America	283.5081	-13.0928	319	27	19.33
cssz-63a	Central and South America	283.8032	-14.0147	317.9	11	10.23
cssz-63b	Central and South America	283.4661	-14.3106	317.9	6	5
cssz-63z	Central and South America	284.1032	-13.7511	317.9	29	19.77
cssz-64a	Central and South America	284.4144	-14.6482	315.7	13	11.96
cssz-64b	Central and South America	284.0905	-14.9540	315.7	8	5
cssz-65a	Central and South America	285.0493	-15.2554	313.2	15	13.68
cssz-65b	Central and South America	284.7411	-15.5715	313.2	10	5
cssz-66a	Central and South America	285.6954	-15.7816	307.7	14.5	13.68
cssz-66b	Central and South America	285.4190	-16.1258	307.7	10	5
cssz-67a	Central and South America	286.4127	-16.2781	304.3	14	13.68
cssz-67b	Central and South America	286.1566	-16.6381	304.3	10	5
cssz-67z	Central and South America	286.6552	-15.9365	304.3	23	25.78
cssz-68a	Central and South America	287.2481	-16.9016	311.8	14	13.68
cssz-68b	Central and South America	286.9442	-17.2264	311.8	10	5
cssz-68z	Central and South America	287.5291	-16.6007	311.8	26	25.78
cssz-69a	Central and South America	287.9724	-17.5502	314.9	14	13.68
cssz-69b	Central and South America	287.6496	-17.8590	314.9	10	5
cssz-69y	Central and South America	288.5530	-16.9934	314.9	29	50.02
cssz-69z	Central and South America	288.2629	-17.2718	314.9	29	25.78

Continued on next page

Table B.2 – continued

Segment	Description	Longitude(°E)	Latitude(°N)	Strike(°)	Dip(°)	Depth (km)
cssz-70a	Central and South America	288.6731	-18.2747	320.4	14	13.25
cssz-70b	Central and South America	288.3193	-18.5527	320.4	9.5	5
cssz-70y	Central and South America	289.3032	-17.7785	320.4	30	50.35
cssz-70z	Central and South America	288.9884	-18.0266	320.4	30	25.35
cssz-71a	Central and South America	289.3089	-19.1854	333.2	14	12.82
cssz-71b	Central and South America	288.8968	-19.3820	333.2	9	5
cssz-71y	Central and South America	290.0357	-18.8382	333.2	31	50.67
cssz-71z	Central and South America	289.6725	-19.0118	333.2	31	24.92
cssz-72a	Central and South America	289.6857	-20.3117	352.4	14	12.54
cssz-72b	Central and South America	289.2250	-20.3694	352.4	8.67	5
cssz-72z	Central and South America	290.0882	-20.2613	352.4	32	24.63
cssz-73a	Central and South America	289.7731	-21.3061	358.9	14	12.24
cssz-73b	Central and South America	289.3053	-21.3142	358.9	8.33	5
cssz-73z	Central and South America	290.1768	-21.2991	358.9	33	24.34
cssz-74a	Central and South America	289.7610	-22.2671	3.06	14	11.96
cssz-74b	Central and South America	289.2909	-22.2438	3.06	8	5
cssz-75a	Central and South America	289.6982	-23.1903	4.83	14.09	11.96
cssz-75b	Central and South America	289.2261	-23.1536	4.83	8	5
cssz-76a	Central and South America	289.6237	-24.0831	4.67	14.18	11.96
cssz-76b	Central and South America	289.1484	-24.0476	4.67	8	5
cssz-77a	Central and South America	289.5538	-24.9729	4.3	14.27	11.96
cssz-77b	Central and South America	289.0750	-24.9403	4.3	8	5
cssz-78a	Central and South America	289.4904	-25.8621	3.86	14.36	11.96
cssz-78b	Central and South America	289.0081	-25.8328	3.86	8	5
cssz-79a	Central and South America	289.3491	-26.8644	11.34	14.45	11.96
cssz-79b	Central and South America	288.8712	-26.7789	11.34	8	5
cssz-80a	Central and South America	289.1231	-27.7826	14.16	14.54	11.96
cssz-80b	Central and South America	288.6469	-27.6762	14.16	8	5
cssz-81a	Central and South America	288.8943	-28.6409	13.19	14.63	11.96
cssz-81b	Central and South America	288.4124	-28.5417	13.19	8	5
cssz-82a	Central and South America	288.7113	-29.4680	9.68	14.72	11.96
cssz-82b	Central and South America	288.2196	-29.3950	9.68	8	5
cssz-83a	Central and South America	288.5944	-30.2923	5.36	14.81	11.96
cssz-83b	Central and South America	288.0938	-30.2517	5.36	8	5
cssz-84a	Central and South America	288.5223	-31.1639	3.8	14.9	11.96
cssz-84b	Central and South America	288.0163	-31.1351	3.8	8	5
cssz-85a	Central and South America	288.4748	-32.0416	2.55	15	11.96
cssz-85b	Central and South America	287.9635	-32.0223	2.55	8	5
cssz-86a	Central and South America	288.3901	-33.0041	7.01	15	11.96
cssz-86b	Central and South America	287.8768	-32.9512	7.01	8	5
cssz-87a	Central and South America	288.1050	-34.0583	19.4	15	11.96
cssz-87b	Central and South America	287.6115	-33.9142	19.4	8	5
cssz-88a	Central and South America	287.5309	-35.0437	32.81	15	11.96
cssz-88b	Central and South America	287.0862	-34.8086	32.81	8	5
cssz-88z	Central and South America	287.9308	-35.2545	32.81	30	24.9
cssz-89a	Central and South America	287.2380	-35.5993	14.52	16.67	11.96
cssz-89b	Central and South America	286.7261	-35.4914	14.52	8	5
cssz-89z	Central and South America	287.7014	-35.6968	14.52	30	26.3
cssz-90a	Central and South America	286.8442	-36.5645	22.64	18.33	11.96
cssz-90b	Central and South America	286.3548	-36.4004	22.64	8	5
cssz-90z	Central and South America	287.2916	-36.7142	22.64	30	27.68
cssz-91a	Central and South America	286.5925	-37.2488	10.9	20	11.96
cssz-91b	Central and South America	286.0721	-37.1690	10.9	8	5
cssz-91z	Central and South America	287.0726	-37.3224	10.9	30	29.06
cssz-92a	Central and South America	286.4254	-38.0945	8.23	20	11.96

Continued on next page

Table B.2 – continued

Segment	Description	Longitude(°E)	Latitude(°N)	Strike(°)	Dip(°)	Depth (km)
cssz-92b	Central and South America	285.8948	-38.0341	8.23	8	5
cssz-92z	Central and South America	286.9303	-38.1520	8.23	26.67	29.06
cssz-93a	Central and South America	286.2047	-39.0535	13.46	20	11.96
cssz-93b	Central and South America	285.6765	-38.9553	13.46	8	5
cssz-93z	Central and South America	286.7216	-39.1495	13.46	23.33	29.06
cssz-94a	Central and South America	286.0772	-39.7883	3.4	20	11.96
cssz-94b	Central and South America	285.5290	-39.7633	3.4	8	5
cssz-94z	Central and South America	286.6255	-39.8133	3.4	20	29.06
cssz-95a	Central and South America	285.9426	-40.7760	9.84	20	11.96
cssz-95b	Central and South America	285.3937	-40.7039	9.84	8	5
cssz-95z	Central and South America	286.4921	-40.8481	9.84	20	29.06
cssz-96a	Central and South America	285.7839	-41.6303	7.6	20	11.96
cssz-96b	Central and South America	285.2245	-41.5745	7.6	8	5
cssz-96x	Central and South America	287.4652	-41.7977	7.6	20	63.26
cssz-96y	Central and South America	286.9043	-41.7419	7.6	20	46.16
cssz-96z	Central and South America	286.3439	-41.6861	7.6	20	29.06
cssz-97a	Central and South America	285.6695	-42.4882	5.3	20	11.96
cssz-97b	Central and South America	285.0998	-42.4492	5.3	8	5
cssz-97x	Central and South America	287.3809	-42.6052	5.3	20	63.26
cssz-97y	Central and South America	286.8101	-42.5662	5.3	20	46.16
cssz-97z	Central and South America	286.2396	-42.5272	5.3	20	29.06
cssz-98a	Central and South America	285.5035	-43.4553	10.53	20	11.96
cssz-98b	Central and South America	284.9322	-43.3782	10.53	8	5
cssz-98x	Central and South America	287.2218	-43.6866	10.53	20	63.26
cssz-98y	Central and South America	286.6483	-43.6095	10.53	20	46.16
cssz-98z	Central and South America	286.0755	-43.5324	10.53	20	29.06
cssz-99a	Central and South America	285.3700	-44.2595	4.86	20	11.96
cssz-99b	Central and South America	284.7830	-44.2237	4.86	8	5
cssz-99x	Central and South America	287.1332	-44.3669	4.86	20	63.26
cssz-99y	Central and South America	286.5451	-44.3311	4.86	20	46.16
cssz-99z	Central and South America	285.9574	-44.2953	4.86	20	29.06
cssz-100a	Central and South America	285.2713	-45.1664	5.68	20	11.96
cssz-100b	Central and South America	284.6758	-45.1246	5.68	8	5
cssz-100x	Central and South America	287.0603	-45.2918	5.68	20	63.26
cssz-100y	Central and South America	286.4635	-45.2500	5.68	20	46.16
cssz-100z	Central and South America	285.8672	-45.2082	5.68	20	29.06
cssz-101a	Central and South America	285.3080	-45.8607	352.6	20	9.36
cssz-101b	Central and South America	284.7067	-45.9152	352.6	5	5
cssz-101y	Central and South America	286.5089	-45.7517	352.6	20	43.56
cssz-101z	Central and South America	285.9088	-45.8062	352.6	20	26.46
cssz-102a	Central and South America	285.2028	-47.1185	17.72	5	9.36
cssz-102b	Central and South America	284.5772	-46.9823	17.72	5	5
cssz-102y	Central and South America	286.4588	-47.3909	17.72	5	18.07
cssz-102z	Central and South America	285.8300	-47.2547	17.72	5	13.72
cssz-103a	Central and South America	284.7075	-48.0396	23.37	7.5	11.53
cssz-103b	Central and South America	284.0972	-47.8630	23.37	7.5	5
cssz-103x	Central and South America	286.5511	-48.5694	23.37	7.5	31.11
cssz-103y	Central and South America	285.9344	-48.3928	23.37	7.5	24.58
cssz-103z	Central and South America	285.3199	-48.2162	23.37	7.5	18.05
cssz-104a	Central and South America	284.3440	-48.7597	14.87	10	13.68
cssz-104b	Central and South America	283.6962	-48.6462	14.87	10	5
cssz-104x	Central and South America	286.2962	-49.1002	14.87	10	39.73
cssz-104y	Central and South America	285.6440	-48.9867	14.87	10	31.05
cssz-104z	Central and South America	284.9933	-48.8732	14.87	10	22.36
cssz-105a	Central and South America	284.2312	-49.4198	0.25	9.67	13.4

Continued on next page

Table B.2 – continued

Segment	Description	Longitude(°E)	Latitude(°N)	Strike(°)	Dip(°)	Depth (km)
cssz-105b	Central and South America	283.5518	-49.4179	0.25	9.67	5
cssz-105x	Central and South America	286.2718	-49.4255	0.25	9.67	38.59
cssz-105y	Central and South America	285.5908	-49.4236	0.25	9.67	30.2
cssz-105z	Central and South America	284.9114	-49.4217	0.25	9.67	21.8
cssz-106a	Central and South America	284.3730	-50.1117	347.5	9.25	13.04
cssz-106b	Central and South America	283.6974	-50.2077	347.5	9.25	5
cssz-106x	Central and South America	286.3916	-49.8238	347.5	9.25	37.15
cssz-106y	Central and South America	285.7201	-49.9198	347.5	9.25	29.11
cssz-106z	Central and South America	285.0472	-50.0157	347.5	9.25	21.07
cssz-107a	Central and South America	284.7130	-50.9714	346.5	9	12.82
cssz-107b	Central and South America	284.0273	-51.0751	346.5	9	5
cssz-107x	Central and South America	286.7611	-50.6603	346.5	9	36.29
cssz-107y	Central and South America	286.0799	-50.7640	346.5	9	28.47
cssz-107z	Central and South America	285.3972	-50.8677	346.5	9	20.64
cssz-108a	Central and South America	285.0378	-51.9370	352	8.67	12.54
cssz-108b	Central and South America	284.3241	-51.9987	352	8.67	5
cssz-108x	Central and South America	287.1729	-51.7519	352	8.67	35.15
cssz-108y	Central and South America	286.4622	-51.8136	352	8.67	27.61
cssz-108z	Central and South America	285.7505	-51.8753	352	8.67	20.07
cssz-109a	Central and South America	285.2635	-52.8439	353.1	8.33	12.24
cssz-109b	Central and South America	284.5326	-52.8974	353.1	8.33	5
cssz-109x	Central and South America	287.4508	-52.6834	353.1	8.33	33.97
cssz-109y	Central and South America	286.7226	-52.7369	353.1	8.33	26.73
cssz-109z	Central and South America	285.9935	-52.7904	353.1	8.33	19.49
cssz-110a	Central and South America	285.5705	-53.4139	334.2	8	11.96
cssz-110b	Central and South America	284.8972	-53.6076	334.2	8	5
cssz-110x	Central and South America	287.5724	-52.8328	334.2	8	32.83
cssz-110y	Central and South America	286.9081	-53.0265	334.2	8	25.88
cssz-110z	Central and South America	286.2408	-53.2202	334.2	8	18.92
cssz-111a	Central and South America	286.1627	-53.8749	313.8	8	11.96
cssz-111b	Central and South America	285.6382	-54.1958	313.8	8	5
cssz-111x	Central and South America	287.7124	-52.9122	313.8	8	32.83
cssz-111y	Central and South America	287.1997	-53.2331	313.8	8	25.88
cssz-111z	Central and South America	286.6832	-53.5540	313.8	8	18.92
cssz-112a	Central and South America	287.3287	-54.5394	316.4	8	11.96
cssz-112b	Central and South America	286.7715	-54.8462	316.4	8	5
cssz-112x	Central and South America	288.9756	-53.6190	316.4	8	32.83
cssz-112y	Central and South America	288.4307	-53.9258	316.4	8	25.88
cssz-112z	Central and South America	287.8817	-54.2326	316.4	8	18.92
cssz-113a	Central and South America	288.3409	-55.0480	307.6	8	11.96
cssz-113b	Central and South America	287.8647	-55.4002	307.6	8	5
cssz-113x	Central and South America	289.7450	-53.9914	307.6	8	32.83
cssz-113y	Central and South America	289.2810	-54.3436	307.6	8	25.88
cssz-113z	Central and South America	288.8130	-54.6958	307.6	8	18.92
cssz-114a	Central and South America	289.5342	-55.5026	301.5	8	11.96
cssz-114b	Central and South America	289.1221	-55.8819	301.5	8	5
cssz-114x	Central and South America	290.7472	-54.3647	301.5	8	32.83
cssz-114y	Central and South America	290.3467	-54.7440	301.5	8	25.88
cssz-114z	Central and South America	289.9424	-55.1233	301.5	8	18.92
cssz-115a	Central and South America	290.7682	-55.8485	292.7	8	11.96
cssz-115b	Central and South America	290.4608	-56.2588	292.7	8	5
cssz-115x	Central and South America	291.6714	-54.6176	292.7	8	32.83
cssz-115y	Central and South America	291.3734	-55.0279	292.7	8	25.88
cssz-115z	Central and South America	291.0724	-55.4382	292.7	8	18.92

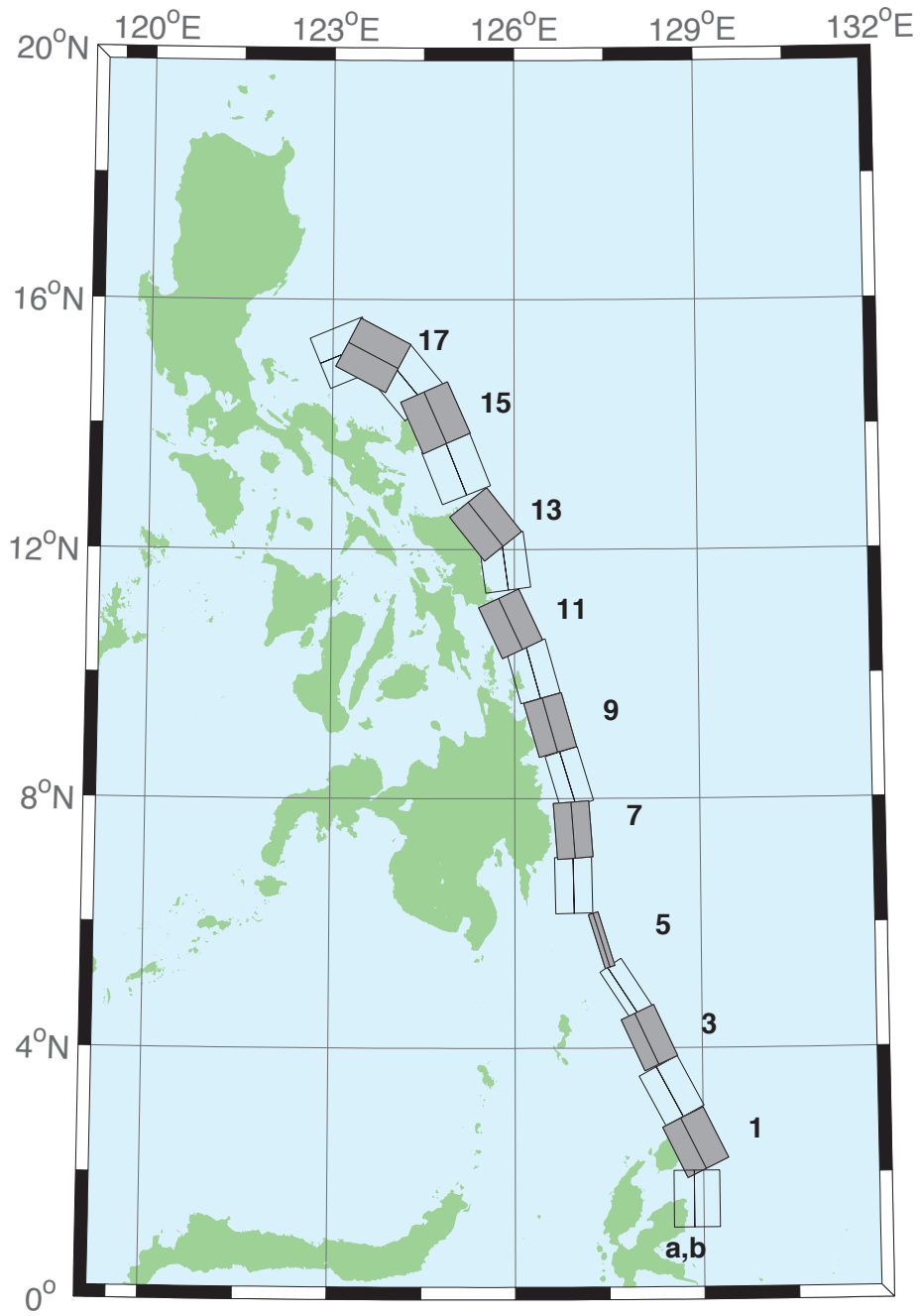


Figure B.3: Eastern Philippines Subduction Zone unit sources.

Table B.3: Earthquake parameters for Eastern Philippines Subduction Zone unit sources.

Segment	Description	Longitude(°E)	Latitude(°N)	Strike(°)	Dip(°)	Depth (km)
epsz-1a	Eastern Philippines	128.5521	2.3289	153.6	44.2	27.62
epsz-1b	Eastern Philippines	128.8408	2.4720	153.6	26.9	5
epsz-2a	Eastern Philippines	128.1943	3.1508	151.9	45.9	32.44
epsz-2b	Eastern Philippines	128.4706	3.2979	151.9	32.8	5.35
epsz-3a	Eastern Philippines	127.8899	4.0428	155.2	57.3	40.22
epsz-3b	Eastern Philippines	128.1108	4.1445	155.2	42.7	6.31
epsz-4a	Eastern Philippines	127.6120	4.8371	146.8	71.4	48.25
epsz-4b	Eastern Philippines	127.7324	4.9155	146.8	54.8	7.39
epsz-5a	Eastern Philippines	127.3173	5.7040	162.9	79.9	57.4
epsz-5b	Eastern Philippines	127.3930	5.7272	162.9	79.4	8.25
epsz-6a	Eastern Philippines	126.6488	6.6027	178.9	48.6	45.09
epsz-6b	Eastern Philippines	126.9478	6.6085	178.9	48.6	7.58
epsz-7a	Eastern Philippines	126.6578	7.4711	175.8	50.7	45.52
epsz-7b	Eastern Philippines	126.9439	7.4921	175.8	50.7	6.83
epsz-8a	Eastern Philippines	126.6227	8.2456	163.3	56.7	45.6
epsz-8b	Eastern Philippines	126.8614	8.3164	163.3	48.9	7.92
epsz-9a	Eastern Philippines	126.2751	9.0961	164.1	47	43.59
epsz-9b	Eastern Philippines	126.5735	9.1801	164.1	44.9	8.3
epsz-10a	Eastern Philippines	125.9798	9.9559	164.5	43.1	42.25
epsz-10b	Eastern Philippines	126.3007	10.0438	164.5	43.1	8.09
epsz-11a	Eastern Philippines	125.6079	10.6557	155	37.8	38.29
epsz-11b	Eastern Philippines	125.9353	10.8059	155	37.8	7.64
epsz-12a	Eastern Philippines	125.4697	11.7452	172.1	36	37.01
epsz-12b	Eastern Philippines	125.8374	11.7949	172.1	36	7.62
epsz-13a	Eastern Philippines	125.2238	12.1670	141.5	32.4	33.87
epsz-13b	Eastern Philippines	125.5278	12.4029	141.5	32.4	7.08
epsz-14a	Eastern Philippines	124.6476	13.1365	158.2	23	25.92
epsz-14b	Eastern Philippines	125.0421	13.2898	158.2	23	6.38
epsz-15a	Eastern Philippines	124.3107	13.9453	156.1	24.1	26.51
epsz-15b	Eastern Philippines	124.6973	14.1113	156.1	24.1	6.09
epsz-16a	Eastern Philippines	123.8998	14.4025	140.3	19.5	21.69
epsz-16b	Eastern Philippines	124.2366	14.6728	140.3	19.5	5
epsz-17a	Eastern Philippines	123.4604	14.7222	117.6	15.3	18.19
epsz-17b	Eastern Philippines	123.6682	15.1062	117.6	15.3	5
epsz-18a	Eastern Philippines	123.3946	14.7462	67.4	15	17.94
epsz-18b	Eastern Philippines	123.2219	15.1467	67.4	15	5
epsz-19a	Eastern Philippines	121.3638	15.7400	189.6	15	17.94
epsz-19b	Eastern Philippines	121.8082	15.6674	189.6	15	5
epsz-20a	Eastern Philippines	121.6833	16.7930	203.3	15	17.94
epsz-20b	Eastern Philippines	122.0994	16.6216	203.3	15	5
epsz-21a	Eastern Philippines	121.8279	17.3742	184.2	15	17.94
epsz-21b	Eastern Philippines	122.2814	17.3425	184.2	15	5

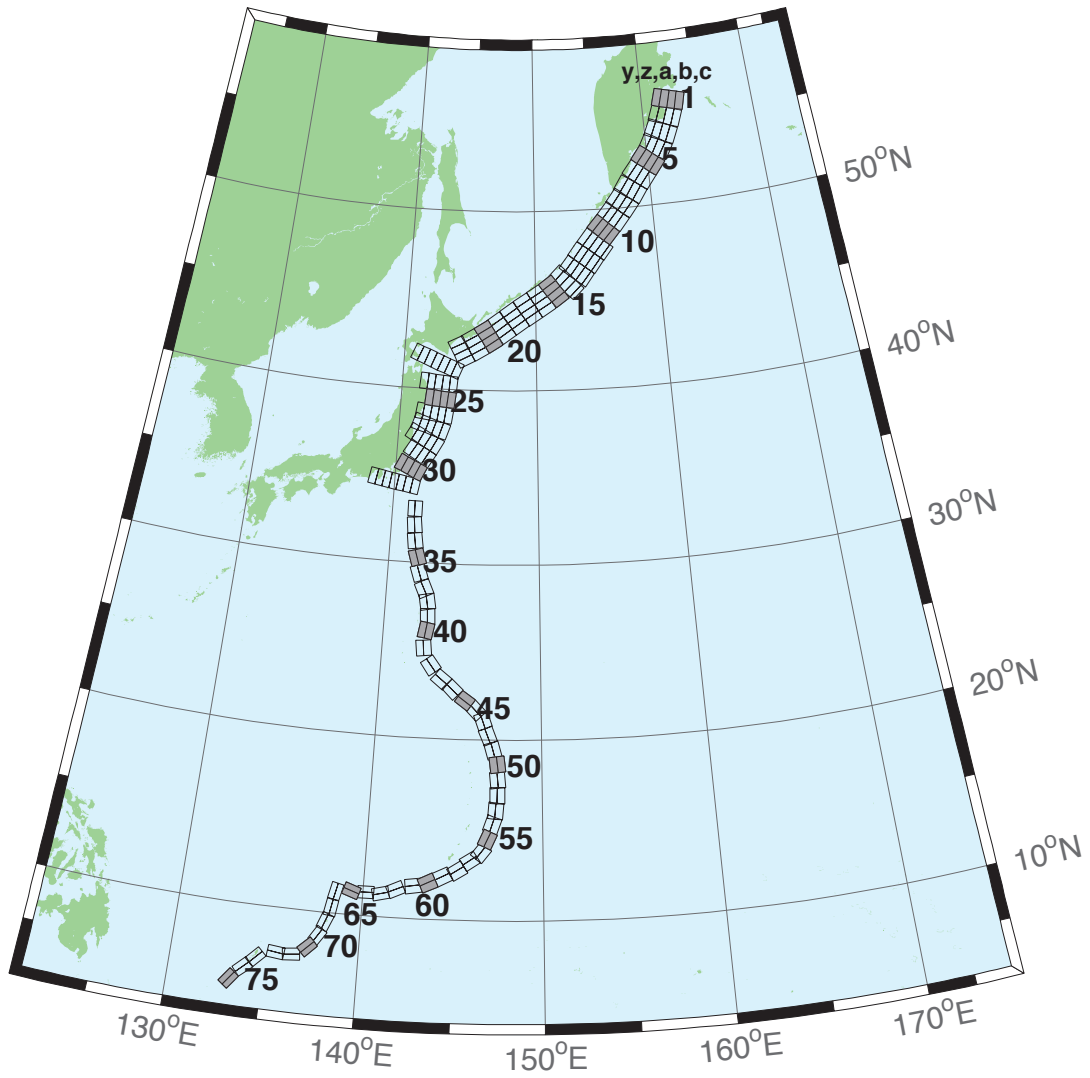


Figure B.4: Kamchatka-Kuril-Japan-Izu-Mariana-Yap Subduction Zone unit sources.

Table B.4: Earthquake parameters for Kamchatka-Kuril-Japan-Izu-Mariana-Yap Subduction Zone unit sources.

Segment	Description	Longitude(°E)	Latitude(°N)	Strike(°)	Dip(°)	Depth (km)
kisz-1a	Kamchatka-Kuril-Japan-Izu-Mariana-Yap	162.4318	55.5017	195	29	26.13
kisz-1b	Kamchatka-Kuril-Japan-Izu-Mariana-Yap	163.1000	55.4000	195	25	5
kisz-1y	Kamchatka-Kuril-Japan-Izu-Mariana-Yap	161.0884	55.7050	195	29	74.61
kisz-1z	Kamchatka-Kuril-Japan-Izu-Mariana-Yap	161.7610	55.6033	195	29	50.37
kisz-2a	Kamchatka-Kuril-Japan-Izu-Mariana-Yap	161.9883	54.6784	200	29	26.13
kisz-2b	Kamchatka-Kuril-Japan-Izu-Mariana-Yap	162.6247	54.5440	200	25	5
kisz-2y	Kamchatka-Kuril-Japan-Izu-Mariana-Yap	160.7072	54.9471	200	29	74.61
kisz-2z	Kamchatka-Kuril-Japan-Izu-Mariana-Yap	161.3488	54.8127	200	29	50.37
kisz-3a	Kamchatka-Kuril-Japan-Izu-Mariana-Yap	161.4385	53.8714	204	29	26.13
kisz-3b	Kamchatka-Kuril-Japan-Izu-Mariana-Yap	162.0449	53.7116	204	25	5
kisz-3y	Kamchatka-Kuril-Japan-Izu-Mariana-Yap	160.2164	54.1910	204	29	74.61
kisz-3z	Kamchatka-Kuril-Japan-Izu-Mariana-Yap	160.8286	54.0312	204	29	50.37
kisz-4a	Kamchatka-Kuril-Japan-Izu-Mariana-Yap	160.7926	53.1087	210	29	26.13
kisz-4b	Kamchatka-Kuril-Japan-Izu-Mariana-Yap	161.3568	52.9123	210	25	5
kisz-4y	Kamchatka-Kuril-Japan-Izu-Mariana-Yap	159.6539	53.5015	210	29	74.61
kisz-4z	Kamchatka-Kuril-Japan-Izu-Mariana-Yap	160.2246	53.3051	210	29	50.37
kisz-5a	Kamchatka-Kuril-Japan-Izu-Mariana-Yap	160.0211	52.4113	218	29	26.13
kisz-5b	Kamchatka-Kuril-Japan-Izu-Mariana-Yap	160.5258	52.1694	218	25	5
kisz-5y	Kamchatka-Kuril-Japan-Izu-Mariana-Yap	159.0005	52.8950	218	29	74.61
kisz-5z	Kamchatka-Kuril-Japan-Izu-Mariana-Yap	159.5122	52.6531	218	29	50.37
kisz-6a	Kamchatka-Kuril-Japan-Izu-Mariana-Yap	159.1272	51.7034	218	29	26.13
kisz-6b	Kamchatka-Kuril-Japan-Izu-Mariana-Yap	159.6241	51.4615	218	25	5
kisz-6y	Kamchatka-Kuril-Japan-Izu-Mariana-Yap	158.1228	52.1871	218	29	74.61
kisz-6z	Kamchatka-Kuril-Japan-Izu-Mariana-Yap	158.6263	51.9452	218	29	50.37
kisz-7a	Kamchatka-Kuril-Japan-Izu-Mariana-Yap	158.2625	50.9549	214	29	26.13
kisz-7b	Kamchatka-Kuril-Japan-Izu-Mariana-Yap	158.7771	50.7352	214	25	5
kisz-7y	Kamchatka-Kuril-Japan-Izu-Mariana-Yap	157.2236	51.3942	214	29	74.61
kisz-7z	Kamchatka-Kuril-Japan-Izu-Mariana-Yap	157.7443	51.1745	214	29	50.37
kisz-8a	Kamchatka-Kuril-Japan-Izu-Mariana-Yap	157.4712	50.2459	218	31	27.7
kisz-8b	Kamchatka-Kuril-Japan-Izu-Mariana-Yap	157.9433	50.0089	218	27	5
kisz-8y	Kamchatka-Kuril-Japan-Izu-Mariana-Yap	156.5176	50.7199	218	31	79.2
kisz-8z	Kamchatka-Kuril-Japan-Izu-Mariana-Yap	156.9956	50.4829	218	31	53.45
kisz-9a	Kamchatka-Kuril-Japan-Izu-Mariana-Yap	156.6114	49.5583	220	31	27.7
kisz-9b	Kamchatka-Kuril-Japan-Izu-Mariana-Yap	157.0638	49.3109	220	27	5
kisz-9y	Kamchatka-Kuril-Japan-Izu-Mariana-Yap	155.6974	50.0533	220	31	79.2
kisz-9z	Kamchatka-Kuril-Japan-Izu-Mariana-Yap	156.1556	49.8058	220	31	53.45
kisz-10a	Kamchatka-Kuril-Japan-Izu-Mariana-Yap	155.7294	48.8804	221	31	27.7
kisz-10b	Kamchatka-Kuril-Japan-Izu-Mariana-Yap	156.1690	48.6278	221	27	5
kisz-10y	Kamchatka-Kuril-Japan-Izu-Mariana-Yap	154.8413	49.3856	221	31	79.2
kisz-10z	Kamchatka-Kuril-Japan-Izu-Mariana-Yap	155.2865	49.1330	221	31	53.45
kisz-11a	Kamchatka-Kuril-Japan-Izu-Mariana-Yap	154.8489	48.1821	219	31	27.7
kisz-11b	Kamchatka-Kuril-Japan-Izu-Mariana-Yap	155.2955	47.9398	219	27	5
kisz-11y	Kamchatka-Kuril-Japan-Izu-Mariana-Yap	153.9472	48.6667	219	31	79.2
kisz-11z	Kamchatka-Kuril-Japan-Izu-Mariana-Yap	154.3991	48.4244	219	31	53.45
kisz-11c	Kamchatka-Kuril-Japan-Izu-Mariana-Yap	156.0358	47.5374	39	57.89	4.602
kisz-12a	Kamchatka-Kuril-Japan-Izu-Mariana-Yap	153.9994	47.4729	217	31	27.7
kisz-12b	Kamchatka-Kuril-Japan-Izu-Mariana-Yap	154.4701	47.2320	217	27	5
kisz-12y	Kamchatka-Kuril-Japan-Izu-Mariana-Yap	153.0856	47.9363	217	31	79.2
kisz-12z	Kamchatka-Kuril-Japan-Izu-Mariana-Yap	153.5435	47.7046	217	31	53.45
kisz-12c	Kamchatka-Kuril-Japan-Izu-Mariana-Yap	155.2208	46.8473	37	57.89	4.602
kisz-13a	Kamchatka-Kuril-Japan-Izu-Mariana-Yap	153.2239	46.7564	218	31	27.7
kisz-13b	Kamchatka-Kuril-Japan-Izu-Mariana-Yap	153.6648	46.5194	218	27	5

Continued on next page

Table B.4 – continued

Segment	Description	Longitude(°E)	Latitude(°N)	Strike(°)	Dip(°)	Depth (km)
kisz-13y	Kamchatka-Kuril-Japan-Izu-Mariana-Yap	152.3343	47.2304	218	31	79.2
kisz-13z	Kamchatka-Kuril-Japan-Izu-Mariana-Yap	152.7801	46.9934	218	31	53.45
kisz-13c	Kamchatka-Kuril-Japan-Izu-Mariana-Yap	154.3957	46.1257	38	57.89	4.602
kisz-14a	Kamchatka-Kuril-Japan-Izu-Mariana-Yap	152.3657	46.1514	225	23	24.54
kisz-14b	Kamchatka-Kuril-Japan-Izu-Mariana-Yap	152.7855	45.8591	225	23	5
kisz-14y	Kamchatka-Kuril-Japan-Izu-Mariana-Yap	151.5172	46.7362	225	23	63.62
kisz-14z	Kamchatka-Kuril-Japan-Izu-Mariana-Yap	151.9426	46.4438	225	23	44.08
kisz-14c	Kamchatka-Kuril-Japan-Izu-Mariana-Yap	153.4468	45.3976	45	57.89	4.602
kisz-15a	Kamchatka-Kuril-Japan-Izu-Mariana-Yap	151.4663	45.5963	233	25	23.73
kisz-15b	Kamchatka-Kuril-Japan-Izu-Mariana-Yap	151.8144	45.2712	233	22	5
kisz-15y	Kamchatka-Kuril-Japan-Izu-Mariana-Yap	150.7619	46.2465	233	25	65.99
kisz-15z	Kamchatka-Kuril-Japan-Izu-Mariana-Yap	151.1151	45.9214	233	25	44.86
kisz-16a	Kamchatka-Kuril-Japan-Izu-Mariana-Yap	150.4572	45.0977	237	25	23.73
kisz-16b	Kamchatka-Kuril-Japan-Izu-Mariana-Yap	150.7694	44.7563	237	22	5
kisz-16y	Kamchatka-Kuril-Japan-Izu-Mariana-Yap	149.8253	45.7804	237	25	65.99
kisz-16z	Kamchatka-Kuril-Japan-Izu-Mariana-Yap	150.1422	45.4390	237	25	44.86
kisz-17a	Kamchatka-Kuril-Japan-Izu-Mariana-Yap	149.3989	44.6084	237	25	23.73
kisz-17b	Kamchatka-Kuril-Japan-Izu-Mariana-Yap	149.7085	44.2670	237	22	5
kisz-17y	Kamchatka-Kuril-Japan-Izu-Mariana-Yap	148.7723	45.2912	237	25	65.99
kisz-17z	Kamchatka-Kuril-Japan-Izu-Mariana-Yap	149.0865	44.9498	237	25	44.86
kisz-18a	Kamchatka-Kuril-Japan-Izu-Mariana-Yap	148.3454	44.0982	235	25	23.73
kisz-18b	Kamchatka-Kuril-Japan-Izu-Mariana-Yap	148.6687	43.7647	235	22	5
kisz-18y	Kamchatka-Kuril-Japan-Izu-Mariana-Yap	147.6915	44.7651	235	25	65.99
kisz-18z	Kamchatka-Kuril-Japan-Izu-Mariana-Yap	148.0194	44.4316	235	25	44.86
kisz-19a	Kamchatka-Kuril-Japan-Izu-Mariana-Yap	147.3262	43.5619	233	25	23.73
kisz-19b	Kamchatka-Kuril-Japan-Izu-Mariana-Yap	147.6625	43.2368	233	22	5
kisz-19y	Kamchatka-Kuril-Japan-Izu-Mariana-Yap	146.6463	44.2121	233	25	65.99
kisz-19z	Kamchatka-Kuril-Japan-Izu-Mariana-Yap	146.9872	43.8870	233	25	44.86
kisz-20a	Kamchatka-Kuril-Japan-Izu-Mariana-Yap	146.3513	43.0633	237	25	23.73
kisz-20b	Kamchatka-Kuril-Japan-Izu-Mariana-Yap	146.6531	42.7219	237	22	5
kisz-20y	Kamchatka-Kuril-Japan-Izu-Mariana-Yap	145.7410	43.7461	237	25	65.99
kisz-20z	Kamchatka-Kuril-Japan-Izu-Mariana-Yap	146.0470	43.4047	237	25	44.86
kisz-21a	Kamchatka-Kuril-Japan-Izu-Mariana-Yap	145.3331	42.5948	239	25	23.73
kisz-21b	Kamchatka-Kuril-Japan-Izu-Mariana-Yap	145.6163	42.2459	239	22	5
kisz-21y	Kamchatka-Kuril-Japan-Izu-Mariana-Yap	144.7603	43.2927	239	25	65.99
kisz-21z	Kamchatka-Kuril-Japan-Izu-Mariana-Yap	145.0475	42.9438	239	25	44.86
kisz-22a	Kamchatka-Kuril-Japan-Izu-Mariana-Yap	144.3041	42.1631	242	25	23.73
kisz-22b	Kamchatka-Kuril-Japan-Izu-Mariana-Yap	144.5605	41.8037	242	22	5
kisz-22y	Kamchatka-Kuril-Japan-Izu-Mariana-Yap	143.7854	42.8819	242	25	65.99
kisz-22z	Kamchatka-Kuril-Japan-Izu-Mariana-Yap	144.0455	42.5225	242	25	44.86
kisz-23a	Kamchatka-Kuril-Japan-Izu-Mariana-Yap	143.2863	41.3335	202	21	21.28
kisz-23b	Kamchatka-Kuril-Japan-Izu-Mariana-Yap	143.8028	41.1764	202	19	5
kisz-23v	Kamchatka-Kuril-Japan-Izu-Mariana-Yap	140.6816	42.1189	202	21	110.9
kisz-23w	Kamchatka-Kuril-Japan-Izu-Mariana-Yap	141.2050	41.9618	202	21	92.95
kisz-23x	Kamchatka-Kuril-Japan-Izu-Mariana-Yap	141.7273	41.8047	202	21	75.04
kisz-23y	Kamchatka-Kuril-Japan-Izu-Mariana-Yap	142.2482	41.6476	202	21	57.12
kisz-23z	Kamchatka-Kuril-Japan-Izu-Mariana-Yap	142.7679	41.4905	202	21	39.2
kisz-24a	Kamchatka-Kuril-Japan-Izu-Mariana-Yap	142.9795	40.3490	185	21	21.28
kisz-24b	Kamchatka-Kuril-Japan-Izu-Mariana-Yap	143.5273	40.3125	185	19	5
kisz-24x	Kamchatka-Kuril-Japan-Izu-Mariana-Yap	141.3339	40.4587	185	21	75.04
kisz-24y	Kamchatka-Kuril-Japan-Izu-Mariana-Yap	141.8827	40.4221	185	21	57.12
kisz-24z	Kamchatka-Kuril-Japan-Izu-Mariana-Yap	142.4312	40.3856	185	21	39.2
kisz-25a	Kamchatka-Kuril-Japan-Izu-Mariana-Yap	142.8839	39.4541	185	21	21.28
kisz-25b	Kamchatka-Kuril-Japan-Izu-Mariana-Yap	143.4246	39.4176	185	19	5
kisz-25y	Kamchatka-Kuril-Japan-Izu-Mariana-Yap	141.8012	39.5272	185	21	57.12

Continued on next page

Table B.4 – continued

Segment	Description	Longitude(°E)	Latitude(°N)	Strike(°)	Dip(°)	Depth (km)
kisz-25z	Kamchatka-Kuril-Japan-Izu-Mariana-Yap	142.3426	39.4907	185	21	39.2
kisz-26a	Kamchatka-Kuril-Japan-Izu-Mariana-Yap	142.7622	38.5837	188	21	21.28
kisz-26b	Kamchatka-Kuril-Japan-Izu-Mariana-Yap	143.2930	38.5254	188	19	5
kisz-26x	Kamchatka-Kuril-Japan-Izu-Mariana-Yap	141.1667	38.7588	188	21	75.04
kisz-26y	Kamchatka-Kuril-Japan-Izu-Mariana-Yap	141.6990	38.7004	188	21	57.12
kisz-26z	Kamchatka-Kuril-Japan-Izu-Mariana-Yap	142.2308	38.6421	188	21	39.2
kisz-27a	Kamchatka-Kuril-Japan-Izu-Mariana-Yap	142.5320	37.7830	198	21	21.28
kisz-27b	Kamchatka-Kuril-Japan-Izu-Mariana-Yap	143.0357	37.6534	198	19	5
kisz-27x	Kamchatka-Kuril-Japan-Izu-Mariana-Yap	141.0142	38.1717	198	21	75.04
kisz-27y	Kamchatka-Kuril-Japan-Izu-Mariana-Yap	141.5210	38.0421	198	21	57.12
kisz-27z	Kamchatka-Kuril-Japan-Izu-Mariana-Yap	142.0269	37.9126	198	21	39.2
kisz-28a	Kamchatka-Kuril-Japan-Izu-Mariana-Yap	142.1315	37.0265	208	21	21.28
kisz-28b	Kamchatka-Kuril-Japan-Izu-Mariana-Yap	142.5941	36.8297	208	19	5
kisz-28x	Kamchatka-Kuril-Japan-Izu-Mariana-Yap	140.7348	37.6171	208	21	75.04
kisz-28y	Kamchatka-Kuril-Japan-Izu-Mariana-Yap	141.2016	37.4202	208	21	57.12
kisz-28z	Kamchatka-Kuril-Japan-Izu-Mariana-Yap	141.6671	37.2234	208	21	39.2
kisz-29a	Kamchatka-Kuril-Japan-Izu-Mariana-Yap	141.5970	36.2640	211	21	21.28
kisz-29b	Kamchatka-Kuril-Japan-Izu-Mariana-Yap	142.0416	36.0481	211	19	5
kisz-29y	Kamchatka-Kuril-Japan-Izu-Mariana-Yap	140.7029	36.6960	211	21	57.12
kisz-29z	Kamchatka-Kuril-Japan-Izu-Mariana-Yap	141.1506	36.4800	211	21	39.2
kisz-30a	Kamchatka-Kuril-Japan-Izu-Mariana-Yap	141.0553	35.4332	205	21	21.28
kisz-30b	Kamchatka-Kuril-Japan-Izu-Mariana-Yap	141.5207	35.2560	205	19	5
kisz-30y	Kamchatka-Kuril-Japan-Izu-Mariana-Yap	140.1204	35.7876	205	21	57.12
kisz-30z	Kamchatka-Kuril-Japan-Izu-Mariana-Yap	140.5883	35.6104	205	21	39.2
kisz-31a	Kamchatka-Kuril-Japan-Izu-Mariana-Yap	140.6956	34.4789	190	22	22.1
kisz-31b	Kamchatka-Kuril-Japan-Izu-Mariana-Yap	141.1927	34.4066	190	20	5
kisz-31v	Kamchatka-Kuril-Japan-Izu-Mariana-Yap	138.2025	34.8405	190	22	115.8
kisz-31w	Kamchatka-Kuril-Japan-Izu-Mariana-Yap	138.7021	34.7682	190	22	97.02
kisz-31x	Kamchatka-Kuril-Japan-Izu-Mariana-Yap	139.2012	34.6958	190	22	78.29
kisz-31y	Kamchatka-Kuril-Japan-Izu-Mariana-Yap	139.6997	34.6235	190	22	59.56
kisz-31z	Kamchatka-Kuril-Japan-Izu-Mariana-Yap	140.1979	34.5512	190	22	40.83
kisz-32a	Kamchatka-Kuril-Japan-Izu-Mariana-Yap	141.0551	33.0921	180	32	23.48
kisz-32b	Kamchatka-Kuril-Japan-Izu-Mariana-Yap	141.5098	33.0921	180	21.69	5
kisz-33a	Kamchatka-Kuril-Japan-Izu-Mariana-Yap	141.0924	32.1047	173.8	27.65	20.67
kisz-33b	Kamchatka-Kuril-Japan-Izu-Mariana-Yap	141.5596	32.1473	173.8	18.27	5
kisz-34a	Kamchatka-Kuril-Japan-Izu-Mariana-Yap	141.1869	31.1851	172.1	25	18.26
kisz-34b	Kamchatka-Kuril-Japan-Izu-Mariana-Yap	141.6585	31.2408	172.1	15.38	5
kisz-35a	Kamchatka-Kuril-Japan-Izu-Mariana-Yap	141.4154	30.1707	163	25	17.12
kisz-35b	Kamchatka-Kuril-Japan-Izu-Mariana-Yap	141.8662	30.2899	163	14.03	5
kisz-36a	Kamchatka-Kuril-Japan-Izu-Mariana-Yap	141.6261	29.2740	161.7	25.73	18.71
kisz-36b	Kamchatka-Kuril-Japan-Izu-Mariana-Yap	142.0670	29.4012	161.7	15.91	5
kisz-37a	Kamchatka-Kuril-Japan-Izu-Mariana-Yap	142.0120	28.3322	154.7	20	14.54
kisz-37b	Kamchatka-Kuril-Japan-Izu-Mariana-Yap	142.4463	28.5124	154.7	11	5
kisz-38a	Kamchatka-Kuril-Japan-Izu-Mariana-Yap	142.2254	27.6946	170.3	20	14.54
kisz-38b	Kamchatka-Kuril-Japan-Izu-Mariana-Yap	142.6955	27.7659	170.3	11	5
kisz-39a	Kamchatka-Kuril-Japan-Izu-Mariana-Yap	142.3085	26.9127	177.2	24.23	17.42
kisz-39b	Kamchatka-Kuril-Japan-Izu-Mariana-Yap	142.7674	26.9325	177.2	14.38	5
kisz-40a	Kamchatka-Kuril-Japan-Izu-Mariana-Yap	142.2673	26.1923	189.4	26.49	22.26
kisz-40b	Kamchatka-Kuril-Japan-Izu-Mariana-Yap	142.7090	26.1264	189.4	20.2	5
kisz-41a	Kamchatka-Kuril-Japan-Izu-Mariana-Yap	142.1595	25.0729	173.7	22.07	19.08
kisz-41b	Kamchatka-Kuril-Japan-Izu-Mariana-Yap	142.6165	25.1184	173.7	16.36	5
kisz-42a	Kamchatka-Kuril-Japan-Izu-Mariana-Yap	142.7641	23.8947	143.5	21.54	18.4
kisz-42b	Kamchatka-Kuril-Japan-Izu-Mariana-Yap	143.1321	24.1432	143.5	15.54	5
kisz-43a	Kamchatka-Kuril-Japan-Izu-Mariana-Yap	143.5281	23.0423	129.2	23.02	18.77
kisz-43b	Kamchatka-Kuril-Japan-Izu-Mariana-Yap	143.8128	23.3626	129.2	15.99	5

Continued on next page

Table B.4 – continued

Segment	Description	Longitude(°E)	Latitude(°N)	Strike(°)	Dip(°)	Depth (km)
kisz-44a	Kamchatka-Kuril-Japan-Izu-Mariana-Yap	144.2230	22.5240	134.6	28.24	18.56
kisz-44b	Kamchatka-Kuril-Japan-Izu-Mariana-Yap	144.5246	22.8056	134.6	15.74	5
kisz-45a	Kamchatka-Kuril-Japan-Izu-Mariana-Yap	145.0895	21.8866	125.8	36.73	22.79
kisz-45b	Kamchatka-Kuril-Japan-Izu-Mariana-Yap	145.3171	22.1785	125.8	20.84	5
kisz-46a	Kamchatka-Kuril-Japan-Izu-Mariana-Yap	145.6972	21.3783	135.9	30.75	20.63
kisz-46b	Kamchatka-Kuril-Japan-Izu-Mariana-Yap	145.9954	21.6469	135.9	18.22	5
kisz-47a	Kamchatka-Kuril-Japan-Izu-Mariana-Yap	146.0406	20.9341	160.1	29.87	19.62
kisz-47b	Kamchatka-Kuril-Japan-Izu-Mariana-Yap	146.4330	21.0669	160.1	17	5
kisz-48a	Kamchatka-Kuril-Japan-Izu-Mariana-Yap	146.3836	20.0690	158	32.75	19.68
kisz-48b	Kamchatka-Kuril-Japan-Izu-Mariana-Yap	146.7567	20.2108	158	17.07	5
kisz-49a	Kamchatka-Kuril-Japan-Izu-Mariana-Yap	146.6689	19.3123	164.5	25.07	21.41
kisz-49b	Kamchatka-Kuril-Japan-Izu-Mariana-Yap	147.0846	19.4212	164.5	19.16	5
kisz-50a	Kamchatka-Kuril-Japan-Izu-Mariana-Yap	146.9297	18.5663	172.1	22	22.1
kisz-50b	Kamchatka-Kuril-Japan-Izu-Mariana-Yap	147.3650	18.6238	172.1	20	5
kisz-51a	Kamchatka-Kuril-Japan-Izu-Mariana-Yap	146.9495	17.7148	175.1	22.06	22.04
kisz-51b	Kamchatka-Kuril-Japan-Izu-Mariana-Yap	147.3850	17.7503	175.1	19.93	5
kisz-52a	Kamchatka-Kuril-Japan-Izu-Mariana-Yap	146.9447	16.8869	180	25.51	18.61
kisz-52b	Kamchatka-Kuril-Japan-Izu-Mariana-Yap	147.3683	16.8869	180	15.79	5
kisz-53a	Kamchatka-Kuril-Japan-Izu-Mariana-Yap	146.8626	16.0669	185.2	27.39	18.41
kisz-53b	Kamchatka-Kuril-Japan-Izu-Mariana-Yap	147.2758	16.0309	185.2	15.56	5
kisz-54a	Kamchatka-Kuril-Japan-Izu-Mariana-Yap	146.7068	15.3883	199.1	28.12	20.91
kisz-54b	Kamchatka-Kuril-Japan-Izu-Mariana-Yap	147.0949	15.2590	199.1	18.56	5
kisz-55a	Kamchatka-Kuril-Japan-Izu-Mariana-Yap	146.4717	14.6025	204.3	29.6	26.27
kisz-55b	Kamchatka-Kuril-Japan-Izu-Mariana-Yap	146.8391	14.4415	204.3	25.18	5
kisz-56a	Kamchatka-Kuril-Japan-Izu-Mariana-Yap	146.1678	13.9485	217.4	32.04	26.79
kisz-56b	Kamchatka-Kuril-Japan-Izu-Mariana-Yap	146.4789	13.7170	217.4	25.84	5
kisz-57a	Kamchatka-Kuril-Japan-Izu-Mariana-Yap	145.6515	13.5576	235.8	37	24.54
kisz-57b	Kamchatka-Kuril-Japan-Izu-Mariana-Yap	145.8586	13.2609	235.8	23	5
kisz-58a	Kamchatka-Kuril-Japan-Izu-Mariana-Yap	144.9648	12.9990	237.8	37.72	24.54
kisz-58b	Kamchatka-Kuril-Japan-Izu-Mariana-Yap	145.1589	12.6984	237.8	23	5
kisz-59a	Kamchatka-Kuril-Japan-Izu-Mariana-Yap	144.1799	12.6914	242.9	34.33	22.31
kisz-59b	Kamchatka-Kuril-Japan-Izu-Mariana-Yap	144.3531	12.3613	242.9	20.25	5
kisz-60a	Kamchatka-Kuril-Japan-Izu-Mariana-Yap	143.3687	12.3280	244.9	30.9	20.62
kisz-60b	Kamchatka-Kuril-Japan-Izu-Mariana-Yap	143.5355	11.9788	244.9	18.2	5
kisz-61a	Kamchatka-Kuril-Japan-Izu-Mariana-Yap	142.7051	12.1507	261.8	35.41	25.51
kisz-61b	Kamchatka-Kuril-Japan-Izu-Mariana-Yap	142.7582	11.7883	261.8	24.22	5
kisz-62a	Kamchatka-Kuril-Japan-Izu-Mariana-Yap	141.6301	11.8447	245.7	39.86	34.35
kisz-62b	Kamchatka-Kuril-Japan-Izu-Mariana-Yap	141.7750	11.5305	245.7	35.94	5
kisz-63a	Kamchatka-Kuril-Japan-Izu-Mariana-Yap	140.8923	11.5740	256.2	42	38.46
kisz-63b	Kamchatka-Kuril-Japan-Izu-Mariana-Yap	140.9735	11.2498	256.2	42	5
kisz-64a	Kamchatka-Kuril-Japan-Izu-Mariana-Yap	140.1387	11.6028	269.6	42.48	38.77
kisz-64b	Kamchatka-Kuril-Japan-Izu-Mariana-Yap	140.1410	11.2716	269.6	42.48	5
kisz-65a	Kamchatka-Kuril-Japan-Izu-Mariana-Yap	139.4595	11.5883	288.7	44.16	39.83
kisz-65b	Kamchatka-Kuril-Japan-Izu-Mariana-Yap	139.3541	11.2831	288.7	44.16	5
kisz-66a	Kamchatka-Kuril-Japan-Izu-Mariana-Yap	138.1823	11.2648	193.1	45	40.36
kisz-66b	Kamchatka-Kuril-Japan-Izu-Mariana-Yap	138.4977	11.1929	193.1	45	5
kisz-67a	Kamchatka-Kuril-Japan-Izu-Mariana-Yap	137.9923	10.3398	189.8	45	40.36
kisz-67b	Kamchatka-Kuril-Japan-Izu-Mariana-Yap	138.3104	10.2856	189.8	45	5
kisz-68a	Kamchatka-Kuril-Japan-Izu-Mariana-Yap	137.7607	9.6136	201.7	45	40.36
kisz-68b	Kamchatka-Kuril-Japan-Izu-Mariana-Yap	138.0599	9.4963	201.7	45	5
kisz-69a	Kamchatka-Kuril-Japan-Izu-Mariana-Yap	137.4537	8.8996	213.5	45	40.36
kisz-69b	Kamchatka-Kuril-Japan-Izu-Mariana-Yap	137.7215	8.7241	213.5	45	5
kisz-70a	Kamchatka-Kuril-Japan-Izu-Mariana-Yap	137.0191	8.2872	226.5	45	40.36
kisz-70b	Kamchatka-Kuril-Japan-Izu-Mariana-Yap	137.2400	8.0569	226.5	45	5
kisz-71a	Kamchatka-Kuril-Japan-Izu-Mariana-Yap	136.3863	7.9078	263.9	45	40.36

Continued on next page

Table B.4 – continued

Segment	Description	Longitude(°E)	Latitude(°N)	Strike(°)	Dip(°)	Depth (km)
kisz-71b	Kamchatka-Kuril-Japan-Izu-Mariana-Yap	136.4202	7.5920	263.9	45	5
kisz-72a	Kamchatka-Kuril-Japan-Izu-Mariana-Yap	135.6310	7.9130	276.9	45	40.36
kisz-72b	Kamchatka-Kuril-Japan-Izu-Mariana-Yap	135.5926	7.5977	276.9	45	5
kisz-73a	Kamchatka-Kuril-Japan-Izu-Mariana-Yap	134.3296	7.4541	224	45	40.36
kisz-73b	Kamchatka-Kuril-Japan-Izu-Mariana-Yap	134.5600	7.2335	224	45	5
kisz-74a	Kamchatka-Kuril-Japan-Izu-Mariana-Yap	133.7125	6.8621	228.1	45	40.36
kisz-74b	Kamchatka-Kuril-Japan-Izu-Mariana-Yap	133.9263	6.6258	228.1	45	5
kisz-75a	Kamchatka-Kuril-Japan-Izu-Mariana-Yap	133.0224	6.1221	217.7	45	40.36
kisz-75b	Kamchatka-Kuril-Japan-Izu-Mariana-Yap	133.2751	5.9280	217.7	45	5

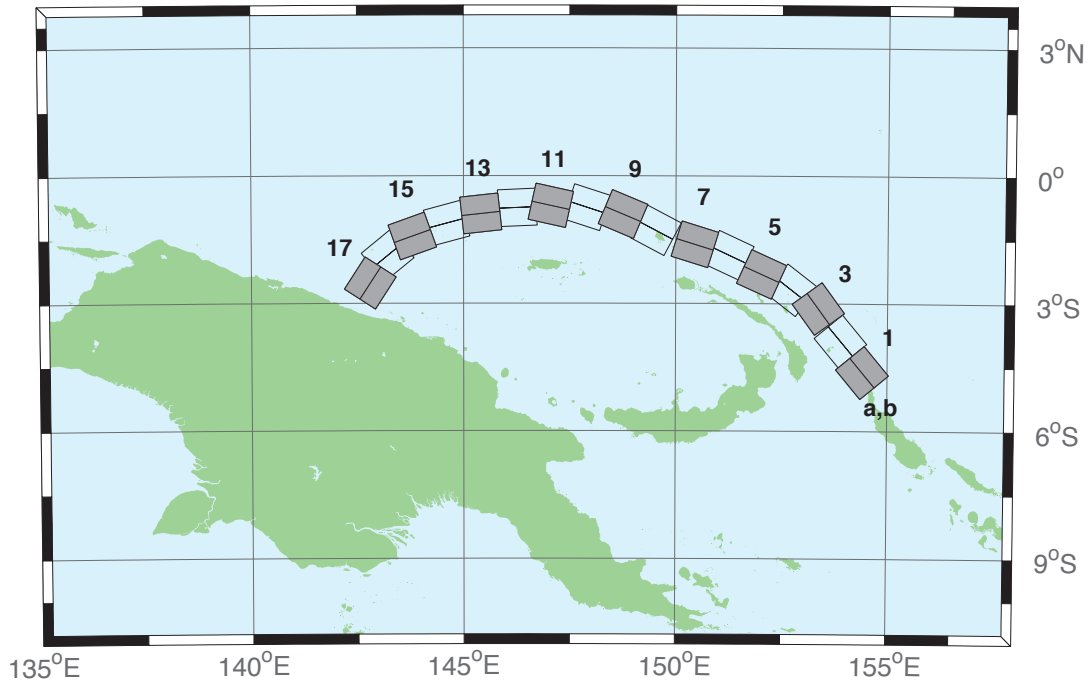


Figure B.5: Manus–Oceanic Convergent Boundary Subduction Zone unit sources.

Table B.5: Earthquake parameters for Manus–Oceanic Convergent Boundary Subduction Zone unit sources.

Segment	Description	Longitude(°E)	Latitude(°N)	Strike(°)	Dip(°)	Depth (km)
mosz-1a	Manus	154.0737	-4.8960	140.2	15	15.88
mosz-1b	Manus	154.4082	-4.6185	140.2	15	2.94
mosz-2a	Manus	153.5589	-4.1575	140.2	15	15.91
mosz-2b	Manus	153.8931	-3.8800	140.2	15	2.97
mosz-3a	Manus	153.0151	-3.3716	143.9	15	16.64
mosz-3b	Manus	153.3662	-3.1160	143.9	15	3.7
mosz-4a	Manus	152.4667	-3.0241	127.7	15	17.32
mosz-4b	Manus	152.7321	-2.6806	127.7	15	4.38
mosz-5a	Manus	151.8447	-2.7066	114.3	15	17.57
mosz-5b	Manus	152.0235	-2.3112	114.3	15	4.63
mosz-6a	Manus	151.0679	-2.2550	115	15	17.66
mosz-6b	Manus	151.2513	-1.8618	115	15	4.72
mosz-7a	Manus	150.3210	-2.0236	107.2	15	17.73
mosz-7b	Manus	150.4493	-1.6092	107.2	15	4.79
mosz-8a	Manus	149.3226	-1.6666	117.8	15	17.83
mosz-8b	Manus	149.5251	-1.2829	117.8	15	4.89
mosz-9a	Manus	148.5865	-1.3017	112.7	15	17.84
mosz-9b	Manus	148.7540	-0.9015	112.7	15	4.9
mosz-10a	Manus	147.7760	-1.1560	108	15	17.78
mosz-10b	Manus	147.9102	-0.7434	108	15	4.84
mosz-11a	Manus	146.9596	-1.1226	102.5	15	17.54
mosz-11b	Manus	147.0531	-0.6990	102.5	15	4.6
mosz-12a	Manus	146.2858	-1.1820	87.48	15	17.29
mosz-12b	Manus	146.2667	-0.7486	87.48	15	4.35
mosz-13a	Manus	145.4540	-1.3214	83.75	15	17.34
mosz-13b	Manus	145.4068	-0.8901	83.75	15	4.4
mosz-14a	Manus	144.7151	-1.5346	75.09	15	17.21
mosz-14b	Manus	144.6035	-1.1154	75.09	15	4.27
mosz-15a	Manus	143.9394	-1.8278	70.43	15	16.52
mosz-15b	Manus	143.7940	-1.4190	70.43	15	3.58
mosz-16a	Manus	143.4850	-2.2118	50.79	15	15.86
mosz-16b	Manus	143.2106	-1.8756	50.79	15	2.92
mosz-17a	Manus	143.1655	-2.7580	33	15	16.64
mosz-17b	Manus	142.8013	-2.5217	33	15	3.7

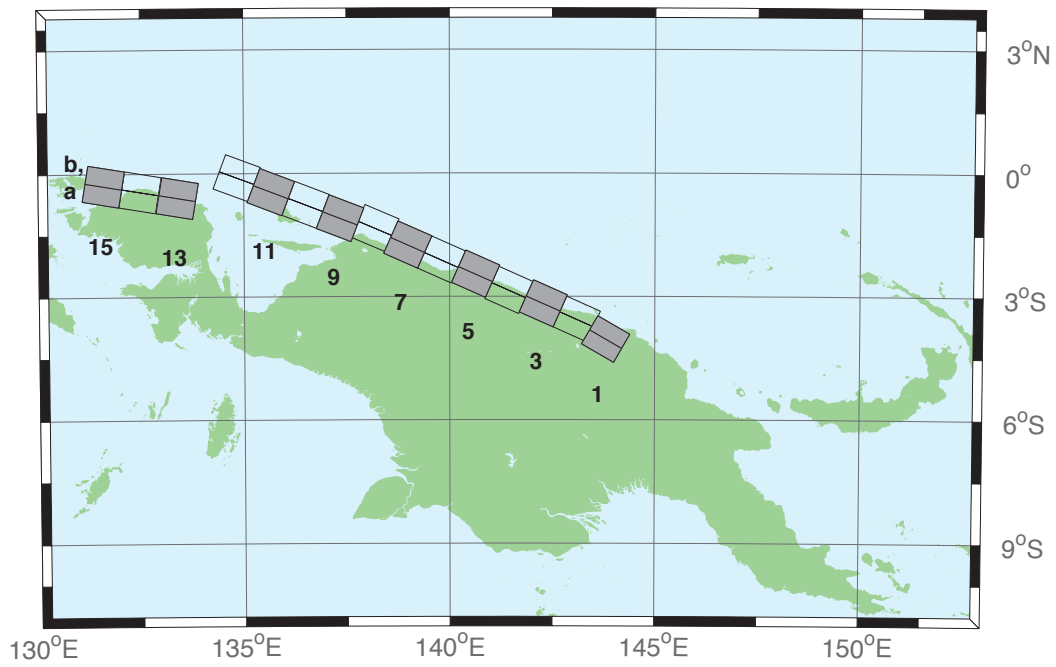


Figure B.6: New Guinea Subduction Zone unit sources.

Table B.6: Earthquake parameters for New Guinea Subduction Zone unit sources.

Segment	Description	Longitude(°E)	Latitude(°N)	Strike(°)	Dip(°)	Depth (km)
ngsz-1a	New Guinea	143.6063	-4.3804	120	29	25.64
ngsz-1b	New Guinea	143.8032	-4.0402	120	29	1.4
ngsz-2a	New Guinea	142.9310	-3.9263	114	27.63	20.1
ngsz-2b	New Guinea	143.0932	-3.5628	114	21.72	1.6
ngsz-3a	New Guinea	142.1076	-3.5632	114	20.06	18.73
ngsz-3b	New Guinea	142.2795	-3.1778	114	15.94	5
ngsz-4a	New Guinea	141.2681	-3.2376	114	21	17.76
ngsz-4b	New Guinea	141.4389	-2.8545	114	14.79	5
ngsz-5a	New Guinea	140.4592	-2.8429	114	21.26	16.14
ngsz-5b	New Guinea	140.6296	-2.4605	114	12.87	5
ngsz-6a	New Guinea	139.6288	-2.4960	114	22.72	15.4
ngsz-6b	New Guinea	139.7974	-2.1175	114	12	5
ngsz-7a	New Guinea	138.8074	-2.1312	114	21.39	15.4
ngsz-7b	New Guinea	138.9776	-1.7491	114	12	5
ngsz-8a	New Guinea	138.0185	-1.7353	113.1	18.79	15.14
ngsz-8b	New Guinea	138.1853	-1.3441	113.1	11.7	5
ngsz-9a	New Guinea	137.1805	-1.5037	111	15.24	13.23
ngsz-9b	New Guinea	137.3358	-1.0991	111	9.47	5
ngsz-10a	New Guinea	136.3418	-1.1774	111	13.51	11.09
ngsz-10b	New Guinea	136.4983	-0.7697	111	7	5
ngsz-11a	New Guinea	135.4984	-0.8641	111	11.38	12.49
ngsz-11b	New Guinea	135.6562	-0.4530	111	8.62	5
ngsz-12a	New Guinea	134.6759	-0.5216	110.5	10	13.68
ngsz-12b	New Guinea	134.8307	-0.1072	110.5	10	5
ngsz-13a	New Guinea	133.3065	-1.0298	99.5	10	13.68
ngsz-13b	New Guinea	133.3795	-0.5935	99.5	10	5
ngsz-14a	New Guinea	132.4048	-0.8816	99.5	10	13.68
ngsz-14b	New Guinea	132.4778	-0.4453	99.5	10	5
ngsz-15a	New Guinea	131.5141	-0.7353	99.5	10	13.68
ngsz-15b	New Guinea	131.5871	-0.2990	99.5	10	5

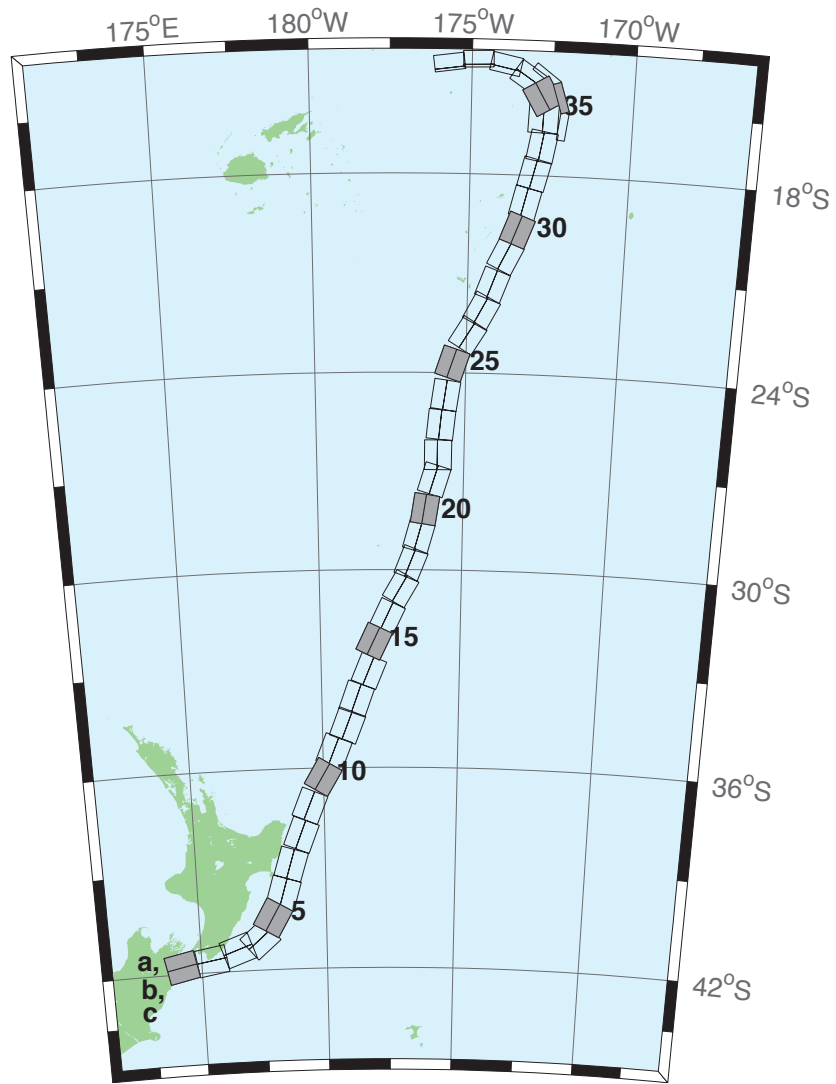


Figure B.7: New Zealand–Kermadec–Tonga Subduction Zone unit sources.

Table B.7: Earthquake parameters for New Zealand–Kermadec–Tonga Subduction Zone unit sources.

Segment	Description	Longitude(°E)	Latitude(°N)	Strike(°)	Dip(°)	Depth (km)
ntsz-1a	New Zealand–Tonga	174.0985	-41.3951	258.6	24	25.34
ntsz-1b	New Zealand–Tonga	174.2076	-41.7973	258.6	24	5
ntsz-2a	New Zealand–Tonga	175.3289	-41.2592	260.6	29.38	23.17
ntsz-2b	New Zealand–Tonga	175.4142	-41.6454	260.6	21.31	5
ntsz-3a	New Zealand–Tonga	176.2855	-40.9950	250.7	29.54	21.74
ntsz-3b	New Zealand–Tonga	176.4580	-41.3637	250.7	19.56	5
ntsz-4a	New Zealand–Tonga	177.0023	-40.7679	229.4	24.43	18.87
ntsz-4b	New Zealand–Tonga	177.3552	-41.0785	229.4	16.1	5
ntsz-5a	New Zealand–Tonga	177.4114	-40.2396	210	18.8	19.29
ntsz-5b	New Zealand–Tonga	177.8951	-40.4525	210	16.61	5
ntsz-6a	New Zealand–Tonga	177.8036	-39.6085	196.7	18.17	15.8
ntsz-6b	New Zealand–Tonga	178.3352	-39.7310	196.7	12.48	5
ntsz-7a	New Zealand–Tonga	178.1676	-38.7480	197	28.1	17.85
ntsz-7b	New Zealand–Tonga	178.6541	-38.8640	197	14.89	5
ntsz-8a	New Zealand–Tonga	178.6263	-37.8501	201.4	31.47	18.78
ntsz-8b	New Zealand–Tonga	179.0788	-37.9899	201.4	16	5
ntsz-9a	New Zealand–Tonga	178.9833	-36.9770	202.2	29.58	20.02
ntsz-9b	New Zealand–Tonga	179.4369	-37.1245	202.2	17.48	5
ntsz-10a	New Zealand–Tonga	179.5534	-36.0655	210.6	32.1	20.72
ntsz-10b	New Zealand–Tonga	179.9595	-36.2593	210.6	18.32	5
ntsz-11a	New Zealand–Tonga	179.9267	-35.3538	201.7	25	16.09
ntsz-11b	New Zealand–Tonga	180.3915	-35.5040	201.7	12.81	5
ntsz-12a	New Zealand–Tonga	180.4433	-34.5759	201.2	25	15.46
ntsz-12b	New Zealand–Tonga	180.9051	-34.7230	201.2	12.08	5
ntsz-13a	New Zealand–Tonga	180.7990	-33.7707	199.8	25.87	19.06
ntsz-13b	New Zealand–Tonga	181.2573	-33.9073	199.8	16.33	5
ntsz-14a	New Zealand–Tonga	181.2828	-32.9288	202.4	31.28	22.73
ntsz-14b	New Zealand–Tonga	181.7063	-33.0751	202.4	20.77	5
ntsz-15a	New Zealand–Tonga	181.4918	-32.0035	205.4	32.33	22.64
ntsz-15b	New Zealand–Tonga	181.8967	-32.1665	205.4	20.66	5
ntsz-16a	New Zealand–Tonga	181.9781	-31.2535	205.5	34.29	23.59
ntsz-16b	New Zealand–Tonga	182.3706	-31.4131	205.5	21.83	5
ntsz-17a	New Zealand–Tonga	182.4819	-30.3859	210.3	37.6	25.58
ntsz-17b	New Zealand–Tonga	182.8387	-30.5655	210.3	24.3	5
ntsz-18a	New Zealand–Tonga	182.8176	-29.6545	201.6	37.65	26.13
ntsz-18b	New Zealand–Tonga	183.1985	-29.7856	201.6	25	5
ntsz-19a	New Zealand–Tonga	183.0622	-28.8739	195.7	34.41	26.13
ntsz-19b	New Zealand–Tonga	183.4700	-28.9742	195.7	25	5
ntsz-20a	New Zealand–Tonga	183.2724	-28.0967	188.8	38	26.13
ntsz-20b	New Zealand–Tonga	183.6691	-28.1508	188.8	25	5
ntsz-21a	New Zealand–Tonga	183.5747	-27.1402	197.1	32.29	24.83
ntsz-21b	New Zealand–Tonga	183.9829	-27.2518	197.1	23.37	5
ntsz-22a	New Zealand–Tonga	183.6608	-26.4975	180	29.56	18.63
ntsz-22b	New Zealand–Tonga	184.0974	-26.4975	180	15.82	5
ntsz-23a	New Zealand–Tonga	183.7599	-25.5371	185.8	32.42	20.56
ntsz-23b	New Zealand–Tonga	184.1781	-25.5752	185.8	18.13	5
ntsz-24a	New Zealand–Tonga	183.9139	-24.6201	188.2	33.31	23.73
ntsz-24b	New Zealand–Tonga	184.3228	-24.6734	188.2	22	5
ntsz-25a	New Zealand–Tonga	184.1266	-23.5922	198.5	29.34	19.64
ntsz-25b	New Zealand–Tonga	184.5322	-23.7163	198.5	17.03	5
ntsz-26a	New Zealand–Tonga	184.6613	-22.6460	211.7	30.26	19.43
ntsz-26b	New Zealand–Tonga	185.0196	-22.8497	211.7	16.78	5
ntsz-27a	New Zealand–Tonga	185.0879	-21.9139	207.9	31.73	20.67

Continued on next page

Table B.7 – continued

Segment	Description	Longitude(°E)	Latitude(°N)	Strike(°)	Dip(°)	Depth (km)
ntsz-27b	New Zealand–Tonga	185.4522	-22.0928	207.9	18.27	5
ntsz-28a	New Zealand–Tonga	185.4037	-21.1758	200.5	32.44	21.76
ntsz-28b	New Zealand–Tonga	185.7849	-21.3084	200.5	19.58	5
ntsz-29a	New Zealand–Tonga	185.8087	-20.2629	206.4	32.47	20.4
ntsz-29b	New Zealand–Tonga	186.1710	-20.4312	206.4	17.94	5
ntsz-30a	New Zealand–Tonga	186.1499	-19.5087	200.9	32.98	22.46
ntsz-30b	New Zealand–Tonga	186.5236	-19.6432	200.9	20.44	5
ntsz-31a	New Zealand–Tonga	186.3538	-18.7332	193.9	34.41	21.19
ntsz-31b	New Zealand–Tonga	186.7339	-18.8221	193.9	18.89	5
ntsz-32a	New Zealand–Tonga	186.5949	-17.8587	194.1	30	19.12
ntsz-32b	New Zealand–Tonga	186.9914	-17.9536	194.1	16.4	5
ntsz-33a	New Zealand–Tonga	186.8172	-17.0581	190	33.15	23.34
ntsz-33b	New Zealand–Tonga	187.2047	-17.1237	190	21.52	5
ntsz-34a	New Zealand–Tonga	186.7814	-16.2598	182.1	15	13.41
ntsz-34b	New Zealand–Tonga	187.2330	-16.2759	182.1	9.68	5
ntsz-34c	New Zealand–Tonga	187.9697	-16.4956	7.62	57.06	6.571
ntsz-35a	New Zealand–Tonga	186.8000	-15.8563	149.8	15	12.17
ntsz-35b	New Zealand–Tonga	187.1896	-15.6384	149.8	8.24	5
ntsz-35c	New Zealand–Tonga	187.8776	-15.6325	342.4	57.06	6.571
ntsz-36a	New Zealand–Tonga	186.5406	-15.3862	123.9	40.44	36.72
ntsz-36b	New Zealand–Tonga	186.7381	-15.1025	123.9	39.38	5
ntsz-36c	New Zealand–Tonga	187.3791	-14.9234	307	57.06	6.571
ntsz-37a	New Zealand–Tonga	185.9883	-14.9861	102	68.94	30.99
ntsz-37b	New Zealand–Tonga	186.0229	-14.8282	102	31.32	5
ntsz-38a	New Zealand–Tonga	185.2067	-14.8259	88.4	80	26.13
ntsz-38b	New Zealand–Tonga	185.2044	-14.7479	88.4	25	5
ntsz-39a	New Zealand–Tonga	184.3412	-14.9409	82.55	80	26.13
ntsz-39b	New Zealand–Tonga	184.3307	-14.8636	82.55	25	5

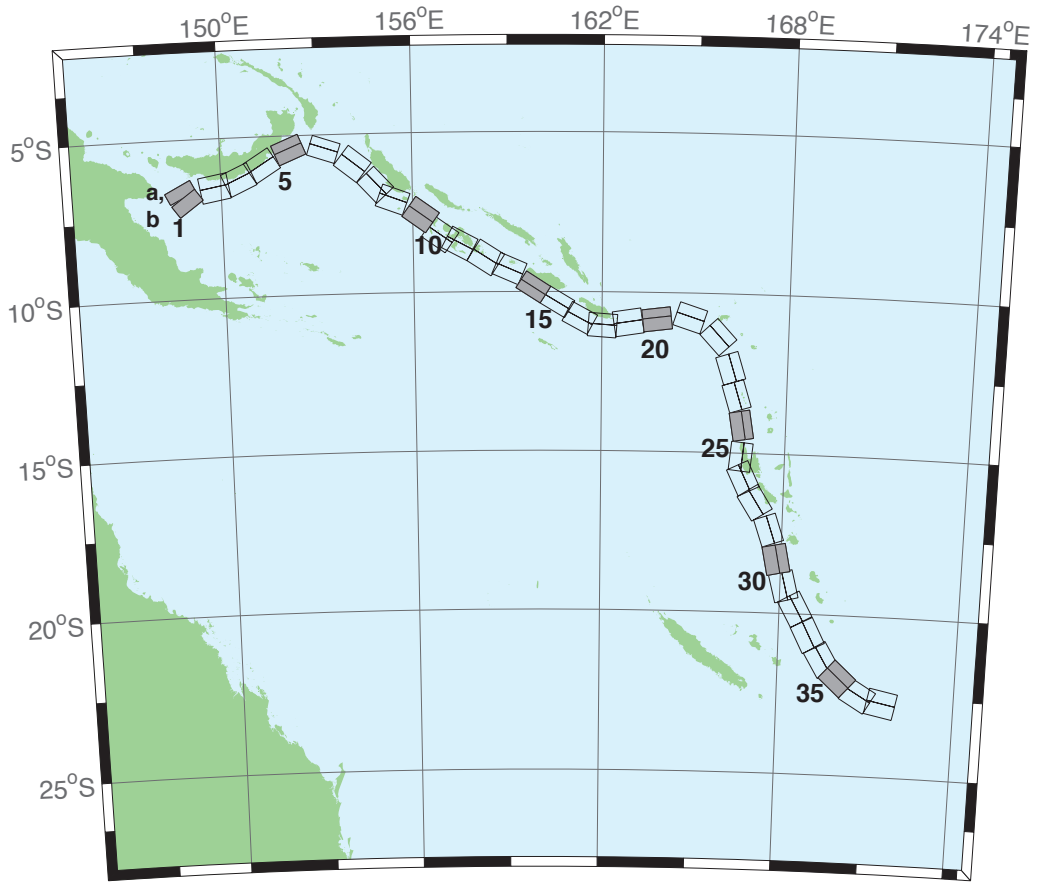


Figure B.8: New Britain–Solomons–Vanuatu Zone unit sources.

Table B.8: Earthquake parameters for New Britain–Solomons–Vanuatu Subduction Zone unit sources.

Segment	Description	Longitude(°E)	Latitude(°N)	Strike(°)	Dip(°)	Depth (km)
nvsz-1a	New Britain–Vanuatu	148.6217	-6.4616	243.2	32.34	15.69
nvsz-1b	New Britain–Vanuatu	148.7943	-6.8002	234.2	12.34	5
nvsz-2a	New Britain–Vanuatu	149.7218	-6.1459	260.1	35.1	16.36
nvsz-2b	New Britain–Vanuatu	149.7856	-6.5079	260.1	13.13	5
nvsz-3a	New Britain–Vanuatu	150.4075	-5.9659	245.7	42.35	18.59
nvsz-3b	New Britain–Vanuatu	150.5450	-6.2684	245.7	15.77	5
nvsz-4a	New Britain–Vanuatu	151.1095	-5.5820	238.2	42.41	23.63
nvsz-4b	New Britain–Vanuatu	151.2851	-5.8639	238.2	21.88	5
nvsz-5a	New Britain–Vanuatu	152.0205	-5.1305	247.7	49.22	32.39
nvsz-5b	New Britain–Vanuatu	152.1322	-5.4020	247.7	33.22	5
nvsz-6a	New Britain–Vanuatu	153.3450	-5.1558	288.6	53.53	33.59
nvsz-6b	New Britain–Vanuatu	153.2595	-5.4089	288.6	34.87	5
nvsz-7a	New Britain–Vanuatu	154.3814	-5.6308	308.3	39.72	19.18
nvsz-7b	New Britain–Vanuatu	154.1658	-5.9017	308.3	16.48	5
nvsz-8a	New Britain–Vanuatu	155.1097	-6.3511	317.2	45.33	22.92
nvsz-8b	New Britain–Vanuatu	154.8764	-6.5656	317.2	21	5
nvsz-9a	New Britain–Vanuatu	155.5027	-6.7430	290.5	48.75	22.92
nvsz-9b	New Britain–Vanuatu	155.3981	-7.0204	290.5	21	5
nvsz-10a	New Britain–Vanuatu	156.4742	-7.2515	305.9	36.88	27.62
nvsz-10b	New Britain–Vanuatu	156.2619	-7.5427	305.9	26.9	5
nvsz-11a	New Britain–Vanuatu	157.0830	-7.8830	305.4	32.97	29.72
nvsz-11b	New Britain–Vanuatu	156.8627	-8.1903	305.4	29.63	5
nvsz-12a	New Britain–Vanuatu	157.6537	-8.1483	297.9	37.53	28.57
nvsz-12b	New Britain–Vanuatu	157.4850	-8.4630	297.9	28.13	5
nvsz-13a	New Britain–Vanuatu	158.5089	-8.5953	302.7	33.62	23.02
nvsz-13b	New Britain–Vanuatu	158.3042	-8.9099	302.7	21.12	5
nvsz-14a	New Britain–Vanuatu	159.1872	-8.9516	293.3	38.44	34.06
nvsz-14b	New Britain–Vanuatu	159.0461	-9.2747	293.3	35.54	5
nvsz-15a	New Britain–Vanuatu	159.9736	-9.5993	302.8	46.69	41.38
nvsz-15b	New Britain–Vanuatu	159.8044	-9.8584	302.8	46.69	5
nvsz-16a	New Britain–Vanuatu	160.7343	-10.0574	301	46.05	41
nvsz-16b	New Britain–Vanuatu	160.5712	-10.3246	301	46.05	5
nvsz-17a	New Britain–Vanuatu	161.4562	-10.5241	298.4	40.12	37.22
nvsz-17b	New Britain–Vanuatu	161.2900	-10.8263	298.4	40.12	5
nvsz-18a	New Britain–Vanuatu	162.0467	-10.6823	274.1	40.33	29.03
nvsz-18b	New Britain–Vanuatu	162.0219	-11.0238	274.1	28.72	5
nvsz-19a	New Britain–Vanuatu	162.7818	-10.5645	261.3	34.25	24.14
nvsz-19b	New Britain–Vanuatu	162.8392	-10.9315	261.3	22.51	5
nvsz-20a	New Britain–Vanuatu	163.7222	-10.5014	262.9	50.35	26.3
nvsz-20b	New Britain–Vanuatu	163.7581	-10.7858	262.9	25.22	5
nvsz-21a	New Britain–Vanuatu	164.9445	-10.4183	287.9	40.31	23.3
nvsz-21b	New Britain–Vanuatu	164.8374	-10.7442	287.9	21.47	5
nvsz-22a	New Britain–Vanuatu	166.0261	-11.1069	317.1	42.39	20.78
nvsz-22b	New Britain–Vanuatu	165.7783	-11.3328	317.1	18.4	5
nvsz-23a	New Britain–Vanuatu	166.5179	-12.2260	342.4	47.95	22.43
nvsz-23b	New Britain–Vanuatu	166.2244	-12.3171	342.4	20.4	5
nvsz-24a	New Britain–Vanuatu	166.7236	-13.1065	342.6	47.13	28.52
nvsz-24b	New Britain–Vanuatu	166.4241	-13.1979	342.6	28.06	5
nvsz-25a	New Britain–Vanuatu	166.8914	-14.0785	350.3	54.1	31.16
nvsz-25b	New Britain–Vanuatu	166.6237	-14.1230	350.3	31.55	5
nvsz-26a	New Britain–Vanuatu	166.9200	-15.1450	365.6	50.46	29.05
nvsz-26b	New Britain–Vanuatu	166.6252	-15.1170	365.6	28.75	5
nvsz-27a	New Britain–Vanuatu	167.0053	-15.6308	334.2	44.74	25.46

Continued on next page

Table B.8 – continued

Segment	Description	Longitude(°E)	Latitude(°N)	Strike(°)	Dip(°)	Depth (km)
nvsz-27b	New Britain–Vanuatu	166.7068	-15.7695	334.2	24.15	5
nvsz-28a	New Britain–Vanuatu	167.4074	-16.3455	327.5	41.53	22.44
nvsz-28b	New Britain–Vanuatu	167.1117	-16.5264	327.5	20.42	5
nvsz-29a	New Britain–Vanuatu	167.9145	-17.2807	341.2	49.1	24.12
nvsz-29b	New Britain–Vanuatu	167.6229	-17.3757	341.2	22.48	5
nvsz-30a	New Britain–Vanuatu	168.2220	-18.2353	348.6	44.19	23.99
nvsz-30b	New Britain–Vanuatu	167.8895	-18.2991	348.6	22.32	5
nvsz-31a	New Britain–Vanuatu	168.5022	-19.0510	345.6	42.2	22.26
nvsz-31b	New Britain–Vanuatu	168.1611	-19.1338	345.6	20.2	5
nvsz-32a	New Britain–Vanuatu	168.8775	-19.6724	331.1	42.03	21.68
nvsz-32b	New Britain–Vanuatu	168.5671	-19.8338	331.1	19.49	5
nvsz-33a	New Britain–Vanuatu	169.3422	-20.4892	332.9	40.25	22.4
nvsz-33b	New Britain–Vanuatu	169.0161	-20.6453	332.9	20.37	5
nvsz-34a	New Britain–Vanuatu	169.8304	-21.2121	329.1	39	22.73
nvsz-34b	New Britain–Vanuatu	169.5086	-21.3911	329.1	20.77	5
nvsz-35a	New Britain–Vanuatu	170.3119	-21.6945	311.9	39	22.13
nvsz-35b	New Britain–Vanuatu	170.0606	-21.9543	311.9	20.03	5
nvsz-36a	New Britain–Vanuatu	170.9487	-22.1585	300.4	39.42	23.5
nvsz-36b	New Britain–Vanuatu	170.7585	-22.4577	300.4	21.71	5
nvsz-37a	New Britain–Vanuatu	171.6335	-22.3087	281.3	30	22.1
nvsz-37b	New Britain–Vanuatu	171.5512	-22.6902	281.3	20	5

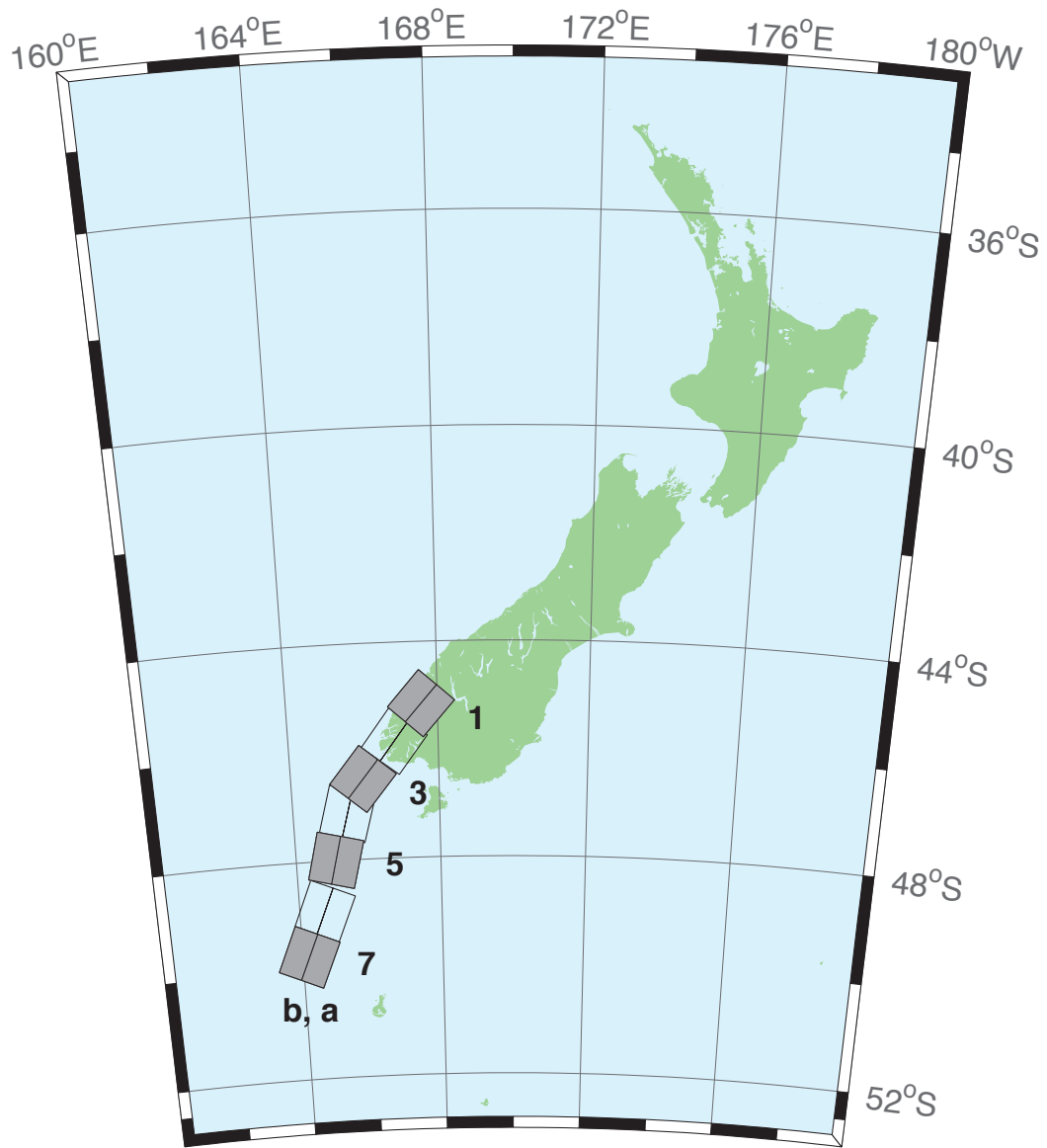


Figure B.9: New Zealand–Puysegur Zone unit sources.

Table B.9: Earthquake parameters for New Zealand–Puysegur Subduction Zone unit sources.

Segment	Description	Longitude(°E)	Latitude(°N)	Strike(°)	Dip(°)	Depth (km)
nzs-1a	New Zealand–Puysegur	168.0294	-45.4368	41.5	15	17.94
nzs-1b	New Zealand–Puysegur	167.5675	-45.1493	41.5	15	5
nzs-2a	New Zealand–Puysegur	167.3256	-46.0984	37.14	15	17.94
nzs-2b	New Zealand–Puysegur	166.8280	-45.8365	37.14	15	5
nzs-3a	New Zealand–Puysegur	166.4351	-46.7897	39.53	15	17.94
nzs-3b	New Zealand–Puysegur	165.9476	-46.5136	39.53	15	5
nzs-4a	New Zealand–Puysegur	166.0968	-47.2583	15.38	15	17.94
nzs-4b	New Zealand–Puysegur	165.4810	-47.1432	15.38	15	5
nzs-5a	New Zealand–Puysegur	165.7270	-48.0951	13.94	15	17.94
nzs-5b	New Zealand–Puysegur	165.0971	-47.9906	13.94	15	5
nzs-6a	New Zealand–Puysegur	165.3168	-49.0829	22.71	15	17.94
nzs-6b	New Zealand–Puysegur	164.7067	-48.9154	22.71	15	5
nzs-7a	New Zealand–Puysegur	164.8017	-49.9193	23.25	15	17.94
nzs-7b	New Zealand–Puysegur	164.1836	-49.7480	23.25	15	5

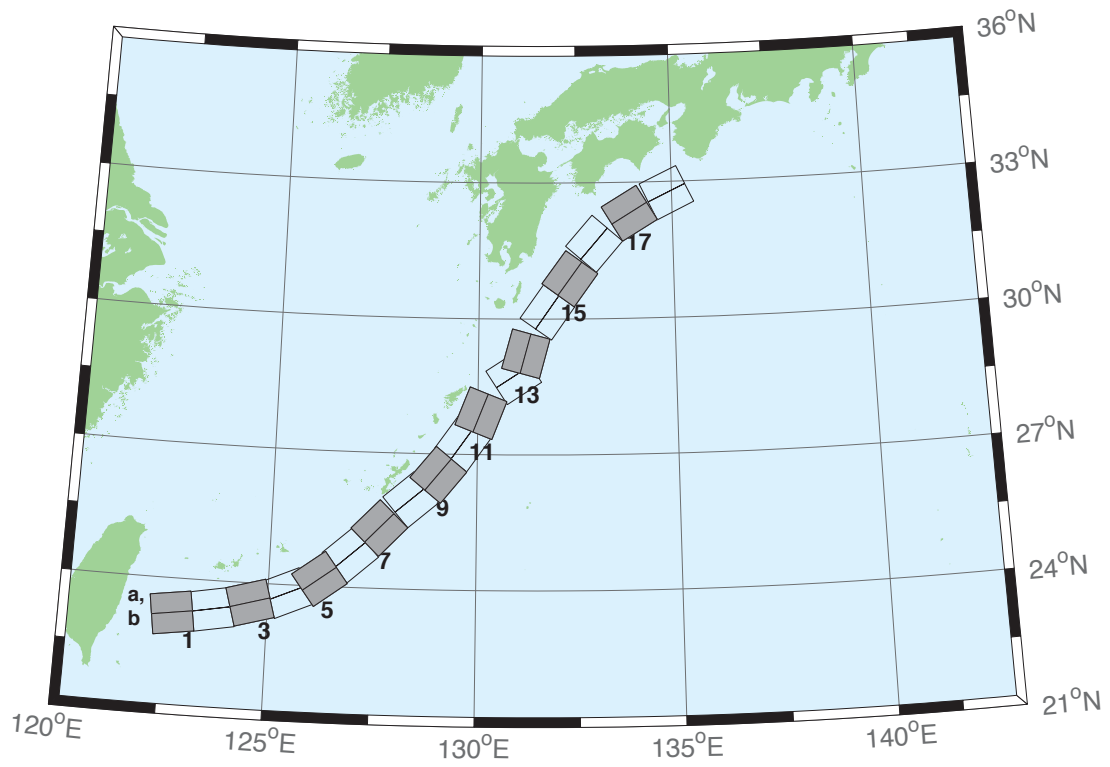


Figure B.10: Ryukyu-Kyushu-Nankai Zone unit sources.

Table B.10: Earthquake parameters for Ryukyu–Kyushu–Nankai Subduction
Zone unit sources.

Segment	Description	Longitude(°E)	Latitude(°N)	Strike(°)	Dip(°)	Depth (km)
rnsz-1a	Ryukyu–Nankai	122.6672	23.6696	262	14	11.88
rnsz-1b	Ryukyu–Nankai	122.7332	23.2380	262	10	3.2
rnsz-2a	Ryukyu–Nankai	123.5939	23.7929	259.9	18.11	12.28
rnsz-2b	Ryukyu–Nankai	123.6751	23.3725	259.9	10	3.6
rnsz-3a	Ryukyu–Nankai	124.4604	23.9777	254.6	19.27	14.65
rnsz-3b	Ryukyu–Nankai	124.5830	23.5689	254.6	12.18	4.1
rnsz-4a	Ryukyu–Nankai	125.2720	24.2102	246.8	18	20.38
rnsz-4b	Ryukyu–Nankai	125.4563	23.8177	246.8	16	6.6
rnsz-5a	Ryukyu–Nankai	125.9465	24.5085	233.6	18	20.21
rnsz-5b	Ryukyu–Nankai	126.2241	24.1645	233.6	16	6.43
rnsz-6a	Ryukyu–Nankai	126.6349	25.0402	228.7	17.16	19.55
rnsz-6b	Ryukyu–Nankai	126.9465	24.7176	228.7	15.16	6.47
rnsz-7a	Ryukyu–Nankai	127.2867	25.6343	224	15.85	17.98
rnsz-7b	Ryukyu–Nankai	127.6303	25.3339	224	13.56	6.26
rnsz-8a	Ryukyu–Nankai	128.0725	26.3146	229.7	14.55	14.31
rnsz-8b	Ryukyu–Nankai	128.3854	25.9831	229.7	9.64	5.94
rnsz-9a	Ryukyu–Nankai	128.6642	26.8177	219.2	15.4	12.62
rnsz-9b	Ryukyu–Nankai	129.0391	26.5438	219.2	8	5.66
rnsz-10a	Ryukyu–Nankai	129.2286	27.4879	215.2	17	12.55
rnsz-10b	Ryukyu–Nankai	129.6233	27.2402	215.2	8.16	5.45
rnsz-11a	Ryukyu–Nankai	129.6169	28.0741	201.3	17	12.91
rnsz-11b	Ryukyu–Nankai	130.0698	27.9181	201.3	8.8	5.26
rnsz-12a	Ryukyu–Nankai	130.6175	29.0900	236.7	16.42	13.05
rnsz-12b	Ryukyu–Nankai	130.8873	28.7299	236.7	9.57	4.74
rnsz-13a	Ryukyu–Nankai	130.7223	29.3465	195.2	20.25	15.89
rnsz-13b	Ryukyu–Nankai	131.1884	29.2362	195.2	12.98	4.66
rnsz-14a	Ryukyu–Nankai	131.3467	30.3899	215.1	22.16	19.73
rnsz-14b	Ryukyu–Nankai	131.7402	30.1507	215.1	17.48	4.71
rnsz-15a	Ryukyu–Nankai	131.9149	31.1450	216	15.11	16.12
rnsz-15b	Ryukyu–Nankai	132.3235	30.8899	216	13.46	4.48
rnsz-16a	Ryukyu–Nankai	132.5628	31.9468	220.9	10.81	10.88
rnsz-16b	Ryukyu–Nankai	132.9546	31.6579	220.9	7.19	4.62
rnsz-17a	Ryukyu–Nankai	133.6125	32.6956	239	10.14	12.01
rnsz-17b	Ryukyu–Nankai	133.8823	32.3168	239	8.41	4.7
rnsz-18a	Ryukyu–Nankai	134.6416	33.1488	244.7	10.99	14.21
rnsz-18b	Ryukyu–Nankai	134.8656	32.7502	244.5	10.97	4.7
rnsz-19a	Ryukyu–Nankai	135.6450	33.5008	246.5	14.49	14.72
rnsz-19b	Ryukyu–Nankai	135.8523	33.1021	246.5	11.87	4.44
rnsz-20a	Ryukyu–Nankai	136.5962	33.8506	244.8	15	14.38
rnsz-20b	Ryukyu–Nankai	136.8179	33.4581	244.8	12	3.98
rnsz-21a	Ryukyu–Nankai	137.2252	34.3094	231.9	15	15.4
rnsz-21b	Ryukyu–Nankai	137.5480	33.9680	231.9	12	5
rnsz-22a	Ryukyu–Nankai	137.4161	34.5249	192.3	15	15.4
rnsz-22b	Ryukyu–Nankai	137.9301	34.4327	192.3	12	5

Appendix C SIFT Testing Report

Point Reyes, California

Jean Newman

1.0 PURPOSE

Forecast models are tested with synthetic tsunami events covering a range of tsunami source locations. Testing is also done with selected historical tsunami events when available.

The purpose of forecast model testing is three-fold. The first objective is to assure that the results obtained with NOAA's tsunami forecast system, which has been released to the Tsunami Warning Centers for operational use, are identical to those obtained by the researcher during the development of the forecast model. The second objective is to test the forecast model for consistency, accuracy, time efficiency, and quality of results over a range of possible tsunami locations and magnitudes. The third objective is to identify bugs and issues in need of resolution by the researcher who developed the Forecast Model or by the forecast software development team before the next version release to NOAA's two Tsunami Warning Centers.

Local hardware and software applications, and tools familiar to the researcher(s), are used to run the Method of Splitting Tsunamis (MOST) model during the forecast model development. The test results presented in this report lend confidence that the model performs as developed and produces the same results when initiated within the forecast application in an operational setting as those produced by the researcher during the forecast model development. The test results assure those who rely on the Point Reyes tsunami forecast model that consistent results are produced irrespective of system.

2.0 TESTING PROCEDURE

The general procedure for forecast model testing is to run a set of synthetic tsunami scenarios and a selected set of historical tsunami events through the forecast system application and compare the results with those obtained by the researcher during the forecast model development and presented in the Tsunami Forecast Model Report. Specific steps taken to test the model include:

1. Identification of testing scenarios, including the standard set of synthetic events, appropriate historical events, and customized synthetic scenarios that may have been used by the researcher(s) in developing the forecast model.
2. Creation of new events to represent customized synthetic scenarios used by the researcher(s) in developing the forecast model, if any.
3. Submission of test model runs with the forecast system, and export of the results from A, B, and C grids, along with time series.
4. Recording applicable metadata, including the specific version of the forecast system used for testing.
5. Examination of forecast model results from the forecast system for instabilities in both time series and plot results.
6. Comparison of forecast model results obtained through the forecast system with those obtained during the forecast model development.
7. Summarization of results with specific mention of quality, consistency, and time efficiency.
8. Reporting of issues identified to modeler and forecast software development team.
9. Retesting the forecast models in the forecast system when reported issues have been addressed or explained.

Synthetic model runs were tested on a DELL PowerEdge R510 computer equipped with two Xeon E5670 processors at 2.93 Ghz, each with 12 MBytes of cache and 32GB memory. The processors are hex core and support hyperthreading, resulting in the computer performing as a 24 processor core machine. Additionally, the testing computer supports 10 Gigabit Ethernet for fast network connections. This computer configuration is similar or the same as the configurations of the computers installed at the Tsunami Warning Centers so the compute times should only vary slightly.

Results

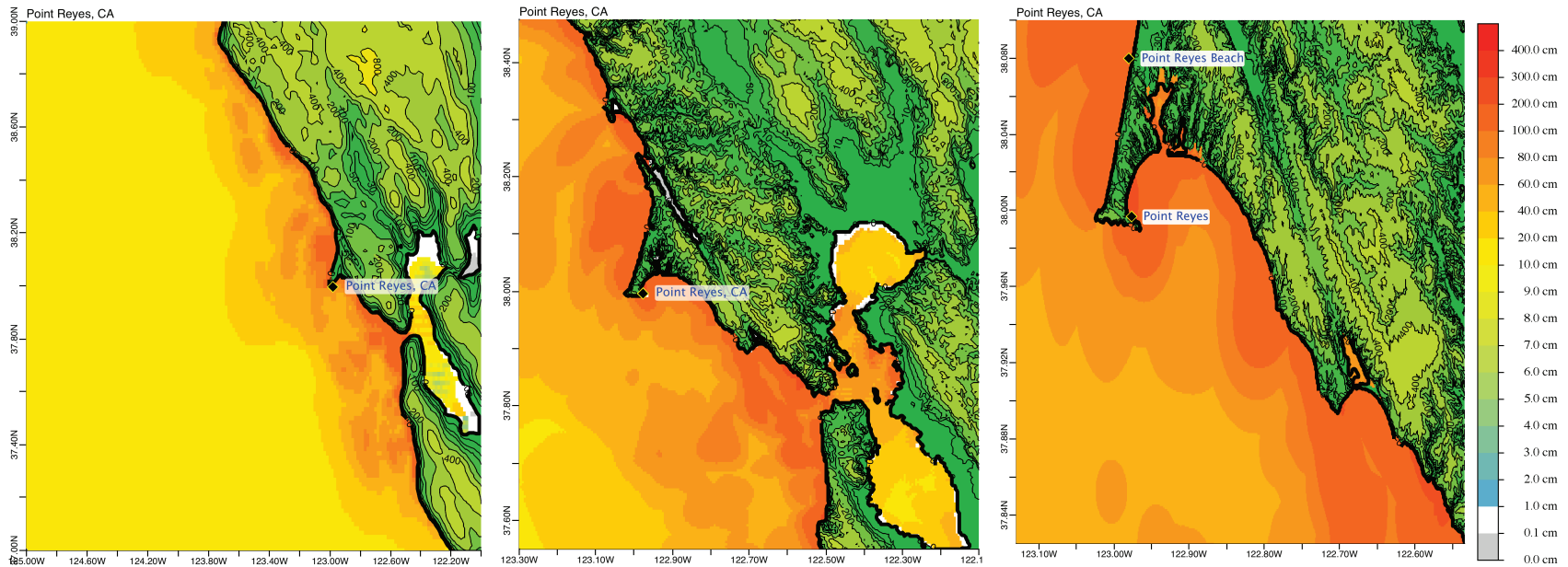
The Point Reyes forecast model was tested with NOAA's tsunami forecast system version 3.2. The same version of the propagation database was used during the model development.

The Point Reyes, California forecast model was tested with five synthetic scenarios and one historical tsunami event. Test results from the forecast system and comparisons with the results obtained during the forecast model development are shown numerically in Table 1 and graphically in Figures 1 to 4. The results show that the forecast model is stable and robust, with consistent and high quality results across geographically distributed tsunami sources and mega-event tsunami magnitudes. The model run time (wall clock time) was under 18 minutes for 8 hours of simulation time, and under 8 minutes for 4 hours. This run time is within the 10 minute run time for 4 hours of simulation time and satisfies time efficiency requirements.

Five synthetic events (there were no timeseries plots in the report for 2 of the cases) were run on the Point Reyes forecast model. The modeled scenarios were stable for all cases tested, with no instabilities or ringing. Results show that the largest modeled height was 401.25 cm and originated in the New Zealand-Kermadec-Tonga (NTSZ 30-39) source. Amplitudes greater than 100 cm were recorded for all test sources. The smallest signal of 119.8 cm was recorded at the far field Central and South American (CSSZ 89-98) source. Direct comparisons, of output from the forecast tool with results of both the historical event (Tohoku, Honshu in report, 2011) and available development synthetic events, demonstrated that the wave pattern were similar in shape, pattern and amplitude.

Table 1. Table of maximum and minimum amplitudes (cm) at the Point Reyes, California warning point for synthetic and historical events tested using SIFT 3.2 and obtained during development.

Scenario Name	Source Zone	Tsunami Source	α [m]	SIFT Max (cm)	Development Max (cm)	SIFT Min (cm)	Development Min (cm)
Mega-tsunami Scenarios							
KISZ 1-10	Kamchatka-Yap-Mariana-Izu-Bonin	A1-A10, B1-B10	25	354.127	354	-175.953	N/A
KISZ 22-31	Kamchatka-Yap-Mariana-Izu-Bonin	A22-A31, B22-B31	25	250.248	251	-176.243	N/A
ASCZ 56-65	Aleutian-Alaska-Cascadia	A56-A65, B56-B65	25	157.536	159	-158.122	N/A
CSSZ 89-98	Central and South America	A89-A98, B89-B98	25	119.796	120	-141.905	N/A
NTSZ 30-39	New Zealand-Kermadec-Tonga	A30-A39, B30-B39	25	401.253	402	-177.000	N/A
Historical Events							
Tohoku 2011	Kamchatka-Kuril-Japan-Izu-Mariana-Yap	n/a	n/a	178.215	n/a	-148.389	n/a



◆ max @14:49 = 250.25 (cm)

◆ min @12:38 = -176.24 (cm)

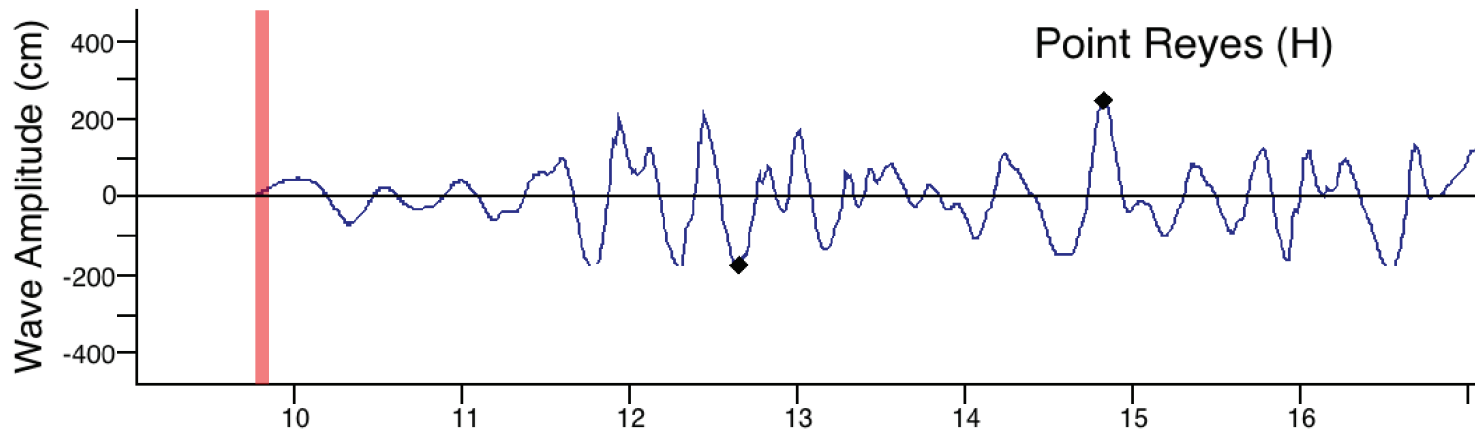
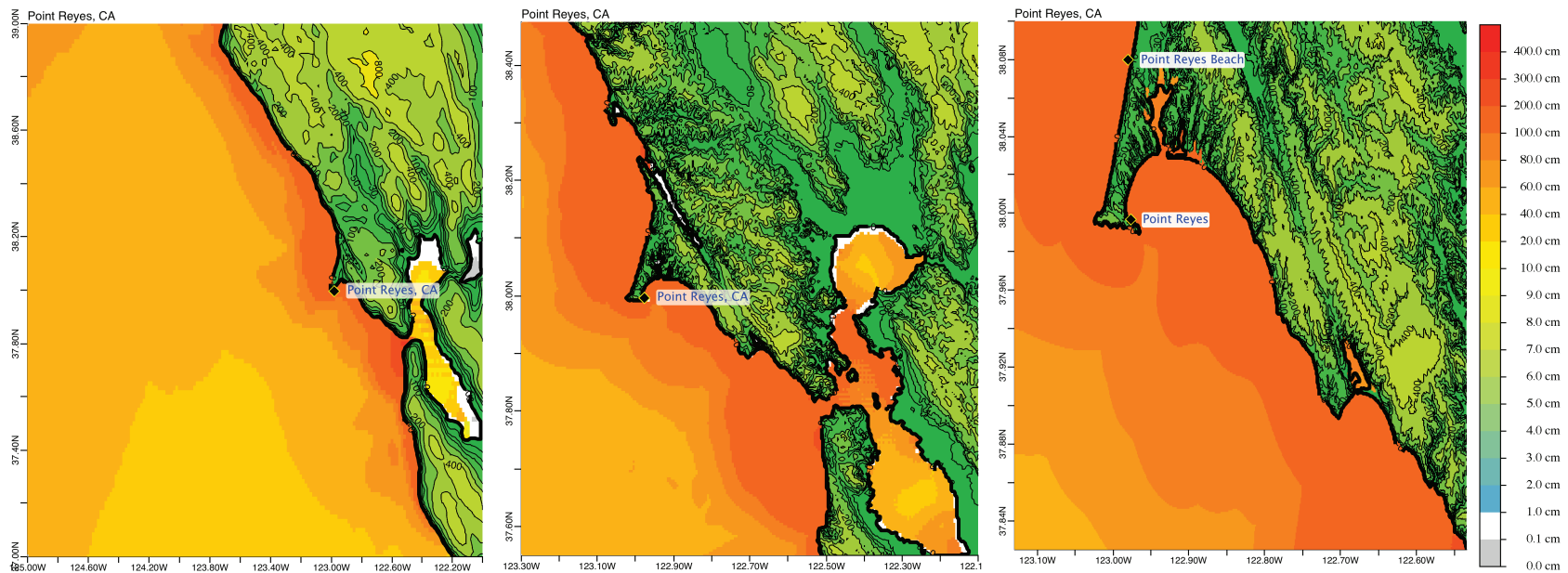


Figure C1 Response of the Point Reyes forecast model to synthetic scenario KISZ 22-31. (a,b, and c) Maximum sea surface elevation for A-, B- and C-grids. (d) Sea surface elevation time series at the C-grid warning point.



◆ max @04:38 = 157.54 (cm)

◆ min @04:19 = -158.12 (cm)

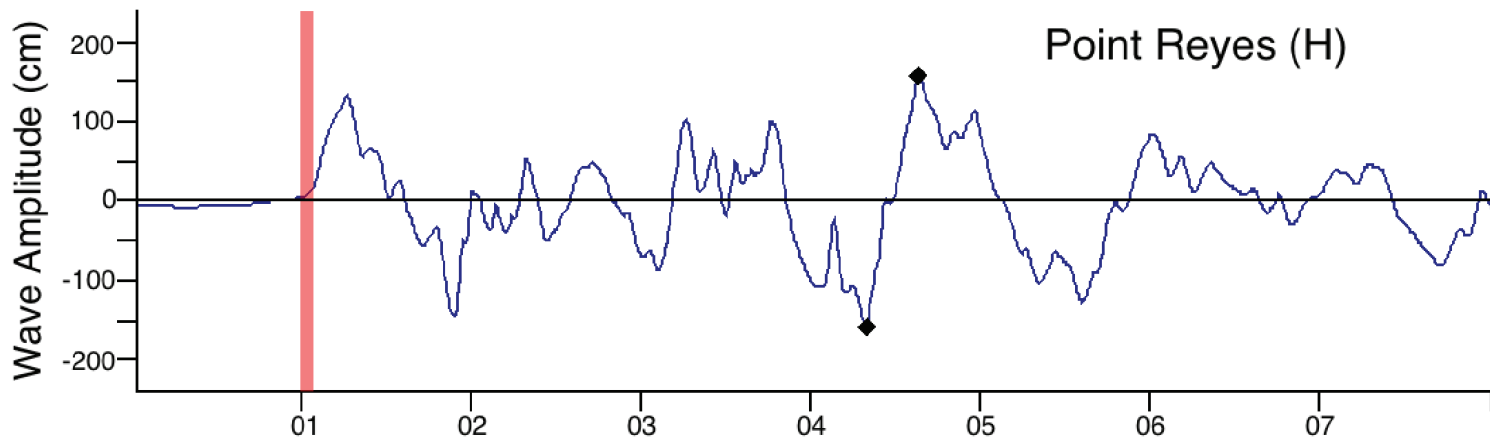


Figure C2 Response of the Point Reyes forecast model to synthetic scenario ACSZ 56-65. (a,b, and c) Maximum sea surface elevation for A-, B- and C-grids. (d) Sea surface elevation time series at the C-grid warning point.

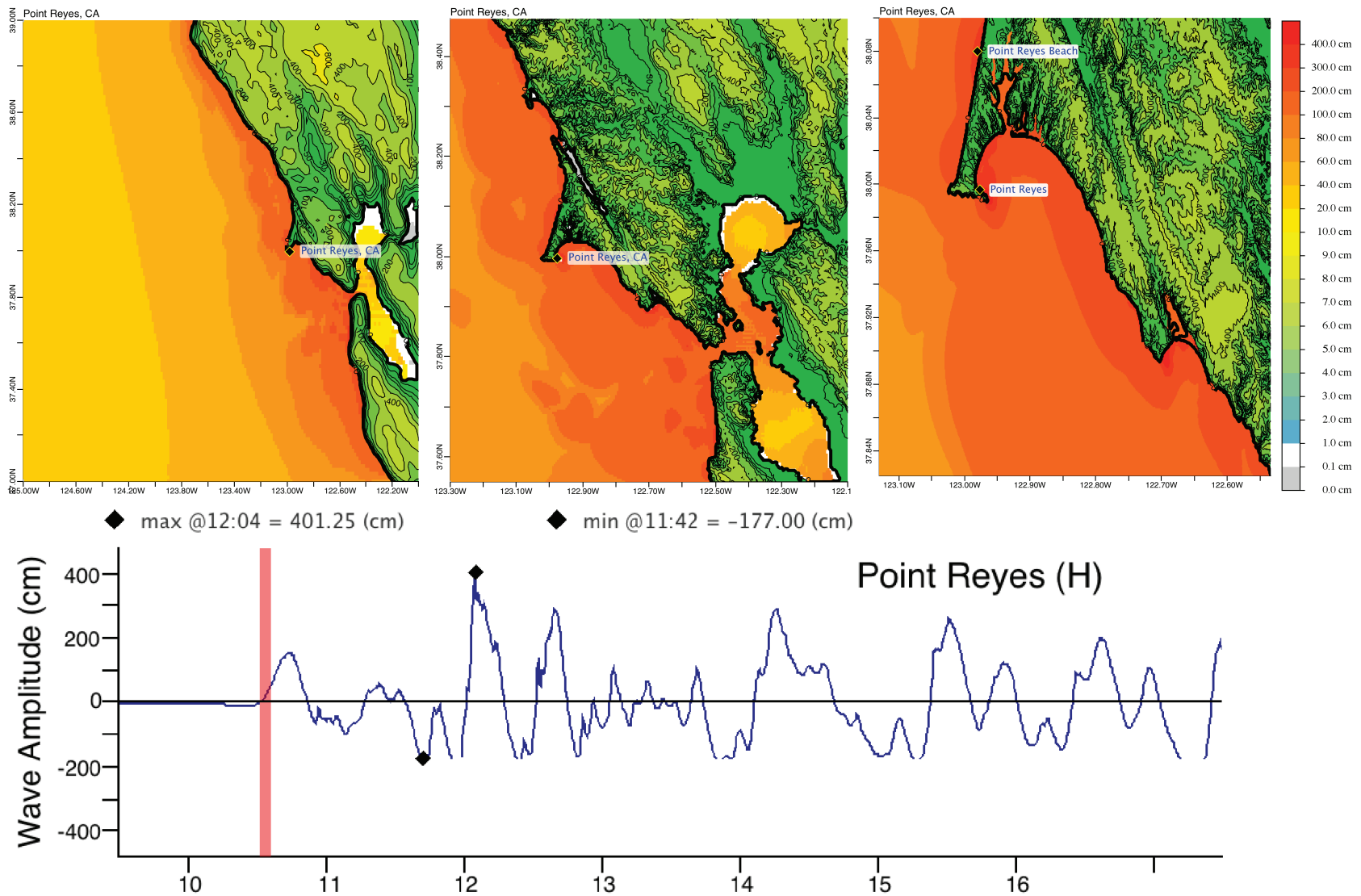


Figure C3 Response of the Point Reyes forecast model to synthetic scenario NTSZ 30-39. (a,b, and c) Maximum sea surface elevation for A-, B- and C-grids. (d) Sea surface elevation time series at the C-grid warning point.

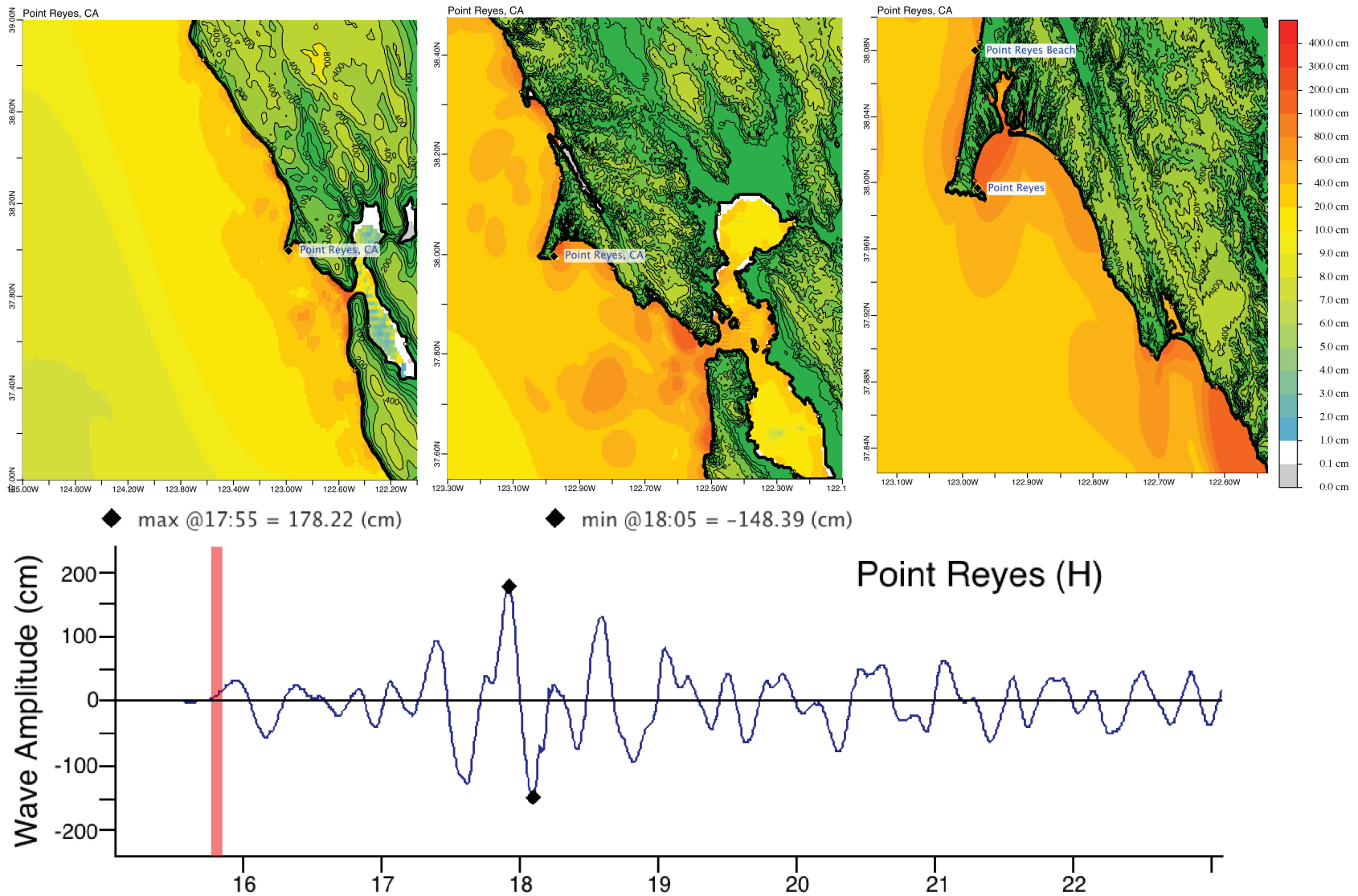


Figure C4 Response of the Point Reyes forecast model to the March 11 Tohoku tsunami. (a,b, and c) Maximum sea surface elevation for A-, B- and C-grids. (d) Sea surface elevation time series at the C-grid warning point.